Spring 2013

Modeling Studies of Antarctic Krill (*Euphausia superba*) Survival During Transport Across the Scotia Sea and Environs

Bettina Andrea Fach
Old Dominion University

Modeling studies of Antarctic krill (*Euphausia superba*) survival during transport across the Scotia Sea and Environs

by

Bettina Andrea Fach
Dipl.-Ing. January 1996, Fachhochschule Wilhelmshaven

A Dissertation Submitted to the Faculty of
Old Dominion University in Partial Fulfillment of the
Requirements for the Degree of

Doctor of Philosophy

Oceanography

Old Dominion University
May 2003

Approved by:

Eileen E. Hofmann (Director)

John M. Klinck (Member)

Ricardo A. Locarnini (Member)

Eugene J. Murphy (Member)

ABSTRACT

Modeling Studies of Antarctic Krill (*Euphausia superba*) Survival During Transport Across the Scotia Sea and Environs

Bettina Andrea Fach
Old Dominion University, 2003
Director: Dr. Eileen E. Hofmann

The Antarctic krill (*Euphausia superba*) populations at South Georgia, which is in the eastern Scotia Sea, are hypothesized to be sustained by import of individuals from upstream regions, such as the western Antarctic Peninsula. To test this hypothesis a modeling framework consisting of the Harvard Ocean Prediction System (HOPS) and a time-dependent, size-structured, physiologically-based krill growth model was developed. The simulated circulation fields obtained from HOPS were used with drifter studies to determine regions and pathways that allow transport of Antarctic krill to South Georgia. Pelagic phytoplankton concentrations along the simulated drifter trajectories were extracted from historical Coastal Zone Color Scanner measurements and sea ice algae concentrations were calculated from sea ice concentration and extent extracted along particle trajectories from Special Sensor Microwave/Imager measurements. As additional food sources, a time series of heterotrophic food was constructed from historical data, and time series of detritus concentrations along simulated drifter trajectories were calculated using phytoplankton concentrations extracted from Coastal Zone Color Scanner measurements together with measured particulate organic carbon to chlorophyll *a* ratios. These food resources, along specified drifter trajectories were then input to the krill growth model to determine the size and viability of krill during transport from the source region to South Georgia.

The drifter simulations showed that krill spawned along the mid to northern portion of the west Antarctic Peninsula continental shelf, coinciding with known krill spawning areas, can be entrained into the Southern Antarctic Circumpolar Current Front and be transported across the Scotia Sea to South Georgia in 10 months or less. Drifters originating on the continental shelf of the Weddell Sea can reach South Georgia as well; however, transport from this region averages about 20

months.

The krill growth model simulations showed that no single food source, such as pelagic phytoplankton, detritus, sea ice algae, or zooplankton, can support continuous growth of Antarctic krill during the 168 to 225 days needed for transport from the western Antarctic Peninsula to South Georgia. However, combinations of the food sources during the transport time enhanced krill survival, with zooplankton (heterotrophic food) and detritus being particularly important during periods of low pelagic phytoplankton concentrations. The growth model simulations also showed that larval and juvenile krill originating along the western Antarctic Peninsula can grow to the 1+ (14 mm to 36 mm) and 2+ (26 mm to 45 mm) sizes observed at South Georgia during the time needed for transport to this region. The additional transport time needed by krill originating in the Weddell Sea allows retention in a potentially high food environment, provided by sea ice, for almost one year. The krill then complete transport to South Georgia in the following year and larval and juvenile krill grow to 2+ (26 mm to 45 mm) and 3+ (35 mm to 60 mm) sizes during transport.

Additional simulations examined the effects of variability in wind stress, the transport through Drake Passage, and changes in the location of the Southern Antarctic Circumpolar Current Front on the transport and growth of Antarctic krill. Sensitivity studies of the simulated circulation showed that the surface wind stress has a minor influence on the overall simulated circulation pattern, but strongly affects the exchange between the continental shelf region of the Antarctic Peninsula and the Antarctic Circumpolar Current through changes in Ekman transport. A 20% decrease in wind stress or a 12% decrease in transport of the Antarctic Circumpolar Current decreases the ability of krill to reach South Georgia, potentially endangering the survival of the local population. A 10 km northward shift in the location of the SACCF also reduces the delivery of krill to South Georgia, especially from the main spawning area along the Western Antarctic Peninsula and in the Bransfield Strait, thereby reducing the potential recruits to the krill populations at South Georgia. A 20% increase in wind stress or a 12% increase in transport through Drake Passage enhances krill transport to South Georgia as long as the SACCF does not change position and can still function as main transport mechanism for krill.

The results of this study show that the krill populations along the Antarctic Peninsula and the Weddell Sea are likely the source populations that provide krill to

the population in South Georgia. However, the successful transport of krill to South Georgia is shown to depend on a multitude of factors, such as the location of the spawning area and timing of spawning, food concentrations during transport, predation, and variations in the location of the SACCF and in sea ice extent. Therefore, this study provides insight into which biological and environmental factors control the successful transport of krill across the Scotia Sea and their survival during that time, and with it insight into krill distribution and production in the Scotia Sea.

ACKNOWLEDGMENTS

First and foremost I would like to thank my advisor, Eileen Hofmann, who has been a wonderful advisor for me. With plenty of encouragement, patience, and support she guided me through this endeavor, fostering my development as a scientist and enabling me to successfully finish my dissertation. Eileen was also very generous in providing opportunities for travels to national and international meetings and cruises, which is gratefully acknowledged. I am also thankful for the contributions and comments of my committee members, John Klinck, Eugene Murphy and Ricardo Locarnini. John's efforts to enlighten me in the mysterious world of circulation models has been tremendous and I appreciate the many opportunities I had to wander into his office and monopolize his time. Eugene, although far away, has provided much advise, guidance, and ideas that helped my work progress over the years. He also made it possible for me to join a research cruise to Antarctica on the RRS *James Clark Ross*, which has been the highlight of my studies. I thank Ricardo for his help in navigating through the often difficult life as a student, always having an open ear and lots of helpful advise.

I am grateful to many people here at CCPO without whom this endeavor would have been much harder to accomplish. Julie Morgan handled all administrative matters very professionally and at the same time provided lots of much needed moral support. Joe Ruettgers helped overcome all computer related problems, no matter what time of day or night. Special thanks go out to all my fellow students who have made this experience so much more pleasurable. I am especially indebted to my long-time office mate Kris Holderied, for her friendship and support, the many scientific discussions, and the frequent trips to 7/11. Without her I would not have been able to achieve this. Tonya Clayton, who has been a wonderful source for life's wisdom and great company. My dear friend Christina Dryden, long-time ally and study companion, Sinan Husrevoğlu who was always there to give excellent advise with any computer problems, and Mike Dinniman for much help with the tricky business of running circulation models and his generosity for always letting me use 'Knudsen'.

Special thanks go out to my great friend Martina Doblin, who has made sure that I don't loose my sanity over finishing my dissertation. Her friendship and constant support greatly helped me accomplish this and mean a lot to me. Thanks

are further ado to my dear friend Rosey Mellion for her continuing friendship over the past years, and also to her parents Pat and Mike, who have provided a supportive family environment far away from home.

I am very grateful to my parents for their unconditional love and support over the past years. They have always believed in me and have gone out of their way to help me realize my dream. And finally to Barış Salihoğlu: I cannot adequately express my heartfelt gratitude for all his support, encouragement, and great cooking throughout this experience.

I wish to thank Professor Alan Robinson, who generously allowed the use of the Harvard Ocean Prediction System and provided the model code. I am indebted to Patrick Haley and Pierre Lermusiaux for their help with HOPS over an extended period of time.

This research was generously supported by the U. S. National Science Foundation, Office of Polar Programs grant number OPP 0087690. The computer facilities and resources were provided by the Commonwealth Center for Coastal Physical Oceanography at Old Dominion University.

Contents

1 INTRODUCTION **1**

2 BACKGROUND **7**

2.1 Circulation Characteristics 7
2.1.1 Large Scale Circulation Characteristics 7
2.1.2 Mesoscale Circulation Characteristics 9
2.2 Krill Life History, Distribution and Variability 11
2.2.1 Krill Life History 11
2.2.2 Krill Distribution 13
2.2.3 Variability 15
2.3 Food Sources and Feeding Behavior of Krill 16
2.4 Modeling Studies 18
2.4.1 Krill Models 18
2.4.2 Circulation Models 19

3 METHODS **22**

3.1 Circulation Model 22
3.1.1 Model Physics 22
3.1.2 Model Structure 24
3.2 Krill Growth Model 33
3.2.1 Model Processes and Parameterizations 34
3.3 Specification of Food Source 40
3.3.1 Phytoplankton 40
3.3.2 Sea Ice Algae 44
3.3.3 Heterotrophic Food 47
3.3.4 Detritus 48
3.4 Simulation Characteristics 51
3.4.1 Circulation Simulations 51
3.4.2 Drifter Trajectories 52
3.4.3 Krill Growth Model 53
3.5 Data Sets for Calibration and Verification of Models 54
3.5.1 Validation of circulation model 54
3.5.2 Validation of krill growth model 60

4 RESULTS **70**

4.1 Reference Simulation 70

4.1.1 Comparison with Hydrography 74

4.1.2 Comparison with Climatology 79

4.2 Model Sensitivity 81

4.2.1 General Circulation 83

4.2.2 Regional Circulation 85

4.2.3 Simulated Drifter Trajectories 87

4.3 Model Drifters 91

4.3.1 Surface Drifters 91

4.3.2 Subsurface Drifters 94

4.3.3 Reference Simulation Transport Pattern 96

4.4 Effect of Environmental Changes 101

4.4.1 Effect of Changes in Wind Stress 102

4.4.2 Effect of Changes in the Transport through Drake Passage . . 106

4.4.3 Effect of Changes in the Location of the Southern ACC Front 106

4.5 Krill Growth Dynamics 110

4.5.1 Effect of Different Food Types 110

4.5.2 Effect of Different Spawning Times 127

4.5.3 Krill Growth Rates 128

4.5.4 Length-frequency Distribution of Krill across the Scotia Sea . 129

5 DISCUSSION **140**

5.1 Circulation model 140

5.1.1 Frontal Structure 140

5.1.2 Eddy Kinetic Energy 141

5.1.3 Hydrography 141

5.1.4 Surface and Subsurface Drifters 143

5.1.5 Effect of Sea Ice Cover 146

5.1.6 Flow Dynamics around South Georgia 147

5.2 Krill Origination Areas and Transport Pathways 148

5.2.1 Weddell Sea 150

5.2.2 Importance of the Southern ACC Front 152

5.2.3 Local Effects around South Georgia 153

5.2.4 Effect of Different Spawning Times on Transport 154

5.2.5 Effect of Environmental Changes 155
5.3 Food Supply 156
5.3.1 Deep Chlorophyll Maximum 158
5.3.2 Selection of Age Group? 159
5.3.3 Estimates of Krill Food Demand 161
5.4 Effect of Variability 163
5.4.1 Variability of Food Sources 163
5.4.2 Variations in Krill Biomass at South Georgia 164
5.4.3 Estimates of Predation 167

6 SUMMARY **171**

7 REFERENCES **174**

List of Tables

1 Characteristics of the three ACC fronts, the Subantarctic Front (SAF), the Polar Front (PF) and the Southern Antarctic Circumpolar Current Front (SACCF). 8

2 Configuration of the HOPS model, values of parameters, and forcing functions used in the simulations. 26

3 Characteristics of the Subantarctic Front (SAF), the Polar Front (PF) and the Southern Antarctic Circumpolar Current Front (SACCF) used to determine the temperature and salinity anomalies for the feature model. 29

4 Summary of the circulation sensitivity simulations showing the change made from the reference simulation and the figures displaying the results. 33

5 Length (L, mm) to wet weight (W, mg), wet weight to dry weight (DW, mg), and dry weight to carbon (C, mg) relationships used in the krill growth model. 35

6 Compression filtration (F^{cf}, $m^3\ d^{-1}$), ice biota grazing (F^{ig}, $m^3\ d^{-1}$), the standard respiration rate (R^s, $\mu\ l\ hr^{-1}$), total ingestion (I_{tot}, mg $C\ d^{-1}$), net production of any size (NP_j, mg $C\ d^{-1}$) and assimilation efficiency A (80%) as used in the krill growth model. 35

7 Summary of POC:Chl$a$ ratios measured for Antarctic waters. For each, the season and location where the measurement was made is given, as well as the relevant reference. 49

8 Summary of the simulations done with different combinations of the food time series. 54

9 Summary of conductivity-temperature-depth recorder (CTD), and expandable bathythermograph (XBT) data sets that can be used to validate the simulated circulation distributions. 57

10 Name, drifter type, latitude and longitude of release locations for WOCE drifters used in this study. 58

11 Source, type, collection method, and space and time coverage of krill data sets available for this study. Western Antarctic Peninsula and South Georgia are abbreviated as WAP and SG, respectively. 61

12 Average simulated surface layer flow speed and direction, and Ekman flow speed and direction over the upper 100 m for 10 drifters defined in Table 10, subjected to ±20% variation in the NCEP wind fields used to force the circulation model. 86
13 Comparison of the average speed of WOCE surface drifters with the average surface speed (m s^{-1}) calculated for the simulated surface drifters released at different times. 93
14 Comparison of the average speed of WOCE ALACE subsurface drifters with the average subsurface speed (m s^{-1}) calculated for the simulated surface drifters released at different times. 97
15 Summary of the total number of simulated drifters reaching South Georgia (at SG), reaching South Georgia from the north (north SG), reaching South Georgia from the south (south SG), reaching within 600 km of South Georgia (600 km SG), and not reaching the South Georgia (not reach) obtained for different circulation scenarios and release times. 100
16 Summary of krill growth simulations for different food types, initial sizes, and release times. 113
17 Summary of krill growth simulations for different food types, initial sizes, and release times. 117
18 Summary of krill growth simulations for different food types, initial sizes, and release times. 120
19 Summary of krill growth simulations for different food types, initial sizes, and release times. 123
20 Summary of krill growth simulations for different food types, initial sizes, and release times. 126
21 Parameters, their associated values, and units as used in equation (24). 144
22 Summary of the total times (days) necessary for different percent (%) of krill to be removed by different rates of predation. 170

List of Figures

1 Base map showing the study region, the locations of the Subantarctic Front (SAF), the Polar Front (PF), the Southern Antarctic Circumpolar Current Front (SACCF), and the southern boundary of the Antarctic Circumpolar Current (dashed line; Bndry). 2

2 Schematic of the modeling framework developed to answer research questions of interest. 6

3 Relationship between size and age of krill obtained from a modified von Bertalanffy growth model (Equation 1) fitted to seasonally oscillating length-at-age krill data given by Siegel (1987). 12

4 Circum-Antarctic map showing the distribution of regions of highest krill concentration as developed by Lubimova et al. (1982), and the climatological locations of the Southern Antarctic Circumpolar Current Front (dashed line) and the southern boundary of the Antarctic Circumpolar Current (dash-dotted line) as given by Orsi et al. (1995). 14

5 Study area with the model domain indicated as a rotated rectangular. 25

6 Wind stress (N m^{-2}) for December 1992 from the NCEP climatology on a 2.5° x 2.5° grid. 30

7 CZCS-derived eight-year (1978-1986) composite of pigment concentration (mg m^{-3}) for January. 41

8 CZCS-derived time series of pigment concentration (mg m^{-3}) along trajectories of three drifters originating at the western Antarctic Peninsula in: A) December (Year Day 335), B) January (Year Day 1), C) February (Year Day 32). 43

9 SSM/I-derived sea ice concentration (% coverage) for June 1988. . . . 45

10 SSM/I-derived time series of sea ice algae concentration (mg m^{-3}) along trajectories of three drifters originating at the western Antarctic Peninsula in A) December (Year Day 335), B) January (Year Day 1), C) February (Year Day 32). 46

11 Time series of heterotrophic food input to the krill growth model. . . 47

12 Measurements of POC and chlorophyll *a* concentrations (*) from several locations during the ANT-X/6 cruise (Dehairs et al., 1997). . . . 50

13 CZCS chlorophyll data-derived time series of detritus concentration (mg C m^{-3}) along trajectories of three drifters originating at the western Antarctic Peninsula in A) December (Year Day 335), B) January (Year Day 1), C) February (Year Day 32). 52
14 Locations of drifters (o) released in the circulation model to simulate krill transport. 53
15 A) Observed potential temperature and B) observed salinity from the WOCE A23 cruise, March to May 1995. 55
16 A) Observed potential temperature and B) observed salinity from the Melville cruise section III, February 1975. 56
17 Drifter trajectories from 27 WOCE/TOGA surface and subsurface drifters used in this study. 59
18 Distribution of Antarctic krill A) surface larvae and B) older krill (>20 mm) in summer (January to March) across the study region extracted from net haul observations obtained during the *Discovery* Investigations, 1926-1940 (Marr, 1962). 63
19 Locations of the length-frequency measurements of Antarctic krill, acquired during BIOMASS, 1980-1985, in the study region (Thorley and Trathan, 1994). 64
20 Locations of Antarctic krill length-frequency measurements from A) FIBEX cruises (January - March 1981), B) SIBEX1 cruises (November - December 1984), C) SIBEX2 cruises (January - March 1985). . 65
21 Summarized length-frequency distributions for Antarctic krill from measurements made during the FIBEX cruises (January - March 1981) for A) west Antarctic Peninsula, B) Bransfield Strait, C) Weddell Sea, D) Elephant Island/Scotia Sea region, E) open Scotia Sea stations, and F) South Georgia. 66
22 Summarized length-frequency distributions for Antarctic krill from measurements made during the SIBEX1 cruises (October - December 1983) for A) west Antarctic Peninsula, B) Bransfield Strait, C) Elephant Island/Scotia Sea, and D) PPS2 (November-December 1984) regions. 67

23 Summarized length-frequency distributions for Antarctic krill measurements made during the SIBEX2 cruises (January - March 1985) for A) southwestern Antarctic Peninsula, B) west Antarctic Peninsula, C) Bransfield Strait, and D) Elephant Island/Scotia Sea regions. 67
24 Location of the British Antarctic Survey Core Programme survey boxes near South Georgia after Watkins (1999). 69
25 Barotropic streamfunction (Sv) A) at the start of the simulation (1 October) and B) after 180 days of simulation (30 March). 71
26 Eddy kinetic energy ($cm^{-2}\ s^{-2}$) on day 180 of the reference simulation (March 30). 73
27 Simulated A) temperature and B) salinity along the Melville III section obtained by averaging the model-derived distributions for days 130 to 150, which correspond to February. 76
28 Simulated A) temperature and B) salinity along the WOCE A23 section obtained by averaging the model-derived distributions for days 190 to 210, which correspond to April. 78
29 Climatological observations of A) potential temperature and B) salinity along the Melville II section obtained from the WOA 1998 climatology. 80
30 Climatological observations of A) potential temperature and B) salinity along the WOCE A23 section obtained from the WOA 1998 climatology. 82
31 Barotropic streamfunction (Sv) after 180 days of simulation (30 March) with A) 20% increased wind stress and B) 20% decreased wind stress. 84
32 Simulated surface drifter trajectories for drifters A) 1 and 2, B) 3 and 4, and C) 5, 7, and 9, released in December that experience NCEP winds (solid line), NCEP winds with a 20% increase in wind speed (dashed line), and NCEP winds with a 20% decrease in wind speed (dotted line). 88
33 Simulated surface drifter trajectories for drifters A) 6, B) 8, and C) 10, released in December that experience NCEP winds (solid line), NCEP winds with a 20% increase in wind speed (dashed line), and NCEP winds with a 20% decrease in wind speed (dotted line). 89

34 Trajectories followed by A) WOCE surface drifter 22047 (+), and B) WOCE surface drifter 22050 (+), and those followed by simulated surface drifters released at day 30 ($\star$), day 60 ($\square$), day 90 ($\triangle$), day 120 ($\triangledown$), and day 150 ($\diamond$). 92
35 Trajectories followed by A) WOCE ALACE subsurface float 204 (+),and B) WOCE ALACE subsurface float 250 (+), and those followed by simulated drifters released at day 30 ($\star$), day 60 ($\square$), day 90 ($\triangle$), day 120 ($\triangledown$), day 150 ($\diamond$) intervals. 95
36 Initial positions at which surface drifters were released in the simulated circulation fields on A) 1 December, B) 1 January, and C) 1 February. 98
37 Simulated surface drifter trajectories resulting from particles released in January along the west Antarctic Peninsula that reach South Georgia from the north (dashed lines) and from the south (solid lines). . . 102
38 Initial positions at which surface drifters were released in the simulated circulation fields obtained using 20% increased wind speeds on A) 1 December, B) 1 January, and C) 1 February. 104
39 Initial positions at which surface drifters were released in the simulated circulation fields obtained using 20% decreased wind speeds on A) 1 December, B) 1 January, and C) 1 February. 105
40 Initial positions at which surface drifters were released in the simulated circulation fields obtained using 12% increased transport through Drake Passage on A) 1 December, B) 1 January, and C) 1 February. . 107
41 Initial positions at which surface drifters were released in the simulated circulation fields obtained using 12% decreased transport through Drake Passage on A) 1 December, B) 1 January, and C) 1 February. . 108
42 Initial positions at which surface drifters were released in the simulated circulation fields obtained with the SACCF moved 10 km to the north on A) 1 December, B) 1 January, and C) 1 February. 109
43 Simulated growth of 2 mm krill (lower curves), 22 mm krill (middle curves), and 45 mm krill (upper curves) starting in December (Year Day 335) using phytoplankton food only. 111

44 Range of simulated growth of 2 mm krill (lower curves), 22 mm krill (middle curves), and 45 mm krill (upper curves) released in the west Antarctic Peninsula region in December (medium shading), January (dark shading), and February (light shading) obtained for Antarctic krill feeding on A) phytoplankton only, B) phytoplankton and sea ice algae with detritus, C) phytoplankton, copepods and sea ice algae with detritus, and D) detritus only. 114

45 Range of simulated growth of 2 mm krill (lower curves), 22 mm krill (middle curves), and 45 mm krill (upper curves) released in the Bransfield Strait region in December (medium shading), January (dark shading), and February (light shading) obtained for feeding on A) phytoplankton only, B) phytoplankton and sea ice algae with detritus, C) phytoplankton, copepods and sea ice algae with detritus, and D) detritus only. 116

46 Range of simulated growth of 2 mm krill (lower curves), 22 mm krill (middle curves), and 45 mm krill (upper curves) released in the Elephant Island/Scotia Sea region in December (medium shading), January (dark shading), and February (light shading) obtained for feeding on A) phytoplankton only, B) phytoplankton and sea ice algae with detritus, C) phytoplankton, copepods and sea ice algae with detritus, and D) detritus only. 119

47 Range of simulated growth of 2 mm krill (lower curves), 22 mm krill (middle curves), and 45 mm krill (upper curves) released in the southwest Antarctic Peninsula region in December (medium shading), January (dark shading), and February (light shading) obtained for feeding on A) phytoplankton only, B) phytoplankton and sea ice algae with detritus, C) phytoplankton, copepods and sea ice algae with detritus, and D) detritus only. 122

48 Range of simulated growth of 2 mm krill (lower curves), 22 mm krill (middle curves), and 45 mm krill (upper curves) released in the Weddell Sea region in December (medium shading), January (dark shading), and February (light shading) obtained for feeding on A) phytoplankton only, B) phytoplankton and sea ice algae with detritus, C) phytoplankton, copepods and sea ice algae with detritus, and D) detritus only. 125
49 Simulated daily growth rates of 2 mm, 22 mm, and 45 mm krill feeding on all food sources combined when starting transport from the west Antarctic Peninsula in January. 129
50 Simulated distribution of larval krill across the study area for individuals that were released in December (•), January (▲), and February (♦). 130
51 Simulated distribution of older krill (>20 mm) across the study area for individuals that were released in A) December, B) January, and C) February. 131
52 Simulated length-frequency distribution of Antarctic krill (January - March) for individuals released in December for the regions: A) southwestern Antarctic Peninsula, B) western Antarctic Peninsula, C) Bransfield Strait, D) Weddell Sea, E) Elephant Island/Scotia Sea region, F) open Scotia Sea, and G) South Georgia. 133
53 Simulated length-frequency distribution of Antarctic krill at South Georgia extrapolated to the potential length of krill in January for individuals arriving at A) the west side of the Island, B) the east side of the Island, and C) all of South Georgia. Total number of individuals, N, found in each area in the simulations is shown. 137
54 Thirty-day average of the simulated current velocity (cm s^{-1}) across the SAF between 57.247°S, 65.05°W and 57.677°S, 65.833°W, which corresponds to the locations of Melville II stations 24 and 21. 145
55 Distribution of five areas around the Antarctic Peninsula that can potentially provide Antarctic krill to South Georgia. 150
56 Transport pathways over 10 months for drifters released at different points in the Weddell-Scotia Confluence in November. 151

57 Simulated growth of 22 mm krill (lower curves), 33 mm krill (middle curves), and 45 mm krill (upper curves) released in November (Year Day 305) in the Weddell-Scotia Confluence. 151
58 Estimates of krill loss due to different rates of predation. 169
A1 Range of CZCS-derived time series of pigment concentration (mg m^{-3}) along trajectories of drifters originating at the west Antarctic Peninsula (region 1) starting in A) December (Year Day 335), B) January (Year Day 1), C) February (Year Day 32). 200
A2 Range of CZCS-derived time series of pigment concentration (mg m^{-3}) along trajectories of drifters originating in the Bransfield Strait area (region 2) starting in A) December (Year Day 335), B) January (Year Day 1), C) February (Year Day 32). 201
A3 Range of CZCS-derived time series of pigment concentration (mg m^{-3}) along trajectories of drifters originating in the Scotia Sea/Elephant Island area (region 3) starting in A) December (Year Day 335), B) January (Year Day 1), C) February (Year Day 32). 202
A4 Range of CZCS-derived time series of pigment concentration (mg m^{-3}) along trajectories of drifters originating in the southwestern Antarctic Peninsula area (region 4) starting in A) December (Year Day 335), B) January (Year Day 1), C) February (Year Day 32). . . . 203
A5 Range of CZCS-derived time series of pigment concentration (mg m^{-3}) along trajectories of drifters originating in the Weddell Sea area (region 5) starting in A) December (Year Day 335), B) January (Year Day 1), C) February (Year Day 32). 204
A6 Range of SSM/I-derived time series of sea ice algae concentration (mg m^{-3}) along trajectories of drifters originating at the west Antarctic Peninsula (region 1) starting in A) December (Year Day 335), B) January (Year Day 1), C) February (Year Day 32). 205
A7 Range of SSM/I-derived time series of sea ice algae concentration (mg m^{-3}) along trajectories of drifters originating in the Bransfield Strait area (region 2) starting in A) December (Year Day 335), B) January (Year Day 1), C) February (Year Day 32). 206

A8 Range of SSM/I-derived time series of sea ice algae concentration (mg m^{-3}) along trajectories of drifters originating in the Scotia Sea/Elephant Island area (region 3) starting in A) December (Year Day 335), B) January (Year Day 1), C) February (Year Day 32). 207

A9 Range of SSM/I-derived time series of sea ice algae concentration (mg m^{-3}) along trajectories of drifters originating in the southwestern Antarctic Peninsula area (region 4) starting in A) December (Year Day 335), B) January (Year Day 1), C) February (Year Day 32). . . . 208

A10 Range of SSM/I-derived time series of sea ice algae concentration (mg m^{-3}) along trajectories of drifters originating in the Weddell Sea area (region 5) starting in A) December (Year Day 335), B) January (Year Day 1), C) February (Year Day 32). 209

A11 Range of CZCS chlorophyll data-derived time series of detritus concentration (mg C m^{-3}) along trajectories of drifters originating at the west Antarctic Peninsula (region 1) starting in A) December (Year Day 335), B) January (Year Day 1), C) February (Year Day 32). . . . 210

A12 Range of CZCS chlorophyll data-derived time series of detritus concentration (mg C m^{-3}) along trajectories of drifters originating in the Bransfield Strait area (region 2) starting in A) December (Year Day 335), B) January (Year Day 1), C) February (Year Day 32). 211

A13 Range of CZCS chlorophyll data-derived time series of detritus concentration (mg C m^{-3}) along trajectories of drifters originating in the Scotia Sea/Elephant Island area (region 3) starting in A) December (Year Day 335), B) January (Year Day 1), C) February (Year Day 32).212

A14 Range of CZCS chlorophyll data-derived time series of detritus concentration (mg C m^{-3}) along trajectories of drifters originating in the southwestern Antarctic Peninsula area (region 4) starting in A) December (Year Day 335), B) January (Year Day 1), C) February (Year Day 32). 213

A15 Range of CZCS chlorophyll data-derived time series of detritus concentration (mg C m^{-3}) along trajectories of drifters originating in the Weddell Sea area (region 5) starting in A) December (Year Day 335), B) January (Year Day 1), C) February (Year Day 32). 214

1 INTRODUCTION

Antarctic krill, *Euphausia superba*, has long been recognized as an important component of the Antarctic marine food web. Many of the top predator populations that are part of the Antarctic marine food web, such as whales, seals, seabirds, penguins and fish, are dependent on krill as a food source (Fraser, 1936; Marr, 1962; Knox, 1970). Therefore, much research has been conducted to better understand the life history, physiology, behavior and distribution of this species (e.g. Nicol et al., 1992; El-Sayed, 1994; Siegel and Loeb, 1994). However, critical information about the behavior, distribution and reproduction of this very abundant and important species in the Southern Ocean is still missing, due in part to the wide distribution of this species in a habitat that spans a vast area (up to 36 x 10^6 km^2) and includes the continental shelf and open ocean. Thus, much of the research on this organism is still restricted to limited studies aboard ship (Nicol and de la Mare, 1993).

Information adequate to determine whether Antarctic krill represent a single or multiple breeding population, which has considerable implications for understanding the distribution and management of this species (Everson and Miller, 1994), is still lacking. Length-frequency distribution (Fevolden and George, 1984) or morphometric measurements (Siegel, 1986) are unable to distinguish between different stocks of krill. However, enzyme structure analysis suggests that there is only a single krill breeding population (Fevolden, 1988; Miller and Hampton, 1989a). This result argues for a source region for Antarctic krill that, with the aid of ocean currents, supplies different areas thereby maintaining a homogeneous population.

The waters around South Georgia (Fig. 1), in the east of the Scotia Sea, contain a persistent population of krill, which provides the primary food for many of the marine mammals, and seabirds that inhabit this region (Croxall et al., 1988). This area is also the site of a commercial krill fishery (Murphy et al., 1997). Early analyses of the length-frequency distribution of Antarctic krill populations around South Georgia led to the conclusion that the local population is not self-sustaining (Marr, 1962; Mackintosh, 1972). The apparent lack of a local population that undergoes reproduction with subsequent recruitment is surprising considering the large top predator populations that depend on Antarctic krill (Everson, 1984). More recent analyses of length-frequency distributions suggest that the youngest dominant year class around South Georgia in mid-summer is the 2+ (3 years old) year class (Murphy

The Journal *Deep-Sea Research* was used as a model for this dissertation

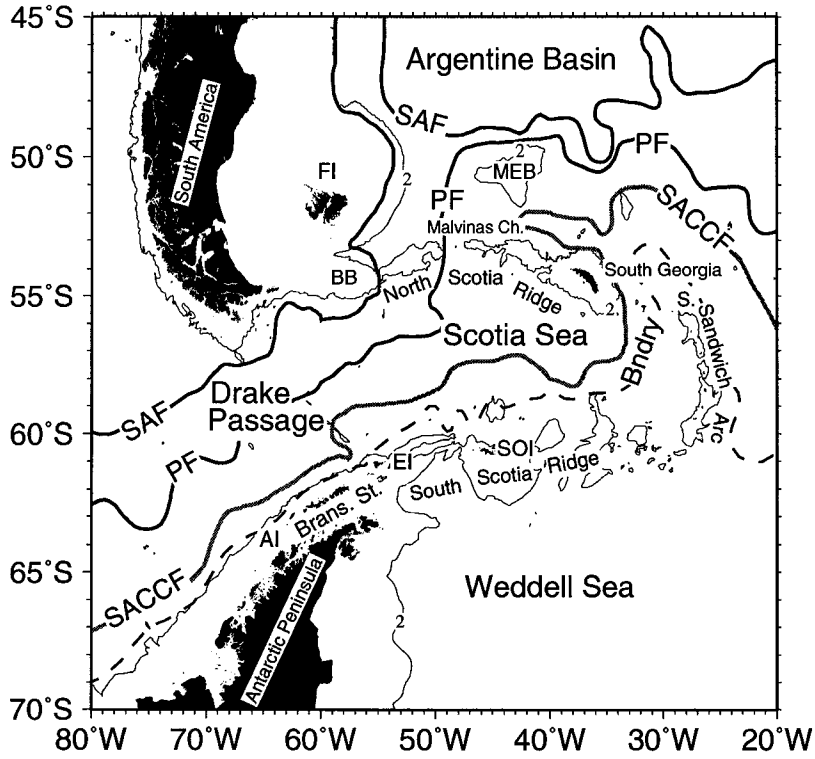

Fig. 1. Base map showing the study region, the locations of the Subantarctic Front (SAF), the Polar Front (PF), the Southern Antarctic Circumpolar Current Front (SACCF), and the southern boundary of the Antarctic Circumpolar Current (dashed line; Bndry). The front locations were determined from historical hydrographic data given in Orsi et al. (1995). The thin line represents the 2000-m isobath. Geographic names are abbreviated as Falkland Islands (FI), Burdwood Bank (BB), Malvinas Chasm (Malvinas Ch.), Maurice Ewing Bank (MEB), South Orkney Islands (SOI), Elephant Island (EI), Anvers Island (AI), and Bransfield Strait (Brans. St.).

et al., 1998; Watkins et al., 1999). Also, Watkins et al. (1999) showed that the krill population at the eastern end of South Georgia tend to be smaller and lack larger year classes relative to the krill populations at the western end of the Island.

Because there is a persistent krill population at South Georgia in spite of no obvious local recruitment, the inference is that this is a sink population which depends on a source population elsewhere. However, direct observations that support krill transport from another region to South Georgia are few. Distributions of various Antarctic krill life stages between the Antarctic Peninsula and South Georgia suggest a spatial separation of stages, with older stages being further eastward from the Antarctic Peninsula, suggesting that this area is a source region for krill popu-

lations observed downstream in the Scotia Sea (Marr, 1962). Brinton (1985) used length-frequency analyses of krill collected from net samples at locations across the Scotia Sea to show that krill size increases towards South Georgia. This has been supported by Siegel (1992), who found evidence that krill are exported from the Antarctic Peninsula region. Transport of krill from this region to South Georgia is accomplished by the large-scale ocean currents (Priddle et al., 1988; Witek et al., 1988). Another potential krill source region is the Weddell Sea (Marr, 1962; Maslennikov and Solyankin, 1988; review by Atkinson et al., 2001). Thus, these observations of potential krill source populations provide the basis for the first research question in this study: **What origination areas and transport pathways provide a sustained recruitment for the Antarctic krill population found around South Georgia, and how do different spawning times at the source affect the transport and survival of krill?**

More recently, the issue of krill transport to South Georgia from an upstream source was tested with modeling studies (Hofmann et al., 1998; Murphy et al., 1998). These studies show that the currents associated with the Antarctic Circumpolar Current (ACC) can transport particles from the Antarctic Peninsula to South Georgia in 140 to 160 days. The currents associated with the Southern ACC Front (SACCF) and southern boundary of the ACC, which flow along the outer continental shelf of the west Antarctic Peninsula, appear to be the primary transport pathways (Hofmann et al., 1998).

Krill of all sizes can potentially be transported by ocean currents. However, passive transport of larval and juvenile krill is most likely because older krill are strong swimmers, with swimming speeds up to 8 times its body length per second (Kils, 1982). For 40 mm krill, this swimming speed is similar to the average speed (30 cm s^{-1}) of the SACCF (Orsi et al., 1995). Modeling studies (Hofmann et al., 1998; Hofmann and Lascara, 2000) suggest that krill with initial sizes of 2 mm and 10 mm can develop to 10-12 mm and 20-30 mm sizes, respectively, in 140 to 160 days, which is the time required for transport between the Antarctic Peninsula and South Georgia by the mean circulation.

Most krill spawning in the Antarctic Peninsula region occurs between December and February (Ross and Quetin, 1986). Chlorophyll concentrations in the Scotia Sea are typically low (<0.6 mg m^{-3}, Comiso et al., 1993) and transport during and subsequent to the spawning season will place larval and juvenile krill in a low food

environment during a time when their potential food supply is declining even further. Thus, while transport of krill across the Scotia Sea to South Georgia is feasible, sufficient food supply during transport or delivery of viable krill to South Georgia is not guaranteed. However, krill are omnivores and exploitation of food sources other than pelagic phytoplankton, such as zooplankton, is possible (Kawaguchi et al., 1986; Daly, 1990; Nordhausen et al., 1992), as is feeding on sea ice algae (Marshall, 1988; Daly and Macaulay, 1991), which has been observed for larval and juvenile krill, and detritus feeding (Holm-Hansen and Huntley, 1984; Kawaguchi et al., 1986; Daly, 1990; Nordhausen et al., 1992). Also, the temperature gradient that krill experience while moving across the Scotia Sea may affect metabolic processes and thus growth (Quetin et al., 1994).

The processes that allow krill to survive transport to South Georgia underlie the second research question: **How are krill growth dynamics influenced by the varying environmental conditions, especially food availability, encountered during transport, and how do krill respond to and use variable food and sea ice environments encountered during transport to enhance survival?** Related to this research question is the third research question: **Do environmental and biological factors combine to select a particular age group of krill that successfully completes transport?**

Surveys of several regions throughout the Southern Ocean have shown strong spatial and temporal variations in krill standing stock (Everson, 1983; Hampton, 1985; Priddle et al., 1988; Miller and Hampton, 1989b; Everson and Miller, 1994). Numerous studies have shown that krill abundance around South Georgia were much reduced in at least four years during the last 20 years (Priddle et al., 1988; Brierley et al., 1997), which affected many krill predators. These variations have been related to key physical-biological interactions such as variations in sea-ice extent further upstream and fluctuations of recruitment in the potential source population on the west Antarctic Peninsula (Murphy et al., 1998). Therefore, the fourth research question addressed in this study is directed at understanding the factors producing this variability: **Are observed episodic variations in krill biomass at South Georgia the result of variations in the upstream source population, variations produced during transport, variations produced by local population processes, or a combination of these factors?**

To answer these research questions, a modeling framework that couples physi-

cal and biological processes was developed to investigate the transport and survival of larval, juvenile and adult stages of Antarctic krill under different environmental conditions (Fig. 2). A primitive equations model, the Harvard Ocean Prediction System (HOPS), developed by the Ocean Dynamics Group at Harvard University (Lozano et al., 1994), is used to simulate the flow field, and temperature and salinity distributions of the Scotia Sea, which provide the environmental structure and characteristics. Drifters are released in the circulation model and are tracked over time, providing transport pathways along which time series of food concentrations can be determined. A time-dependent, size-structured, physiologically-based krill growth model (Hofmann and Lascara, 2000) is used to examine the growth dynamics of Antarctic krill from 2 mm (Calyptopis I) to 60 mm (adults) presented with the time series of food concentration. Because the model is size structured, it incorporates ontogenic changes in physiology that occur as the animal ages. For certain aspects of the research questions to be investigated, an individual-based model of krill growth is more appropriate, which is also developed. The circulation model results are combined with the krill growth model to provide simulations of krill growth and development during transport across the Scotia Sea (Fig. 2).

The goal of this research is to understand different environmental and biological factors that influence the successful transport of krill across the Scotia Sea and their survival during this transport. Ultimately, the interpretation of transport mechanisms will lead to a better understanding of the factors controlling krill distribution and production, which is needed for management of this commercially fished species.

The next chapter presents background information on the circulation pattern in the study area, krill distribution and variability, and the feeding behavior of krill. The numerical model used to model the circulation in the study area and the krill-growth model are described in Chapter 3. This chapter also provides a description of the various food time series developed for input to the growth model, details of the simulations, and a description of the data sets used for verification of the model results. Chapter 4 provides a description of the reference simulation and additional simulations undertaken to address the research questions. Seasonal and mesoscale variations observed in the simulated environmental and krill distributions are discussed in Chapter 5 and are placed within the context of observations. The final chapter provides a summary of the key findings from this study.

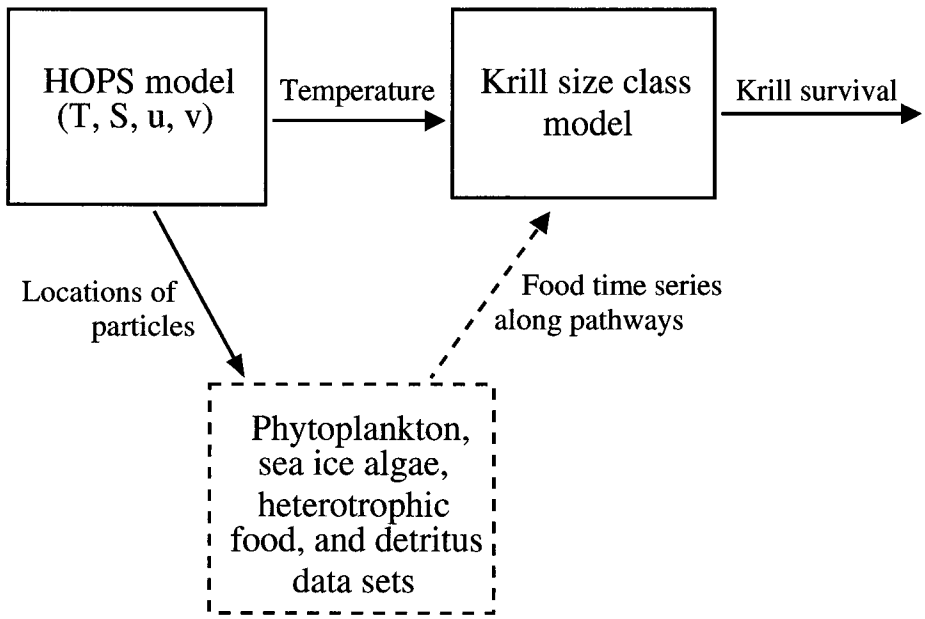

Fig. 2. Schematic of the modeling framework used to address the four research questions of interest. The solid-line boxes indicate the two models used and the dashed-line box indicates the data types used with the model. The solid arrows indicate the inputs and outputs of the models and the dashed arrow indicates the data sets input into the krill growth model.

2 BACKGROUND

This chapter provides a review of topics needed to provide context and validity for the models used in this study. In the following section, an overview of the general oceanic circulation in the region of research is given. The current knowledge of krill distribution and variability around the Antarctic Peninsula and in the Scotia Sea is next outlined, and is followed by a description of known feeding behavior of krill.

2.1 Circulation Characteristics

2.1.1 Large Scale Circulation Characteristics

The Scotia Sea is bounded by the North Scotia Ridge along the north, by the South Sandwich Arc to the east and by the South Scotia Ridge to the south (Fig. 1). It connects to the South Pacific Ocean via Drake Passage to the west. The large scale flow of the Scotia Sea consists of northeastward flow in which high speed frontal regions are embedded (Orsi et al., 1995). It is in the Scotia Sea where the ACC and the Weddell Gyre, two major circulation features in the Southern Ocean, meet.

Three deep reaching, distinctly circumpolar fronts are seen within the ACC. In the southern Drake Passage, the SACCF and the southern boundary of the ACC (Bndry) flow close to the edge of the continental shelf west of the Antarctic Peninsula (Fig. 1). The Bndry is found over the continental slope and the SACCF is located approximately 100 km north of the slope (Orsi et al., 1995). The fronts of the ACC meander and lateral frontal shifts of as much as 100 km over 10 days have been observed (Hofmann and Whitworth, 1985; Nowlin and Klinck, 1986). To the north of the SACCF, flows the Polar Front (PF) and further north the Subantarctic Front (SAF). The SACCF and the Bndry flow across the entire Scotia Sea (Fig. 1). The SACCF then leaves the Scotia Sea to flow along the eastern and northern continental slope of South Georgia after which it turns clockwise, due to interactions with bottom topography, to continue its circumpolar path (Orsi et al., 1995).

The fronts are clearly indicated by large scale horizontal property gradients (Nowlin and Clifford, 1982) and pronounced isopycnal tilt through the deep water column (Orsi et al., 1995). They separate different water mass regimes and the SAF is characterized in particular by a rapid northward sinking of the salinity minimum associated with Antarctic Intermediate Water (AAIW) from near the surface (<34.0) to depths greater than 400 m (<34.3) (Orsi et al., 1995). The PF is

characterized by a large temperature gradient along the potential temperature (θ) minimum (θ <2°C) of the Antarctic Surface Water (AASW) that starts to descend northwards, while the SACCF is indicated by a distinct temperature gradient along the potential temperature maximum (θ >1.8°C) of the Upper Circumpolar Deep Water (UCDW) as it shoals southward to 500 m (Orsi et al., 1995).

The widths of the fronts in Drake Passage have been measured (Sciremammano et al., 1980; Nowlin and Clifford, 1982) and all three fronts are associated with strong baroclinic currents (Nowlin and Clifford, 1982; Hofmann, 1985) and large geostrophic volume transport (Nowlin and Clifford, 1982; Orsi et al., 1995). The approximate width, speed and the geostrophic volume transport relative to 1000 m of the three fronts are given in Table 1.

Table 1. Characteristics of the three ACC fronts, the Subantarctic Front (SAF), the Polar Front (PF) and the Southern Antarctic Circumpolar Current Front (SACCF).

Characteristic	SAF	PF	SACCF	Source
Width (km)	44±8	60±18	37±12	Nowlin and Clifford (1982)
Transport (Sv)	27	22	14.5	Nowlin and Clifford (1982)
Speed (cm s^{-1})	43	40	30	Nowlin and Clifford (1982); Hofmann (1985)

For the setup of the circulation model discussed in Section 3, the baroclinic transport of the ACC is important. Early measurements of the baroclinic transport of the ACC flow through Drake Passage gave estimates of 110-138 x 10^6 m^3 s^{-1} [1 x 10^6 m^3 s^{-1} = 1 Sverdrup (Sv)] (Nowlin et al., 1977), 139±36 Sv (Bryden and Pillsbury, 1977), and 127±14 Sv (Fandry and Pillsbury, 1979). Subsequent measurements gave a mean net transport estimate above 2500 m of 125±10 Sv (Whitworth, 1983; Whitworth and Peterson 1985). Whitworth et al. (1982) showed that during seven crossings of Drake Passage the geostrophic transport relative to 3000 dbar averaged 103 Sv, and gave three estimates of net transport, determined by referencing shipboard data with mooring data, of 117, 144 and 134 Sv. For a detailed summary of the measurements of volume transport of the ACC through Drake Pas-

sage see Peterson (1988, Table 1) and Orsi et al. (1995, Table 2). In addition, Orsi et al. (1995) calculated the total baroclinic transport to be 100 Sv relative to 3000 m. Other baroclinic transport values of importance for the setup of the circulation model are the transport of the Weddell Sea Gyre and the Brazil Current, which have been calculated to be approximately 29.5 Sv (Fahrbach et al., 1994), and 9.6-10.2 Sv (Stramma, 1989), respectively.

East of the Antarctic Peninsula, where the ACC and the Weddell Gyre meet, cold water (<0°C) originating on the western continental shelf and slope of the Weddell Sea is injected into the Scotia Sea and follows the flow eastward (Whitworth et al., 1994). Weddell Sea water is also transported westward at the tip of the Antarctic Peninsula. There the circulation is characterized by dense, cold (<0°C), fresh (<34.6) and oxygenated (>6 ml l^{-1}) water flowing westward over the outer shelf down to depths of 800 m (Nowlin and Zenk, 1988), which is thought to be part of the Antarctic Slope Current (Nowlin and Zenk, 1988; Jacobs, 1991). North of the South Shetland Islands (Fig. 1) the Antarctic Slope Current carries water of Weddell Sea origin to the west (Nowlin and Zenk, 1988; Capella et al., 1990).

2.1.2 Mesoscale Circulation Characteristics

Recent studies have shown mesoscale variability associated with the flow on the continental shelf west of the Antarctic Peninsula (Stein, 1992), in Bransfield Strait (Niiler et al., 1991) and in Drake Passage (Joyce and Patterson, 1977; Peterson et al., 1982; Bryden, 1983; Hofmann and Whitworth, 1985; Klinck, 1985; Gille and Kelly, 1996; Moore et al., 1999). Such changes may have an influence on krill transport. The frontal structure of the ACC causes the relative vorticity between bands of flow with different velocity to give rise to numerous eddies (Joyce and Patterson, 1977; Peterson et al., 1982; Bryden, 1983). The current cores migrate laterally (Nowlin et al., 1977; Hofmann and Whitworth, 1985; Klinck, 1985) and can meander as much as 100 km with time scales of 10 days. These meanders can develop into closed current rings, which were first reported by Joyce and Patterson (1977). Since this first report of current rings, observations of warm and cold core rings have been numerous (Gordon et al., 1977; Joyce et al., 1981; Peterson et al., 1982; Pillsbury and Bottero, 1984; Hofmann and Whitworth, 1985).

Satellite altimeter measurements provide additional evidence of mesoscale variability in the flow of the ACC and show increased levels of eddy variability along the

axis of the ACC (Shum et al., 1990; Chelton et al., 1990; Gille, 1994), particularly in the Scotia Sea (Fu and Chelton, 1984, 1985). Cheney et al. (1983) showed that mesoscale variability associated with the ACC is nearly continuous around Antarctica and that the largest variability is associated with regions of major topographic features, such as are found in the Scotia Sea (Fig. 1). Strong topographic influence on the flow of the ACC and the PF has been described in many other studies involving the analysis of hydrographic data from ship surveys (Gordon et al. 1978; Lutjeharms and Baker, 1980; Orsi et al., 1995), moorings (Inoue, 1985), drifting buoys (Hofmann, 1985; Patterson, 1985), and satellite altimeters (Chelton et al., 1990; Gille, 1994, Moore et al., 1999).

In the Scotia Sea to the south of South Georgia, the flow shifts sharply northward because of interacting with the South Sandwich Arc (Orsi et al., 1995). The relatively clear frontal structure from the Drake Passage region may be affected by the bathymetry in the South Georgia region, as currents pass through the North Scotia Ridge (Mackintosh, 1946; Deacon, 1982). In addition, a series of eddy-like structures have been observed near South Georgia, that seem to be linked to water from the Weddell Sea and the ACC meeting east of the Antarctic Peninsula (Foster and Middleton, 1984). The energy of these eddies increases downstream of the South Orkney Islands (Fig. 1) as the region over which the eddies occur expands (Foster and Middleton, 1984). These eddies are found in the waters to the east and west of South Georgia (Foster and Middleton, 1984).

Bryden (1983) summarized the characteristics of eddy variability in the Southern Ocean and showed that eddy variability has been found everywhere measurements were made. The spatial scales of mesoscale eddies vary from 30 km to 100 km and their surface velocities are typically 30 cm s^{-1} or greater, and the eddies are vertically coherent from surface to bottom. Bryden and Heath (1985) reported eddies from the southwestern Pacific Ocean north of the SAF, that varied over horizontal scales of 60 km and temporal scales of 20 days, and moved southeastward at ca. 12 cm s^{-1}.

Mesoscale eddies are known to retain and concentrate planktonic organisms (Angel and Fasham, 1983; Heywood and Priddle, 1987; Perissinotto and Duncombe Rae, 1990; Niiler et al., 1991), an important food source for krill. Therefore, mesoscale eddies could play a major role in the transport and retention of krill and their food supply.

2.2 Krill Life History, Distribution and Variability

2.2.1 Krill Life History

Antarctic krill are believed to have a life span of 6 years (Siegel, 1987) and so the life history is divided into 6 age groups (0 to 5+) that correspond to different length krill (Fig. 3). The growth curve illustrated in Fig. 3 is the seasonal von Bertalanffy growth curve derived by Siegel (1987), which uses a simple sinusoidal change in the seasonal growth rate to reproduce change of krill length as

$$L_t = L_\infty[1 - e^{(-k(t-t_0)+\frac{ck\sin[2\pi(t-t_s)]}{2\pi})}], \quad (1)$$

where L_t is krill length (mm) at time t, expressed in days, and L_∞ is the maximum size of krill (mm). Values of the equation constants are: L_∞ = 61 mm, k = 0.4728 d^{-1}, t_0 = 0.1418 d, c = 0.9598, and t_s = -0.0272 d. Time is then transformed into the age of krill in years. This type of growth curve assumes that krill grow constantly throughout their lives at various rates.

After spawning the embryonal and early larval stages of krill undergo a descent-ascent cycle in which embryos sink rapidly through the water column to depths of 200 m to 500 m and after hatching, larvae ascend to the surface where they begin feeding (Marr, 1962; Hempel and Hempel, 1986; Hofmann et al., 1992). While ascending, the larvae develop through two non-feeding (Nauplius, Metanauplius) and several feeding (Calyptopis 1-3) developmental stages. Larvae develop through 3 Calyptopis stages and 6 Furcilia stages before reaching the juvenile stage at about 15 mm during their first winter (Fig. 3). The size range corresponding to the juvenile stage is 14-36 mm (Siegel, 1987). Krill then develop into subadult (26-45 mm) and adult stages (35-60 mm) in the second and third years of their life (Siegel, 1987). From age group 3+ onwards, all krill are sexually mature adult stages (Fig. 3). This can result in three or more spawns in this part of their life history (Siegel, 1987). Denys et al. (1981) showed that adult krill can molt into an earlier subadult stage after spawning. In addition, krill have been observed to shrink by molting if starved (Ikeda and Dixon, 1982; Nicol et al., 1992), which is not incorporated in the krill growth model given by equation (1). Thus, a given age group of krill can include krill that may have shrunk to that size, thereby overlapping separate age groups. As a result, krill age cannot be predicted solely from length.

The measurement of temporal increases in quantities of fluorescent age-pigments,

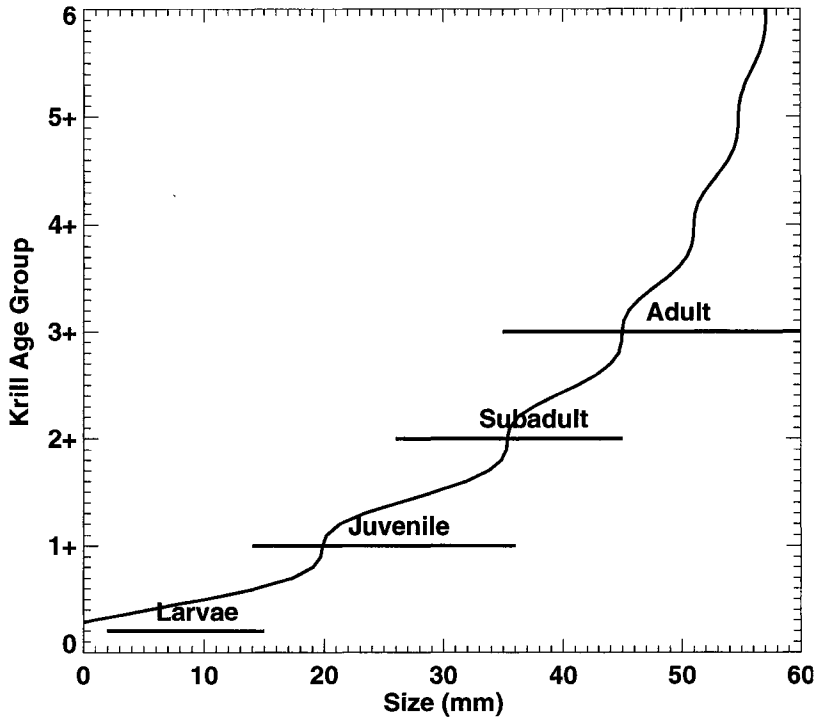

Fig. 3. Relationship between size and age of krill obtained from a modified von Bertalanffy growth model (equation 1) fitted to seasonally oscillating length-at-age krill data given by Siegel (1987). Horizontal lines denote the range of sizes associated with different krill ages for krill from the western Antarctic Peninsula and the Weddell Sea (Siegel, 1987). Age group 3+ and older are considered adults.

such as lipofuscin, has been suggested as a method which obviates the problems associated with size-related measures of age (Ettershank, 1983; 1984; 1985; Nicol et al., 1991). Lipofuscin accumulates as a function of metabolic rate, not the passage of clock time (Ettershank, 1983), and Ettershank (1984) showed that it can be used to discriminate three age classes of mature female krill from a single haul whose bodily dimensions largely overlapped.

In addition, it has been suggested that the relationship between the number of crystalline cones in the krill eye or the diameter of the krill eye and the body length may indicate whether krill experienced shrinkage (Sun et al.; 1995, Sun, 1997). This was confirmed by Shin and Nicol (2002), who demonstrated that fed and starved krill are distinguishable by the relationship between the eye diameter and body length. Krill eye diameter does not decrease in starving animals even when they shrink in

size, while it continues to increase for well-fed krill. This provides an approach for distinguishing starved and well-fed krill. However, any imprints caused by starving in winter will be blurred by summer as the starved krill start active growth (Shin and Nicol, 2002).

2.2.2 Krill Distribution

The first large-scale descriptions of krill distributions were based on net samples obtained during the *Discovery* cruises (Marr, 1962), which show that krill inhabit the broad, circumpolar region between the Antarctic continent and the Antarctic PF (Fig. 4). However, most krill aggregations are confined to areas affected by the seasonal change of annual pack ice (Marr, 1962; Mackintosh, 1972) such as the Antarctic Peninsula region (Comiso et al. 1993).

Krill Biomass

During the Biological Investigations of Marine Antarctic Systems and Stocks (BIOMASS) program, the mesoscale distribution of krill around the Antarctic Peninsula was examined using hydro-acoustic techniques, which showed that this region contains high concentrations of krill (Everson and Miller, 1994). Within the western Antarctic Peninsula region, especially large (up to 15.49 g m^{-2} in summer 1985/86 or even 165.7 g m^{-2}) concentrations of krill have been observed in the Bransfield Strait-South Shetland Island area (e.g. Kalinowski et al., 1985; Siegel, 1988).

Biomass estimates for krill in the Bransfield Strait, Elephant Island and Drake Passage from net samples and from hydro-acoustic data prior to 1987 are summarized by Godlewska and Rakusa-Suszczewski (1988, Table 1). They include estimates from BIOMASS cruises showing mean density values from 0.075 to 44.607 g m^{-2}. Comparison between these data sets is difficult because different methods (hydro-acoustic and net sampling) were used and different subareas were analyzed (Siegel, 1992).

In addition, other studies also found that high krill population densities, with a mean summer biomass ranging from 6.1 g m^{-2} (1987/88) to less than 4.5 g m^{-2} (1989/90) (Siegel, 1992) exist in the Antarctic Peninsula region. A more recent net sampling study of krill distribution around Elephant Island (cf. Fig. 1) measured a mean krill density of 13.3 g m^{-2} (Siegel et al., 2002).

Hydro-acoustic observations of krill density during the Palmer Long-Term Ecological Research (LTER) program at the western Antarctic Peninsula showed that

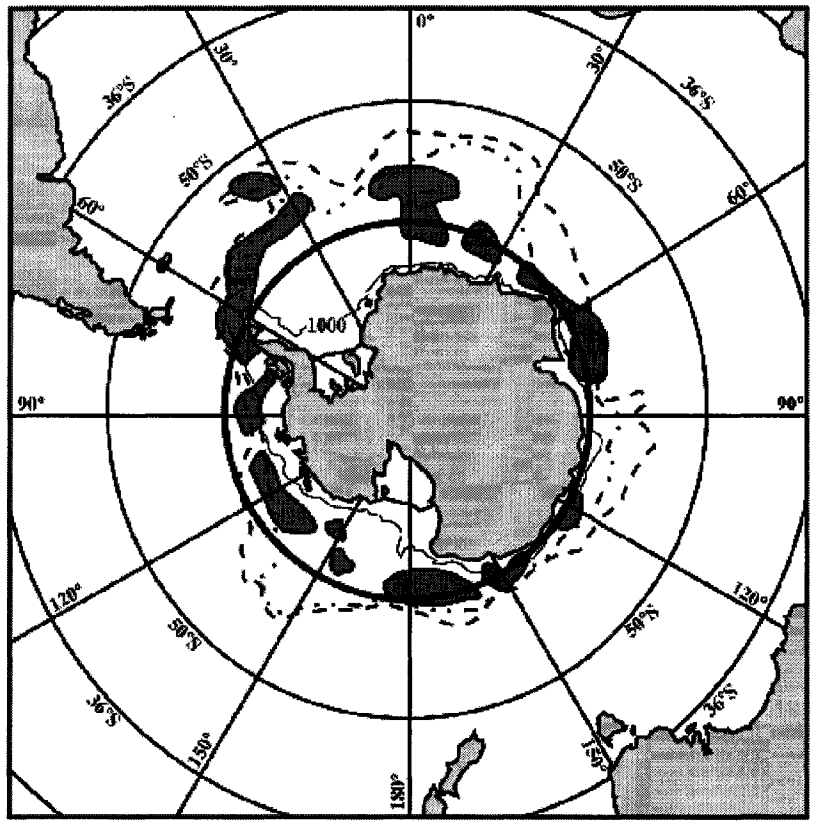

Fig. 4. Circum-Antarctic map showing the distribution of regions of highest krill concentration as developed by Lubimova et al. (1982), and the climatological locations of the Southern Antarctic Circumpolar Current Front (dashed line) and the southern boundary of the Antarctic Circumpolar Current (dash-dotted line) as given by Orsi et al. (1995).

summer biomass was associated with aggregations of high mean biomass (>150 g m^{-2}) (Lascara et al., 1999).

Developmental Migration and Passive Transport

Analyses of krill spatial distributions suggest that developmental migration from the inshore regions of Bransfield Strait to the outer shelf break regions of the South Shetland Islands occurs (Siegel, 1988; Brinton, 1991). Siegel (1992) used results from a net sampling survey to show such a migration from inshore to the outer shelf regions and back for the continental shelf west of the Antarctic Peninsula. Gravid females were mostly found on the outer shelf, while spent females tended to be found in inshore regions, a pattern confirmed by later studies (Lascara et al., 1999; Siegel,

2002). This suggested that spawning occurs in the outer shelf regions west of the Antarctic Peninsula. Consequently, surface currents, like those associated with the ACC, that flow and meander close to the edge of the continental shelf in this area, can potentially entrain larval krill spawned at the shelf edge. Once entrained in high speed surface currents, krill can be transported downstream.

A similar transport mechanism has been suggested for krill in the King George Island region (South Shetland Islands, cf. Fig. 1). Passively drifting krill patches could potentially pass through an area the size of Bransfield Strait in one to two weeks (Everson and Murphy, 1987). In addition, the suggestion that krill larvae found across the Scotia Sea are not produced locally, but are advected into the region by currents is supported by different developmental stages collected in the Scotia Sea north of the South Orkney Islands and east of Elephant Island (Brinton and Townsend, 1984).

2.2.3 Variability

Strong spatial and temporal variations in krill standing stock have been detected in surveys of several regions throughout the Southern Ocean (Everson, 1983; Hampton, 1985; Priddle et al., 1988; Miller and Hampton, 1989b; Everson and Miller, 1994). An extensive hydro-acoustic mapping of the seasonal and regional variability in krill stocks west of the Antarctic Peninsula show a seasonal reduction of krill stock, with a winter minimum, and across-shelf differences in length-frequency distribution, with small adults (<40 mm) generally located in inshore regions (Lascara et al., 1999). Summer biomass was associated with aggregations of small cross-sectional area (<2000 m^2) and high mean biomass (>150 g m^{-2}) in the upper 50 m of the water column, while winter observations were characterized mostly by large cross-sectional area (>10000 m^2) and low mean biomass (<10 g m^{-2}) below 100 m depth. Moreover, a correlation between Circumpolar Deep Water (CDW) and the spatial aggregation of reproducing krill was found (Lascara et al., 1999). This is in agreement with Siegel (1992), who showed that the mean biomass in a winter survey was 0.55 g m^{-2}, only 2.8% of the maximum observed summer stock. Seasonal variation thereby exceeded a factor of 35, while the krill summer stock varied only a factor of 1.6 interannually. The krill biomass data summarized by Godlewska and Rakusa-Suszczewski (1988, Table 1) changed by a factor of at least 21 from summer to winter (Siegel, 1992) and maximum interannual differences fluctuated by a factor of 8.9 (Siegel, 1992).

Interannual variability of krill around South Georgia is a well recognized phenomenon and was first documented in the period of commercial whaling when year-to-year fluctuations in the abundance of whales close to the island were evident from catch statistics (Harmer, 1931; Kemp and Bennet, 1932). During the *Discovery* Investigations, interannual differences in sizes of scientific catches of krill were correlated to sea surface temperatures (Mackintosh, 1972), with substantially greater krill catches in colder years. Later analysis of historical data sets suggested that the variability within the South Georgia ecosystem may be the manifestation of periodic variations across the Scotia Sea and indeed the whole Southern Ocean (Priddle et al., 1988; Sahrhage, 1988; Murphy et al., 1995; Fedoulov et al., 1996; Whitehouse et al., 1996). During the last 20 years, krill abundance around South Georgia was much reduced in at least four years (Priddle et al., 1988; Brierley et al., 1997), which affected many krill predators. A closer look at the variability of krill at South Georgia was taken by Brierley et al. (1999), who showed through hydro-acoustic estimates of krill density, that the magnitude of krill densities and between-year gradients of density between Elephant Island (cf. Fig. 1) and South Georgia mirrored each other for seven austral summers. They concluded that krill densities at both locations are linked, and subject to the same gross physical and biological factors acting over the same temporal and spatial scales. These factors included key physical-biological interactions like variations in sea-ice extent further upstream and fluctuations of recruitment in the potential source population on the west Antarctic Peninsula (Murphy et al., 1998).

2.3 Food Sources and Feeding Behavior of Krill

During austral spring and summer, Antarctic krill have been observed to feed on many different sizes and types of phytoplankton, as shown by feeding studies (Quetin and Ross, 1985; Schnack, 1985) and growth rate studies (Holm-Hansen and Huntley, 1984). Phytoplankton biomass is extremely low (less than 0.1 mg m^{-3}) in the months March to October (austral winter), which has led to a variety of hypotheses that try to explain how krill survive this season. The exploitation of a food source other than pelagic phytoplankton as a winter food source seems to be a strategy for overwinter survival of krill (Kawaguchi et al., 1986; Daly, 1990; Nordhausen et al., 1992), since krill do not seem to have substantial reserve lipids (Clarke, 1984).

Phytoplankton concentrated in surface waters as well as phytoplankton concen-

trations at depths can provide a food source for krill. Krill are known to migrate vertically (Marr, 1962; Nast, 1979; Kalinowski and Witek, 1980; Everson and Ward, 1980; Godlewska, 1996) and are therefore able to use phytoplankton present at greater depths within and just beneath the photic zone.

Subsurface phytoplankton concentrations cannot be detected in Coastal Zone Color Scanner (CZCS) satellite images because satellites represent depth-weighted averages of pigments in near-surface waters, i.e., they are limited by the optical attenuation depth (Smith, 1981). Chlorophyll *a* has been detected at depth in higher concentrations during summer/fall than in winter/spring (El-Sayed and Weber, 1982), and below the photic zone in various parts of the Southern Ocean during summer (Smith and Nelson, 1986; Bianchi et al., 1992; Tréguer and Jacques, 1992; W. O. Smith et al., 1996; Smith et al., 1996). Smith et al. (1996) used historical chlorophyll data obtained since the 1960s and found that during the growing season (November to March) mean chlorophyll *a* concentrations west of the Antarctic Peninsula, down to a depth of 100 m, are relatively high (>1.0 mg m^{-3}) with levels of chlorophyll *a* increasing below 50 m. This shows that deep chlorophyll *a* maxima do occur in this region, which provide a potential food source for krill. During other studies, like the European *Polarstern* Study (EPOS), increased chlorophyll *a* concentrations at depth in the Elephant Island and South Orkney Island region were found during the months of October and November of 1988 (Bianchi et al., 1992; Tréguer and Jacques, 1992). Phytoplankton blooms that extend to 100 m are also often associated with ice edge blooms (Smith and Nelson, 1986) which may extend to about 250 km from the ice edge (Smith and Nelson, 1985).

Krill have been observed feeding on sea ice algae underneath fast ice (Marschall, 1988; Daly and Macaulay, 1991). However, it appears that mostly larvae and juveniles use this food source. In addition, this habitat seems to provide young krill with protection from predators, because small animals are able to retreat into holes and crevices (Daly, 1990). Not all sea ice is necessarily associated with sea ice algae though, and during times of low light during winter, krill may need an alternative food source.

An alternative food source has been suggested by Nordhausen et al. (1992), who observed various copepod species in the stomachs and guts of Antarctic krill, and were able to show in laboratory experiments that krill actively feed on copepods. Additional studies (e.g. Hopkins et al., 1993; Pakhomov et al., 1997) show that

Antarctic krill can feed on zooplankton outside of phytoplankton bloom periods.

Kawaguchi et al. (1986) observed that krill in the Lützow-Holm Bay, near the Japanese Antarctic Station Syowa (69°S, 39°E), were found underneath fast ice close to the sea floor (38-40 m) feeding mainly on detritus. Also Holm-Hansen and Huntley (1984) suggest that detritus may be an important food source for krill, since little is known about the ability of krill to distinguish between living and non-living organic carbon particles. Daly (1990) found evidence in gut contents of krill larvae caught in the marginal ice zone of the Scotia and Weddell Seas during austral winter, that larvae ingested detrital material in addition to phytoplankton and heterotrophic organisms. Calculations of metabolic demands showed that sea ice algae and phytoplankton alone are not enough to sustain krill and that detritus and heterotrophic organisms seem to be additional food sources (Daly, 1990).

Actual shrinking in size due to starvation has also been suggested as mechanism by which krill survive low food concentrations during winter (Ikeda and Dixon, 1982; Nicol et al., 1992). This may be an additional survival strategy for krill, although the studies discussed above suggest that krill have omnivorous feeding behavior.

2.4 Modeling Studies

2.4.1 Krill Models

Mathematical models provide one approach for exploring the downstream transport of krill by currents, and the effect of physical and biological factors on transport patterns and residence times. To date, only a small number of numerical models have been developed for krill. Astheimer et al. (1985) and Astheimer (1986) developed a phenomenological model of individual krill growth, which did not explicitly include metabolic processes and the calculation of net production, and therefore cannot be applied to a wide range of environments. Hofmann et al. (1992) developed a model for the embryos and early larval stages of Antarctic krill that was embedded in a limited-area circulation model to investigate transport and pathways of early life stages of krill (Capella et al., 1992). These models only consider the early life stages and do not include feeding, and as a result are not applicable to the older stages of krill. In addition, krill population dynamics have been modeled by Murphy and Reid (2001) who combined a krill population size model with a size-based selection function to generate length-frequency distributions observed in predator diets at

South Georgia in summer.

A time-dependent, size-structured, physiological krill growth model was developed by Hofmann and Lascara (2000) to examine the growth dynamics of krill from Calyptopis I to adult stages (2-60 mm). They found that the model produces spring and summer growth rates for different size classes that are consistent with observations when krill is feeding on phytoplankton. However, the simulated annual growth cycle, especially for larval and subadult krill, best matches observations when winter respiration rates are reduced and an additional winter food source (sea ice algae) is available. Later modeling studies used an improved version of the above krill growth model to assess the food sources needed to sustain Antarctic krill during transport across the Scotia Sea to South Georgia (Fach et al., 2002), using initial drifter paths from a Lagrangian model presented in Hofmann et al. (1998). Their simulation results show that phytoplankton concentrations across the Scotia Sea are not sufficient to support krill during transport, and that the inclusion of sea ice algae as winter food does significantly not alter this result. Given these results, the importance of other food sources such as heterotrophic food becomes apparent, as well as a possible survival strategy for krill that invalues overwintering under sea ice, resulting in a longer, interrupted transport (Fach et al., 2002).

2.4.2 Circulation Models

An early attempt at running an eddy-resolving model of the Southern Ocean, between 24°S and 79°S, was the Fine Resolution Antarctic Model, FRAM (FRAM Group, 1991; Webb et al., 1991), which is a primitive equation numerical model based on the model of Semtner (1974) and Cox (1984). FRAM is configured with a horizontal grid spacing of 0.5° in the east-west and 0.25° in the north-south direction, using 32 vertical layers. However, representation of the circulation through Drake passage obtained by FRAM differed from observations, because it showed two fronts instead of three (Gross et al., 1995), and the SACCF formed from a bifurcation of the PF as it entered Drake Passage (Gross et al., 1995).

There are numerous modeling studies of Southern Ocean dynamics, however none of them have focused on the connection between the Antarctic Peninsula and the eastern Scotia Sea. Barnier et al. (1998) modified the Semi-spectral Primitive Equation Model (SPEM) from Rutgers University (Haidvogel et al., 1991) to study the circulation of the South Atlantic. The model domain extended from 16°S to the

Antarctic continent and longitudinally from 68°W to 20°E. The resolution of the model was 1.375° in longitude and 1.375 x cos(latitude) in latitude, which does not resolve mesoscale eddies (Barnier et al., 1998). Drake Passage was located on one of the open boundaries and was parameterized to allow inflow of 130 Sv into the South Atlantic. No fronts appear in the simulation results. Similar results were obtained in a companion study using the same model (Marchesiello et al., 1998). The simulated circulation patterns showed good agreement with known climatological circulation features in the South Atlantic, especially in the confluence region between the Brazil Current and the Malvinas Current. Sensitivity studies show the detailed features of the circulation to be influenced by the bottom topography.

Another study focusing on the circulation dynamics of the South Atlantic Ocean used the Ocean Parallel model discussed in detail by Penduff et al. (2001). This model is based on the primitive equations Ocean Parallel model version 8.1 (Madec et al., 1998) and uses the same configuration as the 1/3° Atlantic model developed for the CLIPPER (high resolution modeling of the Atlantic) project (Tréguier et al., 1999). In contrast to the circulation study of Barnier et al. (1998) described above, this model allows a larger part of the ACC to flow into the Scotia Sea. The simulated circulation shows a smaller Malvinas Current, but tends to distort the complex dynamics of the confluence region of this current with the Brazil Current.

Beckmann et al. (1999) developed the Bremerhaven Regional Ice Ocean Simulations (BRIOS) model, to investigate the large scale circulation and water mass distribution in the Weddell Sea. Ice-ocean dynamics were subsequently added to BRIOS (Timmermann et al., 2002a; 2002b). The original, circumpolar model which was forced with climatological data from a sea ice-mixed layer model, included shallow shelf areas as well as the major sub-ice shelf areas. The simulated circulation fields obtained with BRIOS showed a pronounced and persistent double-cell structure of the Weddell Gyre with a maximum transport of 60 Sv. Beckmann et al. (1999) show that the water masses from sub-ice shelf cavities contribute significantly to the water mass formation along the continental slope, and affect water mass characteristics throughout the Weddell Sea by increasing the stability of near-surface stratification, preventing deep ocean convection. With the coupling of BRIOS to a sea ice model, BRIOS-2 was created and forced with 6-hourly wind data of the European Centre for Medium-Range Weather Forecasts (ECMWF) reanalysis. Circulation simulations with this model underestimate summer sea ice coverage, but

winter sea ice extent, thickness and drift are well reproduced (Timmermann et al., 2002a). Simulations of ice-ocean dynamics revealed a strong correlation between atmospheric forcing and sea ice formation (Timmermann et al., 2002b) and show that interannual atmospheric variability propagates into the deep ocean and the sub-ice shelf cavities.

Matano et al. (2002) used the Modular Ocean Model (MOM) to study the northwestern Weddell Sea and its interaction with the Scotia Sea, focusing on circulation pathways, associated stratification, and volume transports. They find that the main route for inter-basin exchange of Weddell Sea Deep Water is into the Scotia Sea through the South Scotia Ridge and the Bransfield Strait, while no advective transport along the eastern side of the South Sandwich Arc was found. Analysis of Lagrangian drifters indicated that fluxes in this region are more likely to be related to eddy-driven mixing than to mean flow advection. A south-flowing jet formed in the simulated circulation fields at the outer shelf off the Antarctic Peninsula.

Apart from regional models there are many global models available, some of which are mentioned here briefly. These models will not be discussed in detail, since their resolution is too coarse to address the research questions of interest to this study. From the FRAM effort discussed above, the Ocean Circulation and Climate Advanced Modeling Project (OCCAM) was developed and two high resolution (1/4° and 1/8°) models of the World Ocean, including the Arctic Ocean and marginal seas such as the Mediterranean, are available (Webb et al., 1998). The Max-Planck-Institut für Meteorologie, in Hamburg, Germany is running the Hamburg Ocean Primitive Equation Model (HOPE), a global general circulation model of the ocean based on the primitive equations (Wolff et al., 1997). Other global models include Estimating the Circulation and Climate of the Ocean (ECCO) (Stammer et al., 1999), the Naval Research Laboratory Ocean Prediction System (Wallcraft, 1991), the Hybrid Coordinate Ocean Model (HYCOM) (Bleck, 2002), and the Parallel Ocean Program (POP) developed at the Naval Postgraduate School and Los Alamos National Laboratory (Smith et al., 1992).

3 METHODS

Described below are the two models which are used to investigate and quantify the relative importance of physical and biological processes determining krill survival and transport across the Scotia Sea to South Georgia. Following this, four potential food sources for krill and their implementation in the simulations of krill growth and development are discussed. The last section describes observational programs that provide data sets adequate for validating results from the circulation and krill growth models.

3.1 Circulation Model

The proposed research requires a realistic representation of the circulation along the Antarctic Peninsula, in the Scotia Sea, and around South Georgia. In particular, the ACC with its frontal structure, needs to be resolved properly, since this is the largest current in this region and is thought to be the primary krill transport mechanism. The circulation model also needs to be able to resolve mesoscale variability such as eddies, because of the possible importance of these features in retaining krill and providing food sources for extended periods. The circulation model also needs the capability of tracking drifters over time and space to investigate transport mechanisms of krill. From the discussion in the previous section, it is apparent that such a circulation model is currently not available for the study region.

The circulation model that is used in this study is the Harvard Ocean Prediction System (HOPS) Primitive Equation Model for coastal and deep water, which is applicable to any oceanic region that may have an arbitrary coastline and open boundary segments (Lozano et al., 1994). A primitive equation (PE) model was chosen, because quasi-geostrophic models do not allow inclusion of the steep bottom topography that is present in the study region. Also, the flow in quasigeostrophic models is assumed to be geostrophic with small departures dependent only on planetary vorticity (Rossby waves), which limits the ability to resolve rapid changes in the flow associated with fronts.

3.1.1 Model Physics

The PE model is based on the Navier-Stokes equations in a rotating coordinate system, assuming the hydrostatic and the Boussinesq approximations (Spall, 1988;

Spall and Robinson, 1989). As described in Lozano et al. (1994), further assumptions include geopotentials lying on concentric spheres, a constant gravitational field throughout the domain, and a rigid surface. The basic structure of the model is based on an early version of the Modular Ocean Model (MOM) (Bryan, 1969; Cox, 1984) and uses a double sigma stretched vertical coordinate system based on a piecewise linear sigma coordinate system (Simmons and Burridge, 1981). Only the vertical component of the Earth's rotation vector is retained, solid boundaries are rigid and impermeable, and heat and salt fluxes normal to those boundaries are zero. The basic state variables for the HOPS model are temperature, salinity and velocity. The model is solved numerically using a B-grid in space, and steps in time using leap-frog with lagged friction, as described in Bryan (1969). The primitive equations under all those above assumptions are written as can be found in Pedlosky (1987).

The mass conservation equation (incompressibility condition) is

$$\frac{\partial u}{\partial x} + \frac{\partial v}{\partial y} + \frac{\partial w}{\partial z} = 0, \tag{2}$$

where u and v are the horizontal velocities, and w is the vertical velocity. The momentum equation is written as

$$\frac{D\vec{u}}{Dt} + f\vec{e}_z \times \vec{u} = -\nabla p + Div\ \tau + \vec{F}_m, \tag{3}$$

where $\frac{D\vec{u}}{Dt}$ is the change of the horizontal velocity vector $\vec{u}$ over time, f is the Coriolis parameter, and $\vec{e}_z$ is a unit vector in the vertical direction. The horizontal pressure gradient is given by ∇p, Div is the three dimensional divergence operator, and τ is the shear stress. The final term, $\vec{F}_m$, is a parameterization for additional subgrid scale physics such as shear instability, bottom stress, horizontal lateral diffusivity and mixing, and internal waves.

The hydrostatic equation is

$$\frac{\partial p}{\partial z} = -g\rho, \tag{4}$$

with g being the gravitational acceleration, and ρ being the water density. The conservation equations for temperature (T) and salt (S) are of the form

$$\frac{DT}{Dt} = Div\ \vec{q}_T + F_T, \tag{5}$$

$$\frac{DS}{Dt} = Div\ \vec{q}_S + F_S, \tag{6}$$

where $\vec{q}_T$ and $\vec{q}_S$ are the heat and salinity flux vectors. The subgrid scale parameterizations involving salt and temperature are given by F_T and F_S, respectively. The equation of state for seawater is written as

$$\rho = \rho(T, S, p). \tag{7}$$

This particular circulation model was chosen because it has useful features, such as terrain-following coordinates which allow a smooth transition from the coast to deep sea in areas where the topography is steeply sloping. In the vertical dimension, the model structure consists of flat upper layers, in order to support higher accuracy in the upper ocean and the main thermocline (Lozano et al., 1994). This is necessary because the study region includes shallow, coastal areas with depths of 100s of meters, and the open ocean with depths of up to 7000 m near South Georgia. For krill advection, the upper 500 m are important and therefore need to be represented accurately. However, bottom topography has a large impact on the speed and the path of the ACC in the region of interest (Gordon et al., 1978; Klinck, 1985) and influences the locations of the circumpolar fronts (Orsi et al., 1993; 1995), which makes it necessary to include the whole water column in the model. Frontal eddies found in the Drake Passage region are usually found to be 30-40 km in horizontal scale (Joyce and Patterson, 1977) and need an average time of 14 days to move through a region (Bryden and Pillsbury, 1977). Depending on the grid spacing chosen for the model, HOPS is eddy admitting, but only small grid spacing (i.e. 10 km and less) allows the resolution of mesoscale eddies.

3.1.2 Model Structure

The model domain includes the Antarctic and Subantarctic regions of the South Atlantic and South Pacific Oceans between the longitudes 85°W and 25°W and the latitudes 43°S and 73°S and is rotated counterclockwise by 22° from the horizontal plane (Fig. 5). The rotation of the model domain enables the ACC to enter Drake Passage in the east and exit into the South Atlantic without encountering model boundaries.

A uniform 10-km grid with 311 grid points of longitude by 221 grid points of latitude is used to represent the model domain. The choice of the appropriate grid spacing is influenced by the need for high resolution of the flow while maintaining realistic simulation times. Therefore, this grid spacing is chosen in order to resolve

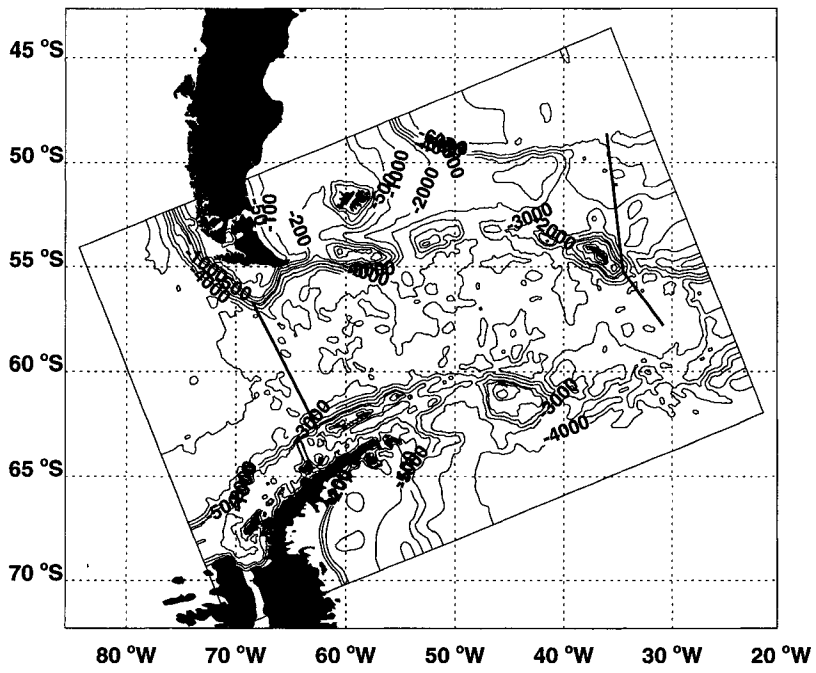

Fig. 5. Study area with the model domain indicated as a rotated rectangular. Contours are bottom topography in meters. Heavy lines indicate the locations of the Melville II (across Drake Passage) and WOCE A23 (near South Georgia) hydrography sections used to validate circulation model results.

mesoscale eddies. In the vertical direction 21 layers are defined, with flat upper layers in order to support higher accuracy in the upper ocean. Since the model uses terrain-following coordinates, the layers increase in thickness with depth so that depths of 4000 m can be resolved. A summary of the model setup is given in Table 2.

Bottom Topography

Correct representation and input of the bottom topography is crucial to the successful implementation of the HOPS model because the discrete form of the pressure gradient terms may produce large systematic errors over steep topography (Messinger, 1982), such as is present in the study area. Such errors may be reduced by systematic smoothing of the bathymetry. The digital earth topography database of land and sea floor elevations ETOPO5 (NOAA, 1988) is used to specify the bottom topography and is smoothed according to the hydrostatic consistency criterion, which involves the bottom slope and the horizontal and vertical resolution of the grid to reduce pressure gradient errors and to avoid hydrostatic inconsistency (Messinger, 1982; Haney, 1991). For this implementation of HOPS, this criterion means that

Table 2. Configuration of the HOPS model, values of parameters, and forcing functions used in the simulations. Abbreviations are used as follows: temperature (T), salinity (S), National Centers for Environmental Prediction (NCEP), Sverdrup (Sv).

Model parameters	Values
Horizontal resolution	10 x 10 km, grid rotated counterclockwise by 22°
	311 x 211 grid points (Longitude x Latitude)
Vertical resolution	21 levels (finer at surface, coarser at bottom)
Time step	36 minutes
Initialization	Antonov et al. (1998) and Boyer et al. (1998)
	climatological T and S fields with feature model
	of frontal jets
Continental boundaries	represented by landmask with three islands
	(Falkland Islands, South Georgia,
	South Shetland Islands)
Ocean bathymetry	ETOPO5 data, with 2 slightly enhanced features,
	smoothed to respect pressure gradient error
	criterion
Eddy viscosity coefficient	background = 5 $cm^2\ s^{-1}$
	wind-mixed surface layer = 10^3 $cm^2\ s^{-1}$
Bottom drag coefficient	$C_D = 2.5 \text{ x } 10^{-3}$
Shapiro Filter	fourth order for momentum, tracers and transport
	second order filter for vorticity
Ekman factor	$ekfac = 0.7$
Dynamical surface forcing	monthly wind stress from NCEP reanalysis
Baroclinic transport	Drake Passage: 140 Sv
	Weddell Gyre: 30 Sv
	Brazil Current: 5 Sv
Model spin up time	2 months

the continental slope off the Antarctic Peninsula, South America, and around South Georgia is approximately 10% gentler in the simulations than in reality. The position of the shelf break is similar to the actual shelf break, but the slope extends at the most one grid point (10 km) further into the deep ocean. In addition, two channels east of Burdwood Bank (south of the Falkland Islands) in the North Scotia Ridge near 54.5°S, 54°W and 53°S, 48.5°W (Fig. 5) are deepened by approximately 150 m and widened by one grid point (10 km) to connect the deep waters south of the North Scotia Ridge with the Malvinas Chasm (cf. Fig. 1). This is necessary due to the flow constraints resulting from these topographic features, which reduce flow through these channels and result in high flow speeds near the features, thereby making the flow unstable. At 64°W a ridge across the western Antarctic shelf near Anvers Island (cf. Fig. 1) is raised to a depth of 100 m to better simulate the flow dynamics in the Bransfield Strait. Overall the bottom topography is defined to be as close as possible to the real conditions and includes all topographic features in this region (Fig. 5).

Boundary Conditions

The land masses, including three major islands, the Falkland Islands, South Georgia and the South Shetland Islands, are defined as closed boundaries in the model domain, which are rigid and impermeable. The baroclinic transport of the flow is imposed on all open boundaries by the choice of the streamfunction at the boundary, including the transport of the ACC, the Brazil Current, and the Weddell Gyre. The transport of the ACC in the Drake Passage is defined to be 140 Sv, the Weddell Sea Gyre 30 Sv, and Brazil Current is defined to be 5 Sv. These transport values correspond to observations made of the ACC, Weddell Gyre and the Brazil current as described in Section 2.1. In this setup, the Brazil Current affects the retroflection of the Malvinas Current as discussed later in section 4.1.2, but the details of this deflection are not important for the Scotia Sea flow. The resolution of the Weddell Gyre is more important to the circulation simulations, as it determines the exchange of water across the southern boundary of the Scotia Sea.

Initialization

Objectively analyzed fields of temperature and salinity obtained from the National Oceanographic Data Center (NODC) World Ocean Atlas (WOA) 1998 (Antonov et al., 1998; Boyer et al., 1998) are used to initialize the model. This data set is an

interpolation of existing observations onto a worldwide grid with a spacing of one degree in latitude and longitude and standard depth levels. The structure of the temperature and salinity distributions used to initialize the model are taken from the annual mean fields available from this data set and are interpolated onto the uniform model grid.

Frontal Jets

Another important element of simulating the Scotia Sea circulation is the use of a feature model to realistically resolve the observed fronts in the ACC (cf. Fig. 1). Using the WOA 1998 climatologies by Antonov et al. (1998) and Boyer et al. (1998) as initial conditions produced unrealistic slow flow through Drake Passage, because the climatological temperature and salinity data distributions are a smoothed representation of the meandering fronts. Feature models (e.g., Gangopadhyay et al., 1997) provide an approach to create dynamically consistent features such as mesoscale rings, or frontal jets which are not resolved in climatological distributions. For the region of interest in this study, the frontal locations are well known (Orsi et al., 1995).

Frontal jets are an important part of the ACC, as they provide flow speeds approaching 0.5 m s^{-1} that contrasts with flow between the jets which can be half to a quarter of these speeds (Nowlin and Clifford, 1982; Hofmann, 1985; Orsi et al., 1995). The original gridded climatology on a one-degree grid is too coarse to represent such narrow features. Therefore, the fronts are restored by creating additional data points at a 50-km spacing and creating fronts along the locations taken from Orsi et al. (1995). At each line segment defining a front, additional values of temperature and salinity are added at 2-km intervals along a line that extends 150 km to each side and is perpendicular to the front. The standard depth, temperature values from the Levitus et al. (1994) and salinity values from the Levitus and Boyer (1994) climatologies are interpolated to these locations, as well as the temperature and salinity anomaly determined by equation 8 below. These additional points, along with the original climatology, are interpolated onto the model grid using an optimal analysis procedure (Bretherton et al., 1976).

A temperature front is defined by an anomaly (Ta) which is assumed to decay exponentially with depth, z in m, and horizontal distance from the front location, y_r in m (positive to the left, facing downstream) as

$$Ta = \Delta T \; y_r e^{-(\frac{y_r}{2W})^2} \; e^{\frac{z}{Z_d}} \; min(1, \frac{-z}{Z_s}), \tag{8}$$

where ΔT is the temperature gradient across the front, W and Z_d are the width and depth scales of the front in m, respectively, and Z_s is the surface layer depth in m defined for each front. The temperature anomaly has the horizontal shape (*Ta shape*) of the derivative of the Gaussian

$$Ta \; shape = y_r e^{-(\frac{y_r}{2W})^2}. \tag{9}$$

A minimum function keeps the frontal structure from intruding into the surface mixed layer, thereby defining the front for the depths between Z_s and Z_d. Equations similar to equations (8, 9) are used to define the salinity anomaly of a front. The five parameters that are used to define each front, derived from the observations discussed in section 2.1.1 (Table 1), are given in Table 3.

Once the fronts are initialized by the feature model they are maintained during the full year of the simulation, despite meanders and eddy formation. This occurs because either certain processes for front formation are included in the model, or simply that the potential energy of the initial density distribution dissipates slowly.

Table 3. Characteristics of the Subantarctic Front (SAF), the Polar Front (PF) and the Southern Antarctic Circumpolar Current Front (SACCF) used to determine the temperature and salinity anomalies for the feature model.

Front	W (km)	Z_d (m)	Z_s (m)	ΔT (°C)/100 km	ΔS/100 km
SAF	40	1200	150	0.96	-0.15
PF	40	1200	150	1.2	-0.15
SACCF	30	1200	300	1.0	-0.09

Dynamical Surface Forcing

Local winds are strong over the region included in the model domain, with the time-averaged zonal wind stress through Drake Passage being a factor of three larger than mid-latitude winds (Trenberth et al., 1989). The wind is an important forcing for the circulation, which means it must be included as an external forcing to the

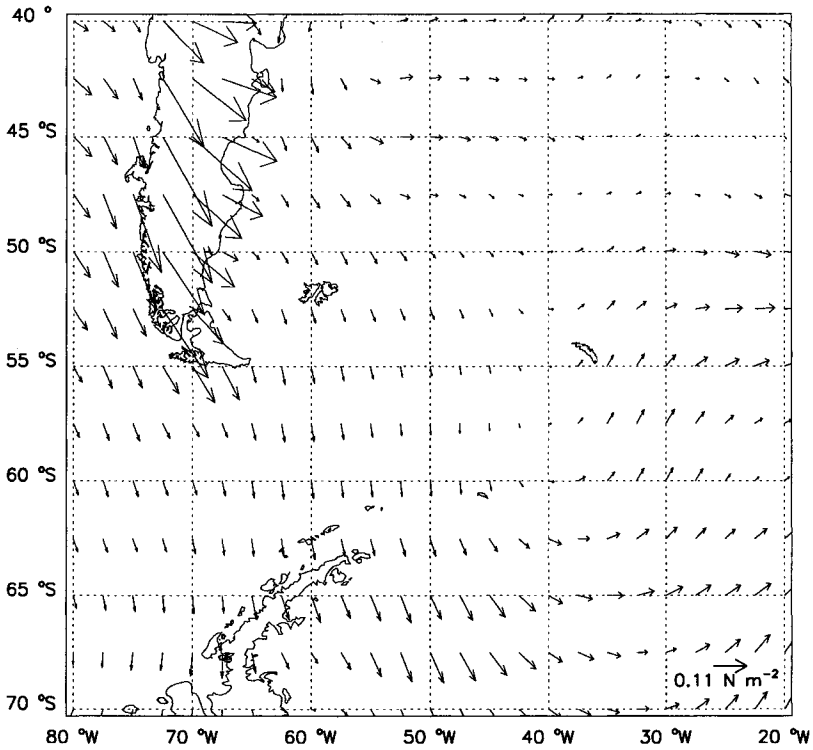

Fig. 6. Wind stress (N m^{-2}) for December 1992 from the NCEP climatology on a 2.5° x 2.5° grid.

model. The NCEP monthly wind stress data set, available over 13 years (1982 to 1994, Kalany et al., 1996) on a 2.5° x 2.5° latitude and longitude grid is used to provide dynamical surface forcing to the model. The monthly data, chosen for three consecutive years (1992-1994) of the available 13 years, are interpolated onto the model grid and the wind fields (Fig. 6) are used to force the circulation model.

Shapiro Filter

Waves shorter than two grid intervals are created by finite differencing schemes and are falsely interpreted as belonging to the longer wave components due to aliasing. Therefore, a Shapiro filter is used to dampen the two- to three-grid-interval waves, leaving middle and long waves relatively unaffected (Shapiro, 1971). The Shapiro filter used in the model is a fourth-order filter for momentum, tracers and transport, and a second-order filter for vorticity. The model is sensitive to changes in the choice of Shapiro filter for vorticity, because choosing a fourth-order filter removes

less variability over time and makes the flow too smooth, which slightly inhibits mesoscale eddy formation.

Circulation Model Spin-up

The model is started on 1 October, 1992 and a spin-up of two months is sufficient to develop a realistic flow field that reproduces observed flow features in the area, including mesoscale variability as described in detail in section 4.1. The length of time allowed for spin-up was determined to be two months by assessing the appearance of mesoscale variability versus the desire to keep the simulation time to a minimum. The circulation model is then run for 10 months from 1 December, 1992 until 30 September, 1993. The resultant simulation is used to provide the flow, temperature and salinity fields of the Scotia Sea and environs.

Circulation Model Simulations and Sensitivity Studies

The model setup described above was used to provide a reference simulation to be used for comparison to other simulations. The influence of changes in environmental forcing such as the wind, the transport through Drake Passage, and the location of the fronts on the transport of krill to South Georgia are also of interest. Therefore, the effect of changes in wind stress on the circulation in the study area are explored by increasing and decreasing the wind stress by an amount which is chosen according to the variability of the NCEP wind data set. Ten years of the NCEP wind time series (1985-1994) were statistically analyzed by calculating variances to determine the variability of wind in the study region. The maximum variability observed is 11.45%, and the minimum variability is 1.78%. Therefore, sensitivity of the circulation to a 20% increase and decrease in winds was tested, to simulate the influence of observed variability and to include possible changes in wind stress due to climate change.

The Ekman factor ($ekfac$), a factor that controls the Ekman depth (from Large et al., 1994; Eq. 24), which translates into the mixed layer depth calculated in the model is used to implement this change in wind stress as

$$h_E = ekfac\ u^*/f, \tag{10}$$

where

$$u^* = \sqrt{(\tau/\rho)}, \tag{11}$$

and h_E is the Ekman depth in m, u^* is the frictional velocity in m s^{-1}, f is the Coriolis parameter in s^{-1}, τ is the wind stress in dynes cm^{-2}, and ρ is the density

in kg m^{-3}. Large et al. (1994) suggest setting $ekfac$ to 0.7; however, the value is somewhat arbitrary. Therefore the ability to increase or decrease this value, if the Ekman depth estimate appears too shallow or too deep in the simulated circulation distribution, is allowed in HOPS. An increase in the wind by 20% translates into a decrease in the Ekman factor to 0.626; a 20% decrease in wind translates into an increase of the Ekman factor to 0.767.

The wind-induced surface Ekman flow is towards the east-northeast and variations in wind speed may affect the exchange between the continental shelf of the Antarctic Peninsula and the open ACC. This is of importance because Antarctic krill are mainly found on and close to the continental shelf of the Antarctic Peninsula, migrating offshore for spawning (Siegel, 1988; Brinton, 1991).

The transport through Drake Passage in the reference simulation was set to 140 Sv. Whitworth et al. (1982) calculated a mean geostrophic transport of 103±12.6 Sv through Drake Passage, and Nowlin and Klinck (1986) review transport estimates for Drake Passage and arrive at an average transport of 134±14 Sv. According to these transport estimates, variations in the transport through Drake Passage of 12% were chosen to simulate possible interannual changes in the transport and its effect on krill transport.

Since the SACCF is the main transport mechanism of krill to South Georgia (Hofmann et al., 1998; Thorpe et al., 2002), it is also of interest to assess the influence of a change in location of this front. The SACCF meanders naturally (Nowlin and Klinck, 1986), but changes in environmental factors due to climate change may shift the fronts of the ACC from their present location. Therefore, the last set of sensitivity simulations considered the flow that would develop with the SACCF shifted 10 km to the north. A summary of all circulation sensitivity simulations is given in Table 4 and the results of each are discussed in section 4.

Drifter Initialization and Implementation

Drifters are released into the simulated surface flow field at 50 m depth in a wide range of initial positions and starting times and tracked over space and time. A depth of 50 m is chosen because krill are found at average depths of 50 m to 70 m (Godlewska, 1996). The trajectories provide particle locations across the Scotia Sea which are then matched with other data sets to obtain time series of available food along specific transport pathways. These time series are then input into the time dependent krill growth model to determine growth and development of Antarctic

Table 4. Summary of the circulation sensitivity simulations showing the change made from the reference simulation and the figures displaying the results. The reference simulation used three years of NCEP winds (1992-1994), a 140 Sv transport through Drake Passage, and frontal locations taken from Orsi et al. (1995).

Simulation	Parameter changed	Results
Reference		Table 12, Figs. 25-35, Fig. 36
Wind up	20% increased winds	Table 12, Fig. 38
Wind down	20% decreased winds	Table 12, Fig. 39
Transport up	12% increased transport	Fig. 40
Transport down	12% increased transport	Fig. 41
Fronts	SACCF moved 10 km to the north	Fig. 42

krill along specific pathways. In addition, drifter trajectories are used for simulated circulation field validation. Drifter locations in the simulated circulation field are calculated using a 16-point cubic Bessel interpolation of the velocity fields at the x and y grid locations of the regular model grid (grid spacing 10 km), and the solution is advanced forward in time with fourth-order Runge-Kutta method with a 36-minute time step.

3.2 Krill Growth Model

The biological model that is used to simulate the growth and development of Antarctic krill is based on the model described in Hofmann and Lascara (2000). This time-dependent, size-structured, physiologically-based model is based on a governing equation for the time-dependent (t) change in the number of krill individuals (N) in a given size class, j, of the form

$$\frac{dN_j}{dt} = -\alpha_j N_j - \beta_j N_j + \alpha_{j-1} N_{j-1} + \beta_{j+1} N_{j+1}, \tag{12}$$

where each size class is defined by a length and carbon weight, as determined by the relationships in Table 5. The rate of transfer between size classes is given by the

coefficients α and β, which are determined by changes in net production based on carbon weight. Net production of any given size class, NP_j, is assumed to be the difference between assimilated ingestion (AI_j) and respiration (R_j) as

$$NP_j = AI_j - R_j, \tag{13}$$

When $NP_j > 0$, the gain in krill biomass (growth) effects a transfer to the next larger size class ($\alpha_j > 0$ and $\beta_j = 0$). For $NP_j < 0$, the loss in krill biomass (shrinkage) is represented by the transfer of individuals to the next smaller size class ($\alpha_j = 0$ and $\beta_j < 0$). These transfers can be expressed in length or biomass by using the conversions given in Table 5.

The model given by equation 12 is configured with 232 size classes to describe the life history of krill from 2 mm (Calyptopis I, first feeding stage) to 60 mm (maximum adult size), with a resolution of 0.25 mm. The size class model is solved numerically using a third-order Adams-Bashforth method (Canuto et al., 1988) with a time step of 0.1 day, which ensures that krill mass and individuals are conserved over the duration of the simulation.

3.2.1 Model Processes and Parameterizations

Observations from field and experimental studies are used to derive functional relationships of the processes affecting krill net production. All of these parameterizations are size-dependent, and in some cases the form of the relationship changes with the size of krill.

Filtration

The primary mode by which krill feed is filtering the water column for available food, such as pelagic phytoplankton or heterotrophic food (Marr, 1962; Schnack, 1985; Quetin and Ross, 1985). Filtration rates for krill have been estimated in numerous laboratory experiments and seem to be dependent on the size of krill (review by Morris, 1984; Quetin and Ross, 1985; Daly, 1990). Observations from those experimental studies were used to derive a relationship between krill dry weight and compression filtration rate F^{cf} (Table 6).

Table 5. Length (L, mm) to wet weight (W, mg), wet weight to dry weight (DW, mg), and dry weight to carbon (C, mg) relationships used in the krill growth model. The krill size range over which the relationships apply and the source for each is indicated.

Equation	Size Range (mm)	Source
$W = 0.0470\,L^{2.121}$	2-5	Ikeda (1984b)
$W = 0.0072\,L^{3.021}$	10-40	Hofmann and Lascara (2000)
$W = 0.0016\,L^{3.423}$	40-60	Hofmann and Lascara (2000)
$DW = 0.216\,W$	2-60	Ikeda & Mitchell (1982)
$C = 0.366\,DW^{1.037}$	2-60	Ikeda & Dixon (1982); Ikeda & Mitchell (1982); Ikeda (1984b); Ikeda & Bruce (1986); Ishii et al. (1987); Ikeda & Kirkwood (1989)

Table 6. Compression filtration (F^{cf}, $m^3\ d^{-1}$), ice biota grazing (F^{ig}, $m^3\ d^{-1}$), the standard respiration rate (R^s, μ l hr^{-1}), total ingestion (I_{tot}, mg C d^{-1}), net production of any size (NP_j, mg C d^{-1}) and assimilation efficiency A (80%) as used in the krill growth model. The krill size range over which the relationships apply and the source for each is indicated.

Equation	Size Range (mm)	Source
$F^{cf} = 0.00085\,DW^{0.825}$	2-25	Morris (1984); Daly (1990)
$F^{cf} = 0.00343\,DW^{0.514}$	> 36	Morris (1984); Quetin & Ross (1985); Schnack (1985); Quetin et al. (1994)
$F^{ig} = 0.05\,F^{cf}$	2-60	Hofmann and Lascara (2000)
$R^s = 0.686\,DW^{1.031}$	< 10	Ikeda (1981); Quetin and Ross (1989)
$R^s = 0.847\,DW^{0.850}$	> 16	Ikeda (1984b)
$AI_j = I_tot * A$	2-60	Hofmann and Lascara (2000)
$NP_j = AI_j - R_j$	2-60	Hofmann and Lascara (2000)

Ingestion

Ingestion (I_j^{cf}) of pelagic phytoplankton is formulated in this model using compression filtration as

$$I_j^{cf} = \gamma_j F_j^{cf} P(t), \tag{14}$$

where F_j^{cf} is the filtration rate for size class j and γ_j is the time krill of size class j spend feeding. The time varying phytoplankton concentration is given by $P(t)$. The constant γ was given the value 0.90 for larval krill ($<$ 12 mm) and 0.75 for larger krill ($>$ 12 mm). This takes into account observations that show krill to alternate between area-intensive feeding and long-distance foraging (Hamner, 1984).

Krill have also been observed feeding on biota associated with sea ice (Marschall, 1988; Daly, 1990) by scraping sea ice algae from the sea ice undersurface using their endopodites (Hamner et al., 1983). Ingestion by grazing of ice biota (I_j^{ig}) is formulated as

$$I_j^{ig} = \gamma_j F_j^{ig} SI(t), \tag{15}$$

where F_j^{ig} is the grazing rate for size class j and $SI(t)$ is the time varying sea ice algae concentration. Sea ice biota is here defined to include phytoplankton and protozoa associated with the ice, as it has been observed that krill feed on *Mesodinium* spp., a phototrophic ciliate, overwintering in brine channels (US Southern Ocean GLOBEC, 2003). Due to absence of appropriate data on grazing of sea ice biota, F_j^{ig} is assumed to be 5% of F_j^{cf}. This specification of F_j^{ig} results in I_j^{ig} rates for maximum values of sea ice biota which are similar to I_j^{cf} for average values of phytoplankton.

In addition, it has been observed that krill actively feed on various copepod species (Nordhausen et al., 1992; Hopkins et al., 1993; Pakhomov et al., 1997). Ingestion of copepods (I_j^{hf}) by use of compression filtration is defined as

$$I_j^{hf} = \gamma_j F_j^{cf} HF(t), \tag{16}$$

with F_j^{cf} being the filtration rate for size class j and the time varying copepod concentration given by $HF(t)$.

Several studies have shown that krill may feed on detritus as an additional food source (Holm-Hansen and Huntley, 1984; Kawaguchi et al., 1986; Daly, 1990). To include detritus feeding in the model, ingestion of detritus (I_j^{df}) filtered from the water column is formulated as

$$I_j^{df} = \gamma_j F_j^{cf} D(t), \tag{17}$$

with the time varying detritus concentration defined as $D(t)$.

Krill is simultaneously presented with a variety of the four food sources phytoplankton, sea ice biota, zooplankton and detritus in the simulations, and the food chosen is dependent on the life stage of krill (i.e. sea ice algae versus heterotrophic food). As sea ice biota become available, small krill (<18 mm) choose to feed on this food source and on detritus entrained in the sea ice as their only food source, as suggested by observations given in Daly (1990). Feeding on the heterotrophic food source is only possible for krill larger than 18 mm, as shown by observations reported by Granéli et al. (1993) and Huntley et al. (1994a). Therefore, all potential food sources are available to only the older krill.

At the same time the availability of food is dependent on the position of krill along the simulated drifter trajectories (i.e. entrainment in an eddy, or presence/absence of sea ice), and in addition the choice of food is dependent on the availability of food sources to krill. Krill prefers feeding on phytoplankton, sea ice algae or heterotrophic food over feeding on detritus and switches to detritus feeding only when all other food sources are scarce. When presented with multiple food sources, feeding on each is done proportionally with equal weighting for each food source. The total ingestion is then defined as

$$I = I_j^{fc} + I_j^{ig} + I_j^{hf} + I_j^{df}. \tag{18}$$

Depending on which food sources are present, total ingestion is defined as the sum of the ingestion terms associated with each available food source. Finally the assimilated ingestion, AI_j, is defined as the total ingestion, times the assimilation efficiency, A. Kato et al. (1982) observed assimilation rates for krill from 72% to 90% when feeding on phytoplankton. Schnack (1985) found ranges of assimilation efficiency of 42.2% to 80.1% in krill (30-55 mm in size) feeding on centric diatoms. The assimilation efficiency in the model is taken to be 80% for all size classes of krill feeding on phytoplankton, sea ice algae or heterotrophic food. This lies in the range of values observed by Kato et al. (1982) for krill feeding on a variety of food types. Unassimilated ingestion is lost as fecal pellets.

Providing detritus as a food source to krill requires a different assimilation rate (A) to be used in the krill growth model, because detrital matter is a food source

with less metabolic value to krill than living matter. Therefore, the assimilation rate for detritus feeding is set to 50%, which is at the lower end of the range reported by Schnack (1985). All size classes of krill are allowed to feed on detritus in the simulations because larvae (Daly, 1990), juvenile and adult krill (Kawaguchi et al., 1986) have been observed feeding on this food source.

Respiration

Metabolic losses due to respiration for each size class (R_j) are assumed to result from three components, standard metabolism (R_j^s), cost due to feeding (R_j^f) and costs associated with overall feeding activity level (R_j^a) (Torres et al., 1994; Quetin et al., 1994), which are expressed as

$$R_j = R_j^s(1 + R_j^f + R_j^a), \tag{19}$$

The relationships used for R_j^s are given in Table 6. Observations from laboratory experiments were used to express standard metabolism as a function of krill size. The metabolic cost of feeding and digestion (R_j^f) is related to the daily ration ingested by krill such that it increases linearly to a value of 1 for rations up to 10%, then remains constant for higher daily rations. The respiration activity factor, (R_j^a), is assumed to depend on seasonal variations in krill activity (Ikeda and Dixon, 1982; Quetin and Ross, 1991). From May to August activity is low, so the minimum standard respiration rate is reduced by 50% and coincides with the minimum day length. During austral summer, when krill are swimming, overall respiration is doubled, taking into account increased metabolic costs associated with swimming (Clarke and Morris, 1983).

Additional Features of Krill Feeding

Another important aspect of krill ingestion is the response of krill to very high concentrations of food. Ishii et al. (1987) found that the ingestion rate of large krill increases with increasing food concentrations. However, it has been suggested that maximum clearance rates for copepods, and therefore ingestion rates, prevail at food concentrations less than the critical concentration and above a feeding threshold (Frost, 1972; Mullin, 1963). Quetin and Ross (1985) showed that the clearance rate of krill first increases linearly with increasing phytoplankton concentration, then levels out at a critical concentration of phytoplankton and decreases once the critical concentration is exceeded, independent of which phytoplankton species was

used as a food source. However, values for the critical concentration and maximum clearing rate changed with species size (30-45 cells ml^{-1} for larger phytoplankton). Hamner (1988), who describes the feeding mechanisms of krill in detail, states that the number of cells captured with every sweep of the legs increases proportionally to the phytoplankton abundance until feeding becomes limited by mastication rate.

Therefore, the simulated krill growth rate is limited to 0.25 mm per time step, thereby limiting the maximum total ingestion of krill to ensure that krill do not grow more than one size class per day. This maximum rate is in excess of observed summer krill growth rates, which range between 0.105 and 0.179 mm d^{-1} (Rosenberg et al., 1986), as well as overall krill growth rates (Siegel and Kalinowski, 1994) and maximum summer growth rates (Ross et al., 2000). However, it is less than the krill growth rate of 0.33 mm d^{-1} estimated by Clarke and Morris (1983).

Krill shrink when they do not encounter enough food to meet their metabolic needs and are starving (Ikeda and Dixon, 1982; Nicol et al., 1992). Ikeda and Dixon (1982) show that the decrease in body wet weight of krill starved over 211 days ranged from 32.1% to 52.2% with a mean decrease of 45%. Thus, for the krill growth model, a loss of krill body wet weight of 45% is assumed to be equivalent to the death of the animal and the simulations are ended at this point. Larval krill of the Calyptopis I stage have less tolerance to starvation (Ikeda, 1984a; 1984b). Therefore, Calyptopis I krill are assumed to die after 6 days without feeding. Additional mortality due to predation is not included in the krill growth model because the model is designed to represent individual animals.

Temperature Effect

The range in temperature (-1.8°C to 4°C) that Antarctic krill encounter across the Scotia Sea is large enough to potentially affect metabolic processes associated with growth (Clarke and Morris, 1983; Quetin et al., 1994). Therefore, the influence of temperature on krill growth rate was included through a Q_{10} relationship. Laboratory measurements of temperature effects on the metabolic processes of euphausiids provide Q_{10} values of 2 (Torres and Childress, 1983) and values calculated for Antarctic krill are as high as 3.5 (Quetin et al., 1994). Experimental observations from which a temperature-dependent growth rate for Antarctic krill can be derived are few (e.g. Poleck and Denys, 1982; Morris and Keck, 1984; Buchholz, 1985; 1991; Ikeda et al., 1985) and the limited data represent different experimental designs, different sized krill, and different feeding frequencies, which are not compatible.

Therefore, the maximum value reported, Q_{10} of 3.5, was used with the model since this represents the maximum effect that can be expected from temperature.

Temperature values along the drifter trajectories, which represent the upper 20 m, were obtained from the WOA 1998 climatology (Antonov et al., 1998; Boyer et al., 1998). These values and the Q_{10} of 3.5 were used to scale the Antarctic krill growth rates obtained from the model, as was done in Fach et al. (2002).

3.3 Specification of Food Source

3.3.1 Phytoplankton

The main environmental forcing used with the krill growth model is the food time series available to krill. Ship-based observations sufficient to construct pelagic phytoplankton distributions across the Scotia Sea do not exist. Therefore, phytoplankton concentrations along particle trajectories were extracted from monthly chlorophyll distributions that were constructed from eight-year composites (1978 to 1986) of Coastal Zone Color Scanner (CZCS) observations from the Scotia Sea (Feldman et al., 1989), which are the only large-scale view of chlorophyll concentration for this region. Ocean color measurements from the Sea-viewing Wide Field-of-view Sensor (SeaWiFS) are not adequate for describing the chlorophyll distribution of this region because the extensive cloud cover, long periods of darkness and seasonal sea ice cover result in considerable gaps in the spatial and temporal coverage. The SeaWiFS composites that extend to the present time do not cover the whole extent of the study area during winter months (June to August) and only cover it marginally in May and September.

The CZCS composite for January (Fig. 7) shows regions of high chlorophyll concentration (10 mg m^{-3}) along the coast of South America, at isolated locations across the Scotia Sea, and along the west Antarctic Peninsula. The minimum concentrations for CZCS-derived chlorophyll is 0.039 mg m^{-3}, which is the threshold concentration for the sensor. This value is used in low chlorophyll periods and provides a low-level background chlorophyll value.

Ninety percent of the signal detected by the satellite originates from the top optical depth of the euphotice zone (Gordon and McCluney, 1975). The euphotic zone is the layer extending from the sea surface to where the light level decays to 1% and is defined to be 4.6 optical depths deep. Thus, most of the phytoplankton present

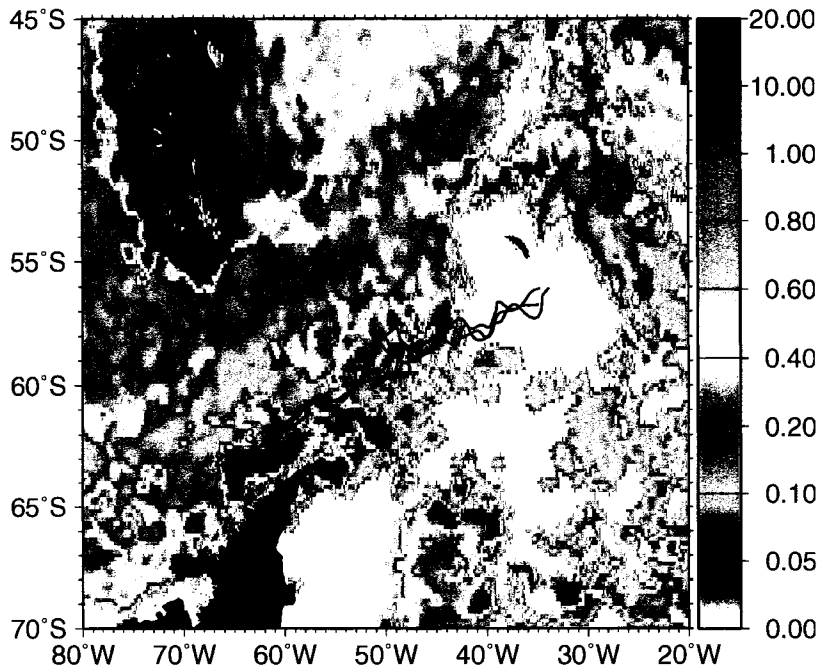

Fig. 7. CZCS-derived eight-year (1978-1986) composite of pigment concentration (mg m^{-3}) for January. Lines indicate the trajectories of three drifters released along the western Antarctic Paninsula.

in the euphotic zone cannot be detected by the CZCS. Standard pigment retrieval algorithms for the CZCS sensor underestimate chlorophyll concentrations below 1.5 mg m^{-3} by a factor of 2.4 (Mitchell and Holm-Hansen, 1991; Sullivan et al., 1993). Therefore, a regional algorithm was developed for the Southern Ocean (Sullivan et al., 1993). Also Dierssen and Smith (2000) calculated that both SeaWiFS and CZCS standard algorithms underestimate the chlorophyll concentration by roughly a factor of 2. More precisely, CZCS underestimates concentrations below 1.5 mg m^{-3} by a factor of 2.2 and above 1.5 mg m^{-3} by

$$c = 10^{(0.45+0.53x)}, \tag{20}$$

where the chlorophyll concentration, c in mg m^{-3}, is calculated with the chlorophyll concentration, x in mg m^{-3}, obtained from the standard chlorophyll algorithm. However, the mean summer pigment (chlorophyll a and phaeopigment) concentration computed with the Southern Ocean algorithm, which was used to construct the chlorophyll distributions used in this study, is within 5% of the *in situ* data (Sullivan

et al., 1993).

The contribution of transient features to the overall food supply is difficult to include in the chlorophyll time series derived from the CZCS observations because the eight-year average that was used to obtain the monthly composites, provides only a static picture. The Scotia Sea region, however, has considerable mesoscale variability in physical and biological distributions (Murphy et al., 1998), which will not be seen in eight-year averages. However, this mesoscale variability is experienced by drifters during transport as they get entrained in circulation features as they move across the Scotia Sea.

Phytoplankton Time Series

The phytoplankton concentration along three particle trajectories (Fig. 7), starting in December (Year Day 335), January (Year Day 1) and February (Year Day 32) (Fig. 8) are first input into the krill growth model. These three drifters were chosen from all drifters originating at the western Antarctic Peninsula because their trajectories show the prominent transport pathways (Fach et al., 2002). It should be noted that the drifter trajectories stop once the drifters reached South Georgia. Therefore, some drifter paths are recorded for a longer time than others.

The chlorophyll concentrations that are encountered along the three drifter trajectories released on the first day of December (Year Day 335), which assumes a November spawning, are between 1 and 12 mg m^{-3} with a one time maximum value of 22 mg m^{-3} (Fig. 8A). The chlorophyll time series for particles released on the first day of January (Year Day 1), which assumes December spawning, show persistent but lower concentrations (Fig. 8B). The chlorophyll time series for particles released on the first day of February (Year Day 32), which assumes January spawning, show similar concentrations as the January release (Fig. 8C). In all three release scenarios, phytoplankton concentrations decrease significantly after the end of April (Year Day 120) since phytoplankton concentrations in the Southern Ocean decrease with the onset of winter as light becomes limiting.

The extracted phytoplankton time series illustrate the large mesoscale variability in food supply that is encountered along trajectories which are not largely separated in space (Fig. 7). The time particles spend in different concentrations of phytoplankton coincides with entrainment of the drifter in eddies, and is a measure of the eddy variability. These entrainments last from five to 20 days. Also, considerable temporal variability in phytoplankton availability occurs depending on the

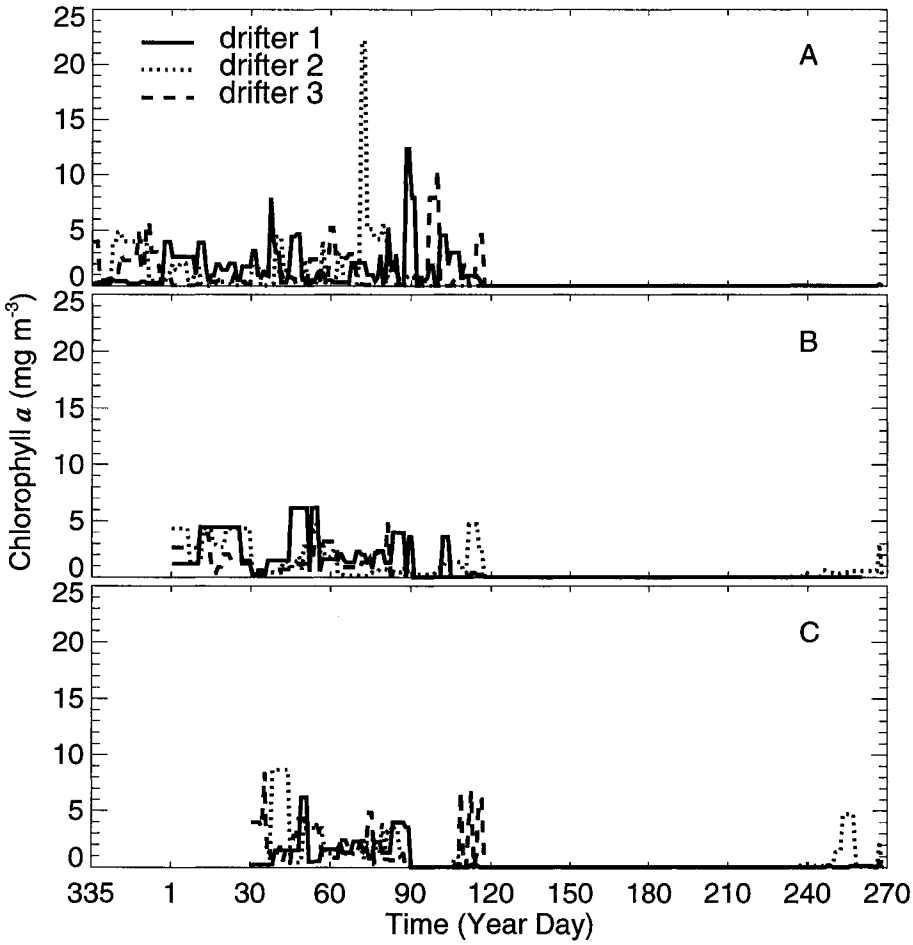

Fig. 8. CZCS-derived time series of pigment concentration (mg m^{-3}) along trajectories of three drifters originating at the western Antarctic Peninsula in: A) December (Year Day 335), B) January (Year Day 1), C) February (Year Day 32).

time a particle leaves the Antarctic Peninsula. Drifters released in December have the chance to encounter high concentrations of phytoplankton food until the end of April, approximately 5 months. A drifter released in February at the same location has only 3 months of potentially high phytoplankton concentrations. These general observations are true for drifters originating at the western and southwestern Antarctic Peninsula, the Bransfield Strait area, the Elephant Island/Scotia Sea region and the Weddell Sea, as shown in Section 4.3.4.

3.3.2 Sea Ice Algae

A large but variable fraction of the Southern Ocean is covered by annually forming sea ice, which covers an area ranging from 4 x 10^6 km^2 at the end of austral summer to 20 x 10^6 km^2 in late winter (Zwally et al., 1979). Algal communities are known to inhabit distinct micro-habitats which are created when pack ice is formed and ages (Garrison et al., 1986; Smetacek et al., 1992; Ackley and Sullivan, 1994). Modeling studies of Antarctic sea ice productivity show that of the 35.7 Tg C produced annually in the Antarctic pack ice, 75% is associated with first-year ice and 50% is associated with the Weddell Sea (Arrigo et al., 1997; 1998). Also the productivity of sea ice algae varies over the year, with the productivity per unit sea ice being greatest in January, but with total production peaking in November due to the more extensive sea ice cover (Arrigo et al., 1998) that exists at the time.

Sea ice algae provides an additional food source for krill especially in austral winter (Marschall, 1988; Daly and Macaulay, 1991). Therefore, sea ice concentrations along the particle trajectories were extracted from Special Sensor Microwave/Imager (SSM/I) measurements during a high-ice year, 1988 (Fig. 9). The June 1988 image is shown (Fig. 9), because this is the time when sea ice coverage is potentially important in krill development (Siegel and Loeb, 1995). The sea ice concentration is stored in pixels representing a 25 km x 25 km area for which one data value is recorded. The percent of sea ice coverage is then used as a proxy for sea ice biota concentrations and was scaled to a sea ice algae concentration using the sea ice algae time series given in Hofmann and Lascara (2000). Because algae concentrations may vary depending on when the sea ice formed, the scaling was done according to the formation time of sea ice in each pixel.

Sea ice concentrations are generated using brightness temperatures derived from passive microwave data. Comparisons of sea ice concentrations and sea ice edges obtained from the satellite sensors with *in situ* and other satellite data show good agreement (Comiso and Sullivan, 1986). In areas of polynya and lead formation and at the sea ice edge, large errors can occur because the emissivity of new sea ice varies continuously with thickness up to several centimeters (Comiso et al., 1989). However, these errors do not affect this analysis because the satellite-derived sea ice distributions are used only to obtain general patterns and trends.

Sea ice-derived food is assumed to be an alternative food source that krill can exploit if they encounter sea ice during transport. This is implemented in the model

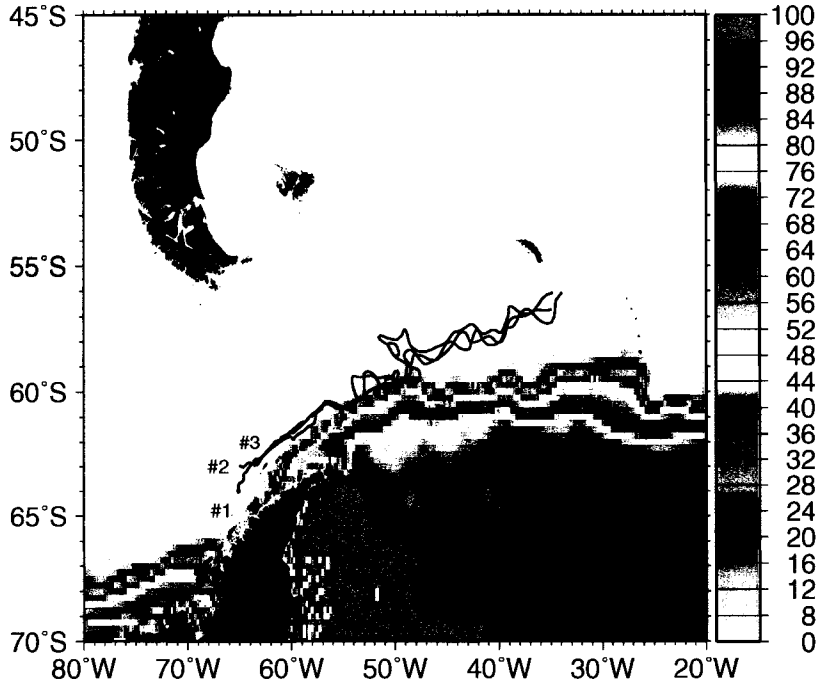

Fig. 9. SSM/I-derived sea ice concentration (% coverage) for June 1988. Lines indicate the trajectories of three drifters released at the western Antarctic Peninsula.

by allowing small krill (<18 mm) to feed only on sea ice-derived food and detritus when sea ice is encountered along a trajectory, while larger krill can feed on sea ice algae and additional food sources, as discussed in section 3.2.1.

Sea Ice-derived Food Time Series

The sea ice algae concentration along the same three drifters released at the western Antarctic Peninsula starting in December (Year Day 335), January (Year Day 1) and February (Year Day 32) (Fig. 10) is input to the krill growth model as an additional winter food source. The sea ice algae concentrations that are encountered along the three drifter trajectories released on the first day of December (Year Day 335), are mostly zero and only one of the drifters encounters sea ice at all (Fig. 10A). The maximum amount of sea ice algae chlorophyll encountered over the complete time of transport is 15 mg m^{-3}. The time series for particles released on the first day on January (Year Day 1) show lower concentrations (Fig. 10B) and the time series for particles released on the first day of February (Year Day 32) shows even

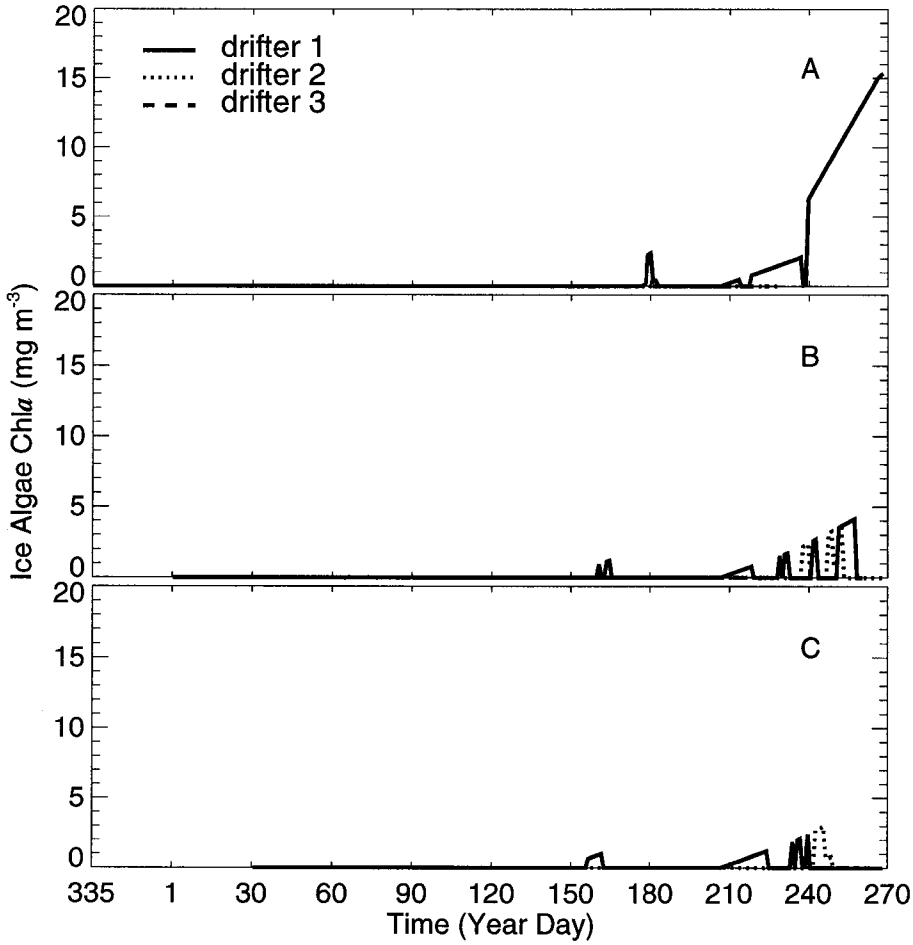

Fig. 10. SSM/I-derived time series of sea ice algae concentration (mg m^{-3}) along trajectories of three drifters originating at the western Antarctic Peninsula in A) December (Year Day 335), B) January (Year Day 1), C) February (Year Day 32).

smaller concentrations of sea ice algae (Fig. 10C). Particles originating at the western Antarctic Peninsula are not likely to encounter sea ice and its associated sea ice algae on their way through the open Scotia Sea, similar to drifters originating in the southwestern Antarctic Peninsula and the Scotia Sea/Elephant Island area. Particles originating in the Bransfield Strait generally pass by pack ice forming off the Antarctic Peninsula during winter, and drifters originating in the Weddell Sea spend most of their transport time under sea ice (see Appendix A).

3.3.3 Heterotrophic Food

Studies (e.g. Hopkins et al., 1993; Pakhomov et al., 1997) show that Antarctic krill can feed on zooplankton outside of phytoplankton bloom periods. Thus, another addition to the food time series available to krill consists of a heterotrophic food source. There are no continuous measurements of copepod concentrations across the Scotia Sea from which a times series of copepod concentrations along drifter paths could be extracted. Therefore, a time series (Fig. 11) was constructed using estimates of mean mesozooplankton biomass in the greater South Georgia region (Atkinson and Snÿder, 1997). This time series assumes that krill encounters occasional patches of high zooplankton concentrations as well as low background concentrations. The low background concentration of copepods was calculated using estimates of low mesozooplankton biomass (Atkinson et al., 2001) and carbon content of mesozooplankton (Atkinson and Snÿder, 1997). Larval krill are not capable of feeding on the large copepods on which the heterotrophic food source is based, due to their small body size. Thus, feeding on the heterotrophic food source is possible only for krill greater than 18 mm in size. Juvenile krill of this size have been observed feeding on copepods (Granéli et al., 1993; Huntley et al., 1994a). The heterotrophic food source as described above (Fig. 11) is used for all drifters independent of origination site.

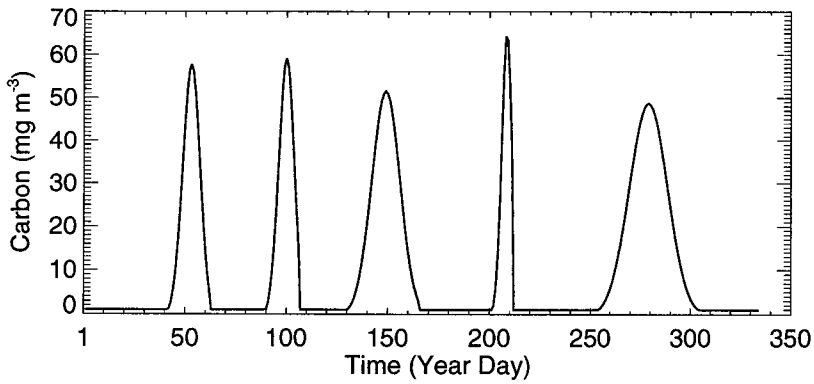

Fig. 11. Time series of heterotrophic food input to the krill growth model.

3.3.4 Detritus

A last addition to the food available to krill is detritus, on which krill have been observed to feed (e.g. Kawaguchi et al., 1986; Holm-Hansen and Huntley, 1984; Daly, 1990). Again, no large scale or temporal data sets of detritus concentration in the area of interest are available. Therefore this food source was constructed using the eight-year composites of CZCS observations described in section 3.3.1 to obtain a conservative estimate of how much chlorophyll *a* is in the area from which detrital material can be estimated.

Particulate organic carbon (POC) is generally considered to be part of the non-living component of sea water and is used in this analysis as a measure of detritus. A direct relationship between detritus and chlorophyll *a* has been reported in the form of POC:Chl*a* ratios (Fabiano et al., 1993; 1995). The POC concentrations are dependent on species composition and physiological state of the phytoplankton (Cota et al., 1992), factors that change over time with specific phytoplankton bloom and season. Therefore, a conversion from chlorophyll *a* concentrations to POC is a somewhat crude and problematic approach for defining POC concentrations. This problem is well understood, but due to the lack of other conversion factors and more specific data on POC concentrations, this method is used in this study.

In general POC:Chl*a* ratios >50 are considered high and may be expected in areas of nutrient deficiency, low temperatures, low light and/or self shading (Fabiano et al., 1993). In the area of interest, several measurements of POC:Chl*a* ratios have been made (Table 7). In the Bellingshausen Sea, Kennedy and Robertson (1995) report the variation of POC and chlorophyll *a* with latitude along 88°W for December 1993. Overall the POC:Chl*a* ratios ranged from 60-739 (Table 7). However, these values are calculated for austral summer, and there are likely to be different ratios in fall and winter.

Brichta and Bathmann (pers. comm.) report average POC:Chl*a* ratios of 29-597 for the continental shelf area of the western Antarctic Peninsula in April, with an average value of 233. Cota et al. (1992) report a mean POC:Chl*a* ratio of 530 in winter that is considerably higher than reported for other areas of the Southern Ocean (Smith and Sakshaug, 1990). Cota et al. (1992) calculated a regression between POC and chlorophyll *a* for the Weddell Sea as

$$\mathrm{POC} = 57.1(\pm 28.9) + 47.2(\pm 30.1)\ \mathrm{Chl}a, \tag{21}$$

Table 7. Summary of POC:Chl*a* ratios measured for Antarctic waters. For each, the season and location where the measurement was made is given, as well as the relevant reference.

POC:Chl*a*	Season	Location	Reference
56-259	Nov-Dec 1980	Elephant Island	v. Bodungen et al. (1986)
260 ± 140 (euphotic zone)	Jan-Feb 1985	Weddell Sea	Nöthig (1988)
>300 (below 100 m)	Jan-Feb 1985	Weddell Sea	Nöthig (1988)
219	Oct-Dec 1986	55°S, 5°E	Scharek (1991)
189	Oct-Dec 1986	58°S, 2°E	Scharek (1991)
138	Jan-Feb 1983	Ross Sea	Cota et al. (1992)
32	Nov 1983	Weddell-Scotia Sea	Cota et al. (1992)
114	March 1986	Weddell Sea	Cota et al. (1992)
530	July-Aug 1988	Weddell-Scotia Sea	Cota et al. (1992)
60-739	Dec 1993	Bellinghausen Sea, 88°W	Kennedy & Robertson (1995)
40-171	Nov-Dec 1992	6°W	Dehairs et al. (1997)
242 (SD=120) (< 1.0 mg chl m^{-3})	Oct-Nov 1992	46-56°S, 6°W	Bathmann et al. (1997)
123 (SD=53) (> 1.0 mg chl m^{-3})	Oct-Nov 1992	46-56°S, 6°W	Bathmann et al. (1997)
29 - 597	April 2000	western Antarctic Peninsula shelf	Brichta & Bathmann (pers. comm.)

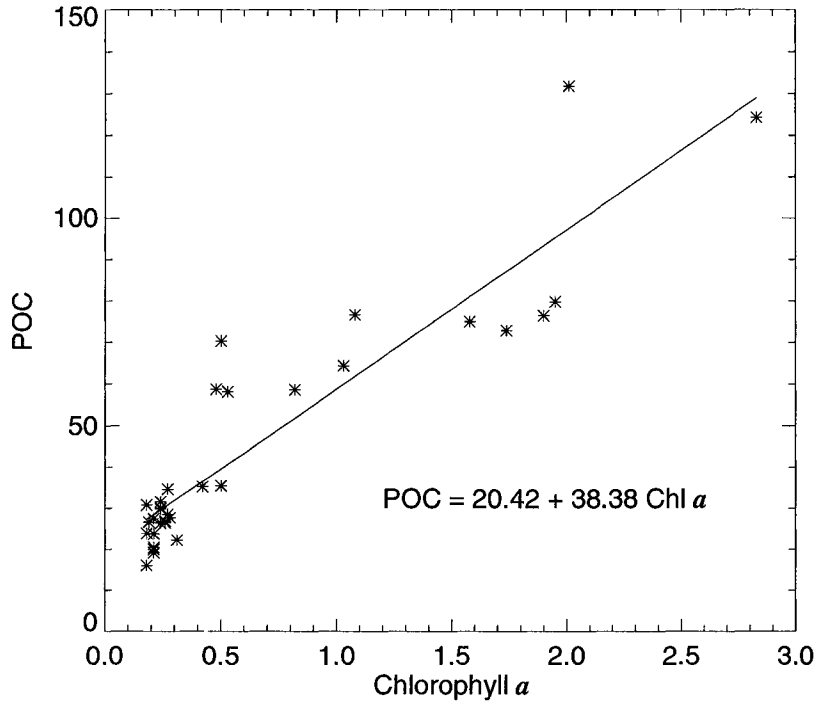

Fig. 12. Measurements of POC and chlorophyll a concentrations ($*$) from several locations during the ANT-X/6 cruise (Dehairs et al., 1997). The linear regression between POC and chlorophyll a fit to these data (solid line) is shown. The units in the linear regression equation are mg C m^{-3} for POC and the intercept, mg Chl$a$ m^{-3} for Chl$a$, and mg C (mg Chl$a$)$^{-1}$ for the ratio 38.38.

with POC and the intercept (57.1±28.9) given in mg C m^{-3}, the ratio (47.2±30.1) having units of mg C (mg Chl a)$^{-1}$, and Chl a given in mg Chl a m^{-3}. It is assumed that the slope of the regression gives an accurate representation of carbon in intact phytoplankton cells.

The chlorophyll a and POC concentrations measured during the ANT X/6 cruise (Table 7) along 6°W in October/November 1992 (Dehairs et al., 1997) are used to calculate a linear regression (Fig. 12) that can be used to estimate POC in the Scotia Sea. The pigment concentrations along simulated drifter paths were extracted from the CZCS data set and converted to summer POC values (October to March) with the ratio of 38, the slope factor of the linear regression (Fig. 12). This value is chosen as a representation of carbon in intact phytoplankton cells as suggested by Cota et al. (1992), and is a conservative estimate for a ratio in high chlorophyll

environments. Bathmann et al. (1997) reported a ratio of 123 (SD=53) for the same area. The calculated ratio of 38 is at the lower end of the previously reported values (Bathmann et al., 1997), but agrees with the slope of 47.2(±30.1) in equation (21) calculated by Cota et al. (1992).

For the winter months (April to September) the average value of 233, which was calculated for the continental shelf area of the western Antarctic Peninsula (Brichta and Bathmann, pers. comm.), is used to convert chlorophyll values extracted along simulated drifter paths to POC, although most of the simulated drifter paths moved through open ocean and processes there vary widely from the continental shelf. Nevertheless, this average value is similar to the average POC:Chl$a$ ratio 242 (SD=120) calculated for regimes with less than 1.0 mg chl m^{-3} in the open ocean in summertime (Bathmann et al., 1997). The value of 233 is close to this average value and therefore provides a useful estimate of the ratio in wintertime, when chlorophyll a values are likely to be below 1.0 mg chl m^{-3}.

Detritus Time Series

The detritus concentrations that are encountered along the same three drifter trajectories (not all shown here) released on the first day of December (Year Day 335), are between 10-200 mg C m^{-3} during the first three months of transport, then increase to 1000 g C m^{-3} in regions characterized by mesoscale patches of high chlorophyll. After April (Year Day 120) the values decrease to between 5 and 15 mg C m^{-3} for the remaining time (Fig. 13A). The time series for particles released on the first day of January (Year Day 1) begin with concentrations up to 200 mg C m^{-3} during austral summer and decrease to values between 5 and 15 mg C m^{-3} in austral winter, decreasing slightly after the beginning of September (Year Day 240) (Fig. 13B). The time series for particles released on the first day on February (Year Day 32) shows similar concentrations as the January release (Fig. 13C), with periods of high detritus concentrations after day 240.

3.4 Simulation Characteristics

3.4.1 Circulation Simulations

The circulation model, with the setup described in section 3.1.2 (Table 2) was started on 1 October 1992 and was used to provide a reference circulation simulation for comparisons to other simulations. Following the reference circulation simulation, a

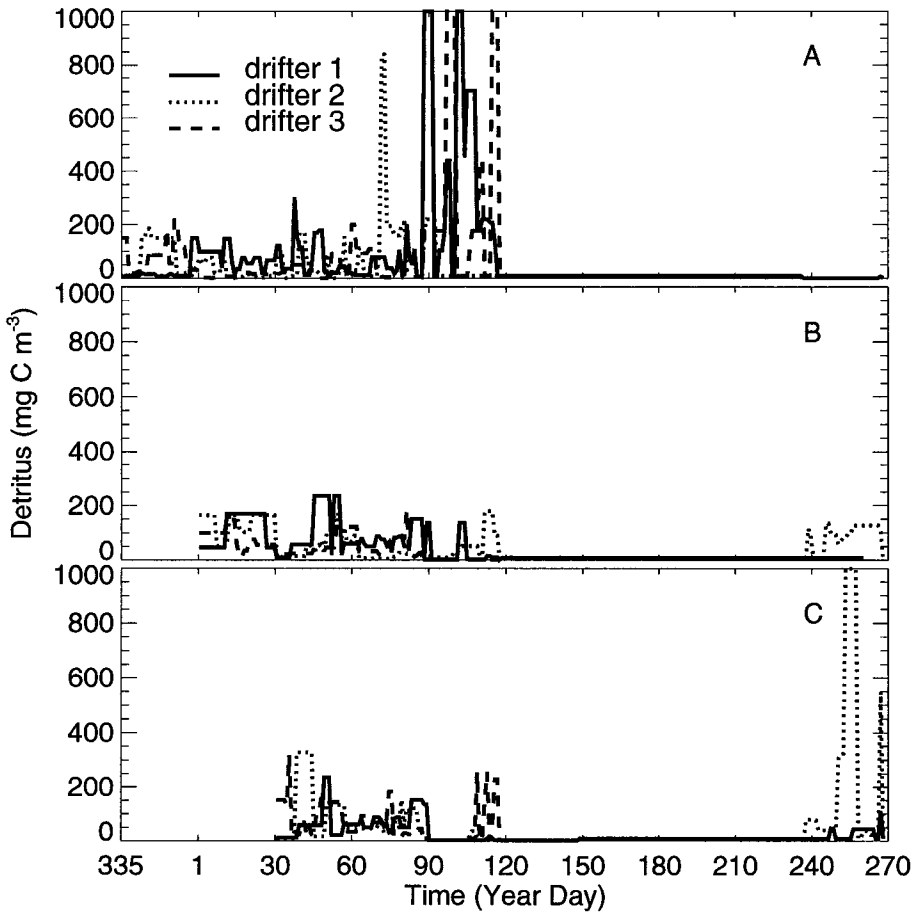

Fig. 13. CZCS chlorophyll data-derived time series of detritus concentration (mg C m^{-3}) along trajectories of three drifters originating at the western Antarctic Peninsula in A) December (Year Day 335), B) January (Year Day 1), C) February (Year Day 32).

set of numerical simulations with the circulation model were done to evaluate the influence of variability in the magnitude of wind, transport through Drake Passage and changes in the location of the SACCF on simulated flow fields (see Table 4 for summary). The results from these simulations are analyzed to help answer research question 2.

3.4.2 Drifter Trajectories

To address the first research question (given on page 3), the transport pathways of drifters released throughout Drake Passage and the Scotia Sea (Fig. 14) at different

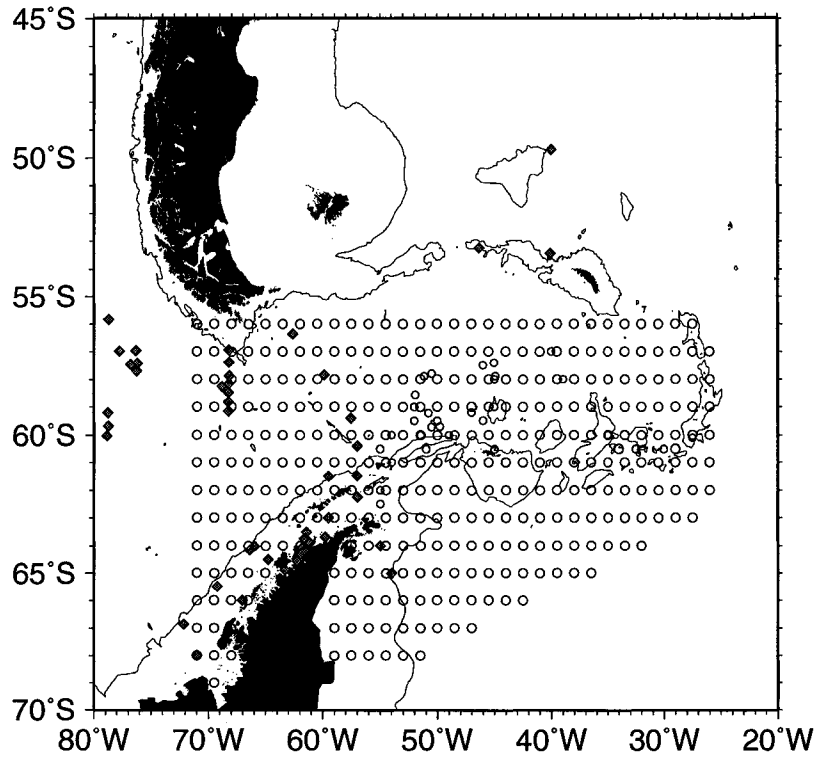

Fig. 14. Locations of drifters (o) released in the circulation model to simulate krill transport. The drifter release locations used to verify circulation simulations are indicated by (♦).

times of the austral summer (on 1 December 1992, 1 January, and 1 February 1993) were simulated using the reference simulation circulation fields. Particle locations were recorded until the end of the simulation on 30 September 1993.

Using the different simulated circulation fields from the set of numerical simulations described above (Table 4), drifter trajectories from drifters released in those circulation fields (Fig. 14) provide the location of krill over time and are used to extract concentrations of different food types in space and time.

3.4.3 Krill Growth Model

To provide a reference for comparison with other krill growth simulations as well as to address the second research question (given on page 4), food time series extracted along the transport pathways of drifters released at different locations throughout the study area (Fig. 14) in the reference circulation at different times of the austral

Table 8. Summary of the simulations done with different combinations of the food time series. The figure showing each food time series is given in column two, and the tables and figures showing the results of the simulations are given in the third column. The different food types are: PP - pelagic phytoplankton, SIF - sea ice-derived food, DF - detritus food, and HF - heterotrophic food.

Food assumption	Food time series	Results
PP	Fig. 8	Table 16-20, Fig. 44-48A
PP + SIF + DF	Fig. 8, Fig. 10, Fig. 13	Table 16-20, Fig. 44-48B
PP + SIF + DF + HF	Fig. 8, Fig. 10, Fig. 13, Fig. 11	Table 16-20, Fig. 44-48C
DF	Fig. 13	Table 16-20, Fig. 44-48D

summer were input into the krill growth model described in section 3.2. Growth and development of krill were recorded until the end of the simulation.

Different food time series extracted from the simulated drifter trajectories produced by the set of numerical simulations described above (Table 4), were input into the krill growth model. Krill growth model simulations produced simulated length-frequency distributions of krill, which are then used to test the effect of the physical environment and biological factors on survival of particular age groups of krill during transport (research question 3). Those simulations are summarized in Table 8 and the results of each are discussed in section 4. The same set of numerical simulations are used to explain episodic variations in krill biomass at South Georgia (research question 4).

3.5 Data Sets for Calibration and Verification of Models

3.5.1 Validation of circulation model

Hydrographic data sets are needed to validate the simulated circulation distributions. Observed temperature, salinity, and velocity distributions are compared to distributions of the same properties as derived by the circulation model. In addition, drifter data from the Drake Passage and Scotia Sea region are compared to passive drifter simulations obtained from the circulation model. Mesoscale variability of

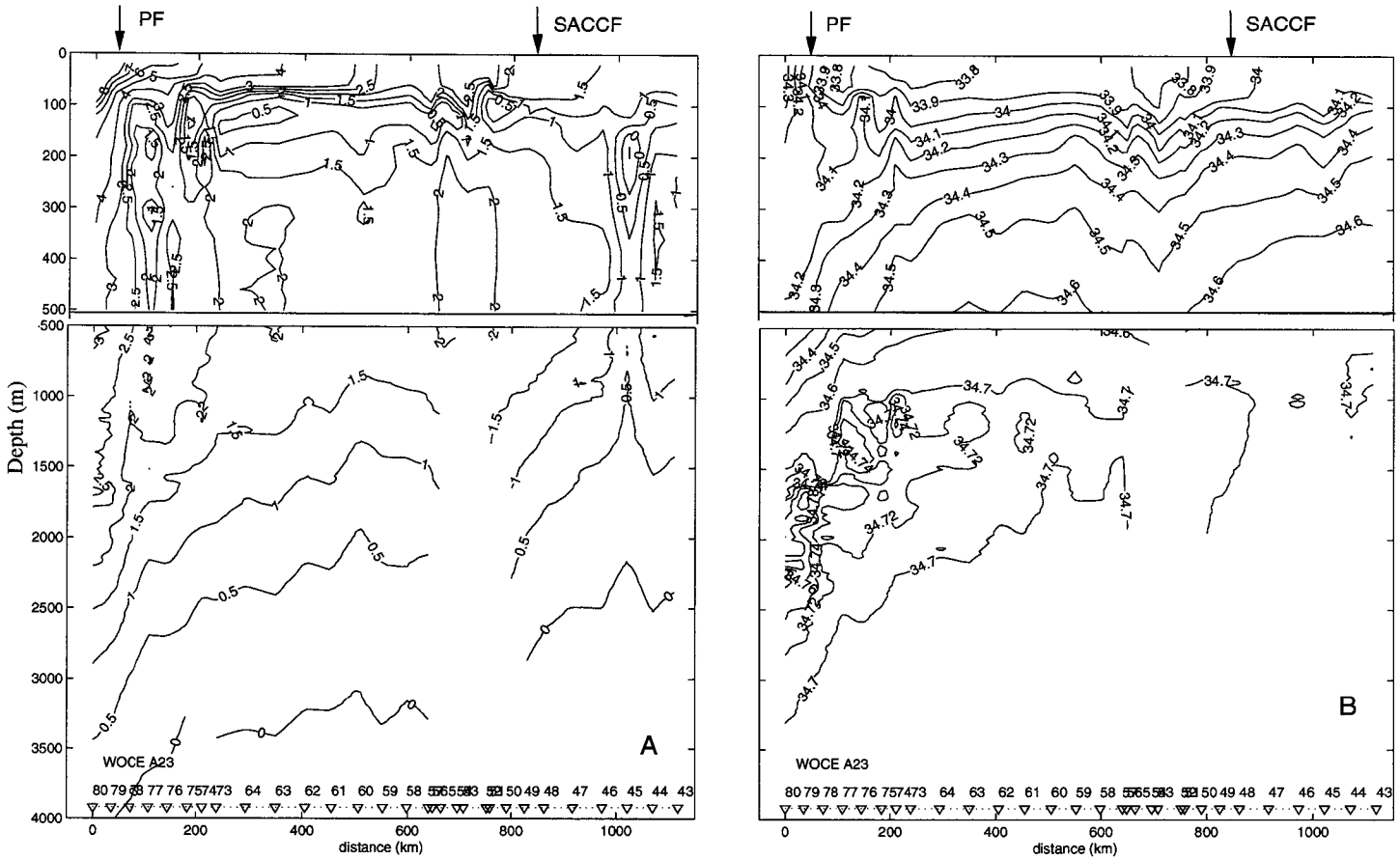

Fig. 15. A) Observed potential temperature and B) observed salinity from the WOCE A23 cruise, March to May 1995. Contour intervals are 0.5°C and 0.05 for temperature and salinity, respectively and arrows indicate locations of the PF and SACCF. Station locations along the transect are shown by ▽. Note vertical scale change in upper and lower panels.

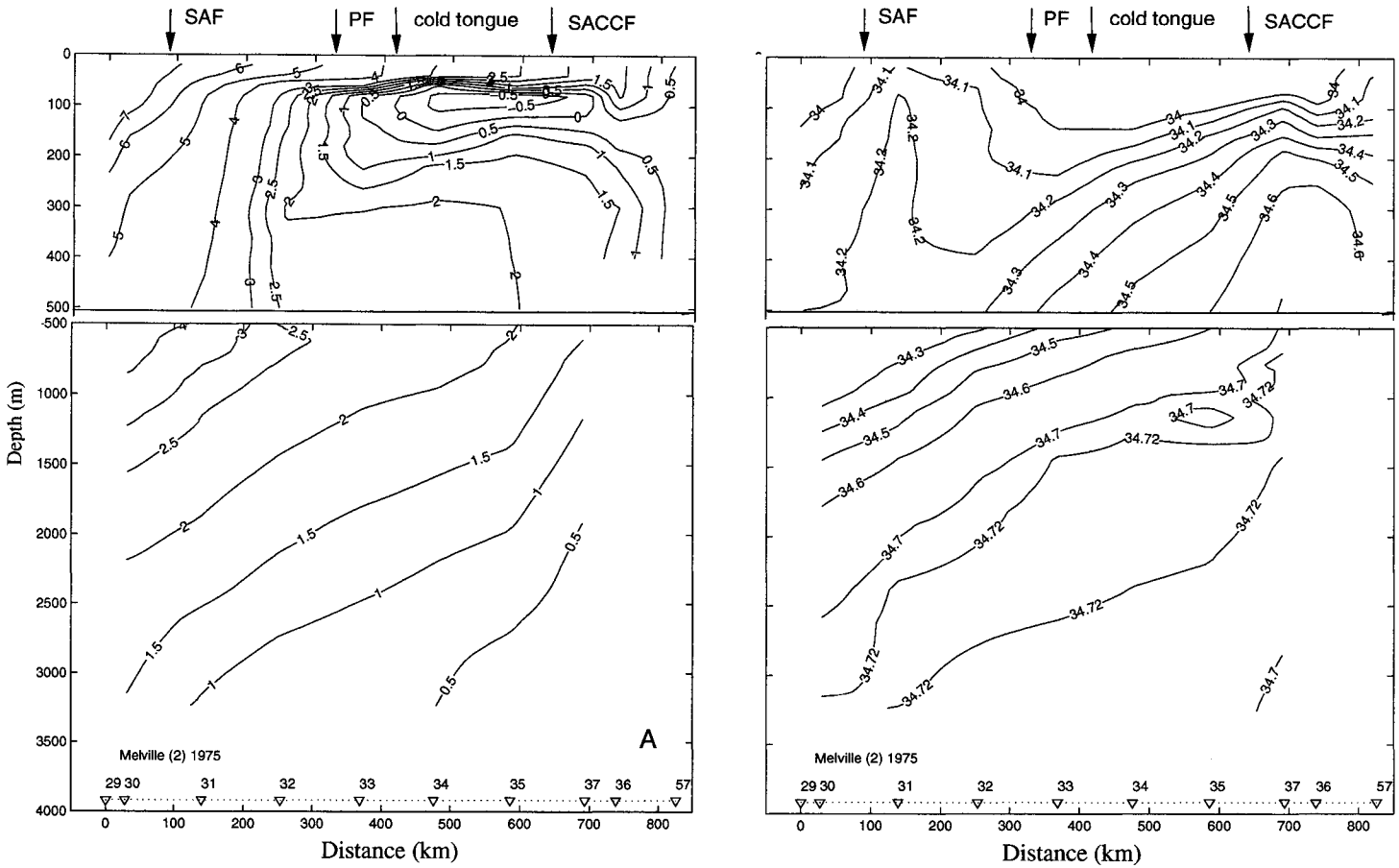

Fig. 16. A) Observed potential temperature and B) observed salinity from the Melville cruise section III, February 1975. Contour intervals are 0.5°C and 0.05 for temperature and salinity, respectively and arrows indicate locations of the SAF, PF, SACCF, and a cold tongue. Station locations along the transect are shown by ▽. Note vertical scale change in upper and lower panels.

the simulated flow is quantified calculating the eddy kinetic energy distribution and comparing it to observations.

Hydrographic Data

Circulation model results are compared to hydrographic data from the Scotia Sea, e.g. the World Ocean Circulation Experiment (WOCE) Section A23 (Heywood and King, 1996). During the A23 cruise eighteen vertical conductivity-temperature-depth (CTD) profiles, 73 stations with expandable bathythermograph (XBT) and chlorophyll *a* data on one specific transect (cf. Fig. 5) across the Scotia Sea close to South Georgia were obtained (Heywood and King, 1996) (Fig. 15).

Other hydrographic data sets are available from several cruises across the Drake Passage, generally from Cape Horn to Livingston Island (Table 9). To assess the accuracy of the simulated temperature and salinity distributions, comparisons are made with the vertical property distributions for WOCE A23 (Fig. 15) and Melville section III (Fig. 16).

Table 9. Summary of conductivity-temperature-depth recorder (CTD), and expandable bathythermograph (XBT) data sets that can be used to validate the simulated circulation distributions.

Source	Data	Type	Coverage	Duration
WOCE	Hydrography	CTD, XBT	Scotia Sea	03-05/1995
WOCE/TOGA		Drifter	Scotia Sea	1991, 1996
FGGE	Drifter		Scotia Sea	1978-1979
Meteor cruise	Hydrography	CTD, XBT	Drake Passage	01/1990
Thompson cruises	Hydrography	CTD, XBT	Drake Passage	02/1976
Melville cruises	Hydrography	CTD, XBT	Drake Passage	02-03/1975
Conrad cruise	Hydrography	CTD, XBT	Drake Passage	02/1975

References: WOCE A23 (Heywood and King, 1996), FGGE (Patterson, 1985), Meteor cruise (Röther et al., 1993), Thompson cruises (Sievers and Nowlin, 1984), Melville cruises (Sievers and Nowlin, 1984), Conrad cruise (Gordon et al., 1977)

Drifter Data

In addition, data from the World Ocean Circulation Experiment/Tropical Ocean Global Atmosphere (WOCE/TOGA) drifters are available (Table 10). In the time

Table 10. Name, drifter type, latitude and longitude of release locations for WOCE drifters used in this study.

Drifter	Drifter Type	Latitude (°S)	Longitude (°W)
WOCE22045	surface	57.839	59.877
WOCE22046	surface	62.216	56.717
WOCE22047	surface	61.471	57.005
WOCE22048	surface	59.417	57.533
WOCE22049	surface	60.417	57.002
WOCE22050	surface	56.245	63.014
WOCE22108	surface	53.279	46.362
WOCE22591	surface	53.445	40.118
WOCE22594	surface	49.704	40.003
ALACE 11	subsurface	56.937	68.245
ALACE 17	subsurface	57.372	68.240
ALACE 18	subsurface	58.168	68.243
ALACE 19	subsurface	57.372	68.240
ALACE 20	subsurface	58.485	68.250
ALACE 21	subsurface	57.868	68.208
ALACE 22	subsurface	58.825	68.253
ALACE 26	subsurface	59.155	68.257
ALACE 204	subsurface	58.268	68.818
ALACE 205	subsurface	56.961	76.330
ALACE 209	subsurface	59.213	78.782
ALACE 211	subsurface	57.702	76.247
ALACE 217	subsurface	57.422	76.177
ALACE 250	subsurface	59.680	78.756
ALACE 290	subsurface	56.984	77.771
ALACE 297	subsurface	55.849	78.714
ALACE 298	subsurface	60.028	78.857
ALACE 299	subsurface	57.459	76.777

from 1991 to 1996, 388 surface and subsurface drifters were released in the Southern Ocean and their position tracked over time (WOCE, 1996) and a select number of these drifters (Table 10, Fig. 17) are used in this study to validate the simulated drifter results. The results of the simulated drifters are then compared with the observed drifter paths and speeds available from the WOCE database (WOCE, 1996). A total of nine surface (50 m) and 18 subsurface (1000 m) drifters were chosen (Table 10) for comparison with the simulated drifter results because of the spatial coverage across the Drake Passage and along the western Antarctic Peninsula (Fig. 17) that they provide. In 1978/1979, 316 satellite-tracked drifting buoys were successfully deployed in the Southern Ocean as part of the First GARP (Global Atmospheric Research Program) Global Experiment (FGGE). Results from these drifter studies, as discussed in Patterson (1985) are also used to validate simulated drifter results.

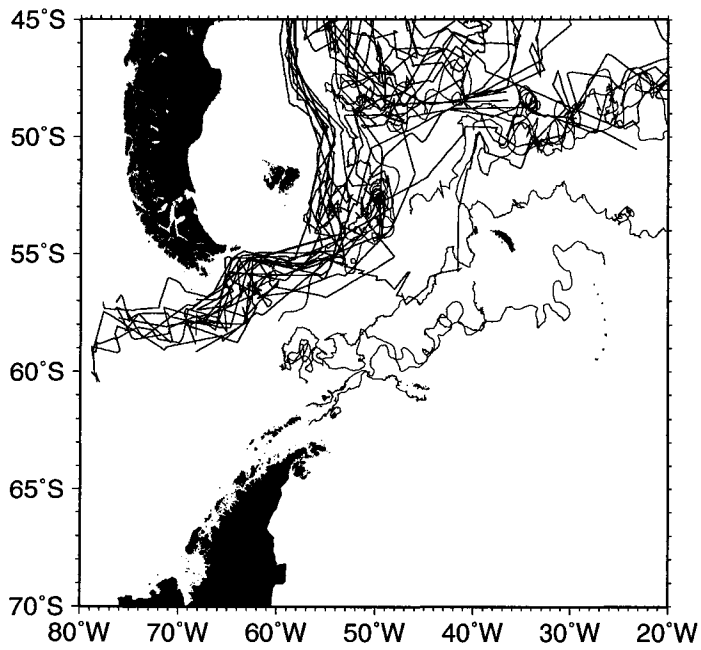

Fig. 17. Drifter trajectories from 27 WOCE/TOGA surface and subsurface drifters used in this study.

Eddy Kinetic Energy

The eddy kinetic energy distribution of the simulated flow at 50 m depth on model

day 180 was calculated and compared to the surface eddy kinetic energy calculated from observations made during FGGE (Patterson, 1985). The 50 m depth corresponds to the depth at which the drifters are released in the circulation model and day 180 (30 March) corresponds to the time when the model has finished spinning up. Kinetic energy (KE) is calculated as

$$KE = \frac{\bar{u}^2 + \bar{v}^2}{2}, \tag{22}$$

where $\bar{u}$ and $\bar{v}$ are the time-averaged simulated horizontal velocities (m s^{-1}). The kinetic energy field is the mean distribution of kinetic energy over a total of 300 days of the model run. The first two months of spin-up time are excluded in the time averaging so that changes in the velocity associated with the model spin-up do not affect the kinetic energy calculation. The eddy kinetic energy (EKE) is calculated as follows

$$EKE = \frac{u'^2 + v'^{2\prime}}{2} \tag{23}$$

where u' and v' are the difference between the simulated velocity at model day 180 and the mean simulated velocity ($u' = u - \bar{u}$, $v' = v - \bar{v}$).

3.5.2 Validation of krill growth model

Krill length-frequency distribution and estimates of krill biomass are two quantities that can be compared to results from krill growth simulations along simulated drifter paths. Krill distribution data from the Scotia Sea and South Georgia regions are needed to compare krill growth model results, and to determine whether krill distributions derived from the simulated drifter results and the krill growth model, match observations.

Data sets from the *Discovery* expeditions (Marr, 1962), the BIOMASS program (Thorley and Trathan, 1994), the LTER program (Lascara, 1996a, 1996b; Lascara, 1999), German expeditions to the Antarctic Peninsula (Siegel, 1985; 1988; 1989; 1992), and the British Antarctic Survey (BAS) krill surveys around South Georgia from hydro-acoustic measurements, net hauls and predator data (Reid et al., 1996; Hill et al., 1996; Croxall et al., 1999; Reid et al., 1999a, 1999b; Watkins, 1999; Watkins et al., 1999) are adequate for initialization and validation of drifter simulations with the circulation model and krill growth model simulations. These data sets

Table 11. Source, type, collection method, and space and time coverage of krill data sets available for this study. Western Antarctic Peninsula and South Georgia are abbreviated as WAP and SG, respectively.

Source	Data Type	Method	Spatial Coverage	Time Coverage
BIOMASS	Biomass	hydro-acoustics	Southern Ocean	1980-1985
	Length-frequency	net tows	(WAP, SG)	1980-1985
	Chlorophyll *a*			1980-1985
Discovery	Length-frequency	net tows	Southern Ocean	1926-1940
Report				
LTER	Biomass	hydro-acoustics	WAP	1991, 1993
	Length-frequency	net tows	WAP	1991, 1993
	Chlorophyll *a*	BOPS	WAP	1991, 1993
German	Biomass	net tows	WAP	1977-1990
cruises	Length-frequency	net tows	WAP	1977-1990
BAS	Length-frequency	net tows, hydro-acoustic	SG	1981-1997
	Length-frequency	predator data	SG	1986, 1991-1997

References: BIOMASS (Thorley and Trathan, 1994), *Discovery* Report (Marr, 1962), LTER (Lascara, 1996; Lascara et al., 1999), German cruises (Siegel, 1985; 1988; 1989; 1992), BAS (Reid et al., 1996; Hill et al., 1996; Croxall et al., 1999; Reid et al., 1999a; 1999b; Watkins, 1999; Watkins et al. 1999)

include length-frequency distributions and krill biomass estimates in the Antarctic Peninsula, Scotia Sea, and South Georgia regions (Table 11).

Discovery Data

The earliest and most comprehensive studies on krill distributions are discussed in the *Discovery* Reports, especially that by Marr (1962). Over the course of 14 years, beginning in 1926, extensive data were obtained on krill behavior, life cycle, and length-frequency distribution at 12,461 stations from 7339 vertical and 5122 horizontal and oblique net tows, respectively. The data cover the whole Southern Ocean, and include a concentration of stations in the South Georgia and Bransfield Strait regions. This data set provides length-frequency distributions throughout the study area (Fig. 18). The length-frequency data were extracted from Marr (1962) by scanning the relevant figures into a computer and digitizing the location of each data point. The resultant data set was then quality controlled to ensure accuracy.

Biomass Data

The objective of the BIOMASS program was to understand the structure and dynamics of the Antarctic marine ecosystem as a basis for the exploitation of potential living resources (El-Sayed, 1977). This was done by conducting three large, international field studies focused on the Antarctic Peninsula and Prydz Bay regions of the Southern Ocean (First International BIOMASS Experiment - FIBEX, Second International BIOMASS Experiment - SIBEX1 and SIBEX2). These studies were designed to quantify the standing stock and productivity of krill populations (El-Sayed, 1994). Field experiments were conducted from 1980-1985 (Table 11), and most data were collected during the summer months. Sampling in the area of interest for this study covered the region extending from Anvers Island northeast to South Georgia and encompassing Bransfield Strait, the South Shetland Islands, Elephant Island and the Weddell/Scotia Confluence (Thorley and Trathan, 1994). The BIOMASS data set contains hydro-acoustic survey data, net haul data comprising krill length-frequency data, bird observation data, and oceanographic data including CTD and chlorophyll *a* data. Although 1093 stations were sampled, equivalent data sets were not obtained at all locations, due to various circumstances during the different cruises. It is the length-frequency data of krill that is most important for comparison with results from this study (Fig. 19).

The three international field studies that were part of BIOMASS were undertaken throughout the 1980s. FIBEX took place from January to March 1981, while SIBEX1 took place in November to December 1983, and SIBEX2 from January to March 1985, with the exception of one cruise on the research vessel *Polarstern* (PSS2) which took place from October to December 1984, earlier than the rest of the SIBEX2 cruises. The length-frequency data is analyzed separately for each of the three field studies, with the exception of the length-frequency data from the PSS2 cruise, which is analyzed together with the SIBEX1 cruises. The sampling locations occupied during the three field studies (Fig. 20) were sub-divided into seven regions for analysis and comparison with the krill growth simulations. The krill length-frequency distribution from each sub-region (Figs. 21-23) provides the comparison with the simulated length-frequency results described in section 4.

Long Term Ecological Research Data

The LTER program was established in 1990 to document interannual and seasonal variations in the pelagic marine ecosystem within continental shelf waters west of the

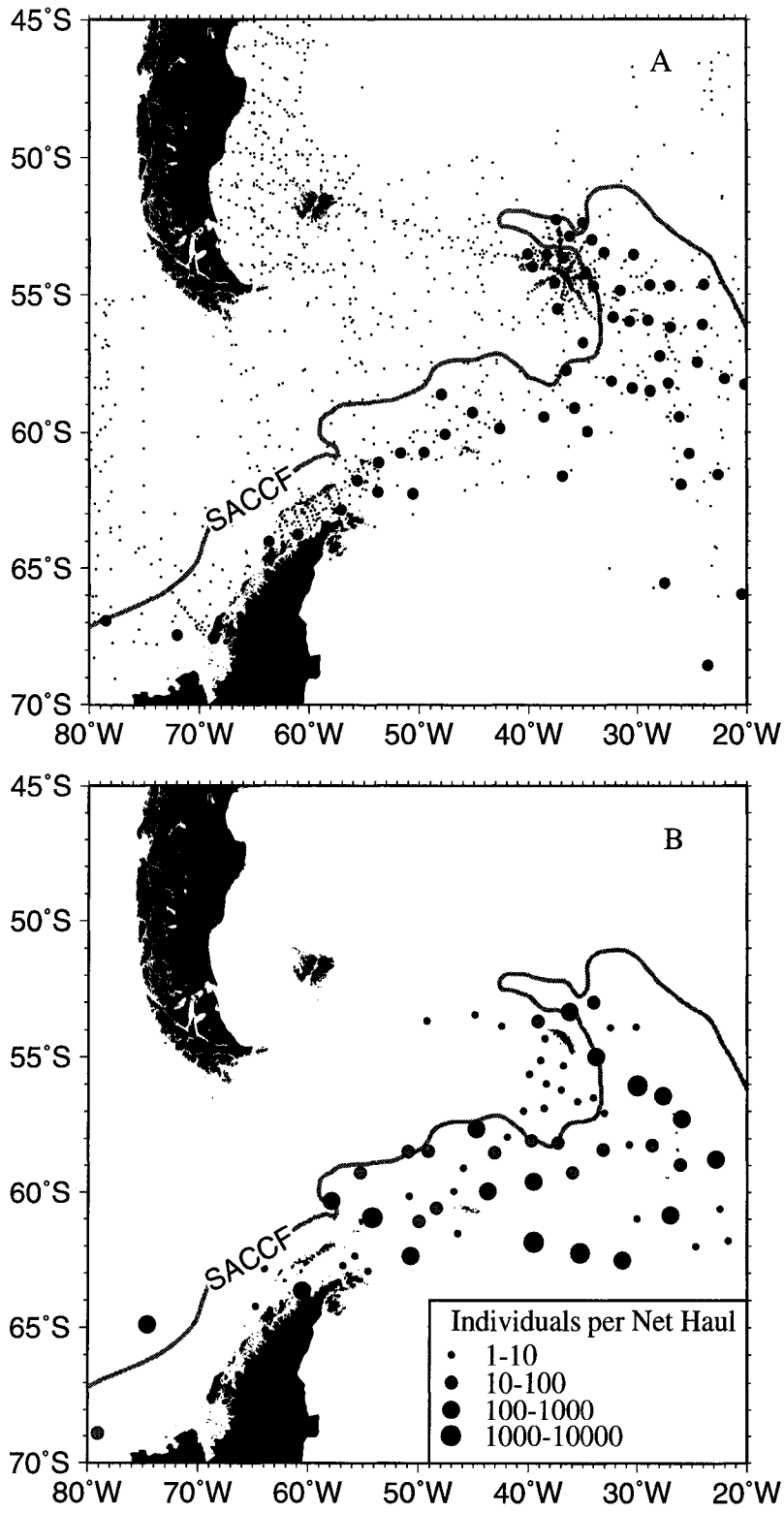

Fig. 18. Distribution of Antarctic krill A) surface larvae and B) older krill (>20 mm) in summer (January to March) across the study region extracted from net haul observations obtained during the *Discovery* Investigations, 1926-1940 (Marr, 1962). The heavy line shows the southern Antarctic Circumpolar Front (SACCF) as given in Orsi et al. (1995). The small dots in the upper panel indicate the distribution of the sampling locations.

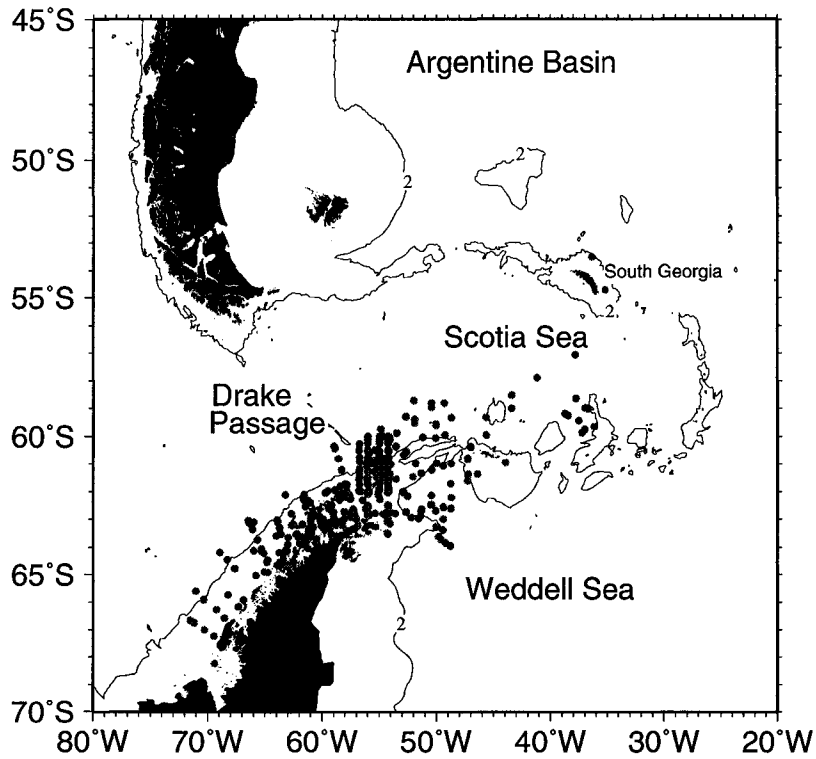

Fig. 19. Locations of the length-frequency measurements of Antarctic krill, acquired during BIOMASS, in the study region (Thorley and Trathan, 1994). The thin line represents the 2000-m isobath.

Antarctic Peninsula (Smith et al., 1995). The LTER cruises spanned all seasons and provided multidisciplinary observations, thus constituting a unique Antarctic data set for that region. Hydro-acoustic measurements and net collections examined the seasonal variability of krill distributions, abundances and population structure west of the Antarctic Peninsula (Lascara et al., 1999). Research cruises are still ongoing and portions of the data sets are available. Hydro-acoustic measurements of krill biomass and net tows were made at 161 stations (Table 11), where the echo sounder was towed below the surface along short transects (1-2 km) in conjunction with net tows (Lascara et al., 1999). For the purpose of this study, the length-frequency distribution of krill as given in Lascara (1996) and Lascara et al., (1999) are used for comparison with model results.

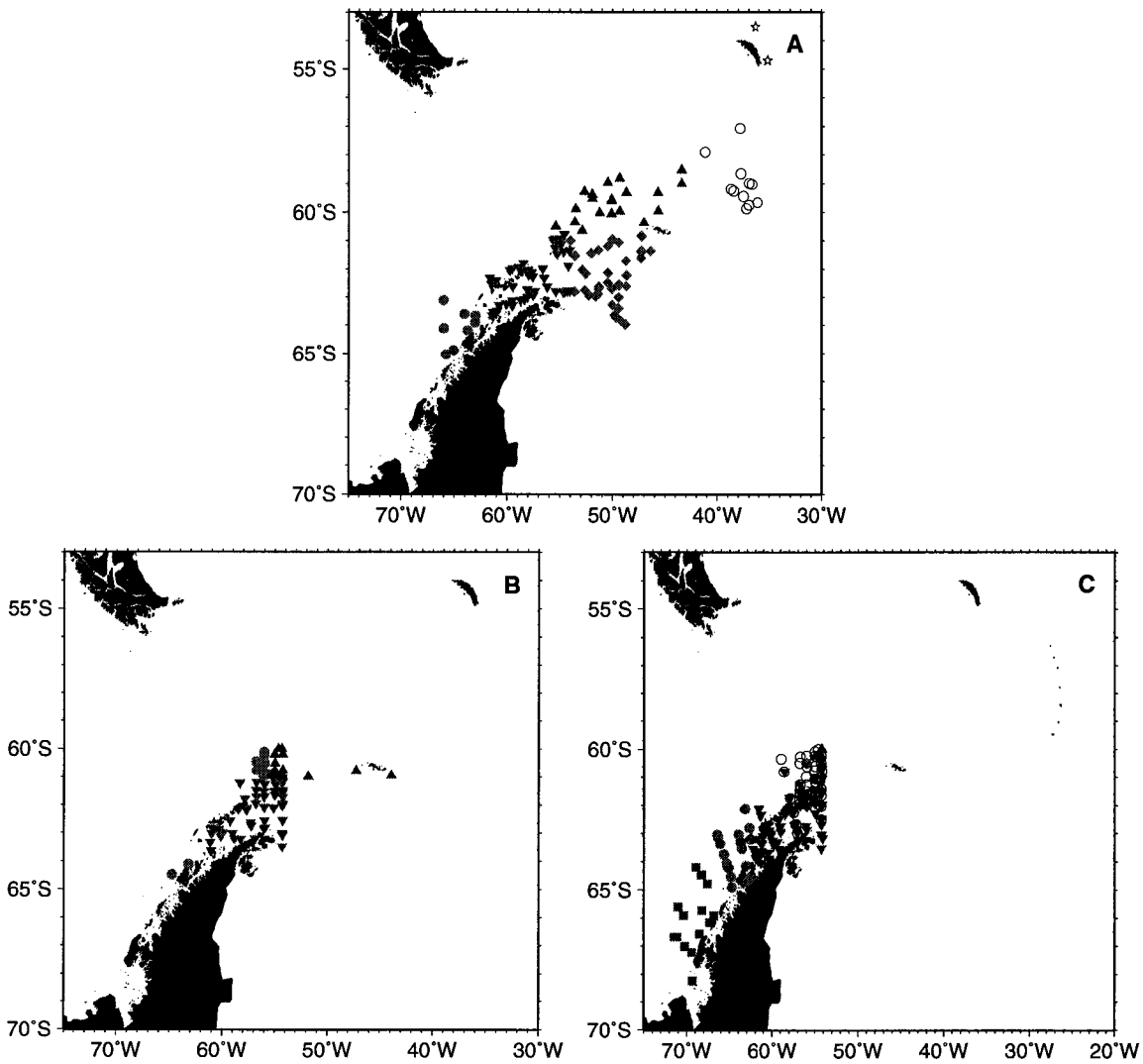

Fig. 20. Locations of Antarctic krill length-frequency measurements from A) FIBEX cruises (January - March 1981), B) SIBEX1 cruises (November - December 1984), C) SIBEX2 cruises (January - March 1985). The measurements in the seven sub-regions used for comparison with the results of the krill growth simulations are designated as: region 1 - west Antarctic Peninsula (•); region 2 - Bransfield Strait (▼); region 3 - Scotia Sea/Elephant Island (▲); region 4 - southwest Antarctic Peninsula (■); and region 5 - Weddell Sea (♦); open Scotia Sea (○) ; and) South Georgia (⋆). Note that the locations of PSS2 stations are shown in panel C by (○).

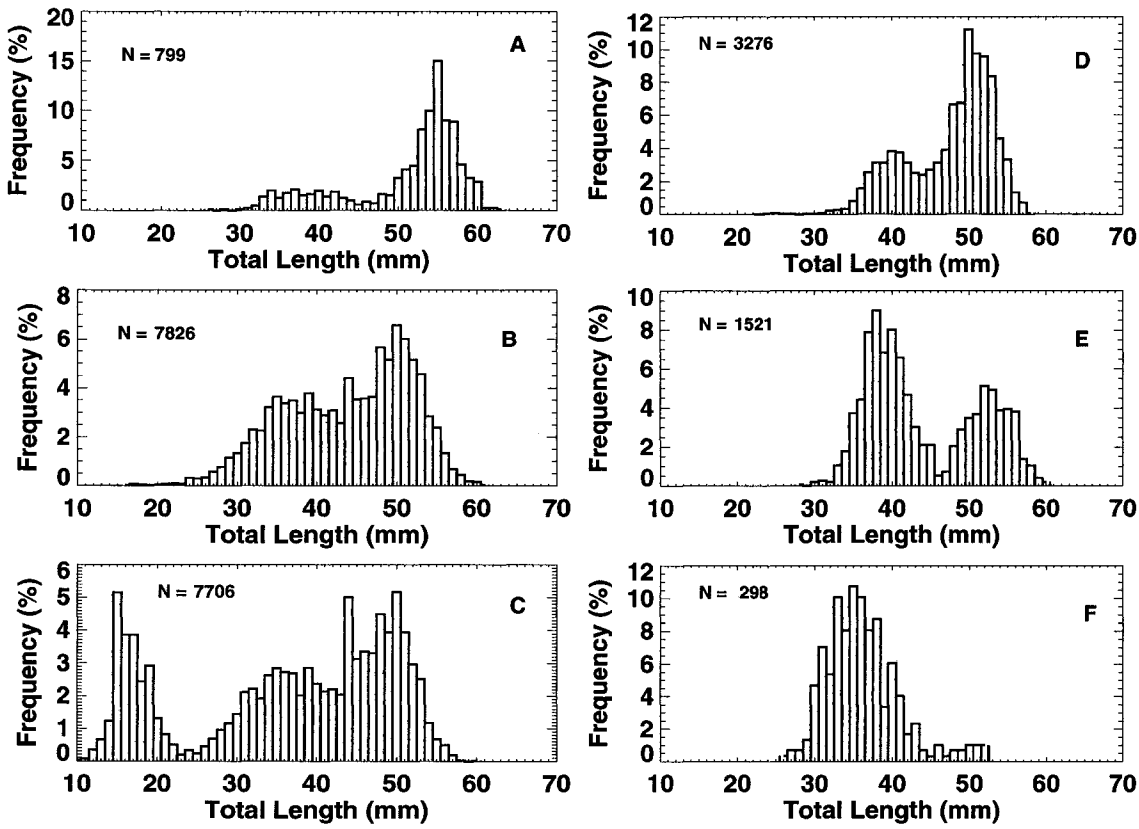

Fig. 21. Summarized length-frequency distributions for Antarctic krill from measurements made during the FIBEX cruises (January - March 1981) for A) west Antarctic Peninsula, B) Bransfield Strait, C) Weddell Sea, D) Elephant Island/Scotia Sea region, E) open Scotia Sea, and F) South Georgia regions. The regions are designated in Figure 20A. The total number of krill individuals, N, sampled in each area is shown.

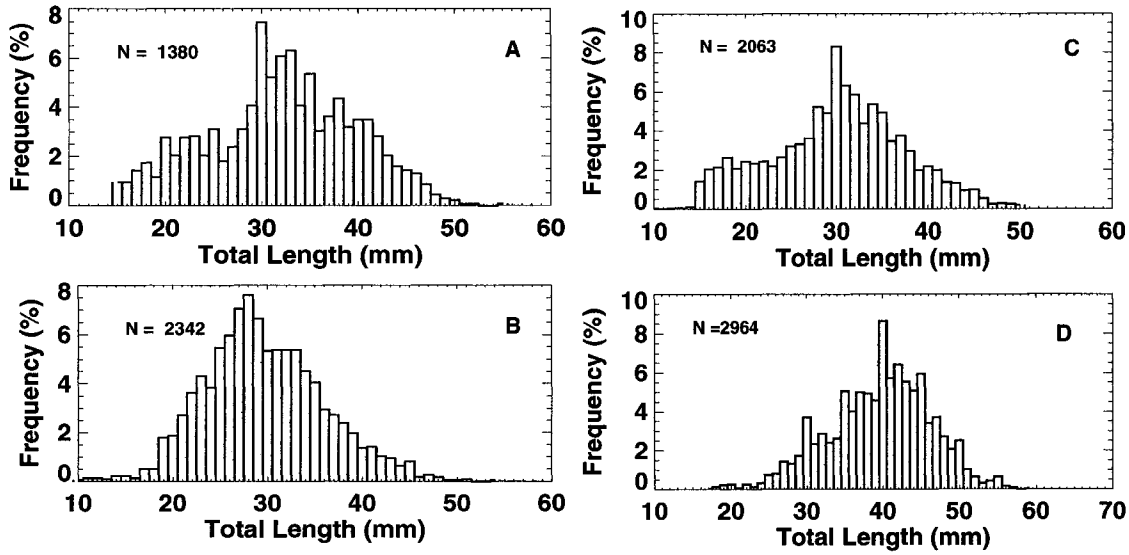

Fig. 22. Summarized length-frequency distribution of Antarctic krill from measurements made during the SIBEX1 cruises (October - December 1983) for A) west Antarctic Peninsula, B) Bransfield Strait, C) Elephant Island/Scotia Sea region, and D) PPS2 (November-December 1984) regions. The regions are designated in Figure 20B. The total number of krill individuals, N, sampled in each area is shown.

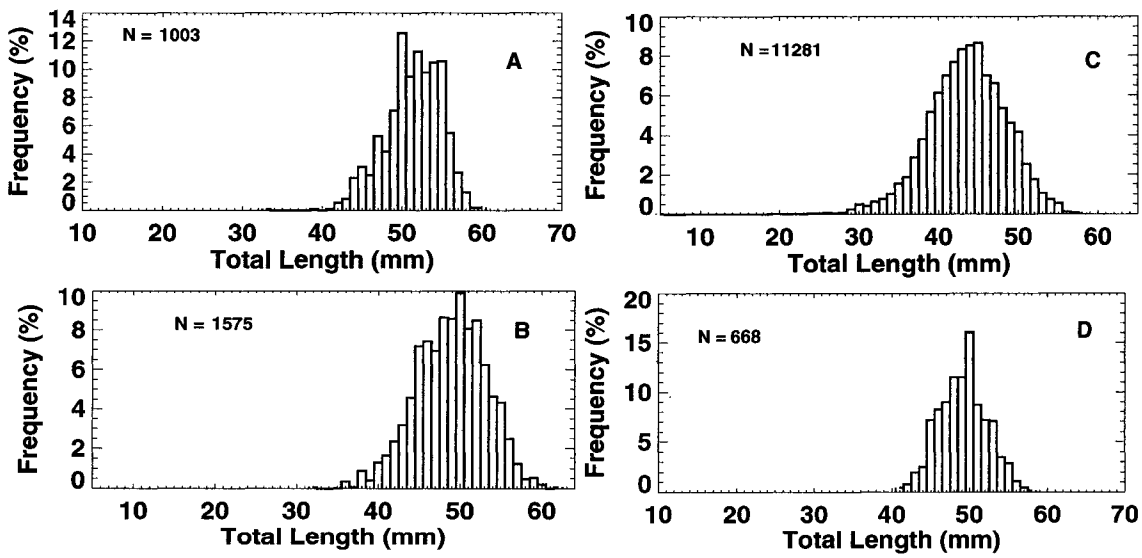

Fig. 23. Length-frequency distribution of Antarctic krill during the SIBEX2 cruises (January - March 1985) compiled for A) southwestern Antarctic Peninsula, B) west Antarctic Peninsula, C) Bransfield Strait, D) Elephant Island/Scotia Sea region. The regions are designated in Figure 20C. The total number of krill individuals, N, sampled in each area is shown.

German Cruise Data

From 1977 to 1990 the Federal Republic of Germany undertook ten expeditions in the months from October to June along the Antarctic Peninsula, which included net tows for krill sampling that covers almost all seasons (Siegel, 1988). Detailed descriptions of these cruises can be found in Siegel (1985; 1988; 1989; 1992), and they are summarized in Table 11. An important advantage of this data set is that standard fishing gear and standardized methods were used throughout (Siegel, 1988). Overall 700 stations were sampled during these cruises, but three cruises (February/March 1981, October/November 1983, March/April 1985) were part of the BIOMASS cruises and are therefore already included in the above data set. The results from the most recent sampling of krill in this area are given in Siegel et al. (2002). These studies provide valuable data on the length-frequency distribution of krill and are used for model validation.

British Antarctic Survey Cruise Data

The British Antarctic Survey carried out 11 surveys at South Georgia between 1981-1997 as part of their Core Programme (Table 11, Watkins et al., 1999), sampling locations mostly inside defined survey boxes: East Core Box located to the east of the Island, and West Core Box located to the north of the Island (Fig. 24). The cruises were mainly carried out in the months of January and February of different years, and the results of net hauls from seven of these cruises are described in detail in Watkins (1999) and Watkins et al. (1999).

In addition net haul data and krill length-frequency data from macaroni penguins (*Eupdyptes chrysolophus*) during the month of February (Hill et al., 1996), fur seal (*Arctocephalus gazella*) and macaroni penguin data of krill length-frequency from December to March 1997/1998 (Reid et al., 1999a; 1999b), predator data and net haul data from February 1986 (Reid et al., 1996), and predator data during the breeding seasons 1986 and 1994 (Croxall et al., 1999) are available (Table 11) for comparison with the simulated length-frequency distribution of Antarctic krill.

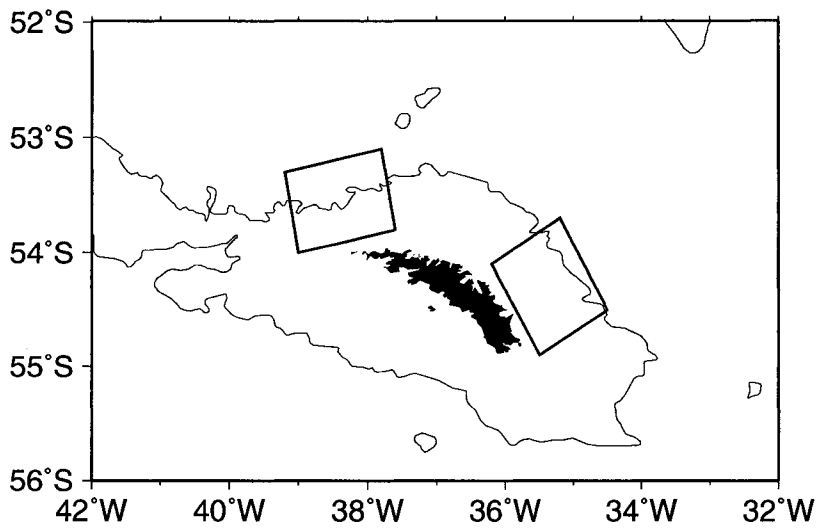

Fig. 24. Location of the British Antarctic Survey Core Programme survey boxes near South Georgia after Watkins (1999). The thin line represents the 2000-m isobath.

4 RESULTS

The circulation model and the krill growth model together with the different food time series described in the previous section, are used to test factors that permit survival of krill during transport across the Scotia Sea to South Georgia. Therefore, the first effort consists of developing simulations of the circulation in the Scotia Sea and comparing the simulated circulation distributions to available data to determine the validity of the fields. Following this, drifter trajectories obtained using the simulated circulation fields are described and are used to determine krill transport patterns across the Scotia Sea. The food supply along the drifter trajectories is next used to determine the fate of Antarctic krill as they are moved across the Scotia Sea by the prevailing circulation.

4.1 Reference Simulation

Basic Circulation Structure

The circulation model with the configuration discussed in section 3, was run from 1 October 1992 to 30 September of the following year. The initial barotropic stream function (Fig. 25A) shows general northeastward flow through Drake Passage and across the Scotia Sea. The transport through Drake Passage is approximately 150 Sv and is separated into three bands, designated by the closely spaced streamlines, which indicate strong flow. These are the three frontal regions, the SAF, PF, and SACCF, of the ACC. The SAF is defined by the closely spaced of streamlines, indicating transport of about 50 Sv, in the north of Drake Passage close to the tip of South America. The SAF turns north just after Burdwood Bank to flow north through a channel between Burdwood Bank and the North Scotia Ridge (cf. Fig. 1) towards the Falkland Islands. At the northern boundary of the model domain, the SAF makes a sharp right turn and flows along 48°S to exit the domain to the east (Fig. 25A). The PF flows parallel to the SAF and turns northeast to flow through a channel in the North Scotia Ridge (53°S, 48.5°W) east of the SAF. The PF has a transport of approximately 30 Sv as shown by the three closely spaced streamlines defining the front. The front diverges and part of it joins flow with the SAF further north, while the rest of the flow is to the east, passing South Georgia to the south, exiting the model domain. Some flow from the SAF diverts north through the same channel as the PF (Fig. 25A).

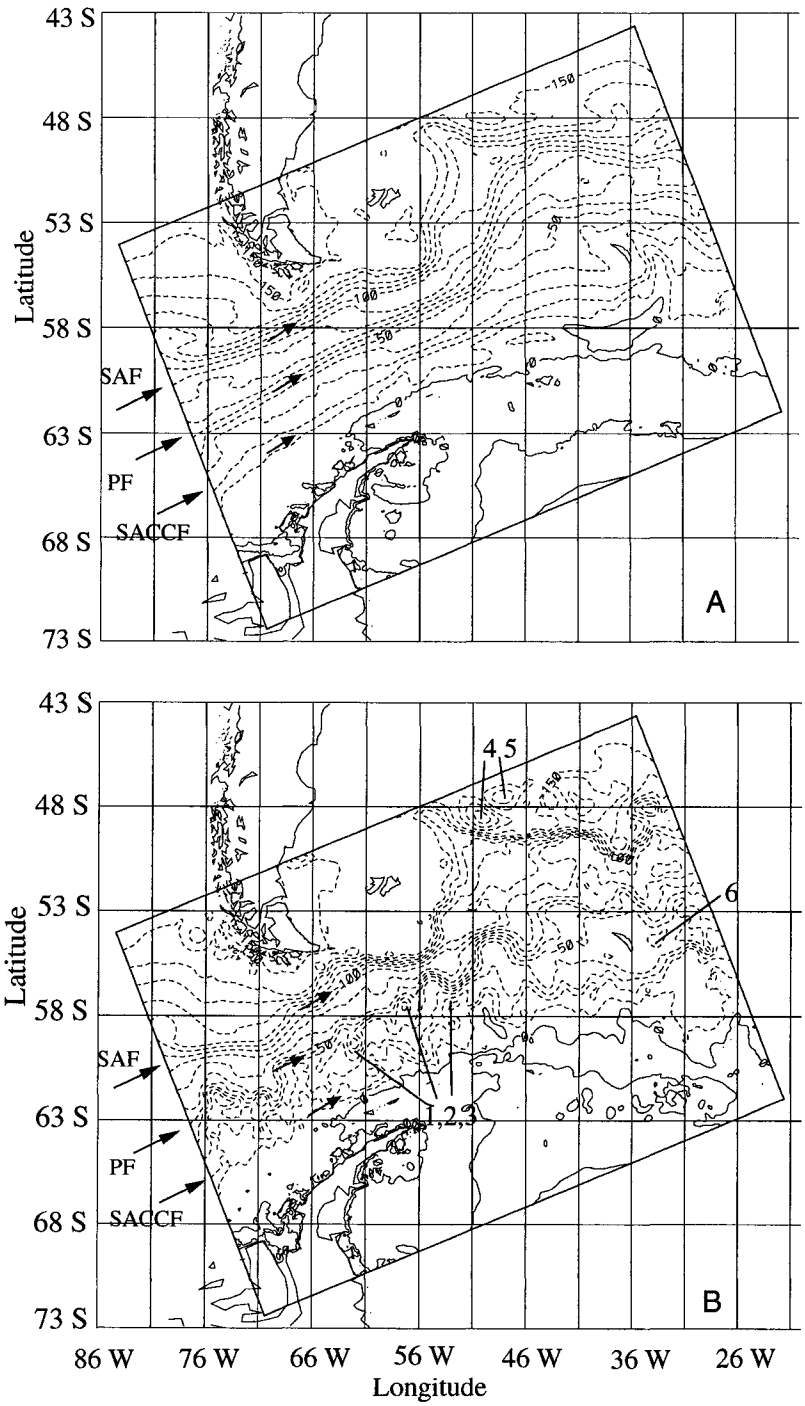

Fig. 25. Barotropic streamfunction (Sv) A) at the start of the simulation (1 October) and B) after 180 days of simulation (30 March). Contour interval is 10 Sv. The direction of the flow is indicated by the arrows. Locations of the Subantarctic Front (SAF), the Polar Front (PF), and the Southern ACC Front (SACCF) are indicated by the large arrows, and the rotated rectangle shows the extent of the model domain. The numbers 1 to 6 mark eddies, which are discussed in the text.

The streamline spacing shows the least number of streamlines associated with the SACCF compared to the other fronts, indicating that it has a transport of approximately 10 Sv (Fig. 25A). The SACCF flows close to the west Antarctic Peninsula continental shelf, parallel to the other two fronts. This front continues its path to the northeast across the Scotia Sea turning north to flow along the east coast of South Georgia and turning east after passing South Georgia. The northern limb of the Weddell Gyre intrudes into the model domain at the southern model boundary at 51°W.

After 180 days of simulation (30 March) considerable mesoscale variability has developed in the simulated circulation distribution (Fig. 25B). The SAF shows closer spaced streamlines through the channel east of Burdwood Bank (cf. Fig. 1) indicating stronger flow through the channel than at the start of the simulation (Fig. 25A). Part of the flow is still diverging and flowing through the channel further east, together with the PF. The PF shows considerable meandering throughout its whole path, with a few visible eddy formations, and accelerated flow through the channel connecting the Scotia Sea with the Malvinas Chasm. The SACCF shows considerable meandering as well. The streamlines move northeast across the Scotia Sea and exit the model domain to the east without turning northward to flow along the east side of South Georgia. In addition, a small fraction of the SACCF combined with flow from the PF, moves east across the Scotia Sea and before reaching South Georgia turns to flow north and then eastward, exiting the model domain to the east of South Georgia.

Overall, the simulated surface circulation matches observations well, with northeastward flow through Drake Passage that is characterized by the banded structure of high speed frontal locations. The locations of the three fronts match observations (cf. Fig. 1), and the locations of the Weddell Gyre and the Weddell Scotia Confluence, where Weddell Sea waters meet Scotia Sea waters, also match observed locations. The transport through Drake Passage, the Weddell Gyre and the Brazil Current are close to the observed transport discussed in section 2.1.1 (Table 1). In addition mesoscale variability that has been observed as described in section 2.1.2, is found in the simulated surface circulation.

Eddy Kinetic Energy Distribution

To quantify the mesoscale variability of the flow in the circulation model, the eddy kinetic energy distribution of the flow at 50 m after 180 days of simulation

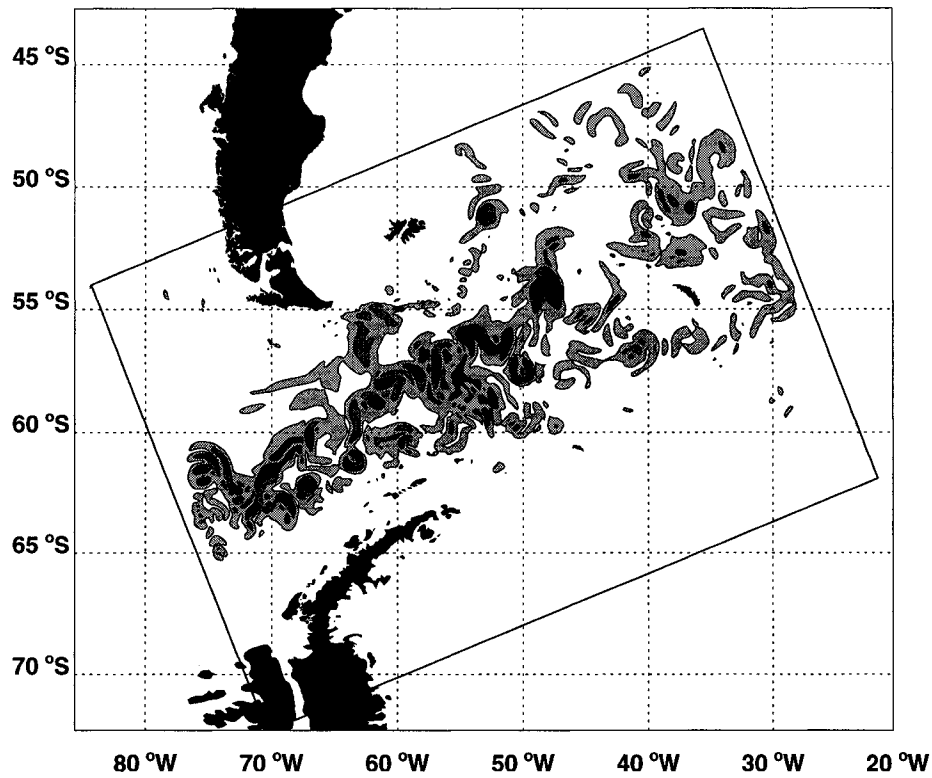

Fig. 26. Eddy kinetic energy (cm^{-2} s^{-2}) on day 180 of the reference simulation (March 30). Contours are shown for 50-250 cm^{-2} s^{-2} (light shading), 250-500 cm^{-2} s^{-2} (medium shading), and >500 cm^{-2} s^{-2} (dark shading).

(Fig. 26) was calculated and compared to the surface eddy kinetic energy calculated from observations made during FGGE (Patterson, 1985) to assess the realism of the simulated surface variability. The simulated circulation after 180 days (30 March) shows that the eddy kinetic energy is especially high in the flow associated with the PF and SACCF (Fig. 26), which meander and create a strong eddy kinetic energy field throughout Drake Passage and the Scotia Sea. The PF produces a strong eddy kinetic energy field over and to the north of the channel connecting the Scotia Sea and the Malvinas Chasm. The pattern of eddy kinetic energy across the Scotia Sea shows an increase that extends northward prior to reaching South Georgia that then moves eastward around the Island. This pattern arises mainly from variability associated with the PF. The variability associated with the SACCF accounts for the band of enhanced eddy kinetic energy that occurs south of South Georgia. Close to the Island, eddy kinetic energy is small, but increases to the north where strong

topographic features are encountered (cf. Fig. 5). Increased eddy kinetic energy occurs where the SAF flows close to the continental shelf of South America, as well as where it flows over the channel between Burdwood Bank and the North Scotia Ridge (cf. Fig. 1) and to the north of this channel.

The eddy kinetic energy in the Scotia Sea shows an eastward extent, with values larger than 500 cm^{-2} s^{-2}. The analysis of the FGGE drifters given in Patterson (1985) show a region of eddy kinetic energy of >500 cm^{-2} s^{-2} in central Drake Passage, which extended to the east into the Scotia Sea, continued northward into the South Atlantic Ocean and followed the continental shelf of South America. Central Drake Passage is also where the eddy kinetic energy is concentrated in the simulated flow (Fig. 26). The simulated eddy kinetic energy values are lower than those given in Patterson (1985) and show only patches of kinetic energy >500 cm^{-2} s^{-2} in the Drake Passage and Scotia Sea. In the eastern Scotia Sea and around South Georgia, Patterson (1985) calculated values of 200-500 cm^{-2} s^{-2}. This is consistent with the simulated values which show lower eddy kinetic energy in this area as compared to Drake Passage.

Thus, the eddy kinetic energy field calculated from the simulated flow (Fig. 26) agrees in distribution and magnitude with the eddy kinetic energy field of the surface flow calculated from the FGGE drifting buoys (Patterson, 1985, Fig. 11a).

4.1.1 Comparison with Hydrography

The reliability of the simulated circulation patterns was determined by comparisons with the Melville section III and the WOCE A23 section described in section 3.5.1. The primary comparisons used in this study are the locations and strengths of the three fronts, the southward extent of the 2.0°C isotherm, and the position of the 2.0°C isotherm or the 34.4, 34.6 or 34.7 isohalines in the water column according to their association with different water masses. The 34.4 isohaline marks the extent of the AASW that is fresher than 34.4, and UCDW is defined by water saltier than 34.4 up to 34.7 (Orsi et al., 1995). Lower Circumpolar Deep Water (LCDW) is defined by salinities above 34.7 (Orsi et al., 1995).

The Melville cruise section III took place in February 1975. The vertical temperature and salinity distributions from this cruise (Fig. 16A,B) are compared to the equivalent simulated vertical distributions (Fig. 27A,B), which are obtained from the average property distributions for model days 130-150, which is equivalent to the

month of February. In general, the observed and simulated temperature and salinity vertical distributions compare well and have similar structures. The 2°C isotherm starts out at about 2400 m in the north of the simulated temperature section (Fig. 27A), which was observed in the Melville III section (Fig. 16A). It rises steeply, and intrudes into the colder water in the south about 550 km south of the north end of the simulated temperature section (Fig. 27A), which is 50 km less than in the observed temperature distribution (Fig. 16A). The 2°C isotherm then reaches the surface of the simulated temperature field (Fig. 27A) about 100 km north of where it is observed to shoal in the Melville III section (Fig. 16A). This is because the surface cold layer, with temperatures less than -0.5°C, seen in the Melville III section (Fig. 16A), is misrepresented in the simulated temperature field (Fig. 27A), indicating that processes necessary for the formation of this layer are missing in the model, as is discussed in detail in section 5.1.3. The observed cold tongue extends about 200 km to the north in the section and has its minimum temperature at 100 m (Fig. 16A). The simulated temperature distribution shows a similar cold tongue feature with the same temperatures and northward extent (Fig. 27A), but the minimum temperatures are found at the surface. The remaining isotherms in the simulated field match observations in starting depths and vertical distribution.

The 34.6 and 34.7 isohalines start at 2300 m and 2900 m at the northern part of the simulated salinity section (Fig. 27B), whereas the observations show these isohalines to start at 1800 m and 2600 m, respectively (Fig. 16B). The simulated isohalines rise towards the surface in the south of the section (Fig. 27B), consistent with the observations (Fig. 16B).

The locations of the three fronts in the ACC are clearly indicated by large horizontal property gradients (Nowlin and Clifford, 1982) and pronounced isopycnal tilt throughout the deep water column (Orsi et al., 1995). The simulated vertical temperature and salinity distributions (Fig. 27, see arrows) show locations of all three fronts that match observed front locations (Fig. 16, see arrows). The tilt in the simulated temperature and salinity distributions at the frontal locations is pronounced (Fig. 27) and matches the observed property gradients in the Melville III section (Fig. 16). For example, the 1.5°C isotherm rises 750 m in the SACCF in the Melville III section (Fig. 16A) and rises 700 m in the SACCF in the simulated temperature distribution (Fig. 27A).

The above comparisons show that for this region of the model domain the sim-

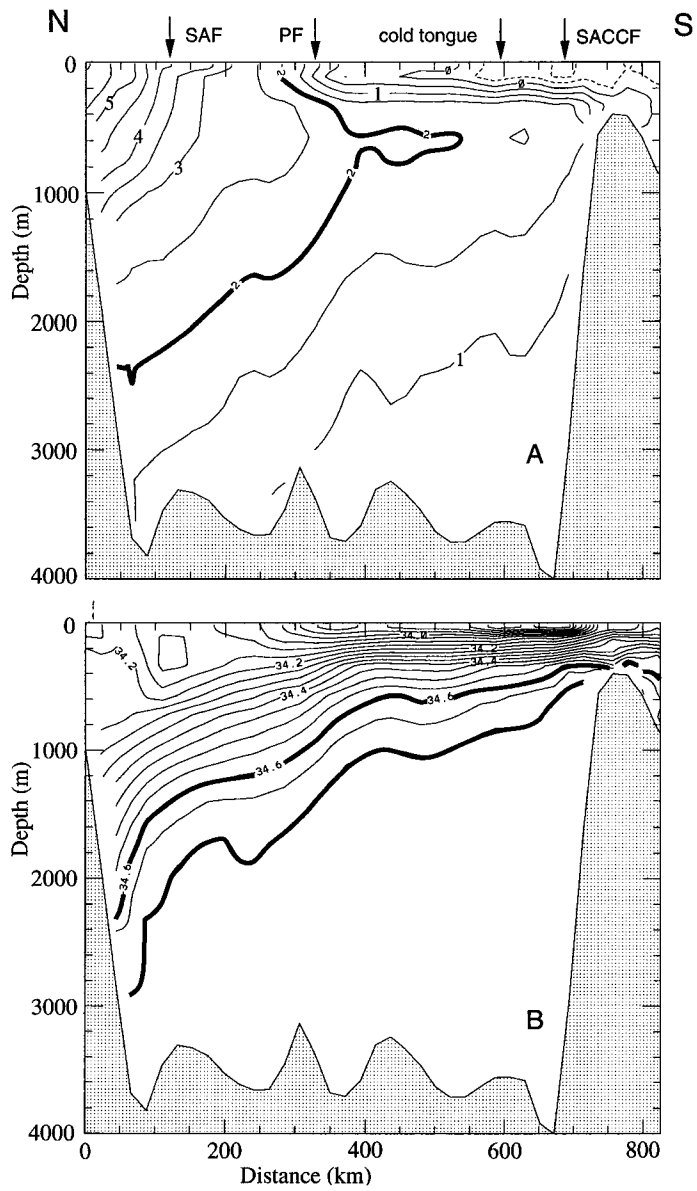

Fig. 27. Simulated A) temperature and B) salinity along the Melville III section obtained by averaging the model-derived distributions for days 130 to 150, which correspond to February. Contour intervals are 0.5°C and 0.05 for temperature and salinity, respectively. The thick lines mark A) the 2°C isotherm and B) the 34.6 and 34.7 isohalines. The dashed lines indicate negative temperatures. Arrows indicate the locations of the three fronts, the SAF, the PF, and the SACCF, and a cold tongue. The northern and southern ends of the section are indicated by N and S, respectively.

ulated water column structure matches observations with the exception of the cold tongue and the depth of the isohalines in the northern part of the section. The fronts are also well resolved in the simulated property fields and their positions match observations.

The WOCE A23 section, located in the eastern Scotia Sea near South Georgia, was obtained between March and May 1995. The vertical temperature and salinity distributions along this section (Figs. 15A,B) are compared to the equivalent simulated vertical distributions from the same time of the year (Figs. 28A,B). The WOCE A23 cruise track changed direction near South Georgia (cf. Fig 5), which makes direct comparison with the model results difficult. However, equivalent simulated vertical sections were derived by combining two sections to represent the WOCE A23 cruise track.

The 2°C isotherm starts out at 2300 m in the northern part of the simulated temperature distribution (Fig. 28A), which agrees with observations from the WOCE A23 cruise (Fig. 15A). It then rises steeply at the position of the PF, then slowly shoals and reaches the surface about 500 km south of where it shoals in the observations (Fig. 15A). The 1.0°C isotherm starts at 3000 m in the north of the simulated temperature section (Fig. 28A), which is also observed (Fig. 15A), and rises steeply to the PF and reaches 2000 m depth to the north of the topographic rise, at 800 km distance from the northern part of the section (Fig. 28A). In the WOCE A23 section the 1.0°C isotherm was observed to shoal to 1500 m (Fig. 15A). This isotherm then shoals to above 600 m at the location of the SACCF in the simulated temperature section (Fig. 28A) similar to observations (Fig. 15A).

The simulated location of the SACCF (Fig. 28, see arrows) is approximately 80 km further north than observed (Fig. 15, see arrows). The location of the PF in the simulated property fields (Fig. 28, see arrows) is moved about 100 km to the south of the observed location (Fig. 15, see arrows). The isotherms in the simulated temperature distribution (Fig. 28A) level out in the southern part of the section and even slightly decline, indicating a reversal in flow. This flow reversal results from an eddy spinning off the SACCF in this region and remaining south of the SACCF (Fig. 25). The observations show a strong feature with cold water centered around station 45 (Fig. 15). This is a cold core eddy, which is not seen in the simulated circulation fields. The weak tilt of the isotherms and isohalines in the simulated property fields (Fig. 28, see arrows) do not show the strong shear north of the PF

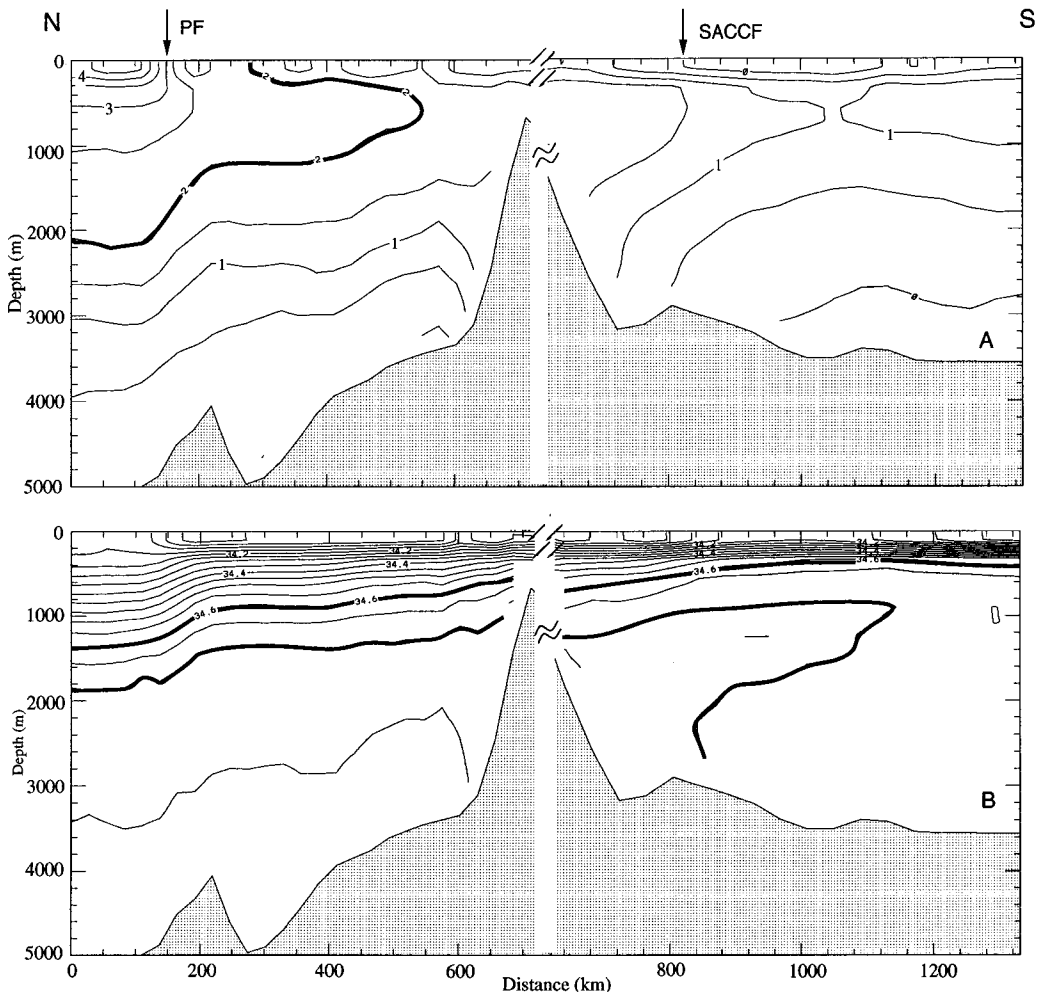

Fig. 28. Simulated A) temperature and B) salinity along the WOCE A23 section obtained by averaging the model-derived distributions for days 190 to 210, which correspond to April. Contour intervals are 0.5°C and 0.05 for temperature and salinity, respectively. The thick lines mark the 2°C isotherm (A) and the 34.6 and 34.7 isohalines (B). Arrows indicate the locations of two fronts, the PF and the SACCF. The northern and southern end of the section are indicated by N and S, respectively. Pairs of lines (//) indicate where the cruise tracks changed direction.

seen in the WOCE A23 section (Fig. 15A), and the simulated PF has a weaker temperature gradient than does the observed PF.

The 34.6 and 34.7 isohalines start at 1400 m and 1900 m in the simulated salinity field (Fig. 28B), respectively, and then rise in the PF, which matches the WOCE A23 section observations (Fig. 15B). The 34.6 isohaline shoals to 400 m at the southern end of the simulated salinity distribution (Fig. 28B), which is also observed. The tongue of water marked by the 34.7 isohaline rises across the whole section of simulated salinity and shoals as expected to approximately 1000 m, but protrudes 100 km further to the south than seen in the observations (Fig. 15B).

The above comparisons show that the simulated isotherms and isohalines are smoother than the observations because they have been averaged over the month of April. Also, the simulated vertical temperature structure shows isotherms that are deeper than observed and the PF is about 100 km further south and the SACCF is about 80 km to the north of observed positions.

4.1.2 Comparison with Climatology

In addition to comparing the simulated circulation patterns with observations of the Melville section III and the WOCE A23 section as described in section 4.1.1, the reliability of the simulated circulation patterns was determined by comparison with the climatology used to initialize the model, which is described in section 3.1.2. Again, the primary comparisons used are the southward extent of the 2.0°C isotherm, and the positions of the 2.0°C isotherm and the 34.4, 34.6 or 34.7 isohalines.

The temperature distribution of the annual climatology along the section that corresponds to the Melville II section shows that the 2°C isotherm starts at 2400 m in the north of the section (Fig. 29A), as observed in the Melville II section (Fig. 16A) and in the simulated temperature field (Fig. 27A). However, the representation of the cold tongue in the climatology differs from observations (Fig. 16A) because the climatology is constructed from an annual mean with a 1° resolution. The cold tongue appears in the climatology (Fig. 29A), but the northern extent is 300 km south of that seen in the observations (Fig. 16A), and the observed cold temperature of -0.5°C (Fig. 16A) is not present. In the simulated temperature field (Fig. 27A), the cold tongue extends to about 400 km from the north of the section and temperatures of -0.5°C are present.

The 34.6 isohaline starts at 1800 m in the northern part of the climatology section

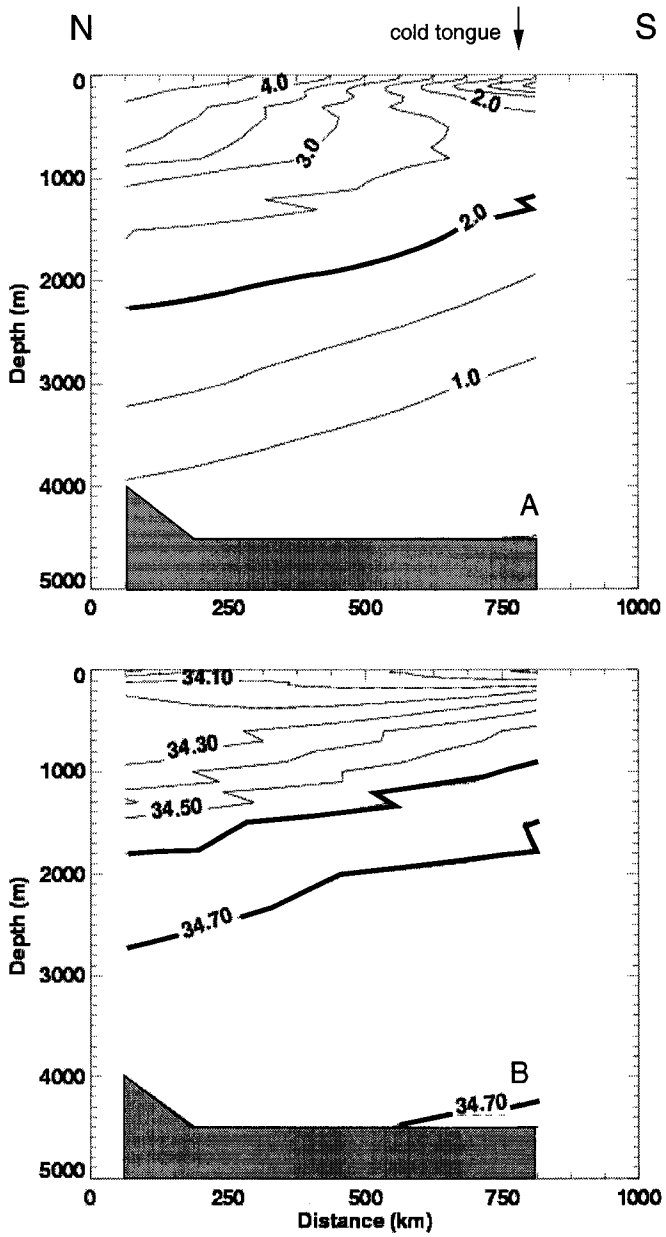

Fig. 29. Climatological observations of A) potential temperature and B) salinity along the Melville II section obtained from the WOA 1998 climatology. Contour intervals are 0.5°C and 0.1 for temperature and salinity, respectively. The thick lines mark the 2°C isotherm (A) and the 34.6 and 34.7 isohalines (B). Arrow indicates the location of the cold tongue.

(Fig. 29B), which agrees with the observations (Fig. 16B), while the simulated salinity field shows this isohaline to be at 2300 m (Fig. 27B). At the northern part of the climatology section the 34.7 isohaline starts at 2750 m (Fig. 29B), which is lower than the 2600 m that is observed (Fig. 16B). The simulated salinity distribution shows the isohaline starting at 2900 m in the north (Fig. 27B).

Comparison of the climatology temperature distribution from the section that corresponds to the WOCE A23 section to the simulated temperature field shows that the simulated 2°C isotherm (Fig. 28A) matches the location of this isotherm in the climatology (Fig. 30A). However, the simulated 2°C isotherm (Fig. 28A) shoals 500 km to the north of where this isotherm appears in the climatology. The 1°C isotherm starts at 3000 m in the simulated temperature field (Fig. 28A) and moves across the section similar to the 1°C isotherm in the climatology (Fig. 30A). However, the 1°C isotherm in the climatology shoals to about 1000 m in the southern part of the section (Fig. 30A) and part of it reaches the surface 75 km from the southern end, which matches observations (Fig. 15A). The simulated 1°C isotherm shoals to the same depth, but reaches the surface 500 km to the north of where this isotherm shoals in the climatology (Fig. 28A).

The location of the 34.6 isohaline in the simulated salinity field (Fig. 28B) agrees with the climatology (Fig. 30B). The simulated salinity field also shows a tongue of 34.7 water moving southward and up across the section (Fig. 28B), which is observed in the observations (Fig. 15B) and is seen in the climatology (Fig. 30B). In the climatological salinity section, the tongue starts at 1600 m and 3800 m respectively (Fig. 30B) and extends across the section. In the simulated salinity field the same isohaline starts at 1850 m and 3400 m in the north and extends across the section, although it stops 200 km from the south of the section (Fig. 15B).

The above comparisons show that there is a good agreement between the simulated temperature and salinity distributions and the climatology, except for the representation of the cold tongue in the Melville II section from Drake Passage. A comparison of the frontal locations is not done here because the fronts in the simulated flow field are initialized with a feature model in addition to this climatology.

4.2 Model Sensitivity

As discussed in section 3, the simulated circulation fields respond strongly to variations in wind forcing. To test this, the wind was changed ±20% (Table 12) by

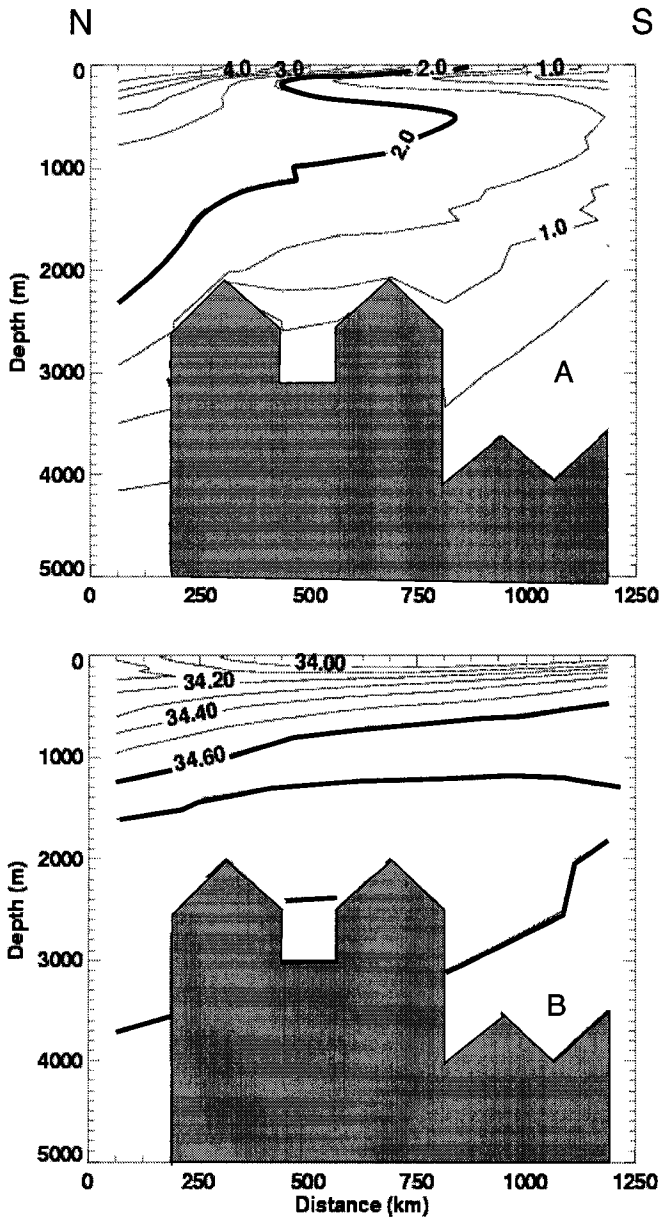

Fig. 30. Climatological observations of A) potential temperature and B) salinity along the WOCE A23 section obtained from the WOA 1998 climatology. Contour intervals are 0.5°C and 0.1 for temperature and salinity, respectively. The thick lines mark the 2°C isotherm (A) and the 34.6 and 34.7 isohalines (B).

changing the Ekman factor, and the resultant sensitivity of the circulation to the change was determined.

4.2.1 General Circulation

The influence of wind on the overall circulation can be seen by comparing the baroclinic streamfunction after 180 days of simulation with increased wind (Fig. 31A) or decreased wind (Fig. 31B) to the reference baroclinic streamfunction after 180 days (Fig. 25B). Considerable mesoscale variability is seen in the surface barotropic streamfunction in both simulations (Fig. 31A,B). Overall the barotropic streamfunction from the decreased and increased wind simulations shows the same flow features as the reference simulation (Fig. 25B). In the increased wind simulation, the SAF shows close streamline spacing indicating an accelerated flow through the channel east of Burdwood Bank (cf. Fig. 1) with a small part of this front diverging and flowing through the channel further east together with the PF. A similar flow is seen in the reference simulation (Fig. 25B). The PF and SACCF show considerable meandering along their paths with a few visible eddies, and the flow of the PF is accelerated over the channel in the North Scotia Ridge connecting the Scotia Sea with the Malvinas Chasm (cf. Fig. 1). The only difference between this simulation and the reference simulation is that the barotropic stream function now shows more pronounced eddies associated with the fronts (Fig. 31A, numbers 1-6). The eddies are visible at the same locations as in the reference simulation, but now are defined by more streamlines or are better defined in shape, indicating they are more strongly developed than in the reference simulation. At the northern boundary near 51°W, two observed eddies changed their form to be slightly more round in shape (Fig. 31A, numbers 1, 2). In addition, a more pronounced eddy which developed from the SACCF is seen to the east of South Georgia (Fig. 31A, number 3).

The barotropic streamfunction of the decreased wind simulation (Fig. 31B) shows fewer developed eddies, and the two eddies observed at the northern model domain boundary in the increased wind simulation have formed a large and a small formation. There is no eddy present to the east of South Georgia in the reduced wind simulation (Fig. 31B).

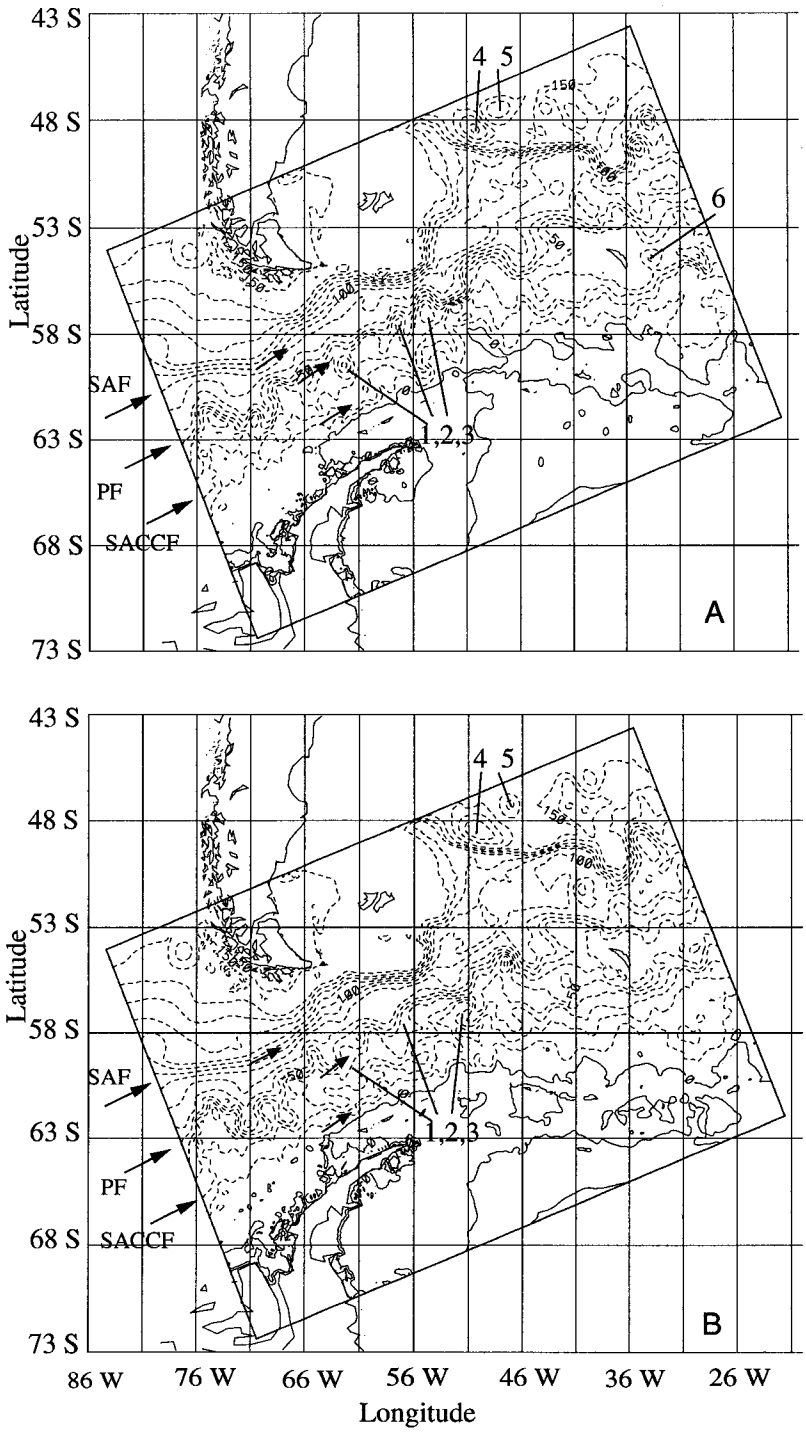

Fig. 31. Barotropic streamfunction (Sv) after 180 days of simulation (30 March) with A) 20% increased wind stress and B) 20% decreased wind stress. Contour interval is 10 Sv. The direction of the flow is indicated by the arrows. Locations of the Subantarctic Front (SAF), the Polar Front (PF), and the Southern ACC Front (SACCF) are indicated by large arrows, and the rotated rectangle shows the extent of the model domain. The numbers 1 to 6 mark eddies, discussed in the text.

4.2.2 Regional Circulation

To further test the influence of wind on the regional circulation, especially along the western Antarctic Peninsula, the flow speed and direction of ten simulated surface drifters are used to examine the model sensitivity to wind. The starting positions of the drifters were chosen to cover different environments in the study area. Drifter 1 is located on the western Antarctic Peninsula shelf in the Bransfield Strait, 2 is located in the vicinity of the SAF, 3 in the vicinity of the PF, 4 and 5 at two different locations on the western Antarctic Peninsula shelf, 6 at the edge of the SACCF, 7 on the Weddell Sea shelf edge, 8 in the middle of the Scotia Sea, 9 close to South Georgia and 10 off the tip of the Antarctic Peninsula.

Decreasing the wind stress over the total study region by 20% changes the surface flow speeds of the drifters over a large range from -68% to 36% (Table 12). Five of the drifters react with increased surface speeds and changed flow direction, while the other five drifters show decreased surface speeds with a change in direction. The smallest change in drifter behavior occurs (drifter 6) at the edge of the SACCF, with a 1% decrease in speed and a 2° change in direction. The largest change occurs (drifter 5) at the southwestern Antarctic Peninsula, with a 68% decrease of surface speed and a 6° change in direction (Table 12).

Increasing the wind stress by 20% changes the surface speed and direction of the ten drifters (Table 12), but the range is less than that observed for decreased wind stress, being between -18% to 23%. Again drifters at the edge of the SACCF (drifter 6) experience the least change, with a 2% decrease in speed and a 15° change in direction. The drifters that show changes in speed and direction are not necessarily the same drifters as those in the decreased wind simulations. For example drifter 2, located in the SAF, experiences decreased speeds in both cases, while drifter 1, in the Bransfield Strait, experiences increased surface speed with decreased winds and decreased surface speed with increased wind. In contrast, drifter 5, at the southwest Antarctic Peninsula, experiences strongly decreased surface flow speeds (68%) with decreased winds and slightly increased flow speed (3%) with increased wind.

Changes in the wind stress distribution used to force the model have different effects on the surface flow speed and direction in different areas in the model domain. A 20% decrease in the wind changes the surface flow speeds and direction of the surface flow more than a 20% increase in wind stress. The increase or decrease of the wind has an almost uniform influence on the Ekman flow, which increases by

Table 12. Average simulated surface layer flow speed and direction, and Ekman flow speed and direction over the upper 100 m for 10 drifters defined in Table 10, subjected to ±20% variation in the NCEP wind fields used to force the circulation model. The simulated speed and direction values are 30-day averages for December. The percent change in surface and Ekman flow speeds is computed relative to the winds used for the reference simulation.

		Initial location		Surface flow			Ekman flow		
Wind		longitude	latitude	speed	change	direction	speed	change	direction
Forcing		(°W)	(°S)	(cm s^{-1})	(%)	(°true)	(cm s^{-1})	(%)	(°true)
NCEP	1	59.0	63.0	0.57		312	0.7		58
	2	60.5	56.0	6.94		167	0.57		66
	3	56.0	58.0	2.60		300	0.5		67
	4	63.5	64.0	3.85		138	0.68		60
	5	69.5	66.0	3.07		140	0.56		82
	6	59.0	61.0	11.33		73	0.58		67
	7	53.0	65.0	3.08		63	0.93		49
	8	44.0	58.0	13.16		330	0.3		67
	9	39.0	56.0	8.69		124	0.22		333
	10	53.0	63.0	6.35		1	0.65		53
NCEP	1	59.0	63.0	0.89	36	263	0.56	-25	58
-20%	2	60.5	56.0	4.79	-44	248	0.46	-24	66
	3	56.0	58.0	3.59	28	336	0.4	-25	67
	4	63.5	64.0	3.23	-19	161	0.54	-26	60
	5	69.5	66.0	1.83	-68	146	0.45	-24	82
	6	59.0	61.0	11.20	-1	75	0.47	-23	67
	7	53.0	65.0	3.34	8	30	0.74	-26	49
	8	44.0	58.0	11.99	-10	348	0.24	-25	67
	9	39.0	56.0	11.88	30	122	0.18	-26	333
	10	53.0	63.0	7.82	19	350	0.52	-25	53
NCEP	1	59.0	63.0	0.54	-5	162	0.84	17	58
+20%	2	60.5	56.0	5.85	-18	173	0.69	17	66
	3	56.0	58.0	2.58	-0.7	252	0.6	17	67
	4	63.5	64.0	5.00	23	141	0.82	17	60
	5	69.5	66.0	3.14	3	141	0.67	16	82
	6	59.0	61.0	11.04	-2	87	0.7	17	67
	7	53.0	65.0	3.63	15	64	1.11	16	49
	8	44.0	58.0	12.52	-5	333	0.36	17	67
	9	39.0	56.0	9.52	9	125	0.27	18	333
	10	53.0	63.0	5.37	-18	2	0.78	17	53

approximately 17% with increased flow and decreases by approximately 25% with decreased wind stress (Table 12).

4.2.3 Simulated Drifter Trajectories

The drifter trajectories resulting from variable wind conditions (Figs. 32, 33) indicate the extent to which the simulated circulation is modified by increases or decreases in the wind field. For normal wind conditions, drifter 1 (Fig. 32A, solid line) flows south in Bransfield Strait and then turns west, exits the Strait, and becomes entrained in the SACCF. Increased winds produce and enhance northward Ekman transport, which moves drifter 1 into the ACC sooner (dashed line). The simulated trajectories for this drifter for normal and increased winds are similar (Fig. 32A, solid and dashed line), except for a northward shift during increased wind conditions.

A 20% reduction in the wind results in the drifter remaining longer in Bransfield Strait before becoming entrained into the ACC (Fig. 32A, dotted line). Under decreased winds, eight months of the total transport time is spent in or near Bransfield Strait. As a consequence, this drifter is transported only as far as 59°W, while the original drifter and the drifter experiencing increased winds are transported halfway across the Scotia Sea in the same time. Clearly, increased wind enhances transport towards South Georgia by accelerating offshore transport and entrainment into the ACC, and moves the drifters on a more northward trajectory. Decreased wind speeds slow and retain particles along the northern Antarctic Peninsula.

Drifter 2 was released in the SAF (Fig. 32A, solid line) and its trajectory follows the SAF as it flows east and then turns north between Burdwood Bank and the North Scotia Ridge (cf. Fig. 1) to flow along the continental shelf east of South America. The trajectories of these drifters do not differ until passing 50°S. After that, the drifter experiencing decreased winds turns north at 47°W and becomes entrained in an eddy. The drifter experiencing increased winds turns north at 42°W, continues to flow northeast and exits the model domain. The original drifter continues on an eastward path turning north at 36°W.

Drifter 3 was released in the central Scotia Sea near the PF (Fig. 32B, solid line) from where it moved northeastward with many meanders, and passed to the north of South Georgia. Increased wind stress produces a similar trajectory that is displaced northward (Fig. 32B, solid line). Decreasing the wind stress produces a simulated drifter trajectory (Fig. 32B, dotted line) that is south of the original drifter path.

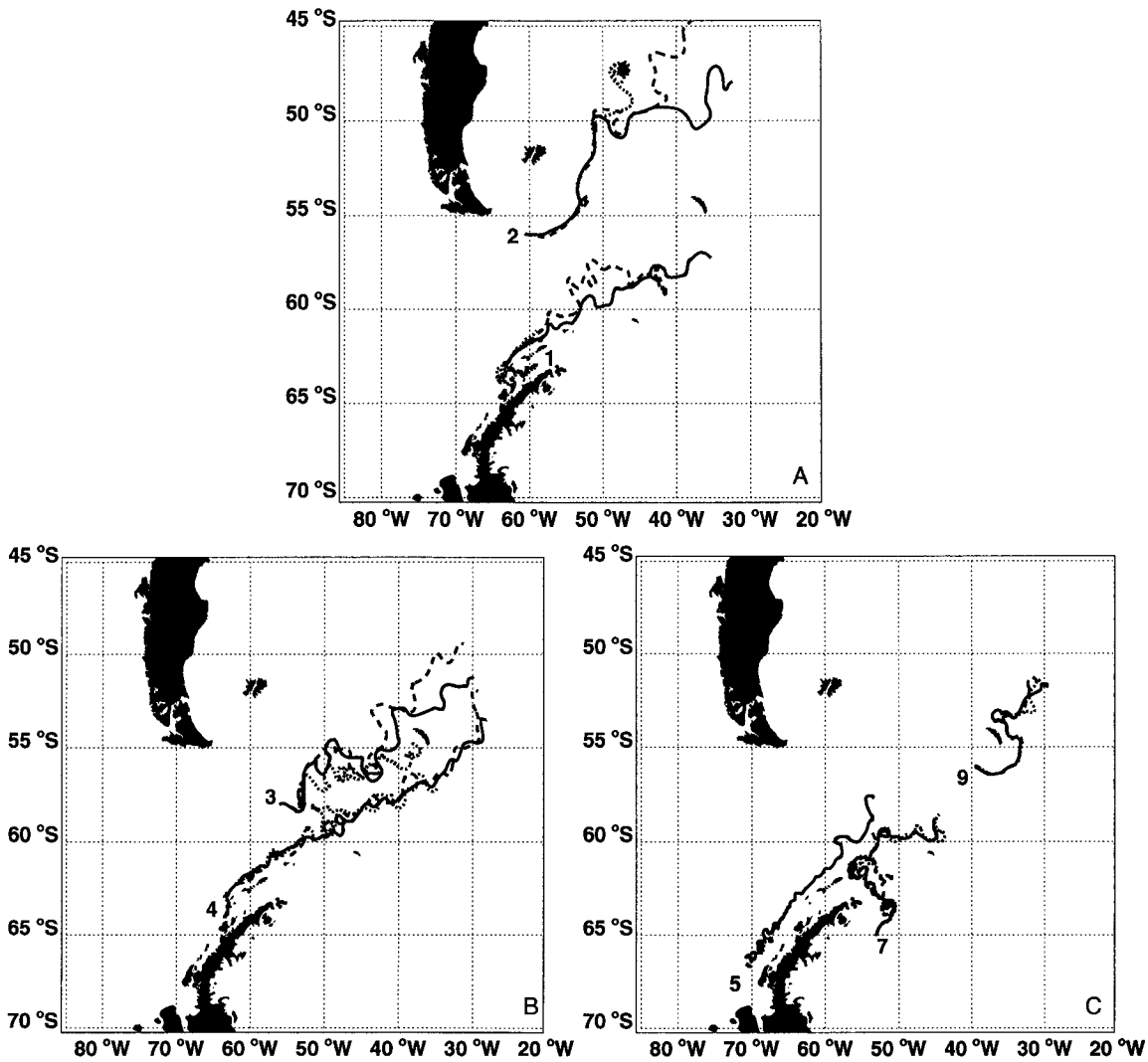

Fig. 32. Simulated surface drifter trajectories for drifters A) 1 and 2, B) 3 and 4, and C) 5, 7, and 9, released in December that experience NCEP winds (solid line), NCEP winds with a 20% increase in wind speed (dashed line), and NCEP winds with a 20% decrease in wind speed (dotted line). Numbers indicate the release point of each drifter as given in Table 12. The choices for specified drifters are described in section 3.5.1.

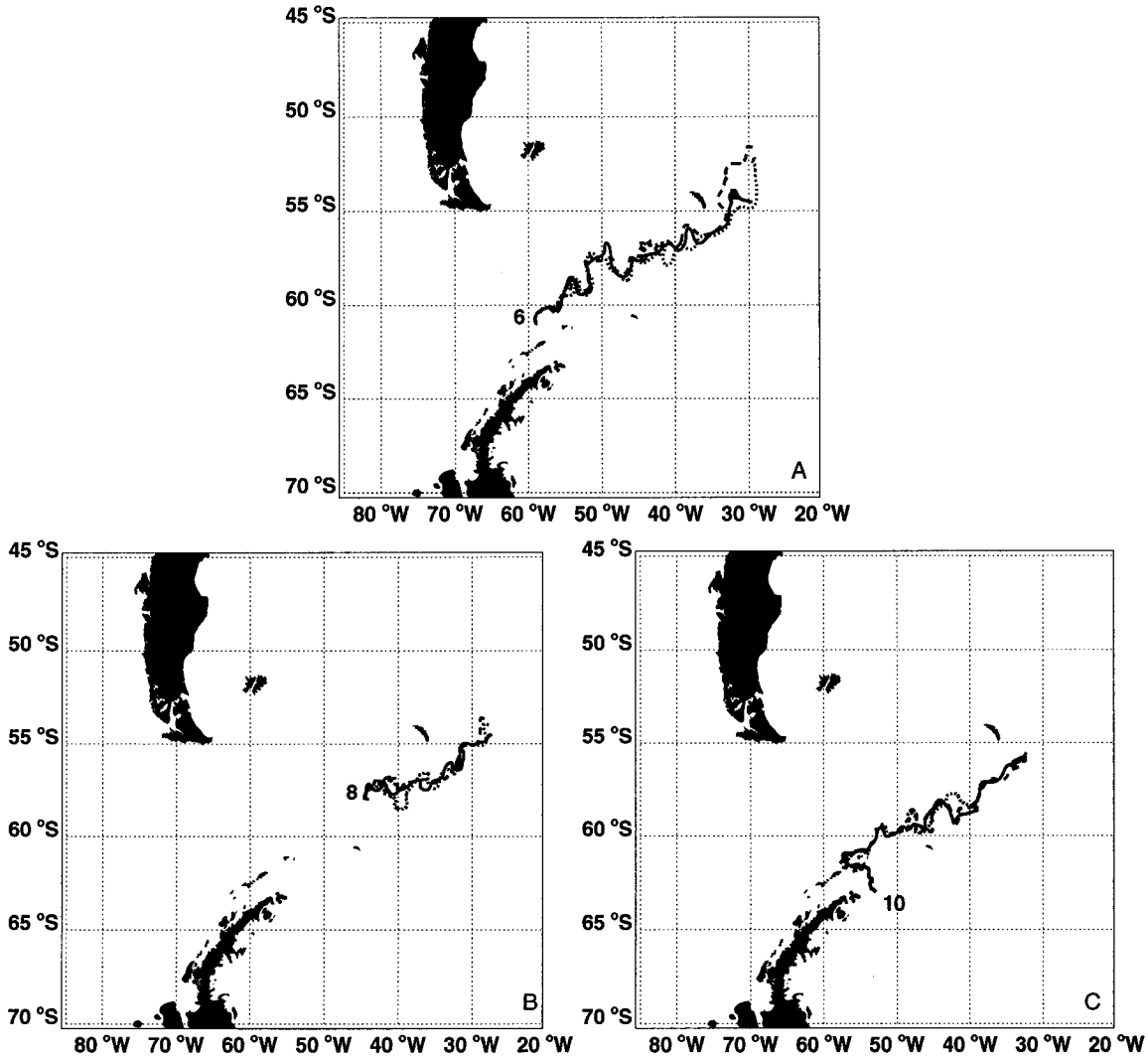

Fig. 33. Simulated surface drifter trajectories for drifters A) 6, B) 8, and C) 10, released in December that experience NCEP winds (sold line), NCEP winds with a 20% increase in wind speed (dashed line), and NCEP winds with a 20% decrease in wind speed (dotted line). Numbers indicate the release point of each drifter as given in Table 12. The choices for specified drifters are described in section 3.5.1.

This drifter moves across the Scotia Sea and is delivered directly to South Georgia.

The simulated trajectory of drifter 4, released on the continental shelf of the western Antarctic Peninsula (Fig. 32B, solid line), moves north until it is entrained into the SACCF and transported across the Scotia Sea, passing South Georgia a considerable distance to the south. Increased winds produce a similar simulated trajectory (Fig. 32B, dashed line) but the drifter ends further to the northeast. Decreased winds also result in a similar simulated trajectory, but the distance covered is less (Fig. 32B, dotted line), with the drifter ending just south of South Georgia. Simulated trajectories from drifters released in other locations, such as drifter 6 (Fig. 33A), drifter 8 (Fig. 33B), drifter 9 (Fig. 32C), and drifter 10 (Fig. 33C) show this same behavior. With increased winds the simulated drifters move faster and cover more distance over the total transport time compared to the simulated drifters that experienced decreased winds.

Drifters released on the southwestern shelf of the Antarctic Peninsula (drifter 5, Fig. 32C) experience changes in the wind differently. After entrainment in an eddy the simulated drifter experiencing NCEP winds is transported northeast along the Antarctic Peninsula and across the Scotia Sea by the SACCF. Decreased wind allows entrainment of the drifter in the eddy for almost ten months and as a result the drifter does not leave the continental shelf. Increased wind speeds transport the drifter first southwest before it turns north and is entrained in the SACCF, and results in decreased northeast transport along the continental shelf.

Drifters originating in the Weddell Sea (drifter 7, Fig. 32C) have almost identical trajectories for NCEP winds and decreased winds. Increasing the wind speeds results in the drifter being entrained in more eddies, and eastward displacement of the trajectory. The drifter is not transported to South Georgia in a decreased wind condition either (Fig. 32C, dotted line). During early spring (October - November) the climatological winds shift from northwesterly to westerly, creating a more offshore component to the Ekman flux. During this time, which slightly precedes the December to February krill spawning season (Ross and Quetin, 1986), this near surface flow will transport particles closer to the fast flowing ACC.

The above analysis shows that the surface wind stress has a minor influence on the overall circulation pattern, indicating that the simulated circulation is largely controlled by the initial density distribution, the frontal features and the bottom topography. However, wind stress does have a strong effect on the exchange between

the continental shelf region of the Antarctic Peninsula and the ACC due to the contribution of the Ekman transport to the overall large-scale surface flow.

4.3 Model Drifters

The simulated circulation patterns are used primarily to track surface drifters over time. Therefore, verification of the simulated flow speeds and directions is needed. This is done by releasing surface and subsurface drifters in the model domain at locations that correspond to release sites of WOCE surface and subsurface drifters (Table 10). The mesoscale variability of the Scotia Sea and the equivalent variability in the simulated circulation fields will preclude exact matching of the simulated and observed drifters. However the general transport direction and average speeds of the observed and simulated paths should match.

4.3.1 Surface Drifters

WOCE drifter 22047 (Fig. 34A), which was released in southern Drake Passage in January 1995, follows the SACCF. The observed trajectory of this drifter is east-northeastward from the tip of the Antarctic Peninsula across the Scotia Sea, passing South Georgia to the south. Eight meanders occur in the path of the drifter and its average speed is 0.234 m s^{-1}. The simulated drifters, with various release times, flow along the same trajectory until 48°W, where drifters move north and some move south of the WOCE surface drifter. The drifters released after 60 and 120 days of simulation turn northward, following the path of the SACCF northward for 30 more days, while the observed drifter moved eastward. The overall agreement of surface drifter paths is good, with all simulated drifter trajectories following the observed drifter trajectory closely. The WOCE drifter took 208 days to complete the trajectory shown in Fig. 34A, while the simulated surface drifters took 216 to 336 days to cover the same distance. This difference in transport time arises because the simulated drifters are entrained in eddies at the beginning of their paths, which results in lagging the observed drifter time. Overall the simulated surface drifters are slower than the WOCE surface drifters (Table 13).

WOCE drifter 22050 (Fig. 34B) starts in March 1995, near the northern side of Drake Passage in the vicinity of the high speed flow of the SAF. The average speed of this drifter is 0.322 m s^{-1} and the observed trajectory is eastward to the edge of the shallow continental shelf of South America, where it turns northward

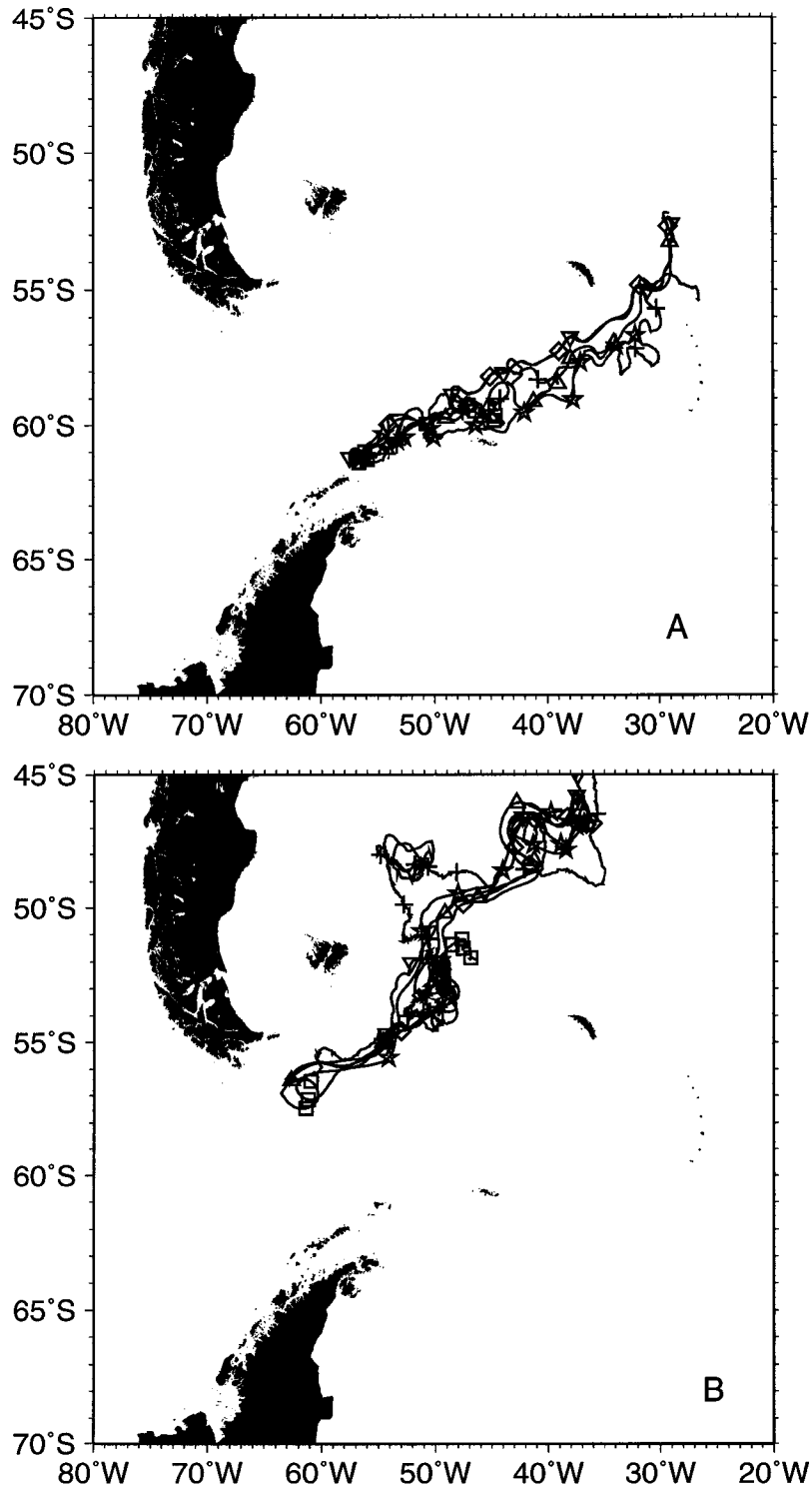

Fig. 34. Trajectories followed by A) WOCE surface drifter 22047 (+), and B) WOCE surface drifter 22050 (+), and those followed by simulated surface drifters released at day 30 ($\star$), day 60 ($\square$), day 90 ($\triangle$), day 120 ($\triangledown$), day 150 ($\diamond$). Symbols mark the position of the simulated and WOCE drifters at 30-day intervals.

Table 13. Comparison of the average speed of WOCE surface drifters with the average surface speed (m s^{-1}) calculated for the simulated surface drifters released at different times. The average simulated drifter speed is based on all drifters released in the simulated circulation fields. The error is the calculated fractional error of average speed to observed average speed.

Observed WOCE Drifter	Simulated Drifters						WOCE Drifter Avg	Error
	Day 30	Day 60	Day 90	Day 120	Day 150	Avg		
WOCE22045	0.296	0.282	0.285	0.293	0.186	0.268	0.374	0.283
WOCE22046	0.100	0.109	0.082	0.088	0.115	0.099	0.156	0.369
WOCE22047	0.080	0.066	0.116	0.142	0.159	0.113	0.234	0.517
WOCE22048	0.160	0.184	0.151	0.202	0.228	0.185	0.339	0.455
WOCE22049	0.133	0.197	0.132	0.152	0.148	0.152	0.212	0.281
WOCE22050	0.127	0.085	0.145	0.157	0.171	0.137	0.322	0.574
WOCE22108	0.157	0.157	0.306	0.220	0.306	0.229	0.458	0.499
WOCE22591	0.191	0.260	0.171	0.193	0.176	0.198	0.299	0.338
WOCE22594	0.199	0.253	0.196	0.314	0.365	0.265	0.321	0.173

between Burdwood Bank and South Georgia (cf. Fig. 1). Near 54°S it is captured by an eddy in which it stays for approximately five months. The WOCE drifter 22050 then moves north and turns east near 48°S where it stays in another eddy-like feature for three months. Near 30°W the drifter turns once again northward. It took 428 days to cover the distance shown in Fig. 34B, with about eight months of this time spent in eddies, which reduced the overall transport distance.

The simulated surface drifters follow the same eastward path taken by WOCE drifter 22050 and turn north along the continental shelf east of Burdwood Bank. However, they are not transported as far north as WOCE drifter 22050, but rather turn east near 50°S and then follow a northeastward path. The simulated drifters move this distance in 216-336 days, because they are not trapped in eddies, as was WOCE drifter 22050. Only the simulated drifter released on day 60 is entrained into a large eddy near its release point and does not move as far northeast as the others. The simulated drifter paths match the observed drifter paths in the first part

of the trajectory, but diverge from the path of WOCE drifter 22050 after passing the Falkland Islands and move northeastward. Again the average speeds of the simulated drifters are slower than that of WOCE drifter 22050 (Table 13).

The best agreement of simulated and observed drifter speeds is with WOCE drifter 22594, with the model-derived speeds being only 17% slower than the observed drifter speeds. The worst agreement is with WOCE drifter 22050, which is 57% faster than the equivalent simulated drifters. On average the model drifters are 38.5% slower than the observed drifters. Possible reasons for this speed difference are discussed in section 5.

4.3.2 Subsurface Drifters

Most of the eighteen Autonomous Lagrangian Circulation Explorer (ALACE) subsurface drifters available from the WOCE study, located at 1000 m depth, passed through the northern side of Drake Passage, an area which is not the focus of the drifter simulations in this study (Table 10, Fig. 17). Two of these WOCE subsurface drifters however, passed further south through Drake Passage and are used for comparison with simulated drifter paths in this region (Fig. 35). The rest of the subsurface drifters are used for a general comparison of the circulation at the northern side of Drake Passage and the South Atlantic.

The ALACE float 204 (Fig. 35A) started at the northern side of Drake Passage in the Pacific Ocean near the high speed flow of the SAF and traveled at an average speed of 0.253 m s^{-1} to the east-northeast. The drifter turned north from the Scotia Sea into the south Atlantic between Burdwood Bank and South Georgia (cf. Fig. 1), and near 49°S the drifter turned again and moved to the east. The subsurface drifter took 354 days to complete this trajectory. The simulated subsurface drifter trajectories follow the same general northeastward path but remain north of the observed trajectory, and also turn north to exit the Scotia Sea into the South Atlantic. However, after moving out of the Scotia Sea, the simulated drifter trajectories turn east-northeast, thereby diverging from the observed northward path. The simulated drifter released on day 30 meets the observed subsurface drifter trajectory at the end of the path. The simulated subsurface drifters released on day 60 and 150 turn south again after entering the South Atlantic and actually get transported back across the North Scotia Ridge into the Scotia Sea before once again moving into the South Atlantic. The simulated drifters need 216 to 336 days to move this distance and are

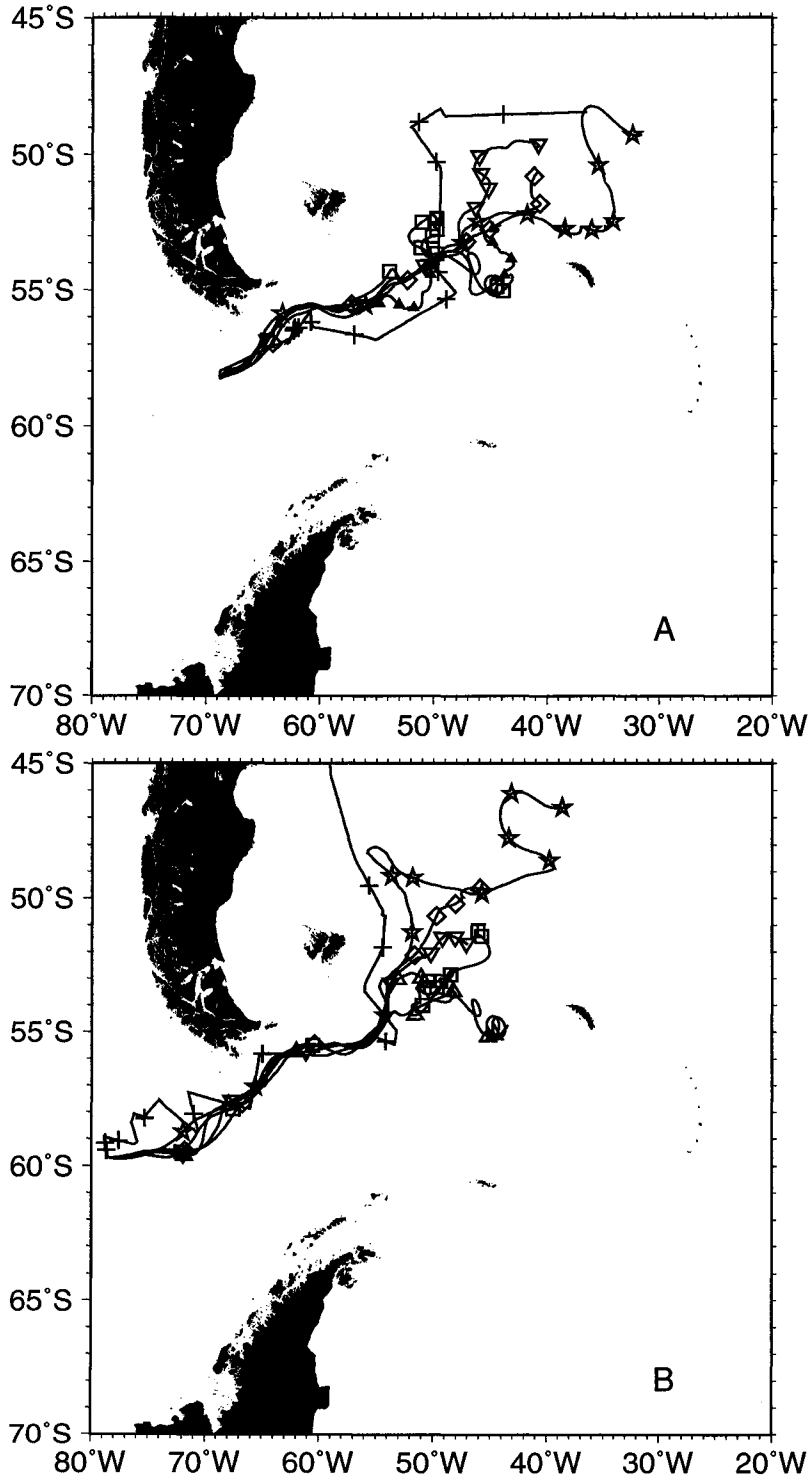

Fig. 35. Trajectories followed by A) WOCE ALACE subsurface float 204 (+), and B) WOCE ALACE subsurface float 250 (+), and those followed by simulated drifters released at day 30 ($\star$), day 60 ($\square$), day 90 ($\triangle$), day 120 ($\triangledown$), day 150 ($\diamond$) intervals. Symbols mark the position of the simulated and WOCE subsurface drifters at 30-day intervals.

overall slower than the observed drifter (Table 14).

The ALACE float 250 (Fig. 35B) started west of Drake Passage in the South Pacific and moved with an average speed of 0.319 m s^{-1} to the northeast along the continental slope east of South America. It then turned north from the Scotia Sea into the South Atlantic where it moved past the Falkland Islands (cf. Fig. 1) to the north. It took 288 days to complete this trajectory. The simulated drifter trajectories follow the observed drifter path exactly and turn into the South Atlantic, but then move into a more northeastward direction.

The simulated drifter released on day 150 turns south again after entering the South Atlantic and is transported back across the North Scotia Ridge into the Scotia Sea where it remains in an eddy. Only the simulated drifter released on day 30 follows a similar northward trajectory along the shelf of South America in the Malvinas (Falkland) Current before turning east at 48°S. The model domain ends at this latitude (cf. Fig. 5) and the incoming flow of the Brazil Current joins the Malvinas Current at this location, turning part of it southward instead of letting the whole current exit to the north. Again, the simulated drifter trajectories require 216 to 336 days to move this distance and are 59.5% slower in speed than the observed drifter (Table 14).

Comparison of the average speed (m s^{-1}) of each simulated drifter with the average speed of the observed subsurface drifter trajectories shows that all of the simulated subsurface drifters are slower than the WOCE ALACE drifters (Table 14). The best agreement between simulated and observed drifter speeds are for drifters ALACE 18 and 19, where the simulated drifters are 44% slower than the observed drifter. The worst agreement is found for drifter ALACE 217, which is 78% faster than the simulated drifter. On average the ALACE subsurface drifters are 59.5% faster than the simulated drifters, which means that the subsurface drifters are even slower in respect to the observed subsurface drifters than the surface drifters in respect to the observed surface drifters. This difference in simulated and observed speeds is explained in detail in section 5.

4.3.3 Reference Simulation Transport Pattern

The simulated drifter pattern resulting from a December release (Fig. 36A) shows a broad area along the western Antarctic Peninsula extending into the Scotia Sea,

that extends from the continental shelf of the Peninsula into Drake Passage,

Table 14. Comparison of the average speed of WOCE ALACE subsurface drifters with the average subsurface speed (m s^{-1}) calculated for the simulated surface drifters released at different times. The average simulated drifter speed is based on all drifters released in the simulated circulation fields. The error is the calculated fractional error of average speed to observed average speed.

Observed WOCE Drifter	Simulated Drifters						WOCE Drifter Avg	Error
	Day 30	Day 60	Day 90	Day 120	Day 150	Avg		
ALACE 11	0.119	0.180	0.154	0.172	0.094	0.144	0.303	0.525
ALACE 17	0.148	0.143	0.112	0.161	0.202	0.153	0.287	0.465
ALACE 18	0.121	0.152	0.123	0.109	0.171	0.135	0.242	0.442
ALACE 19	0.148	0.143	0.112	0.161	0.202	0.153	0.275	0.442
ALACE 20	0.123	0.106	0.151	0.104	0.116	0.120	0.245	0.51
ALACE 21	0.078	0.172	0.158	0.131	0.183	0.144	0.473	0.695
ALACE 22	0.064	0.130	0.051	0.057	0.104	0.081	0.283	0.712
ALACE 26	0.071	0.113	0.099	0.154	0.121	0.112	0.311	0.641
ALACE 204	0.127	0.125	0.103	0.116	0.118	0.118	0.253	0.534
ALACE 205	0.094	0.086	0.157	0.130	0.112	0.116	0.291	0.602
ALACE 209	0.050	0.084	0.112	0.160	0.121	0.105	0.234	0.549
ALACE 211	0.148	0.137	0.043	0.082	0.051	0.092	0.246	0.626
ALACE 217	0.124	0.043	0.017	0.084	0.112	0.076	0.350	0.783
ALACE 250	0.167	0.127	0.159	0.113	0.147	0.143	0.319	0.552
ALACE 290	0.079	0.018	0.120	0.098	0.058	0.074	0.279	0.733
ALACE 297	0.097	0.123	0.129	0.104	0.111	0.113	0.278	0.595
ALACE 298	0.114	0.131	0.117	0.130	0.151	0.128	0.312	0.588
ALACE 299	0.100	0.014	0.064	0.101	0.093	0.074	0.294	0.747

from which particles can reach South Georgia in the 10 months of the simulation. This region includes a total of 81 drifter release points and roughly coincides with the path of the SACCF. North of this area, in the center of the Drake Passage, is a narrow band of locations from which drifters can reach South Georgia from the north. In addition,drifters from four locations south of South Georgia approach the

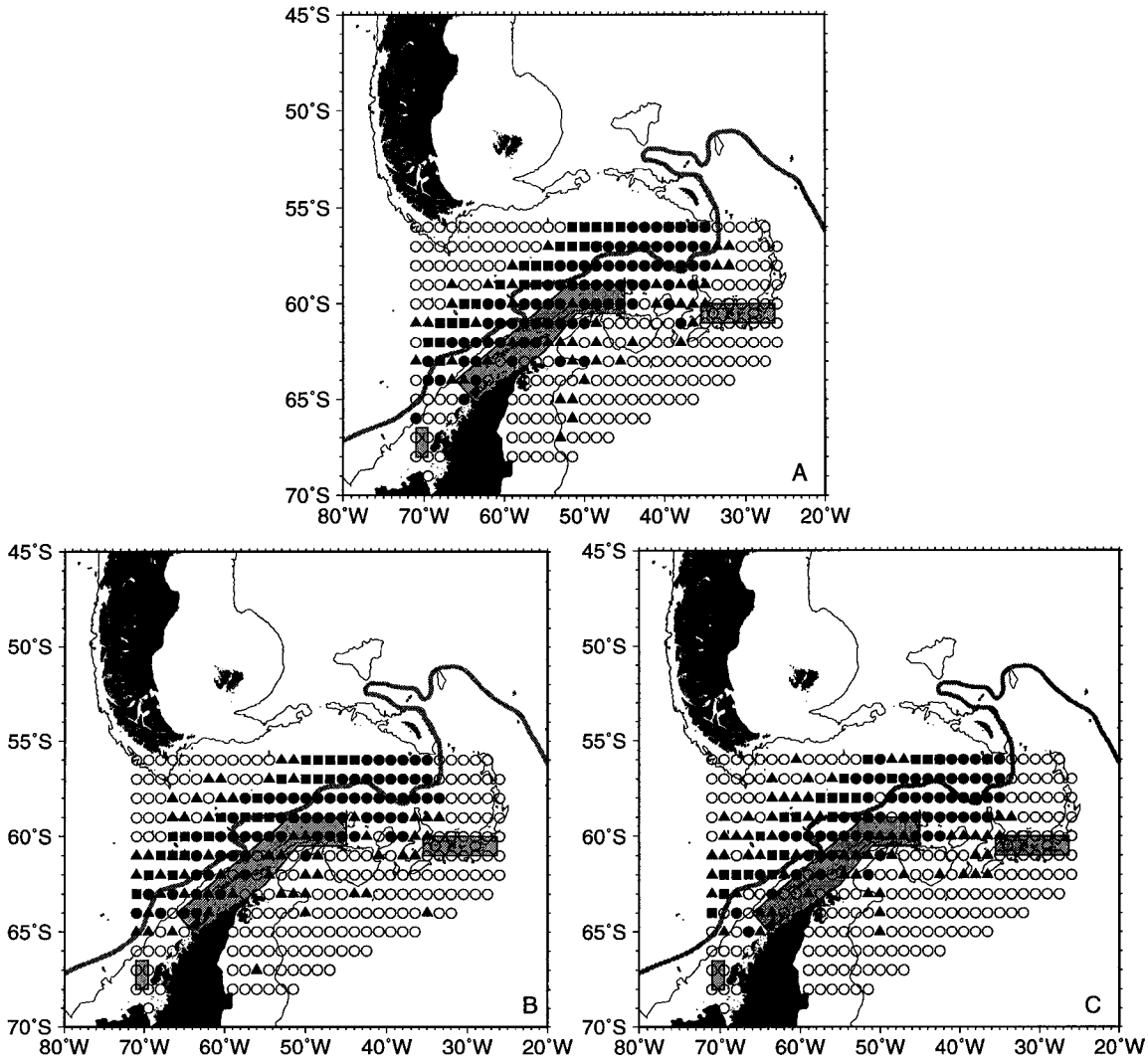

Fig. 36. Initial positions at which surface drifters were released in the simulated circulation fields on A) 1 December, B) 1 January, and C) 1 February. The drifter release points are separated into groups that correspond to drifters that reach South Georgia (•), those that approach South Georgia from the north (■), those that arrive to within 600 km of South Georgia (▲), and those that do not reach South Georgia (○). The areas of consistent Antarctic krill spawning, as identified in Marr (1962), are shown in grey. The thick grey line shows the position of the SACCF and the thin black lines indicate the 2000-m isobath.

Island from the north. North of this narrow band are several locations from which drifters are transported to within 600 km of South Georgia. Six locations along the Weddell Sea continental shelf break, east of the Antarctic Peninsula close to the 2000-m isobath, and several locations east of the tip of the Antarctic Peninsula are sites that allow drifters to be transported to within 600 km of South Georgia in ten months. Drifters originating in the east of the Scotia Sea do not reach South Georgia directly, but rather move within 600 km of the Island. Drifters originating from the spawning area between 35°W and 25°W (Fig. 36A) are not transported near South Georgia but are transported to the east, away from the Island. Five release points in Bransfield Strait, close to the Antarctic Peninsula coastline, result in particle trajectories that do not reach the vicinity of South Georgia, because of transport times longer than ten months. Drifters originating along the southwestern shelf of the Antarctic Peninsula west of 65°W, where another spawning area is located, do not reach South Georgia. Instead, they are transported only small distances to the northeast along the continental shelf. Overall, 108 of the 332 released drifters reach South Georgia and 44 come within 600 km of the Island (Table 15). of the Antarctic Peninsula west of 65°W where another spawning area is located, do not reach South Georgia. Instead, they are transported only small distances to the northeast along the continental shelf. Overall, 108 of the 332 released drifters reach South Georgia and 44 come within 600 km of the Island (Table 15).

The simulated transport pattern for a January release (Fig. 36B) shows that drifters with initial locations at the northern tip of the Antarctic Peninsula and in the eastern Bransfield Strait no longer reach South Georgia. Again a broad area of release locations along the Antarctic Peninsula from which particles can reach South Georgia is present, which coincides with the location of the SACCF. However, a January release results in a reduction in the number of drifters that approach South Georgia from the south (Table 15). To the north of this band there are again a number of locations from which particles can reach South Georgia from the north, but the number of locations has declined from 27 to 23 (Table 15). Only one location in the Weddell Sea and seven locations east of the tip of the Antarctic Peninsula result in drifters that are transported to within 600 km of South Georgia (Table 15). Overall 93 drifters of the 332 released reach South Georgia, while 57 are transported to within 600 km of the Island (Table 15).

The simulated transport pattern for a February release (Fig. 36C) shows even

Table 15. Summary of the total number of simulated drifters reaching South Georgia (SG), reaching South Georgia from the north (north SG), reaching South Georgia from the south (south SG), reaching within 600 km of South Georgia (600 km SG), and not reaching South Georgia (not reach) obtained for different circulation scenarios and release times. The circulation scenarios are discussed in section 3.1.2 and summarized in Table 4. Drake Passage is abbreviated as DP. Drifter release times are 1 December (Dec), 1 January (Jan), and 1 February (Feb).

		Total number of drifters				
Simulation Type	Release Time	at SG	north SG	south SG	600 km SG	not reach
Reference	Dec	108	27	81	44	180
	Jan	93	23	70	57	182
	Feb	87	23	64	60	185
20% increased winds	Dec	105	21	84	51	176
	Jan	96	13	83	54	182
	Feb	84	24	60	58	190
20% decreased winds	Dec	93	19	74	54	185
	Jan	90	23	67	61	181
	Feb	84	16	68	56	192
12% increase in DP transport	Dec	108	22	86	40	184
	Jan	91	26	65	58	183
	Feb	83	20	63	58	191
12% decrease in DP transport	Dec	99	28	71	56	177
	Jan	90	18	72	60	182
	Feb	83	22	61	69	180
SACCF moved 10 km north	Dec	97	25	72	48	187
	Jan	100	21	79	55	177
	Feb	89	25	64	62	181

fewer locations at the western Antarctic Peninsula shelf that allow drifters to reach South Georgia. The total number of drifters reaching South Georgia decreased from 108 in December, 93 in January to 87 in February (Table 15). Drifters released at three additional sites in the western Bransfield Strait do not reach South Georgia,

as well as those released at three sites west of Bransfield Strait and two sites in the Scotia Sea near 50°W. In this simulation, drifters starting west of 63°W mostly reach South Georgia from the north or are transported to within 600 km of South Georgia, while only four drifters released west of 63°W reach the Island. Drifters originating in the Weddell Sea are transported into the vicinity of the Island. Overall, 87 drifters reach South Georgia and 60 are transported to within 600 km of this island (Table 15).

The simulations show that the earlier the release time of particles along the Antarctic Peninsula, the better the chance of reaching South Georgia, especially those originating in the main spawning area off the west Antarctic Peninsula and the Bransfield Strait, which are areas with a large krill population. Late release times also negatively affect the chances of krill survival from the Weddell Sea that are otherwise transported to within 600 km of South Georgia.

The simulated drifters can reach South Georgia from the south or the north of the Island, depending on their release locations. Of these simulated drifters, 60% approach South Georgia from the southern side of the Island (Fig. 37, solid lines). Some of these particles then move on in a northeastward direction away from the Island, while some particles that move closer to the Island follow the flow of the SACCF and wrap around the western side of the Island before moving further northeast. Particles approaching South Georgia northward of 56°S (Fig. 37, dashed lines) turn northward when reaching the eastern continental shelf of South Georgia and are then transported around the northern side of the Island, after which they join particles coming from the south and move off in a northeastwardly direction. Many of the simulated particle trajectories pass near South Georgia, but only two are transported onto the continental shelf of the Island (Fig. 37). These particles reach the 500-m isobath and do not get closer. This is the result of the resolution of the simulated circulation near South Georgia as discussed in section 5.1.1.

4.4 Effect of Environmental Changes

The simulated drifter trajectories show that it is possible for krill originating in known spawning areas along the western Antarctic Peninsula plus the Weddell Sea to be transported to South Georgia. Thus, the influence of variable environmental conditions such as wind, the transport through Drake Passage and the location of the fronts on this basic transport pattern is next assessed.

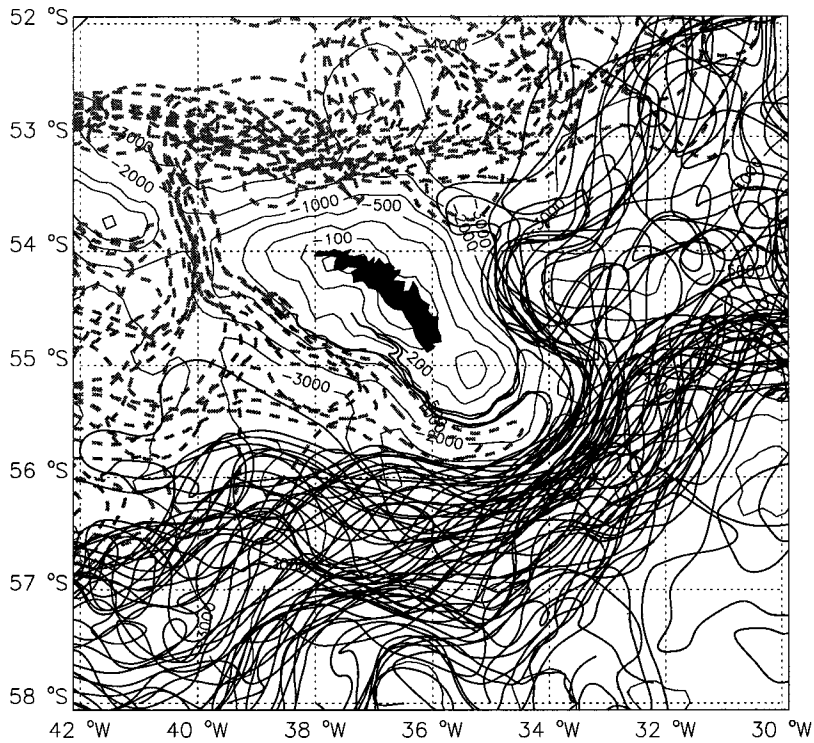

Fig. 37. Simulated surface drifter trajectories of a January release in the reference simulation that reach South Georgia from the north (dashed lines) and from the south (solid lines). Thin black lines indicate the bottom topography, and depth is given in meters.

4.4.1 Effect of Changes in Wind Stress

The simulated transport pattern (Fig. 38A) for drifters released in December in a circulation field obtained using increased wind speed conditions, as discussed in section 3.1.2 (Table 4), shows a pattern similar to the reference simulation (Fig. 36A). A broad area along the western Antarctic Peninsula extending into the Scotia Sea occurs from which particles can reach South Georgia in the 10 months of the simulation. There are only three locations in the Bransfield Strait and one offshore from the Bransfield Strait (61°S, 59°W), from which drifters cannot reach South Georgia. The most notable difference between this simulation and the reference December release simulation (Fig. 36A), is that drifters originating at only three sites along the shelf break in the Weddell Sea are transported to within 600 km of South Georgia. Overall 51 drifters reach the vicinity of South Georgia, with 84

drifters approaching from the south, and 21 drifters approaching from the north. This represents six drifters less than in the reference simulation (Table 15).

The drifter pattern from the January release simulation (Fig. 38B) is similar to that from the January release reference simulation (Fig. 36B). The drifters originating at sites in Bransfield Strait that did not reach South Georgia in the reference simulation remain the same. However, drifters from two additional release sites did not reach South Georgia, because the drifters were retained in the Bransfield Strait for several months before being advected into the fast-moving currents of the SACCF. The increased Ekman transport increased the entrainment of drifters originating in Bransfield Strait into the ACC, as seen in section 4.2 (drifter 1), but this advection into the ACC is not significant enough to transport drifters to South Georgia in the nine months of the simulation. Overall drifters originating at 13 more sites than in the reference January release simulation reached South Georgia from the south, but only 13 reached the Island from the north, which is 10 less than in the reference simulation (Table 15).

The simulated transport pattern for a February release with increased winds (Fig. 38C) shows a pattern similar to that obtained for the reference simulation for a February release (Fig. 36C, Table 15).

The simulated drifter transport patterns obtained for the three release times and a 20% reduction in wind speed (Figs. 39A-C) is similar to that obtained from the reference simulation (Fig. 36A). The primary difference is that fewer sites in Bransfield Strait allow drifters to reach South Georgia (Figs. 39A-C). Another effect of reduced wind is that fewer drifters reach the South Georgia from the north side (Table 15), because many drifters first approach the Island from the south, turn northward and are transported along the western side of the Island (Fig. 37). With reduced winds these drifters do not move far enough to be transported along the northern side of South Georgia.

Increased wind stress over the study area does not facilitate transport of more drifters from Bransfield Strait towards the South Georgia and it has a negative influence on transport times from the Weddell Sea. Decreased wind stress affects drifters from the Bransfield Strait and the Weddell Sea negatively.

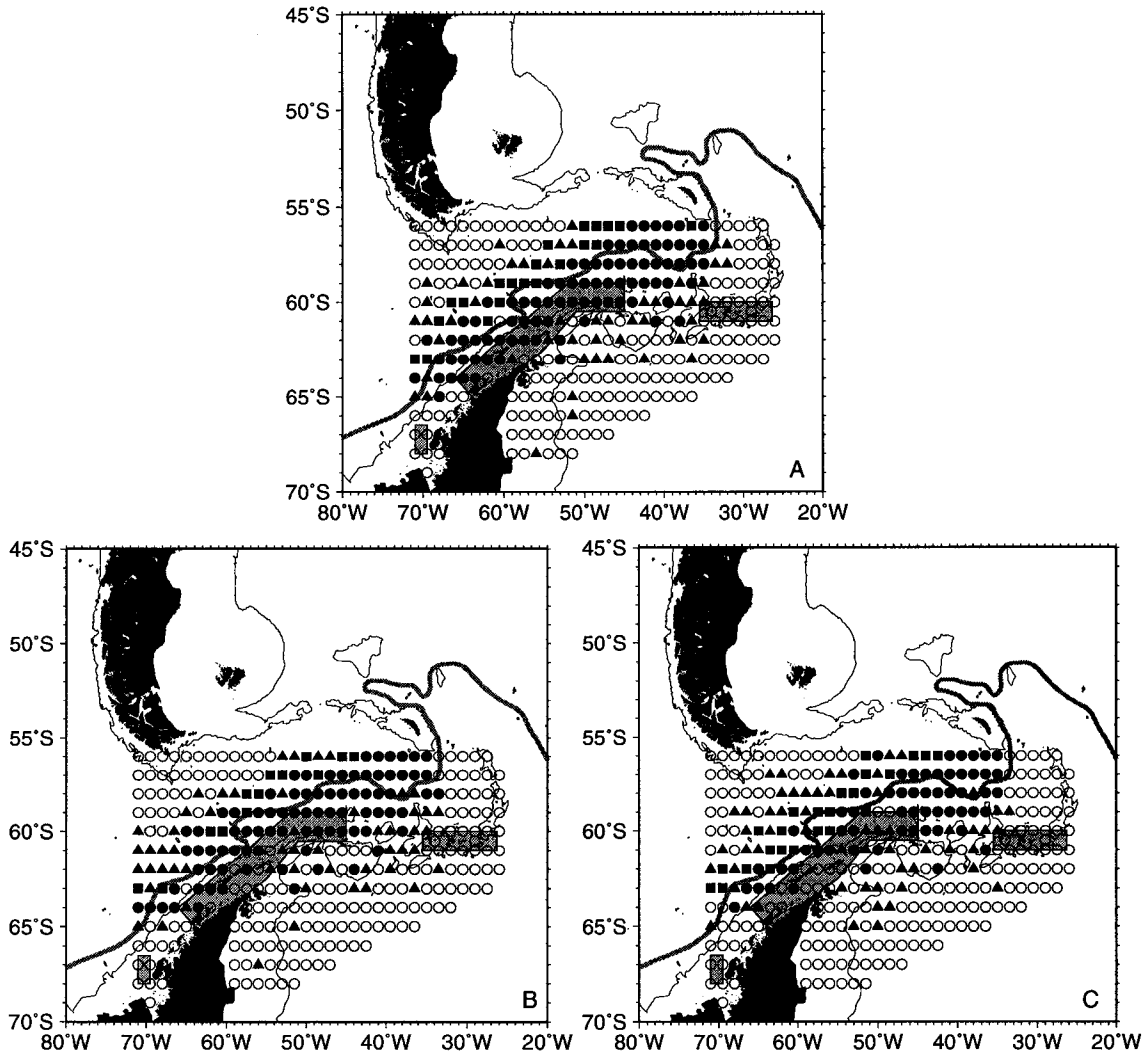

Fig. 38. Initial positions at which surface drifters were released in the simulated circulation fields obtained using 20% increased wind speeds on A) 1 December, B) 1 January, and C) 1 February. The drifter release points are separated into groups that correspond to drifters that reach South Georgia (•), those that approach South Georgia from the north (■), those that arrive to within 600 km of South Georgia (▲), and those that do not reach South Georgia (○). The areas of consistent Antarctic krill spawning, as identified in Marr (1962), are shown in grey. The thick grey line shows the position of the SACCF and the thin black lines indicate the 2000-m isobath.

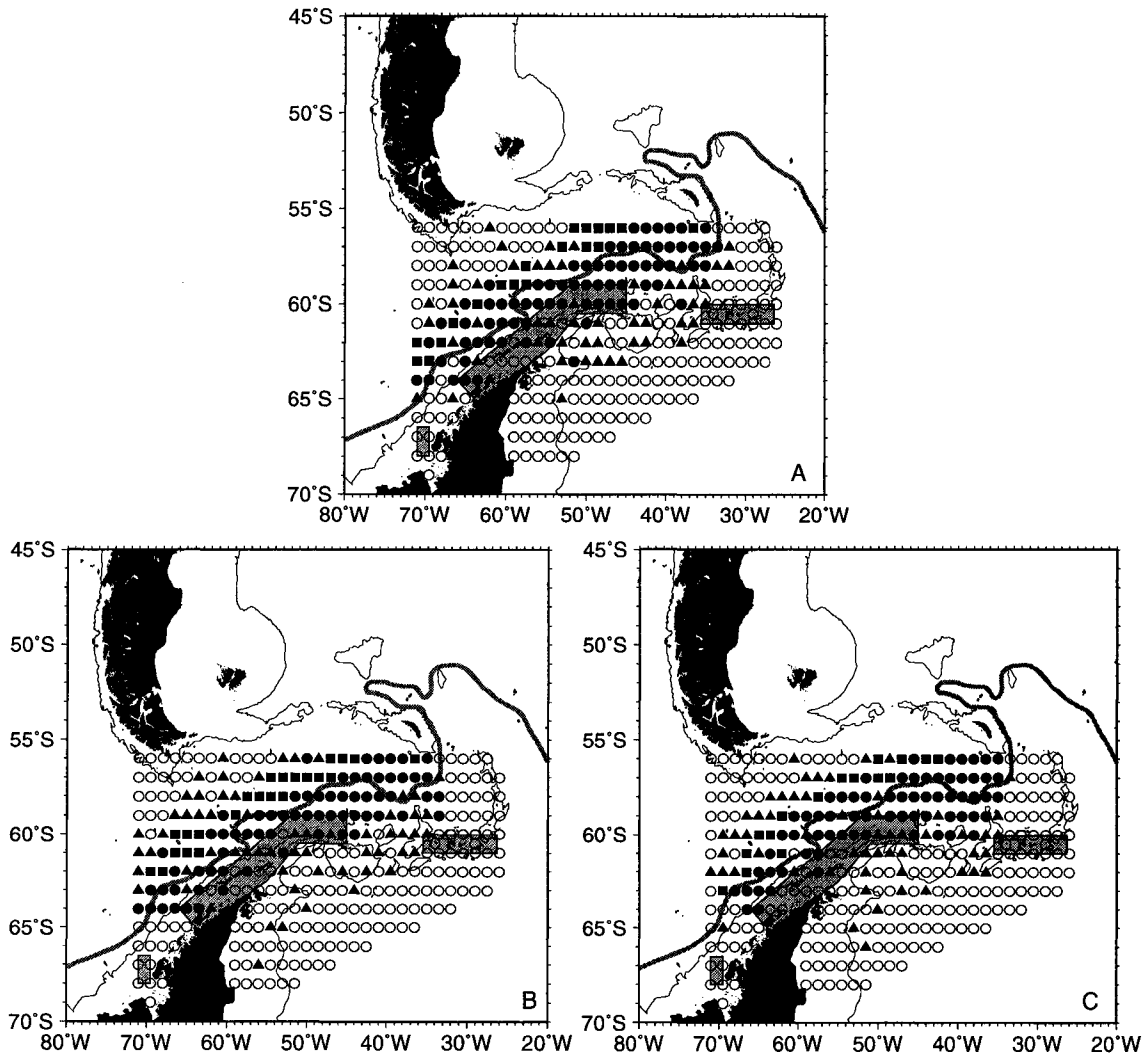

Fig. 39. Initial positions at which surface drifters were released in the simulated circulation fields obtained using 20% decreased wind speeds on A) 1 December, B) 1 January, and C) 1 February. The drifter release points are separated into groups that correspond to drifters that reach South Georgia (•), those that approach South Georgia from the north (■), those that arrive to within 600 km of South Georgia (▲), and those that do not reach South Georgia (○). The areas of consistent Antarctic krill spawning, as identified in Marr (1962), are shown in grey. Thick grey lines shows the position of the SACCF and thin black lines indicate the 2000-m isobath.

4.4.2 Effect of Changes in the Transport through Drake Passage

The simulated drifter transport pattern for the three release times with a circulation field produced by a 12% increase in transport through Drake Passage (Figs. 40A-C), described in section 3.1.2 (Table 4), shows that drifters originating in Bransfield Strait do not reach South Georgia. The currents in Bransfield Strait are not strongly influenced by the transport through Drake Passage. In fact the result of this simulation is quite similar to the simulation with 20% increased winds (Figs. 38A-C). The number of drifters reaching South Georgia for the different release times is summarized in Table 15. For a 12% decrease in transport through Drake Passage the simulated drifter transport patterns produced for all three release times (Figs. 41A-C) are similar to those obtained in the reference simulation (Figs. 36A-C). These simulations also show that earlier release times favor transport to South Georgia (Table 15).

4.4.3 Effect of Changes in the Location of the Southern ACC Front

When the SACCF is moved 10 km north of its climatological location, the simulated drifter transport pattern produced by a December and January release (Figs. 42A,B) shows that drifters originating on the western Antarctic Peninsula continental shelf are not transported to South Georgia. Drifters originating at sites on the outer part of the west Antarctic Peninsula continental shelf, are transported only to within 600 km of South Georgia. Many of the drifters reach South Georgia from the south (Table 15). However, this is not beneficial in terms of krill transport, because these drifters originate in the open ocean, rather than in the krill spawning areas. For a February release the simulated drifter transport pattern (Fig. 42C) shows an even wider range of locations on the western Antarctic Peninsula shelf from which drifters cannot reach South Georgia. As a result, the entire southwestern part of the main krill spawning area does not provide krill to South Georgia.

Thus, moving the SACCF 10 km to the north has a negative influence on transport of krill from the main spawning area along the western Antarctic Peninsula. The SACCF influences transport from the west Antarctic Peninsula continental shelf so much that a move to the north (even of only 10 km) leaves only a fraction of the spawning areas that can potentially supply krill to South Georgia. The simulations also show that earlier release times favor transport to South Georgia (Table 15).

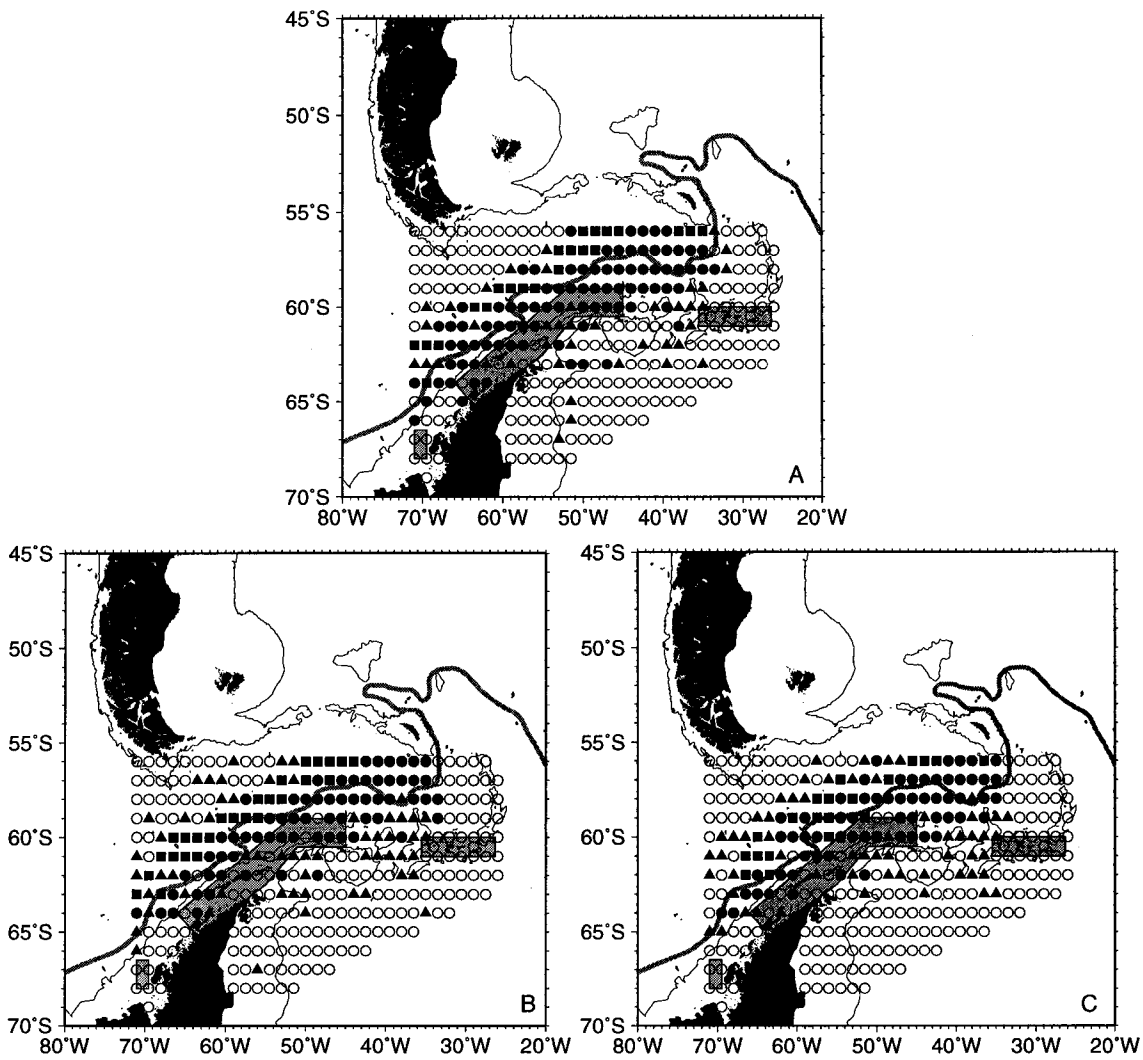

Fig. 40. Initial positions at which surface drifters were released in the simulated circulation fields obtained using 12% increased transport through Drake Passage on A) 1 December, B) 1 January, and C) 1 February. The drifter release points are separated into groups that correspond to drifters that reach South Georgia (•), those that approach South Georgia from the north (■), those that arrive to within 600 km of South Georgia (▲), and those that do not reach South Georgia (○). The areas of consistent Antarctic krill spawning, as identified in Marr (1962), are shown in grey. The thick grey line shows the position of the SACCF and the thin black lines indicate the 2000-m isobath.

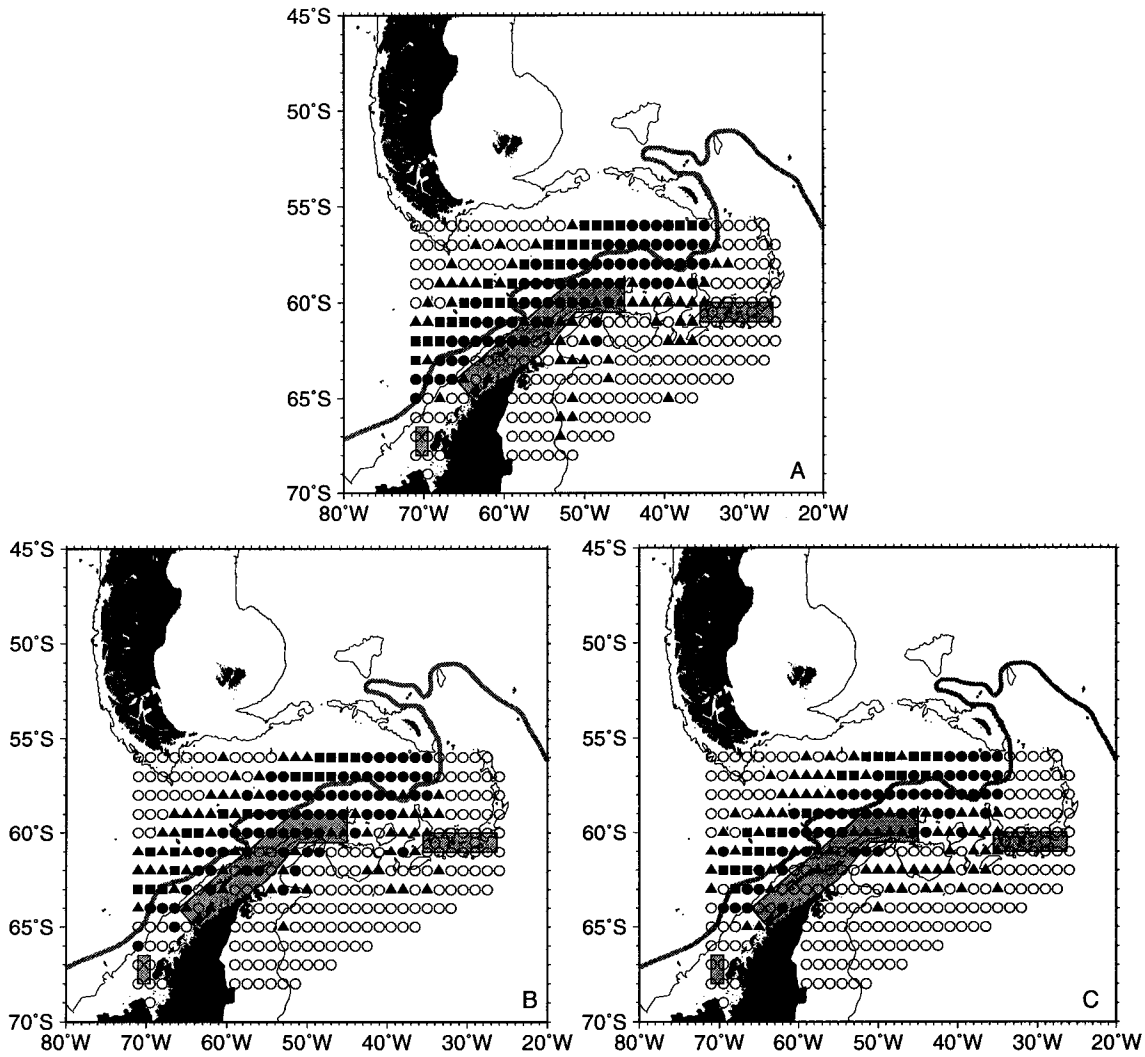

Fig. 41. Initial positions at which surface drifters were released in the simulated circulation fields obtained using 12% decreased transport through Drake Passage on A) 1 December, B) 1 January, and C) 1 February. The drifter release points are separated into groups that correspond to drifters that reach South Georgia (•), those that approach South Georgia from the north (■), those that arrive to within 600 km of South Georgia (▲), and those that do not reach South Georgia (○). The areas of consistent Antarctic krill spawning, as identified in Marr (1962), are shown in grey. The thick grey line shows the position of the SACCF and the thin black lines indicate the 2000-m isobath.

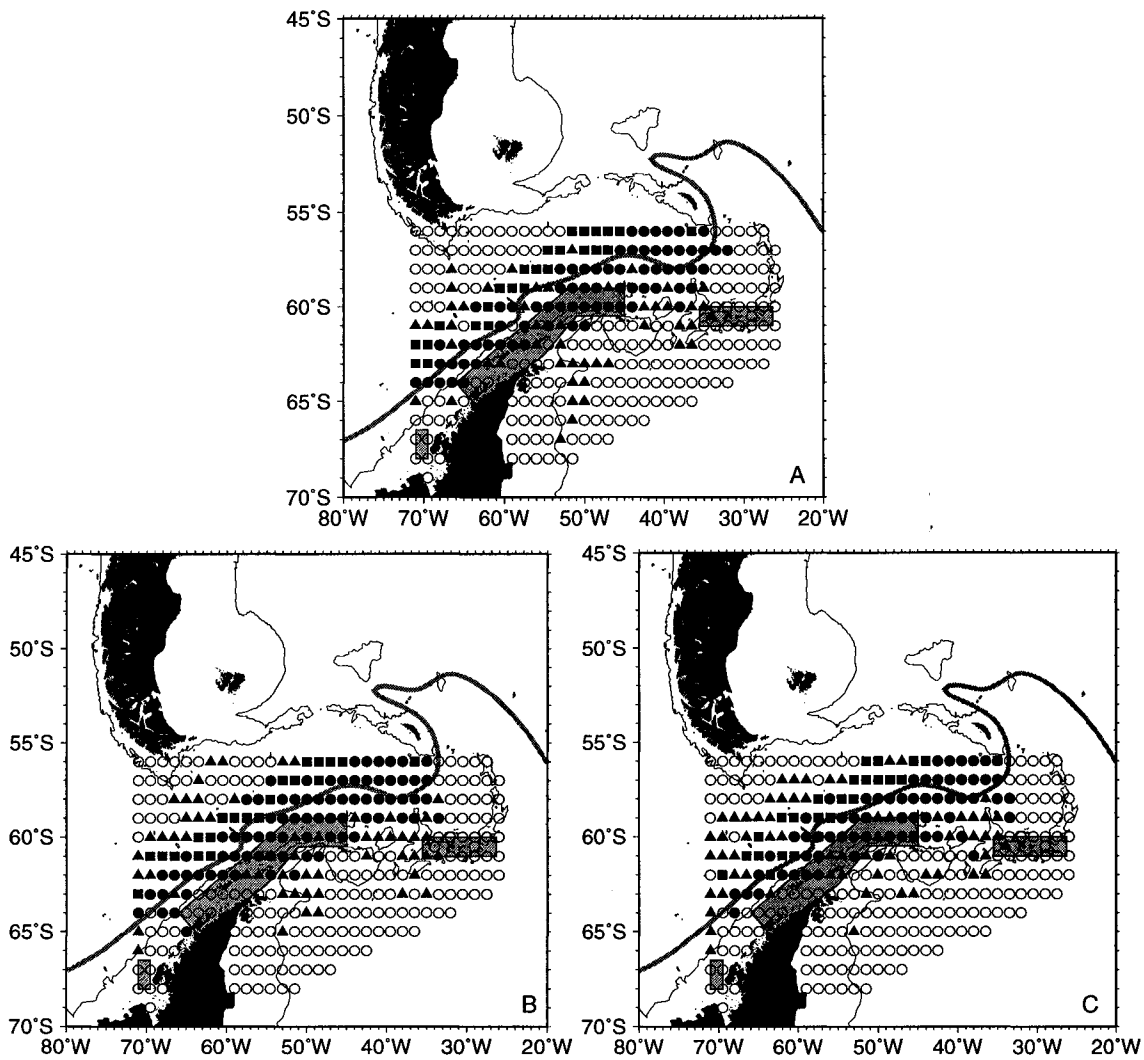

Fig. 42. Initial positions at which surface drifters were released in the simulated circulation fields obtained with the SACCF moved 10 km to the north on A) 1 December, B) 1 January, and C) 1 February. The drifter release points are separated into groups that correspond to drifters that reach South Georgia (•), those that approach South Georgia from the north (■), those that arrive to within 600 km of South Georgia (▲), and those that do not reach South Georgia (○). The areas of consistent Antarctic krill spawning, as identified in Marr (1962), are shown in grey. The thick grey line shows the moved position of the SACCF and the thin black lines indicate the 2000-m isobath.

4.5 Krill Growth Dynamics

Food time series along simulated drifter trajectories obtained from the reference simulation for release sites in the five regions discussed in section 4.3.3 were input to the krill growth model. The results of these simulations are next discussed.

4.5.1 Effect of Different Food Types

Larval krill, with an initial size of 2 mm represent the current season's spawn. Krill of this size are exposed to different phytoplankton time series (Appendix A, Fig. A1A, see also Fig. 8A) extracted along simulated drifter trajectories from region 1. The krill begin feeding in December (Year Day 335) and grow over time to different sizes (Fig. 43), because of the different amounts of food available to them along a given trajectory. Of the larval krill, 38% survive until the end of the simulation and 62% die due to insufficient food (Table 16). The maximum size reached by survivors at the end of the simulation is 13.13 mm and the smallest size when reaching South Georgia is 2.88 mm (note that different drifters have different length simulations depending on when a drifter reaches South Georgia). The 2.88 mm krill never encountered sufficient food to grow in size, but had just enough food to fulfill its relatively low energy demand (Appendix A, Fig. A1A, thick solid line). The other surviving krill managed to grow over the time of transport (Table 16). Krill that grow fast during the first days of the simulation often die when less food is provided, because their energy demand increases with increasing size. Therefore, 62% of the krill die during the simulation, the smallest being 6.13 mm, the largest being 14.38 mm at the time of death.

The simulated growth of 22 mm krill, which corresponds to the 1+ age class (juveniles) (cf. Fig. 3), develops differently than 2 mm krill, reaching a wide range of sizes at the end of the simulation. The smallest surviving krill is 21.88 mm, the largest is 31.63 mm at the end of the simulation (Table 16). Of the juvenile krill, 38% die during the time of the simulation and their sizes at death are between 17.88 and 30.63 mm. Juvenile krill grow slightly faster to bigger sizes than do larval krill, because they can feed on higher daily rations. At the same time, their energy demand is higher. Therefore, juvenile krill shrink more rapidly than larval krill, but can also survive longer periods of shrinking. Death of krill is defined as losing more than 45% of the body wet weight, so larger krill can survive longer than smaller krill, as they have higher initial wet weight (Hofmann and Lascara, 2000).

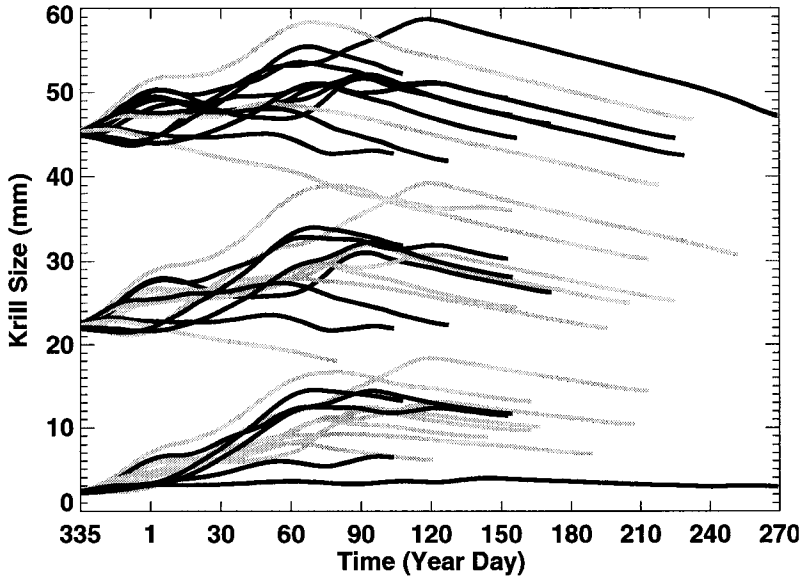

Fig. 43. Simulated growth of 2 mm krill (lower curves), 22 mm krill (middle curves), and 45 mm krill (upper curves) starting in December (Year Day 335) using phytoplankton food only. Krill that survive the time needed for transport to South Georgia are shown by black lines. Krill that die before reaching South Georgia are indicated by grey lines.

The pattern of growing and shrinking for 45 mm krill, which represents adult krill, is similar to that of the juvenile krill, except that shrinking periods are more pronounced and the 45 mm krill survive shrinking longer due to higher initial wet weight. Of the adult krill, 77% survive the entire time of the simulations and are between 41.63 and 51.88 mm in size at the end of the simulation when the simulated drifter reaches South Georgia. The implication is that the food encountered during transport was not sufficient for krill to grow much in size. Krill that died were between 35.88 and 46.63 mm at the time of death.

The effect of temperature on the simulated krill growth is implemented in these simulations by rescaling simulated daily growth rates of krill, which are calculated relative to 0°C, and rescaling them using temperature values extracted along drifter paths and a Q_{10} value of 3.5. Temperature affects growth rates of larval, juvenile, and adult krill noticeably only when krill encounter maxima or minima in the food that is available to them. When increased food concentrations coincide with elevated temperatures, they can increase the growth rate of krill by up to 4%, while the

coincidence of low food concentrations with decreased temperatures may decrease krill growth rates slightly. At the same time these increased growth rates of krill are of short duration and have only a small impact on the final size of krill at the end of the simulation.

Western Antarctic Peninsula

The drifters released in December along the western Antarctic Peninsula (region 1) need between 141 and 306 days to reach South Georgia (see section 4.3.3). As discussed above, phytoplankton food alone (Appendix A, Fig. A1A) is not sufficient to sustain krill originating at the western Antarctic Peninsula and many of these krill, especially larval krill die during the time needed to reach South Georgia (Fig. 44A, Table 16).

Including sea ice algae (Appendix A, Fig. A6A) and detritus (Appendix A, Fig. A11A) as additional food sources results in a significant improvement in krill growth and survival (Fig. 44B). Larval krill survival is more than doubled with additional food. The maximum size of krill at the time that coincides with arriving at South Georgia is 17.38 mm, which is a significant increase in size. Juvenile krill also show enhanced survival with this type of food than with phytoplankton only and all krill survive transport. Similarly the maximum size of survivors increases to 38.38 mm, but the minimum size decreases to 18.63. Adult krill profit from the additional food as well with 100% of the adults surviving the transport time. The maximum size of survivors at the end of the simulation increases to 55.88 mm during the last days of the simulation. This improvement in krill growth and survival is mainly an effect of detritus being available to krill, as most krill from this region do not encounter sea ice algae (Appendix A, Fig. A6A).

Adding heterotrophic food (Fig. 11) to the above food supply improves the growth and survival of juvenile and adult krill (Fig. 44C, Table 16). Larval krill cannot feed on copepods, so initially they do not profit from this additional food source, but as some of them reach a size larger than 18 mm, they start feeding on copepods. Therefore, although the number of survivors stays the same, the maximum size increases to 21.88 mm at the time that coincides with arrival at South Georgia. Juvenile and adult krill can use the additional food supply and the effect is that krill are now growing to sizes between 29.66 mm and 45.13 mm for juvenile krill and 49.13 mm and 59.88 mm for adult krill. In the simulations, all krill manage to grow above their starting size over the time of the simulation.

Table 16. Summary of krill growth simulations for different food types, initial sizes, and release times. The percent (%) and length of krill surviving and dying, respectively, at the end of each simulation is shown. The results are based on the food available along the trajectories of 13 drifters released in region 1, the west Antarctic Peninsula. Abbreviations used in the Table are: P (phytoplankton), PID (phytoplankton, sea ice algae, and detritus), PIDC (phytoplankton, sea ice algae, detritus, and copepods), D (detritus), NA (not applicable).

Food type	Initial size (mm)	Release time (month)	% surviving	Final length (mm)	% dying	Length at death (mm)
		Dec	38	2.88 - 13.13	62	6.13 - 14.38
	2	Jan	31	2.38 - 6.88	69	2.38 - 14.38
		Feb	31	2.38 - 5.13	69	1.88 - 8.88
P		Dec	62	21.88 - 31.63	38	17.88 - 30.63
	22	Jan	31	21.88 - 27.88	69	17.13 - 31.63
		Feb	23	17.88 - 24.63	77	17.13 - 24.38
		Dec	77	41.63 - 51.88	23	35.88 - 46.63
	45	Jan	77	36.63 - 48.13	23	35.13 - 35.88
		Feb	77	36.88 - 44.88	23	35.13 - 42.38
		Dec	85	5.13 - 17.38	15	10.13 - 13.38
	2	Jan	85	2.88 - 14.88	15	2.88 - 10.88
		Feb	77	2.13 - 8.63	23	6.38 - 8.88
PID		Dec	100	18.63 - 38.38	0	NA
	22	Jan	69	19.13 - 36.38	31	17.13 - 18.13
		Feb	92	17.88 - 18.13	8	17.38
		Dec	100	38.13 - 55.88	0	NA
	45	Jan	100	35.88 - 54.13	0	NA
		Feb	100	38.63 - 47.88	0	NA
		Dec	85	5.13 - 21.88	15	10.13 - 13.13
	2	Jan	77	2.88 - 22.38	23	2.88 - 10.88
		Feb	77	2.13 - 6.38	23	6.38 - 8.88
PIDC		Dec	100	29.66 - 45.13	0	NA
	22	Jan	100	23.63 - 44.13	0	NA
		Feb	100	24.88 - 38.13	0	NA
		Dec	100	49.13 - 59.88	0	NA
	45	Jan	100	44.13 - 59.88	0	NA
		Feb	100	44.63 - 55.13	0	NA
		Dec	69	2.13 - 4.38	31	1.88 - 5.63
	2	Jan	38	2.38 - 6.63	62	1.63 - 5.63
		Feb	8	2.38	92	1.63 - 3.38
D		Dec	46	18.13 - 21.65	54	17.13 - 21.88
	22	Jan	15	17.63 - 26.13	85	17.13 - 23.38
		Feb	8	20.63	92	17.13 - 19.63
		Dec	69	36.13 - 42.38	31	35.13 - 36.38
	45	Jan	54	35.38 - 44.63	46	35.13 - 35.38
		Feb	31	37.13 - 40.63	69	35.13 - 37.38

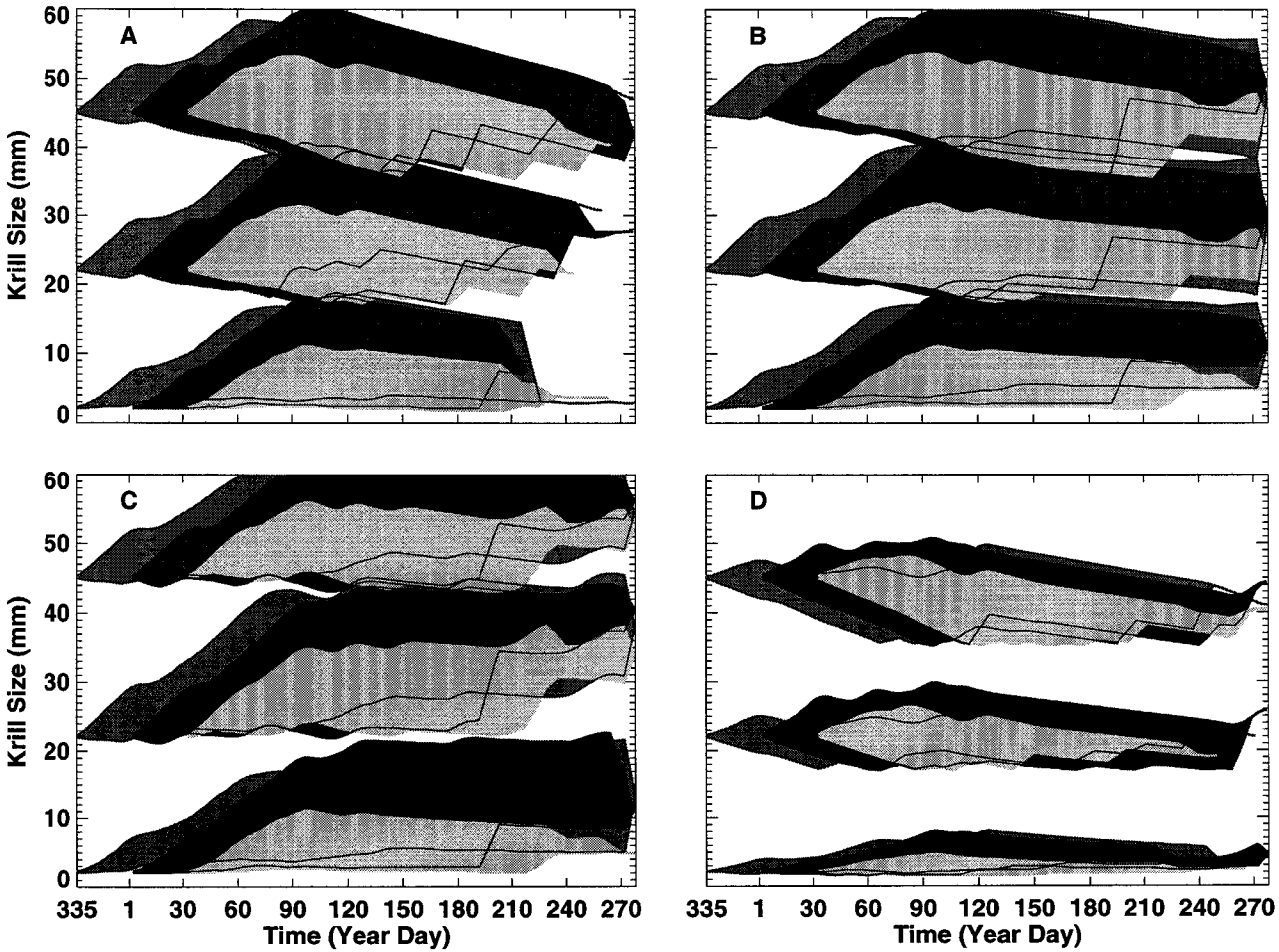

Fig. 44. Range of simulated growth of 2 mm krill (lower curves), 22 mm krill (middle curves), and 45 mm krill (upper curves) released in the west Antarctic Peninsula region in December (medium shading), January (dark shading), and February (light shading) obtained for Antarctic krill feeding on A) phytoplankton only, B) phytoplankton and sea ice algae with detritus, C) phytoplankton, copepods and sea ice algae with detritus, and D) detritus only.

Feeding on detritus (Appendix A, Fig. A11A) as the only food source is not beneficial for krill originating from region 1 (Fig. 44D). Food concentrations are highest during the first five months of the simulation but are still too low for krill to grow much in size. Detritus concentrations decrease during winter (Fig. 13A), so that all krill shrink from then on. Therefore, although 69% of the adult krill survive transport, they only grow to final sizes of 36.13 mm to 42.38 mm. Larval krill, with their lower energy needs, grow slightly more during the first months of the simulation and 69% of the larvae survive transport times. They grow to sizes of 3.13 mm to 4.38 mm by the end of the simulation. All three krill sizes grow to smaller sizes when feeding on detritus only than when feeding on phytoplankton only.

Although the above discussion focuses on December release only, the same can be said for all other release times (Fig. 44, dark and light shading). For krill originating at the western Antarctic Peninsula the combined food of phytoplankton, sea ice algae, detritus and heterotrophic food is the most favorable food supply. In these simulations the phytoplankton food encountered is sufficient for some krill to survive (Appendix A, Fig. A1A), but the detritus encountered (Appendix A, Fig. A11A) provides sufficient food to improve the survival of all krill sizes. The consistent supply of detritus (Appendix A, Fig. A11A) and heterotrophic food (Fig. 11) are the primary food sources that allow survival during times of low food supply in these simulations.

Bransfield Strait

The drifter results presented in section 4.3.3, show that krill originating in Bransfield Strait (region 2) need between 184 and 306 days to reach South Georgia, when released in December. Phytoplankton food alone (Appendix A, Fig. A2A) is not sufficient for krill to survive, with only 33% of the larval krill originating in this region surviving the transport to South Georgia (Fig. 45A, Table 17). The survivors grow to sizes between 4.38 mm and 16.13 mm, which is overall bigger than larval krill from region 1. Only 22% of the juvenile krill survive, growing to 22.13 mm to 35.13 mm in size, while 78% of adult krill survive, reaching sizes of 35.88 mm to 59.88 mm.

The addition of sea ice algae (Appendix A, Fig. A7A) combined with detritus (Appendix A, Fig. A12A) as additional food sources, improves the growth and survival of krill (Fig. 45B) by more than doubling the number of survivors of larval and juvenile krill, similar to what was found for krill originating in region 1. The

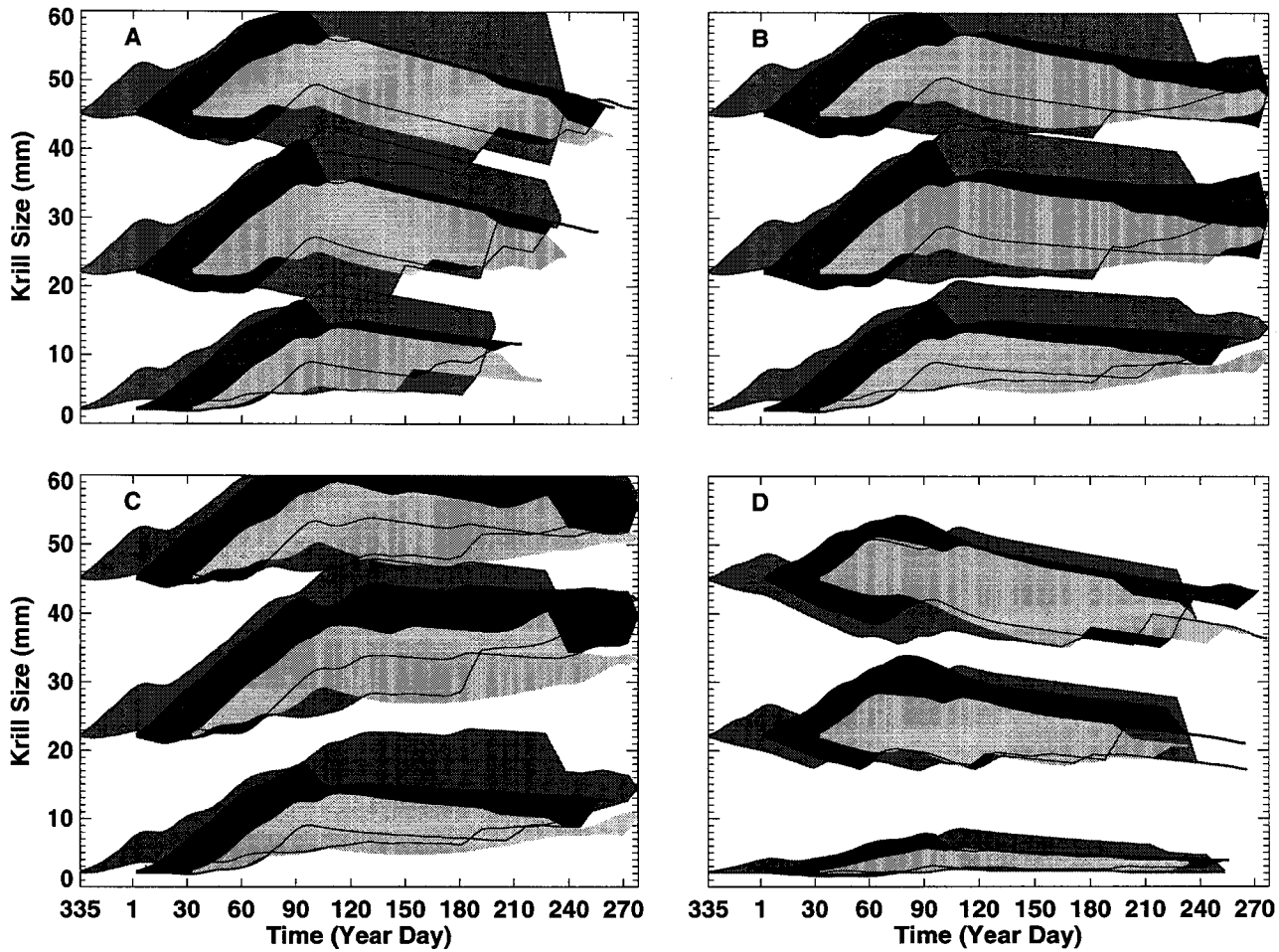

Fig. 45. Range of simulated growth of 2 mm krill (lower curves), 22 mm krill (middle curves), and 45 mm krill (upper curves) released in the Bransfield Strait region in December (medium shading), January (dark shading), and February (light shading) obtained for feeding on A) phytoplankton only, B) phytoplankton and sea ice algae with detritus, C) phytoplankton, copepods and sea ice algae with detritus, and D) detritus only.

Table 17. Summary of krill growth simulations for different food types, initial sizes, and release times. The percent (%) and length of krill surviving and dying, respectively, at the end of each simulation is shown. The results are based on the food available along the trajectories of nine drifters released in region 2, the Bransfield Strait. Abbreviations are: P (phytoplankton), PID (phytoplankton, sea ice algae, and detritus), PIDC (phytoplankton, sea ice algae, detritus, and copepods), D (detritus), NA (not applicable).

Food type	Initial size (mm)	Release time (month)	% surviving	Final length (mm)	% dying	Length at death (mm)
		Dec	33	4.38 - 16.13	67	7.88 - 13.38
	2	Jan	11	17.38	89	8.88 - 11.68
		Feb	11	10.88	89	6.38 - 9.88
P		Dec	22	22.13 - 35.13	78	17.38 - 28.63
	22	Jan	22	25.13 - 40.63	78	22.13 - 28.63
		Feb	22	27.13 - 30.38	78	22.38 - 27.13
		Dec	78	35.88 - 59.88	22	40.88 - 41.63
	45	Jan	44	41.63 - 59.88	56	40.63 - 46.63
		Feb	44	42.88 - 50.38	56	39.63 - 43.88
		Dec	89	6.13 - 18.13	11	8.38
	2	Jan	33	12.13 - 17.38	67	6.88 - 11.38
		Feb	44	8.63 - 11.13	56	7.62 - 9.88
PID		Dec	100	21.13 - 39.63	0	NA
	22	Jan	100	23.88 - 40.63	0	NA
		Feb	100	23.88 - 32.13	0	NA
		Dec	100	41.63 - 59.88	0	NA
	45	Jan	100	43.13 - 59.88	0	NA
		Feb	100	44.13 - 52.13	0	NA
		Dec	89	6.13 - 16.38	11	8.38
	2	Jan	33	12.88 - 12.13	67	6.88 - 11.38
		Feb	44	7.63 - 11.13	56	7.63 - 9.88
PIDC		Dec	100	33.38 - 46.13	0	NA
	22	Jan	100	33.63 - 43.38	0	NA
		Feb	100	32.63 - 40.38	0	NA
		Dec	100	48.63 - 59.88	0	NA
	45	Jan	100	51.88 - 59.88	0	NA
		Feb	100	50.88 - 59.88	0	NA
		Dec	34	2.88 - 3.13	66	1.88 - 6.13
	2	Jan	34	3.63 - 7.13	66	2.63 - 4.63
		Feb	34	2.63 - 3.88	66	2.63 - 3.88
D		Dec	23	17.13 - 18.13	77	17.13 - 18.13
	22	Jan	34	19.88 - 20.88	66	17.13 - 26.13
		Feb	23	20.63 - 23.63	77	17.38 - 21.63
		Dec	78	35.38 - 46.13	22	35.13
	45	Jan	45	37.13 - 51.13	55	35.13 - 43.13
		Feb	56	37.13 - 44.63	44	35.13 - 38.13

survival rate for juvenile and adult krill is now 100%. Again this is due mainly to the availability of detritus to krill. Growth and survival of krill further improves when heterotrophic food is added as an additional food source (Fig. 45C), with 89% larval krill surviving a time that coincides with arrival at South Georgia, growing up to 16.38 mm. In the juvenile and adult krill simulations, all krill survive to reach South Georgia, and their sizes increase to between 33.38 mm to 46.13 mm and 48.63 mm to 59.88 mm, respectively.

For juvenile and adult krill originating in region 2, detritus as the only food source is not beneficial (Fig. 45D, Table 17) and the simulated growth patterns are similar to those obtained for region 1. Surviving krill of all sizes do not grow significantly in the total simulation time. Thus, for juvenile and adult krill originating in the Bransfield Strait region the combined phytoplankton, sea ice algae, detritus and heterotrophic food is the most favorable food supply. Few krill have access to enough sea ice algae that could supply an additional food source (Appendix A, Fig. A7A), but the consistent supply of detritus (Appendix A, Fig. A12A) and heterotrophic food (Fig. 11) is the main reason for them to survive times of low food supply.

Elephant Island/Scotia Sea

The simulated drifters originating in the Elephant Island/Scotia Sea area need between 58 and 277 days to reach South Georgia when released in December (see section 4.3.3). This is considerably less time than that needed by drifters released in other regions. Phytoplankton as the only food source (Appendix A, Fig. A3) is sufficient, as evidenced by 43% of the larvae, 62% of the juvenile, and 86% of the adult krill surviving long enough to reach South Georgia (Fig. 46A, Table 18).

The addition of sea ice algae (Appendix A, Fig. A8A) and detritus (Appendix A, Fig. A13A) improves the growth and survival of krill (Fig. 46B, Table 18) although no sea ice is encountered by krill (Appendix A, Fig. A8A). The addition of heterotrophic food improves the growth and survival of krill (Fig. 46C) because more food is available during the simulation (Fig. 11, Appendix A, Fig. A13A). Most larval krill cannot utilize this food source during the simulation and 86% of the larval krill survive, relative to feeding on phytoplankton only. Juvenile krill survival, however, reaches 95%, and all adult krill survive the time of the simulation.

Detritus concentrations are high along the simulated drifter trajectories originating in this region in the first five months of the simulation (Appendix A, Fig. A13A) compared to other origination areas. As a result, all three sizes of krill grow slightly

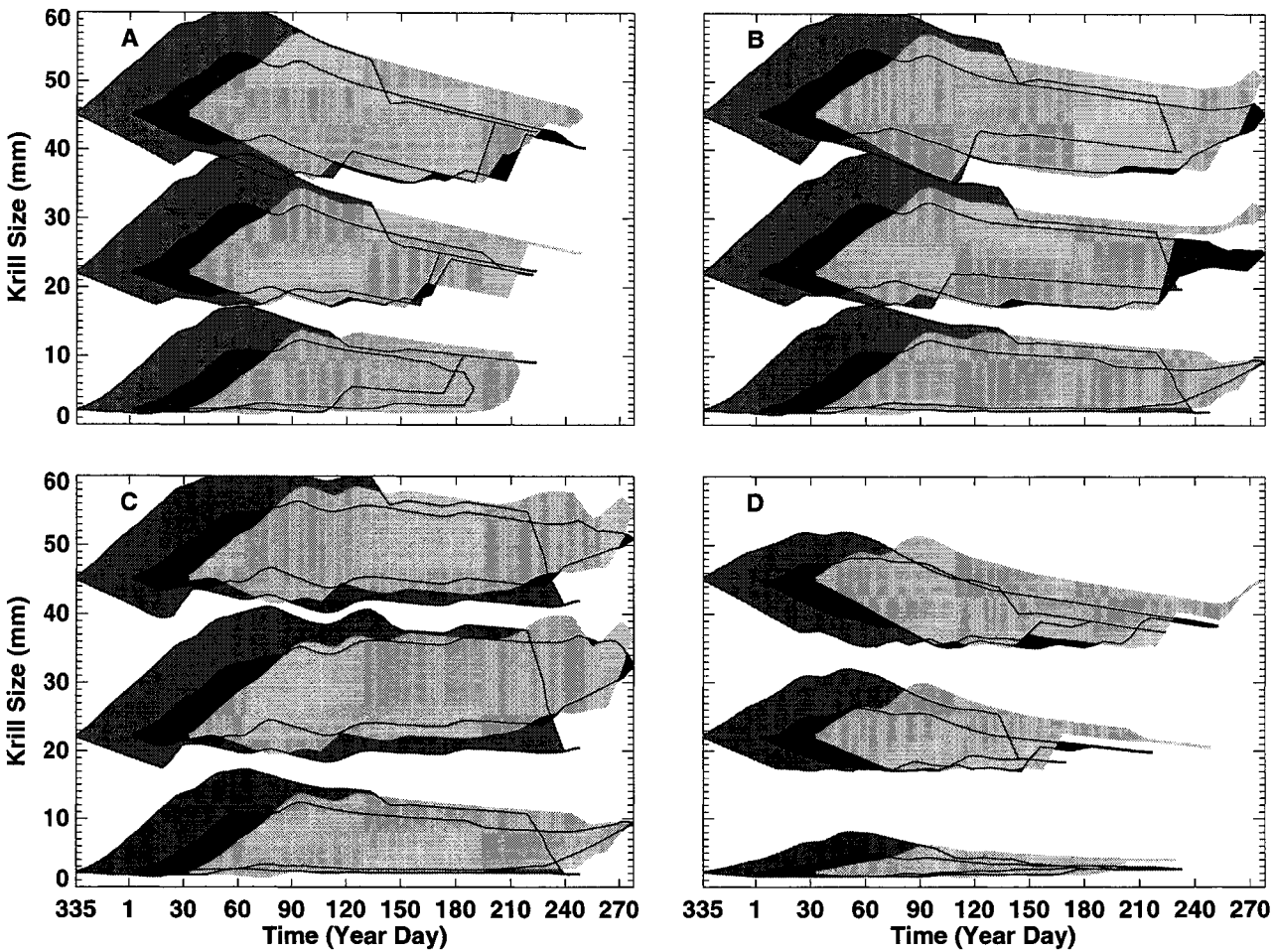

Fig. 46. Range of simulated growth of 2 mm krill (lower curves), 22 mm krill (middle curves), and 45 mm krill (upper curves) released in the Elephant Island/Scotia Sea region in December (medium shading), January (dark shading), and February (light shading) obtained for feeding on A) phytoplankton only, B) phytoplankton and sea ice algae with detritus, C) phytoplankton, copepods and sea ice algae with detritus, and D) detritus only.

Table 18. Summary of krill growth simulations for different food types, initial sizes, and release times. The percent (%) and length of krill surviving and dying, respectively, at the end of each simulation is shown. The results are based on the food available along the trajectories of 21 drifters released in region 3, the Elephant Island/Scotia Sea area. Abbreviations are: P (phytoplankton), PID (phytoplankton, sea ice algae, and detritus), PIDC (phytoplankton, sea ice algae, detritus, and copepods), D (detritus), NA (not applicable).

Food type	Initial size (mm)	Release time (month)	% surviving	Final length (mm)	% dying	Length at death (mm)
		Dec	43	3.13 - 10.63	57	1.88 - 13.38
	2	Jan	33	3.13 - 6.63	67	2.88 - 9.88
		Feb	33	17.88 - 36.63	67	1.88 - 10.88
P		Dec	62	19.13 - 31.88	38	17.13 - 23.63
	22	Jan	43	18.88 - 24.38	57	17.13 - 24.88
		Feb	38	17.88 - 26.63	62	17.13 - 26.63
		Dec	86	35.63 - 52.88	14	35.13 - 39.63
	45	Jan	57	37.38 - 45.38	43	35.13 - 40.38
		Feb	67	35.13 - 47.88	33	35.13 - 45.63
		Dec	86	2.13 - 14.13	14	1.63 - 10.13
	2	Jan	67	3.13 - 10.13	33	4.88 - 9.88
		Feb	71	2.38 - 9.13	29	1.63 - 10.88
PID		Dec	86	19.88 - 34.38	14	17.13
	22	Jan	86	17.88 - 27.63	14	17.13 - 20.88
		Feb	62	19.38 - 33.13	38	17.13 - 20.88
		Dec	95	37.38 - 55.38	5	35.13
	45	Jan	100	36.63 - 47.38	0	NA
		Feb	100	35.13 - 48.63	0	NA
		Dec	86	2.13 - 12.13	14	1.63 - 10.13
	2	Jan	67	3.13 - 10.13	33	4.88 - 9.88
		Feb	71	2.38 - 9.13	29	1.63 - 10.63
PIDC		Dec	95	20.88 - 40.63	5	17.13
	22	Jan	100	23.88 - 37.63	0	NA
		Feb	100	19.88 - 33.88	0	NA
		Dec	100	40.37 - 59.88	0	NA
	45	Jan	100	40.13 - 54.13	0	NA
		Feb	100	41.66 - 57.63	0	NA
		Dec	48	2.13 - 4.13	52	1.63 - 5.63
	2	Jan	24	1.88 - 2.38	76	1.63 - 3.38
		Feb	10	1.88 - 2.38	90	1.63 - 3.88
D		Dec	29	18.38 - 25.38	71	17.13 - 21.63
	22	Jan	10	17.13 - 17.63	90	17.13 - 20.63
		Feb	14	20.38 - 20.88	86	17.13 - 21.63
		Dec	67	35.88 - 43.88	33	35.13 - 36.13
	45	Jan	43	35.88 - 39.13	57	35.13 - 38.13
		Feb	52	35.13 - 45.13	48	35.13 - 39.13

more in the first months (Fig. 46D). But detritus concentrations decrease so drastically that only 29% juvenile krill survive, while 48% of the larval krill and 67% of the adult krill survive the time of the simulation. However, again all krill do not grow significantly over the transport time compared to krill feeding on phytoplankton only.

Krill originating in this area are able to survive transport with phytoplankton as the sole food source. Adding detritus and heterotrophic food sources improves the growth and survival of krill, while no sea ice-derived food is encountered (Appendix A, Fig. A8A) because the drifter paths are away from the advancing sea ice in winter. Again, the continuous supply of detritus and heterotrophic food allow survival of krill during times of low food supply. However, detritus concentrations along the drifter trajectories are so low after the first five months of the simulation (Appendix A, Fig. A13A), that it alone is not an adequate food source.

Southwestern Antarctic Peninsula

Drifters originating at the southwestern Antarctic Peninsula (region 4) need between 211 and 306 days to reach South Georgia (see section 4.3.3) because this region is the farthest away from South Georgia. Feeding on phytoplankton food only is deleterious to krill (Fig. 47A, Table 19). Although sufficient food is available in the first four months to support growth (Appendix A, Fig. A4A), none of the krill survive the time needed to reach South Georgia from this region. The long time required to reach South Georgia and the low food values from April onward, result in essentially no survival.

Providing sea ice algae combined with detritus as an additional food source provides a great improvement (Fig. 47B, Table 19), enabeling 83% of all sizes of krill to survive the time necessary for transport. This is mostly due to the inclusion of detritus, as sea ice algae concentrations are low (Appendix A, Fig. A9A). The growth and survival of krill improves more with the addition of heterotrophic food (Fig. 47C, Table 19). All juvenile and adult krill survive the simulation time and develop to sizes of 26.63 mm to 42.13 mm and 46.38 mm to 57.88 mm for juvenile and adult krill, respectively. Detritus concentrations along trajectories originating from this region (Appendix A, Fig. A14A) are so low during the first months of the simulation that all krill, independent of size feeding on this sole food source, die before the end of the simulation (Fig. 47D, Table 19).

For all sizes of krill originating at the southwestern Antarctic Peninsula the

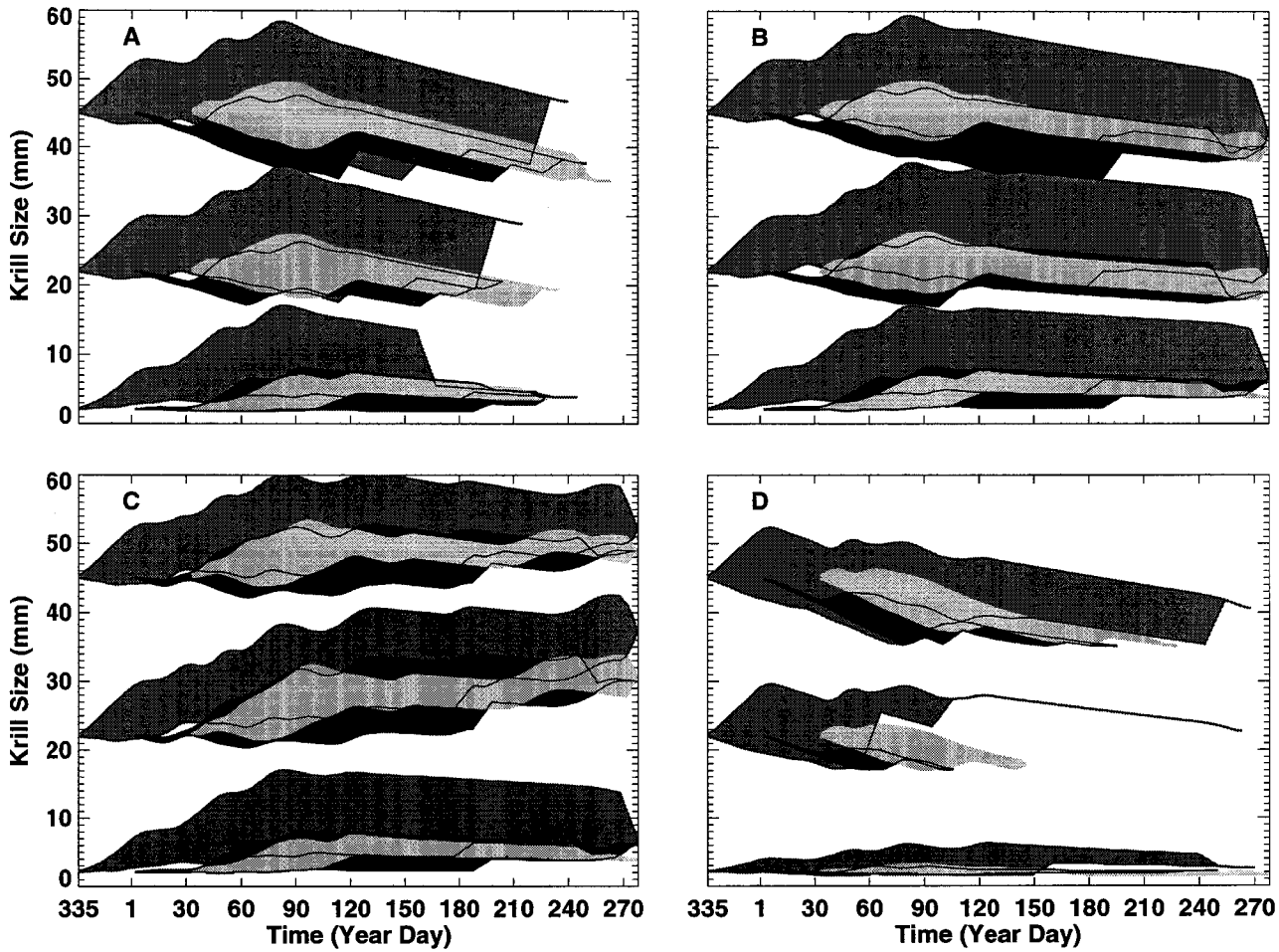

Fig. 47. Range of simulated growth of 2 mm krill (lower curves), 22 mm krill (middle curves), and 45 mm krill (upper curves) released in the southwest Antarctic Peninsula region in December (medium shading), January (dark shading), and February (light shading) obtained for feeding on A) phytoplankton only, B) phytoplankton and sea ice algae with detritus, C) phytoplankton, copepods and sea ice algae with detritus, and D) detritus only.

Table 19. Summary of krill growth simulations for different food types, initial sizes, and release times. The percent (%) and length of krill surviving and dying, respectively, at the end of each simulation is shown. The results are based on the food available along the trajectories of six drifters released in region 4, the southwest Antarctic Peninsula. Abbreviations are: P (phytoplankton), PID (phytoplankton, sea ice algae, and detritus), PIDC (phytoplankton, sea ice algae, detritus, and copepods), D (detritus), NA (not applicable).

Food type	Initial size (mm)	Release time (month)	% surviving	Final length (mm)	% dying	Length at death (mm)
		Dec	0	NA	100	3.13 - 13.38
	2	Jan	0	NA	100	1.88 - 5.88
		Feb	0	NA	100	3.63 - 5.13
P		Dec	0	NA	100	17.38 - 28.88
	22	Jan	0	NA	100	17.13 - 20.63
		Feb	0	NA	100	17.13 - 21.13
		Dec	0	NA	100	35.13 - 46.63
	45	Jan	17	37.63	83	35.13 - 36.13
		Feb	17	35.38	83	35.13 - 39.13
		Dec	83	4.13 - 13.38	17	8.38
	2	Jan	100	2.38 - 6.38	0	NA
		Feb	67	3.88 - 6.13	33	4.13 - 4.88
PID		Dec	83	19.38 - 31.88	17	24.88
	22	Jan	83	17.13 - 23.63	17	17.13
		Feb	83	17.88 - 22.88	17	20.13
		Dec	83	38.88 - 49.38	17	42.88
	45	Jan	100	35.38 - 43.13	0	NA
		Feb	100	37.88 - 43.13	0	NA
		Dec	83	4.13 - 13.38	17	8.88
	2	Jan	100	2.38 - 6.68	0	NA
		Feb	67	3.88 - 6.13	33	4.13 - 4.88
PIDC		Dec	100	26.63 - 42.13	0	NA
	22	Jan	100	23.13 - 35.13	0	NA
		Feb	100	27.88 - 33.88	0	NA
		Dec	100	46.38 - 57.88	0	NA
	45	Jan	100	44.38 - 51.63	0	NA
		Feb	100	47.13 - 52.13	0	NA
		Dec	0	NA	100	1.63 - 4.63
	2	Jan	0	NA	100	1.63 - 2.13
		Feb	0	NA	100	1.63 - 2.38
D		Dec	0	NA	100	17.13 - 13.13
	22	Jan	0	NA	100	17.13
		Feb	0	NA	100	17.13 - 18.38
		Dec	0	NA	100	35.13 - 41.83
	45	Jan	0	NA	100	35.13
		Feb	0	NA	100	35.13 - 36.63

combined food of phytoplankton, sea ice algae, detritus and heterotrophic food is the most favorable food supply. Krill do not encounter much sea ice (Appendix A, Fig. A9A), but detritus and the addition of heterotrophic food increases their chances of survival during times of low food supply. Detritus feeding alone is not beneficial for krill released in this region.

Weddell Sea

Simulations of krill growth for krill originating in region 5, the Weddell Sea continental shelf break area, are different from the above simulations because few of the drifters originating in this region are transported to within 600 km of South Georgia. Most are transported to the Weddell-Scotia Confluence. Phytoplankton food alone is not sufficient to sustain krill (Fig. 48A, Table 20). This is expected because most of the origination sites are underneath sea ice and little pelagic phytoplankton is available (Appendix A, Fig. A5A).

Adding sea ice algae (Appendix A, Fig. A10A) and detritus (Appendix A, Fig. A15A) as additional food sources improves the growth and survival of krill (Fig. 48B, Table 20) because so much sea ice algae is present that krill of all sizes have sufficient food (Appendix A, Fig. A10). All larval krill that survive the simulation time (65%), as well as all juvenile and adult survivors (71% and 100% respectively) grow to large sizes. This growth is within the limit set in the model (maximum daily growth rate of 0.25 mm d^{-1}) but is not realistic. Not all krill from this region survive transport because they leave the sea ice covered area of the Weddell Scotia Confluence at a time of low phytoplankton concentrations.

The addition of heterotrophic food (Fig. 11) improves the survival of juvenile and adult krill (Fig. 48C, Table 20), with more juvenile and adult krill surviving. Again, this growth is not realistic. This food source provides the needed food when krill leave the ice-covered area. Detritus-only feeding is not beneficial for krill originating from region 5 (Fig. 48D). Detritus concentrations along the drifter trajectories are high compared to trajectories from region 4 (Appendix A, Fig. A15), but lower than in all other areas. However, similar to results from other simulations, 12% larval krill, 18% juvenile krill, and 24% adult krill survive the simulation.

Due to the release location in an area largely covered with sea ice, sea ice algae is the dominant food source in this simulation and adding heterotrophic food increases the chances of survival for larger krill. Drifters from this region are not likely to reach South Georgia in the 306 days of this simulation, but instead, most reach

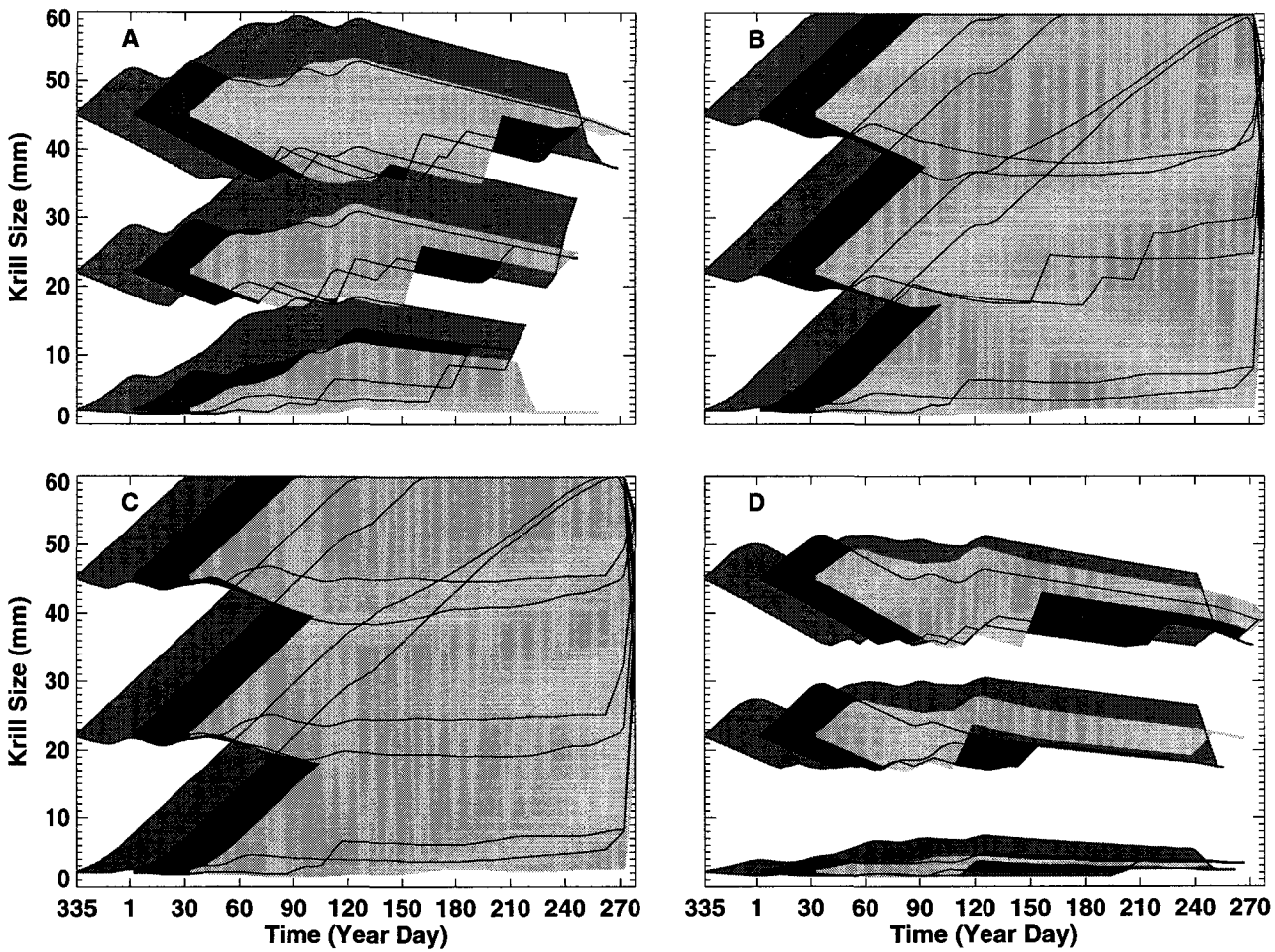

Fig. 48. Range of simulated growth of 2 mm krill (lower curves), 22 mm krill (middle curves), and 45 mm krill (upper curves) released in the Weddell Sea region in December (medium shading), January (dark shading), and February (light shading) obtained for feeding on A) phytoplankton only, B) phytoplankton and sea ice algae with detritus, C) phytoplankton, copepods and sea ice algae with detritus, and D) detritus only.

Table 20. Summary of krill growth simulations for different food types, initial sizes, and release times. The percent (%) and length of krill surviving and dying, respectively, at the end of each simulation is shown. The results are based on the food available along the trajectories of 17 drifters released in region 5, the Weddell Sea. Abbreviations are: P (phytoplankton), PID (phytoplankton, sea ice algae, and detritus), PIDC (phytoplankton, sea ice algae, detritus, and copepods), D (detritus), NA (not applicable).

Food type	Initial size (mm)	Release time (month)	% surviving	Final length (mm)	% dying	Length at death (mm)
		Dec	0	NA	100	1.63 - 14.38
	2	Jan	0	NA	100	1.63 - 10.88
		Feb	0	NA	100	1.63 - 8.83
P		Dec	12	24.88 - 32.63	88	17.13 - 24.13
	22	Jan	0	NA	100	17.13 - 24.13
		Feb	6	22.13	94	17.13 - 24.88
		Dec	18	43.88 - 50.63	82	35.13 - 41.63
	45	Jan	0	NA	100	35.13 - 42.13
		Feb	6	43.13	94	35.13 - 42.38
		Dec	65	5.38 - 59.88	35	6.13 - 15.13
	2	Jan	47	8.13 - 59.88	53	1.88 - 8.13
		Feb	59	2.63 - 53.38	41	1.63 - 8.63
PID		Dec	71	29.38 - 59.88	29	17.38 - 27.63
	22	Jan	65	18.13 - 59.88	35	17.13 - 21.63
		Feb	59	25.88 - 59.88	41	17.13
		Dec	100	40.13 - 59.88	0	NA
	45	Jan	82	42.13 - 59.88	18	36.38 - 40.63
		Feb	82	36.88 - 59.88	18	35.13
		Dec	65	5.38 - 59.88	35	6.13 - 15.13
	2	Jan	47	8.13 - 59.88	53	1.88 - 8.38
		Feb	59	2.63 - 53.13	41	1.63 - 8.63
PIDC		Dec	94	25.13 - 59.88	6	27.88
	22	Jan	82	23.13 - 59.88	18	18.38 - 21.88
		Feb	94	22.38 - 59.88	6	17.63
		Dec	100	45.38 - 59.88	0	NA
	45	Jan	100	45.38 - 59.88	0	NA
		Feb	100	43.63 - 59.88	0	NA
		Dec	12	3.63 - 4.88	88	1.63 - 5.38
	2	Jan	0	NA	100	1.63 - 3.38
		Feb	6	2.88	94	1.63 - 3.13
D		Dec	18	10.13 - 26.13	82	17.13 - 19.88
	22	Jan	0	NA	100	17.13 - 23.13
		Feb	6	19.86	94	17.13 - 21.63
		Dec	24	35.13 - 45.38	76	35.13 - 37.38
	45	Jan	6	38.63	94	35.13 - 40.88
		Feb	18	37.13 - 40.63	82	35.13

the Weddell-Scotia Confluence. Krill are in good condition at that time. Drifters would then need an additional ten months of transport to reach South Georgia, as discussed in section 5.2.2. This would place them at South Georgia in October to December of the following year.

4.5.2 Effect of Different Spawning Times

The range of krill growth rates obtained for the January simulations of drifters originating in region 1 is larger for the different food time series, with the exception of detritus, than those obtained for the December and February simulations (Fig. 44A-C). However, the important results from the simulations are how many krill survive and what size they grow to in the time needed for the simulated drifter to reach South Georgia. As discussed in section 3.3, the length of time when high phytoplankton concentrations are encountered decreases significantly with later spawning times (Fig. 8). This is mirrored in the results for all three initial krill sizes and the first three feeding simulations (Figs. 44A-C) and the numbers of how many krill survive, as well as the maximum size of survivors decrease from the December to the February release. When detritus is the primary food source (Fig. 44D), this is true also and the survival rate or all krill is highest when released in December.

Overall it can be concluded that a December release is the most beneficial time for the survival and growth of krill transported to South Georgia from the western Antarctic Peninsula. Earlier spawning is best, especially for larval krill, which is the most likely size class to get transported to South Georgia. For juveniles and adults, the difference in growth and survival for the different spawning times is small when krill exploit a combination of all food sources.

The effects of different spawning times for krill originating in region 2 (Fig. 45, Table 17) are similar to those for krill originating in region 1. Again December is the most beneficial release time for krill from region 2, when feeding on all food types except detritus. The simulated results for krill feeding on detritus only is also similar to those obtained for krill released in region 1, however, January is the most beneficial start time for detritus only feeding in this simulation (Fig. 45D, Table 17). For krill originating in the Elephant Island/Scotia Sea area (region 3), the southwest Antarctic Peninsula (region 4), and the Weddell Sea (region 5), a December release is most favorable for krill feeding on all four food sources, although differences between release times are small.

4.5.3 Krill Growth Rates

To assess the effect of different food sources on krill growth and survival daily growth rates of krill originating at the west Antarctic Peninsula released in January are examined. Daily growth rates associated with 2 mm krill feeding on all four food sources combined (Fig. 49) range between -0.09 to 0.25 mm d^{-1}. Daily growth rates of 22 mm and 45 mm krill range between -0.125 to 0.25 mm d^{-1} and -0.15 to 0.25 mm d^{-1}, respectively. Periods of shrinking occur in all sizes of krill, but more so for 45 mm krill because larger krill have a higher energy demand than smaller krill. The maximum growth rate for all sizes is 0.25 mm d^{-1} because this is the maximum growth rate allowed in the model to keep growth realistic. Shrinking rates for 45 mm krill are higher than those for 22 mm krill, which are higher than those for 2 mm krill. This reflects the higher metabolic rates of the larger animals. The simulated growth rates are within the range of observed growth rates, 0.105 to 0.179 mm d^{-1} (Rosenberg et al., 1986) and 0.33 mm d^{-1} (Clarke and Morris, 1983).

Different food sources have different effects on the daily growth rates of krill (Fig. 49). At the beginning of transport phytoplankton concentrations are low, but increase rapidly after 10 days. This causes an increase in the growth rate of larval krill over the time of high phytoplankton supply. The growth rate does not increase more rapidly, because the food uptake of krill is limited depending on krill size. The growth rate of juvenile and adult krill increases more rapidly. This is caused by older krill being able to feed on heterotrophic food available at the same time, as well as the fact that larger krill can feed on larger portions of food. A sudden decrease in phytoplankton food causes negative growth rates (shrinking) in all sizes of krill. Until day 90 krill growth rates are closely tied to the phytoplankton concentrations available as food. Constantly high phytoplankton concentrations, such as seen between day 40 and day 50, indicate that krill encountered an eddy with high food concentrations for a period of time.

After day 90 however, other food sources gain more importance. The combination of heterotrophic food and phytoplankton increases growth rates of all krill sizes around day 100, but afterward a period of shrinking starts because of insufficient food. Larval krill has reached sizes of larger than 18 mm at this time and is therefore able to utilize the heterotrophic food as well. Detritus is available as the only food source after day 110, but because of its low metabolic value the amount of detritus available is not enough to sustain growth. Krill encounter four patches of sea ice

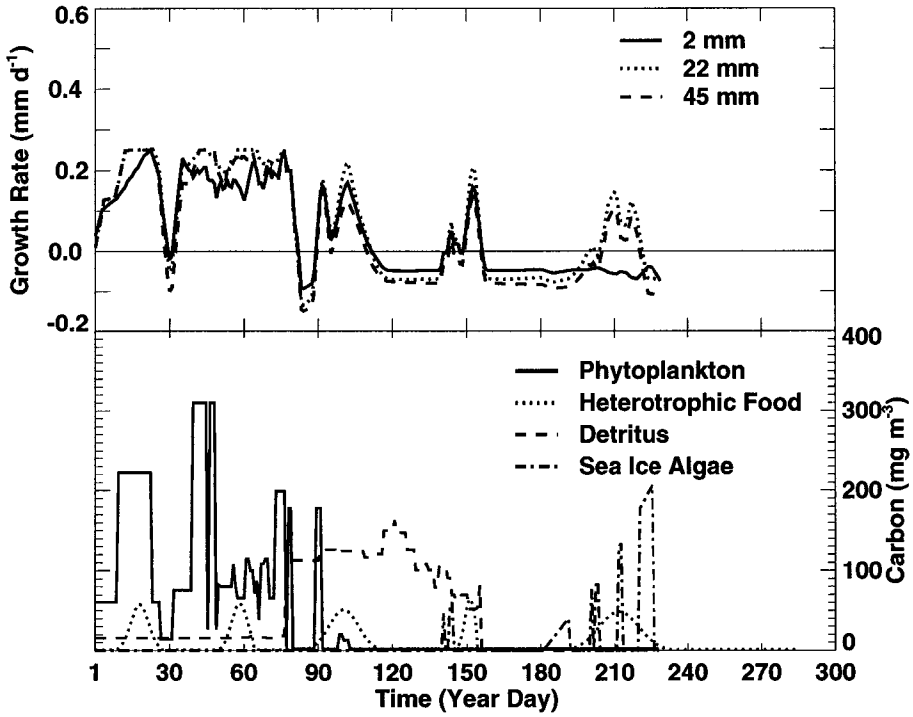

Fig. 49. Simulated daily growth rates of 2 mm, 22 mm, and 45 mm krill feeding on all food sources combined when starting transport from the west Antarctic Peninsula in January. The time series of phytoplankton, sea ice algae, heterotrophic food and detritus are shown.

algae in this simulation after day 200. Larval krill have shrunk below 18 mm by this time and show a decreased growth rate, indicating that low concentrations of sea ice algae alone as a food source have a negative effect on krill growth. This is because the energy needed to feed on this food source is higher than the energy available from the food. Older krill switch between feeding on heterotrophic food and sea ice algae during this time and similar effects on the growth rate of these are observed.

4.5.4 Length-frequency Distribution of Krill across the Scotia Sea

Comparison with *Discovery* Data

The results from the krill growth simulations can be verified by comparing with observed krill length-frequency distributions discussed in section 3.5.2. In these comparisons, time in the simulation is used as a proxy for distance across the Scotia

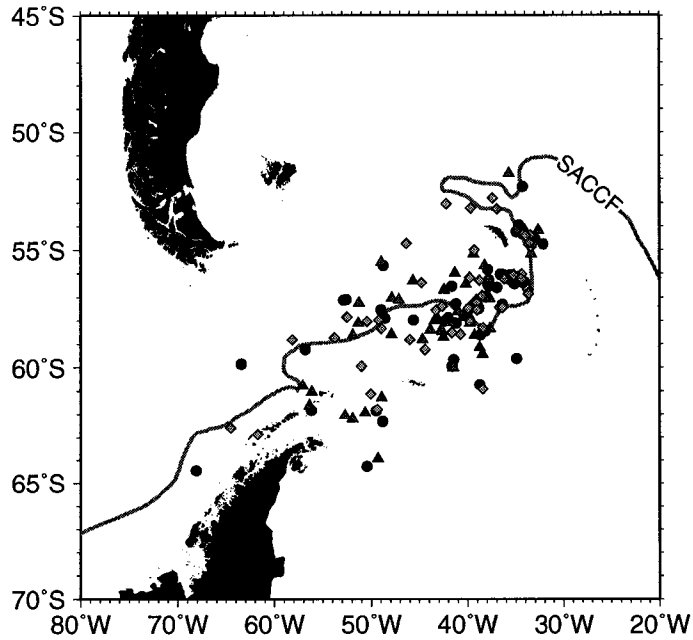

Fig. 50. Simulated distribution of larval krill across the study area for individuals that were released in December (•), January (▲), and February (♦). The climatological location of the SACCF is shown for reference.

Sea. The distribution of larval krill at the end of the reference simulation for krill feeding on phytoplankton, sea ice algae, detritus and heterotrophic food combined (Fig. 50), shows that larval krill are distributed along the path of the SACCF from the Antarctic Peninsula to South Georgia, with most larvae found in the southeastern Scotia Sea. Large numbers of larval krill are found at the eastern and northern side of South Georgia. This distribution compares well to the length-frequency values from *Discovery* observations (cf. Fig. 18A), which show abundant larvae around South Georgia, distributed along the western Antarctic Peninsula, and across the Scotia Sea south of the SACCF. The simulated distributions, however, show larval krill north of the SACCF west of 43°W, which is not seen in the observations.

The simulated length-frequency distributions obtained for older krill (>20 mm) feeding on all four food sources combined (Fig. 51) can be compared to the distribution of the same size krill in summer (January to March) extracted from the *Discovery* data (Fig. 18B). These comparisons show that the earlier the start of the simulation, the further the krill can spread throughout the Scotia Sea by the end of

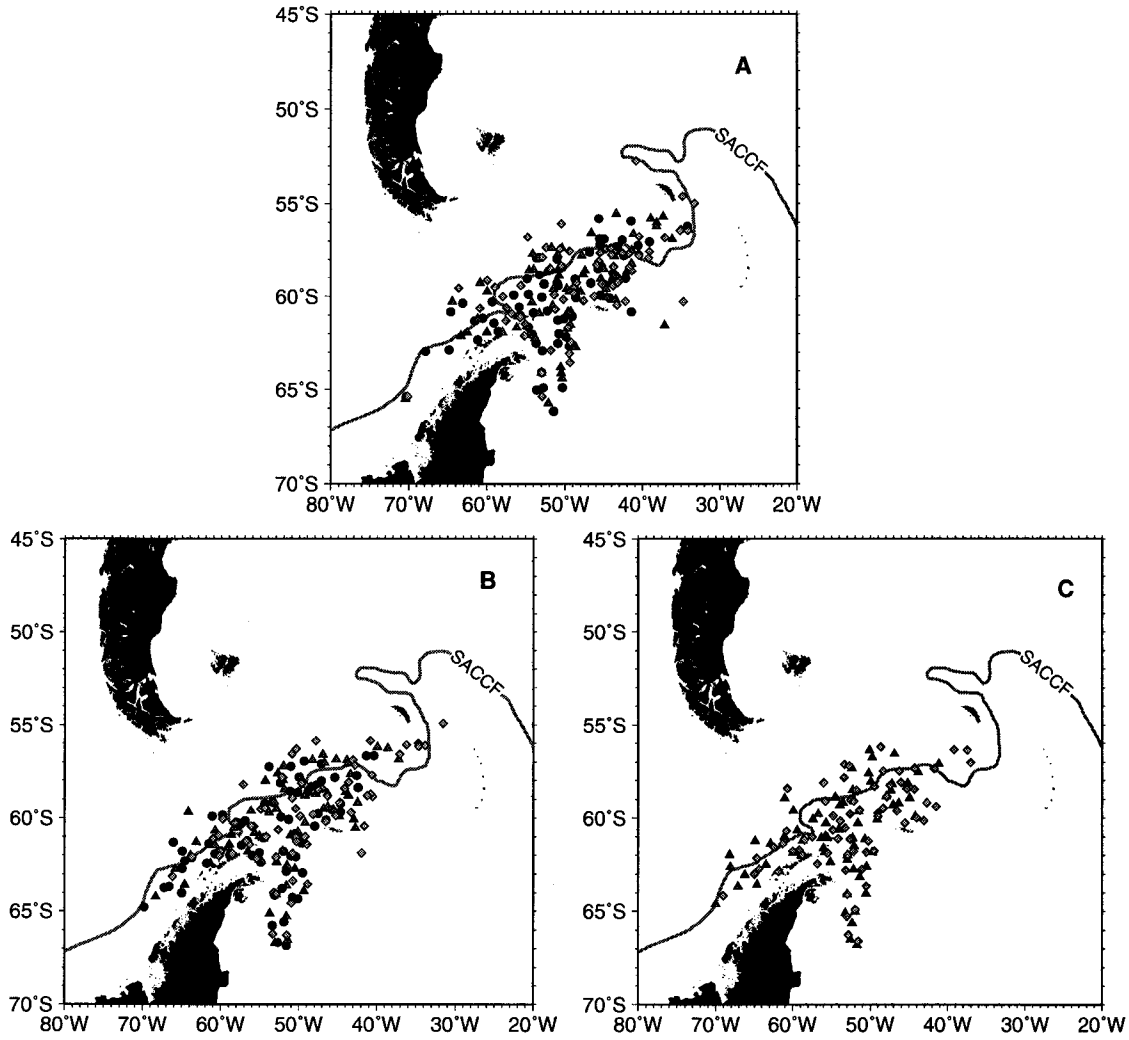

Fig. 51. Simulated distribution of older krill (>20 mm) across the study area for individuals that were released in A) December, B) January, and C) February. Within each set of simulations, the location of the older krill at the end of January (•), February (▲), and March (♦) is shown. The climatological location of the SACCF is shown for reference.

January, February or March. The distribution of older krill is similar to that seen in the *Discovery* data, with older krill being distributed across the whole Scotia Sea along the path of the SACCF. The *Discovery* data (Fig. 18A,B) show larval and older krill in regions around the South Sandwich Islands and near the eastern end of the South Scotia Ridge, which are areas the simulated drifters do not reach. This suggests that krill found in these areas most likely do not originate from the western Antarctic Peninsula or along the continental shelf break of the Weddell Sea. The simulated krill distributions also show larval and older krill located in the western Weddell Sea, which is an area not sampled during the *Discovery* cruises (cf. Fig. 18A).

Comparison with BIOMASS Data

The simulated length-frequency distributions of krill from January to March (Fig. 52), summarized to correspond to the FIBEX geographical regions (Fig. 21), show three dominant sizes of krill which arise from 2 mm, 22 mm and 45 mm krill used to initialize the simulations. These length-frequency distributions are compared to FIBEX data (Fig. 21) and SIBEX2 data (Fig. 23) that took place over the time from January to March.

The simulated length-frequency distribution from the southwestern Antarctic Peninsula region (Fig. 52A) includes a total number of nine krill. Thus, the simulated length-frequency distribution is very different from the SIBEX2 data from the same region (Fig. 23A), the only field study covering this region, due to the small number of krill in the simulated distribution. However, the simulated length-frequency distribution does show krill of 54 mm to 56 mm in size, which are sizes that were common in the SIBEX2 data (Fig. 23A).

The simulated length-frequency distribution for krill found in the western Antarctic Peninsula region (Fig. 52B) can be compared to both FIBEX (Fig. 21A) and SIBEX2 data (Fig. 23B) from the same region. The BIOMASS data from different years show different krill size distributions, with the SIBEX2 data being composed of krill greater than 32 mm with a modal length of 50 mm, while the FIBEX data has a modal length of 55 mm. However, the range of krill in the FIBEX data includes sizes of 25 mm and higher, and in addition the distribution is almost bimodal. The simulated length-frequency distribution shows three main sizes of krill, the smallest of which (<18 mm) was not found in the BIOMASS data, while sizes of 23 mm to 37 mm and again sizes of 42 mm to 60 mm were found during the FIBEX cruises. The

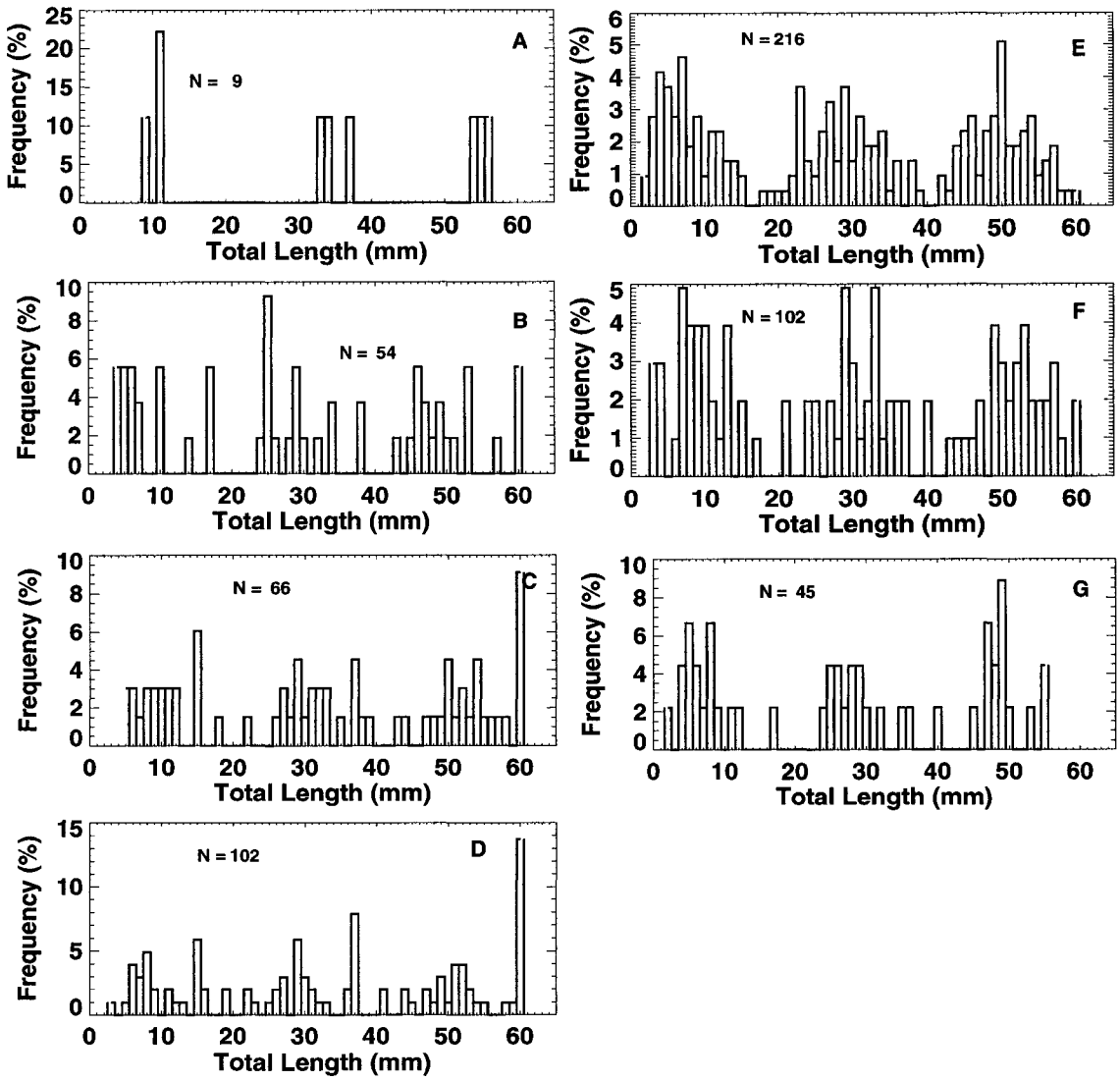

Fig. 52. Simulated length-frequency distribution of Antarctic krill (January - March) for individuals released in December for the regions: A) southwestern Antarctic Peninsula, B) western Antarctic Peninsula, C) Bransfield Strait, D) Weddell Sea, E) Elephant Island/Scotia Sea region, F) open Scotia Sea, and G) South Georgia. Regions are shown in Fig. 20A. Total number of individuals, N, found in each area in the simulations is shown.

smallest size class of krill is produced by using 2 mm krill to initialize the model. However, the fact that no larval krill were found in the BIOMASS data does not mean that there are no larval krill in this area. Rather, this may be due to a sampling bias during the cruises. The net sampling of larval krill is difficult because they are located mostly at the surface. If the net used to capture krill is closed below the surface, larval krill concentrations will be missed.

The FIBEX data (Fig. 21B) and SIBEX2 data (Fig. 23C) for the Bransfield Strait from different years show different krill size distributions. The SIBEX2 data are composed mainly of krill greater than 28 mm with a modal length of 45 mm, while the FIBEX data has a modal length of 50 mm but the range of krill found includes sizes of 16 mm and higher. The simulated length-frequency distribution (Fig. 52C) shows that most krill sizes from 6 mm to 60 mm are found in this region. There is no structure to the length-frequency distribution of the simulations except that 15 mm krill, 29 mm, 38 mm, 50 mm, 54 mm and 60 mm krill are present at higher frequency than other sizes. Again the smallest sizes <15 mm found in the simulated distributions are not found in the BIOMASS data.

In the Weddell Sea region the FIBEX data (Fig. 21C) shows two dominant size groups with modal sizes of 14 mm and 50 mm length krill, and another size group around 35 mm. The simulated length-frequency distribution (Fig. 52D) of krill in the same region shows the same range of krill size but also includes krill smaller than 10 mm. Furthermore, 60 mm krill are present in the simulated distribution, but are absent in the observations.

Observations of krill in the Elephant Island/Scotia Sea region (Fig. 21D, Fig. 23D), show a modal size of krill around 50 mm but the FIBEX data (Fig. 21D) includes additional sizes of smaller krill in its distribution as noted in the previous regions. The simulated length-frequency distribution for this area shows three cohorts of krill with modal sizes of 7 mm, 29 mm, and 50 mm (Fig. 52E). Aside from the cohort of krill sizes under 15 mm, which is not found in the BIOMASS data, the simulated length-frequency distribution is similar to the FIBEX distribution, although the medium size class is composed of smaller krill than in the FIBEX data, which has a modal size of 50 mm plus a smaller peak around 40 mm, and large krill are not as dominant as in the FIBEX data.

The simulated length-frequency distribution of krill found in the open Scotia Sea region is best compared to the FIBEX cruise data from the research vessel

Odissey (ODFX) which covers a similar area (Fig. 21E). In this region the simulated distributions show good agreement with the data, especially the larger krill (Fig. 52F). Three cohorts of krill are centered around 7 mm, 30 mm, and 52 mm, while the ODFX data shows two modal sizes of 38 mm and 52 mm. The simulated larval krill size frequency is not seen in observations.

The comparison of simulated length-frequency distributions for the South Georgia region (Fig. 52G) with ODFX data collected near the Island (Fig. 21F) shows one cohort of krill with a modal size of 35 mm krill in the observed data, while the simulations show a smaller size groups of 24 mm to 32 mm krill in that area. In addition, krill sizes below 10 mm are not found in the observations and in the simulations more krill above 46 mm are found.

Larval sizes of krill are not represented in the BIOMASS length-frequency distributions but these sizes do occur in the simulated length-frequency distributions. The cohorts of large krill in the simulated krill distributions are better compared with the observed data, while the simulated medium-sized krill are on average smaller than in the observed data. This is in part due to the structure of the simulations, with krill being released as 2 mm, 22 mm and 45 mm krill at the beginning of December. By March, all sizes of krill have not had appropriate time to develop and travel large distances across the Scotia Sea. The distribution of krill across the Scotia Sea is more spaced out over the whole study area at the end of the simulation (Fig. 50). Earlier start times may show more appropriate sizes of medium and large krill during the January to March time frame. Also, the BIOMASS data set itself has problems with the comparability of data from different cruises (Thorley and Trathan, 1994). Exact latitude/longitude locations of stations were missing and had to be interpolated, and different ships used different nets for krill collection and also had different methods for determining krill length.

The reference simulation ends at the beginning of October and most krill have moved to South Georgia. Therefore, there are not enough krill at the west Antarctic Peninsula, the Bransfield Strait, and Elephant Island/Scotia Sea region at this time to conduct a meaningful analysis of length-frequency distributions that can be compared to the SIBEX1 data (Fig. 22).

Comparison with South Georgia Data

A comparison between the simulated krill length-frequency distribution at South Georgia with observations is an important validation for the model result. Observa-

tions that can be used for comparison with the simulated results are numerous, but the majority of these observations are in summer or spring. Therefore, the simulated length-frequency data of krill arriving at South Georgia at the end of the reference simulation (October) is extrapolated to obtain krill sizes in the following January by using a summer growth rate for krill of 0.13 mm d^{-1}, which translates into a mean annual growth rate of 0.032 mm d^{-1} (Mauchline, 1980). This is an average value calculated for the growth rate of krill (see review by Siegel and Kalinowski, 1994). The simulation with a December release was chosen because, as shown in the previous section, this is the most beneficial release time for drifters originating in most regions. The resultant krill sizes can be compared to length-frequency distributions from surveys at South Georgia that took place in January-February over 11 years, as described in section 3.

The simulated length-frequency distribution (Fig. 53A) shows that krill of 10 mm to 25 mm reach the western side of South Georgia (defined as west of 36°W) as well as a smaller number of medium-sized krill (45 mm and 46 mm), and large krill (63 mm). Of all the krill that reach South Georgia in the reference simulation, only 5% are transported to the western side of the Island. The simulated length-frequency distribution may be compared with the length-frequency distribution of krill in the West Core Box (cf. Fig. 24) which shows two cohorts (Watkins, 1999; Fig. 3 - cruises JR06, JB10). These cohorts were centered around 38 mm and 49 mm in the JB10 cruise and around 39 mm and 53 mm in the JR06 cruise. The simulated length-frequency distribution shows a small number of krill of larger sizes arriving on the west side of the Island and their length is larger than the modal sizes of the observations, but within the observed range. Krill transported to the western side of South Georgia arrive south of 54°S on the southwest side of the Island, not at the same location as the West Core Box.

The remainder of the simulated krill reach the east side of South Georgia. The corresponding simulated length-frequency distribution (Fig. 53B) shows three cohorts with small krill (5 mm to 28 mm) centered about the modal size 15 mm and two main cohorts of larger krill. The second cohort has a modal size of 43 mm, spanning krill sizes from 33 mm to 48 mm, and the cohort of large krill has modal sizes of 59 mm and 61 mm.

This simulated distribution compares well with the length-frequency distribution of krill in the East Core Box (cf. Fig. 24), which shows krill larger than 25 mm found

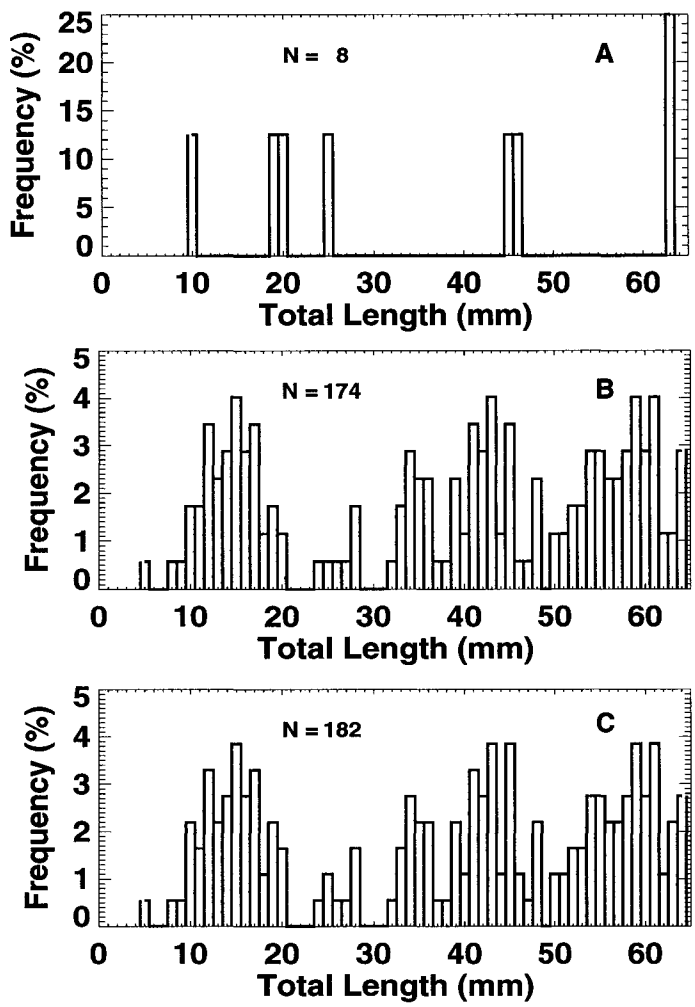

Fig. 53. Simulated length-frequency distribution of Antarctic krill at South Georgia extrapolated to the potential length of krill in January for individuals arriving at A) the west side of the Island, B) the east side of the Island, and C) all of South Georgia. Total number of individuals, N, found in each area in the simulations is shown.

in this area (Watkins, 1999; Fig. 3 - cruise JR03). Observations show that 47 mm krill are the most frequent size of krill and that other size classes, centered at 34 mm, 40 mm, and 52 mm, are present. However, the observations do not show krill smaller than 24 mm present in this area and have considerably less large krill around 60 mm than do the simulated results.

The simulated length-frequency distribution obtained for all simulated krill arriving at South Georgia (Fig. 53C) is similar to the distribution for the east side of the Island (Fig. 53B). Three cohorts are seen, with the smallest from 5 mm to 28 mm centered around the modal size 15 mm, and two main cohorts of larger krill. The medium size cohort and large krill cohort have two modal sizes of 43 mm and 45 mm, while the large cohort is the same as obtained for the east side of South Georgia, 59 mm and 61 mm (Fig. 53B).

The cruises to which this simulated length-frequency distribution can be compared to are the JR17 and JR28 cruises (Watkins, 1999; Fig. 3). The 1996/97 (JR17) cruise shows three different size classes of krill around South Georgia, which are centered around 23 mm, 38 mm, and 48 mm. The main cohort is the one centered around 38 mm, which is also present in the simulated length-frequency data. The 1997/98 (JR28) cruise shows two main cohorts, with modal sizes of 34 mm and 54 mm. These match the two cohorts of larger sized krill in the simulation well (Fig. 53C). Again, krill below 24 mm are not seen in the observations.

Net haul data and length-frequency data collected at the northeast of the Island at the beginning of February (Hill et al., 1996; Fig. 2) showed a mean krill length of 53.1 mm, and a modal size of 55 m, with krill ranging from 28 mm to 65 mm in size. Krill length-frequency data from stomach contents of macaroni penguins (*Eupdyptes chrysolophus*) collected at the same place showed a mean krill size of 55.4 mm (Hill et al., 1996; Fig. 2), a modal size of 59 mm, and a range of krill size from 39 mm to 64 mm. Predator length-frequency data from fur seals (*Arctocephalus gazella*) and macaroni penguins (*Eupdyptes chrysolophus*) in general match those found in net hauls once spatial and temporal bias has been accounted for (Reid et al, 1999). It is known that modal sizes of krill in predator samples are generally slightly greater than the comparable mode in net haul samples, which might suggest a selection of predators for larger krill. At the same time larger krill may be under-represented in nets, so the differences between the two are essentially compensatory (Reid et al, 1999).

Since these data were collected at the northwest coast of South Georgia they are best compared to the simulated length-frequency distributions at the west coast of South Georgia. However, because the simulated length-frequency distribution shows only 5% of the krill are found there and the locations of those krill do not match the locations of the data presented in Hill et al. (1996), the data are compared to the simulated distribution of krill all around South Georgia (Fig. 53C). The simulated length-frequency distribution matches the data in that it shows a similar modal size of 54 mm to 56 mm for the largest cohort that matches the net sample modal size. The simulated krill length-frequency distributions also show a range of 45 mm to 64 mm in length, which matches observations.

5 DISCUSSION

The modeling approach used in this study provides a framework for the investigation of exchanges between krill populations, the food resources necessary for krill survival, and possible responses of krill populations to environmental change. In this chapter the performance of the circulation model is discussed as well as the results of the drifter and krill growth simulations that are described in section 4. Specifically, the discussion focuses on a) the circulation model, b) krill origination areas and transport pathways, c) food supply available to krill, and d) the effect of environmental variability on the transport of krill to South Georgia and their chances of survival.

5.1 Circulation model

5.1.1 Frontal Structure

The HOPS framework is used to simulate the circulation to provide the environmental structure and flow characteristics in Drake Passage and the Scotia Sea. The simulated circulation fields reproduced features of the observed circulation in Drake Passage and in the Scotia Sea (cf. Fig. 25), especially the frontal structure of the flow and the mesoscale variability. The frontal structure of the ACC flow was included in the model through a feature model, because the climatological data used for initialization of the temperature and salinity fields do not resolve the fronts. Once the fronts were initialized in the circulation fields, they did not dissipate over the time of the simulations. This indicates that either frontal dynamics are included in the model, which are too weak to produce the fronts but are strong enough to keep an existing front from dissipating, or that the dissipation of the potential energy of the initial density structure is slow.

The locations of the SACCF and the PF are moved about 100 km from the observed locations of the fronts in the WOCE A23 section in the eastern Scotia Sea. The location of the fronts in the HOPS model, as implemented in this study, is dependent on the bottom topography. The smoothing of the bottom topography (section 3.1.2) makes the continental slopes about 10% gentler and smoothes topographic features, such as deep channels or sea mounts. This influences the location of the fronts. However, it has been shown that all fronts of the ACC meander, and lateral shifts of as much as 100 km over 10 days have been observed in the Drake

Passage (Nowlin et al., 1977; Hofmann and Whitworth, 1985; Klinck, 1985; Nowlin and Klinck, 1986). In fact, during the WOCE A23 cruise a shift of the PF of more than 100 km in one week was observed (Heywood and King, 1996). Therefore, the simulated frontal locations are within the range of observed variability.

5.1.2 Eddy Kinetic Energy

Comparison of the simulated eddy kinetic energy field with the eddy kinetic energy field of the surface flow calculated from FGGE drifting buoys (Patterson, 1985, Fig. 11a) showed that the simulated eddy kinetic energy field is overall lower than that obtained from observations as discussed in section 4.1, but agrees in distribution and magnitude with the eddy kinetic energy field calculated from the FGGE drifters. The simulated eddy kinetic energy values are lower than those given in Patterson (1985) because the surface eddy field obtained from the FGGE drifters included a stronger influence of wind stress than does the equivalent field at 50 m. Also, the eddy kinetic energy fields given in Patterson (1985) are based on a 5° resolution compared to the 10 km resolution of the simulated field, which tends to smooth the kinetic energy field obtained from FGGE drifters.

McClain et al. (1991) presented a similar calculation of surface eddy kinetic energy from the FGGE drifter data that showed bands of eddy kinetic energy greater than 700 cm^2 s^{-2} in Drake Passage and the Scotia Sea, with occasional patches of energy >1000 cm^{-2} s^{-2}. Eddy kinetic energy calculated from Geodetic Satellite (Geosat) data, however, showed lower energies in the study area, between 100 - 500 cm^2 s^{-2} (McClain et al., 1991). This energy is correlated with the bottom topography (Chelton et al., 1990). The eddy kinetic energy calculated from the simulated circulation distributions show similar patters that follow topographic features (cf. Fig. 26).

The simulated eddy kinetic energy levels are within the range of those calculated from observations, thereby showing that the circulation model resolves the characteristics of the eddy field in Drake Passage and the Scotia Sea.

5.1.3 Hydrography

Comparison of simulated vertical temperature and salinity distributions with observations (section 4.1.1) showed that the vertical structure of the different water masses present in the Scotia Sea is not correctly resolved. This mismatch is due to

factors related to implementation of the HOPS model. A primary factor is that, the circulation model is initialized with the WOA 1998 climatological temperature and salinity fields (Antonov et al., 1998; Boyer et al., 1998), which is a smoothed representation of the hydrography in the study region. The data density used to construct this climatology is sparse in some parts of the study region and is is also sparse over the entire region during the austral winter.

Comparison of the simulated vertical temperature and salinity fields with the climatology (section 4.1.2) showed that there is a good agreement between the simulated temperature and salinity distributions and the climatology. This indicates that the simulated property fields are closely related to the initialization of the model and that discrepancies with observations are in part due to the insufficient representation of features in the climatology which then continue over time. One exception of this is the representation of the cold tongue in the Melville II section across Drake Passage. The simulated temperature field shows a cold tongue that does not match the observations and the initial climatology.

The model therefore is initialized with only an approximate representation of the observed hydrography that may not accurately represent the vertical water mass structure. In addition, the model relaxes to the climatological values at the model domain boundaries, which results in water flowing into or out of the model being set to climatological values. If there are any inconsistencies in the temperature and salinity values at the boundaries, then the water masses advected into the model are misrepresented. Therefore, data sets used for initialization of circulation models are of major importance and should be chosen carefully. In the study region, the availability of high quality hydrographic data with good spatial and temporal resolution is lacking, which points to the need for further hydrographic observations and subsequent inclusion into available climatologies.

Further, no surface heating or cooling processes are included in this implementation of HOPS and, therefore, surface waters cannot undergo seasonal heating or cooling. At the same time sea ice cover is not included in this model implementation, and the dynamics associated with sea ice-ocean interactions are consequently missing (see section 5.1.4). Therefore, features such as the cold tongue observed in the Melville III section (cf. Fig. 16) are included in the model simulations through the inadequate initial climatological temperature distribution, which then evolve over time due to wind mixing. The lack of sufficient vertical mixing as a restorative

mechanism may also be one reason why vertical temperature and salinity structures deteriorate over time. For a more accurate representation of the water masses, the inclusion of heat exchange with the atmosphere and sea ice dynamics is needed.

5.1.4 Surface and Subsurface Drifters

The comparison of simulated drifter trajectories with WOCE surface and subsurface drifters (section 4.3) showed that the surface drifters in the model were on average 38% slower than the WOCE drifters and that the subsurface drifters were on average 60% slower than the observed drifters. Part of this disagreement arises from the time variability of the front locations and the probability that a simulated drifter is entrained in a front. The observed convergence at the fronts may be missing because fronts are initialized in the model, so that drifters do not accumulate in fronts. The discrepancy between observed and simulated drifters also arises because the currents associated with the fronts in the simulated circulation fields are slower than observed.

The thermal wind equation

$$\frac{\partial u}{\partial z} = \frac{g}{\rho f}\frac{\partial \rho}{\partial y}, \tag{24}$$

shows that the velocity gradient over depth ($\frac{\partial u}{\partial z}$) is determined by the density gradient ($\frac{\partial \rho}{\partial y}$), the gravitational acceleration (g) in m s^{-2}, the water density (ρ) in kg m^{-3}, and the Coriolis force (f) in s^{-1}. Equation (24) is used to calculate the geostrophic flow speeds at 1000 m across the SAF at day 180 of the simulation, using the parameter values in Table 21 and assuming zero flow at 2500 m.

This calculation gives geostrophic flow speeds at 1000 m depth that are 28% higher than the flow speeds produced in the simulated flow fields, which indicates that the density gradient across the SAF should produce higher geostrophic current velocities.

Comparison of geostrophic flow speeds calculated from directly measured current velocity from current meters deployed along the Melville section II (Nowlin et al. 1977) with the simulated current velocity at the same time and location obtained from the circulation simulations show discrepancies of the same order. The calculated 30-day average current velocity produced by the simulated density gradient

Table 21. Parameters, their associated values, and units as used in equation (24).

Parameter	Value	Units
g	9.81	$m^2\ s^{-1}$
ρ	1028	$kg\ m^{-3}$
f (at 57°S)	-1.22 x 10^{-4}	s^{-1}
∂z	1500	m

across the SAF (Fig. 54) can be compared to the calculated current velocity across the SAF at the same station locations (between station 21 and 24) from the Melville II cruise (Nowlin et al., 1977, Fig. 10). The simulated current velocity agrees with the directly measured velocity in that the high flow velocities at the surface decrease with depth (Fig. 54). However, when simulated and observed current speeds at different depth levels are compared, it can be seen that the simulated current velocity at 1000 m is 15.8 cm s^{-1}, while the observed velocity across the same distance (between Station 21 and 24) is 17.5 cm s^{-1}, which is 11% less than the observed speeds. At 500 m depth this difference between simulated and observed current velocity is 13% and at the surface it is 5%. However, the error bars of the directly measured velocities (Nowlin et al., 1977, Fig. 10) show a standard deviation of about ±10 cm s^{-1} and the simulated current velocities are within the range of this deviation.

There are two main reasons for the noted differences in frontal speeds. The grid spacing of this model is 10 km and is therefore too coarse to define the sharp property gradients that are observed at the fronts. As a result, the weaker density gradients produce smaller current velocities. A higher resolution model would counteract this problem. At the same time the fronts are implemented in this model by using a feature model and are defined by property gradients which may be too weak.

A second reason may be that the horizontal dissipation of energy is so strong that it is extracting kinetic energy, slowing the flow down. At the same time the choice of the horizontal smoothing mechanism, the Shapiro filter, used to dampen the two- to three-grid-interval waves, reduces the steep frontal gradient, which causes slower current speeds.

As discussed previously (section 3.1.2), the bottom topography has a major in-

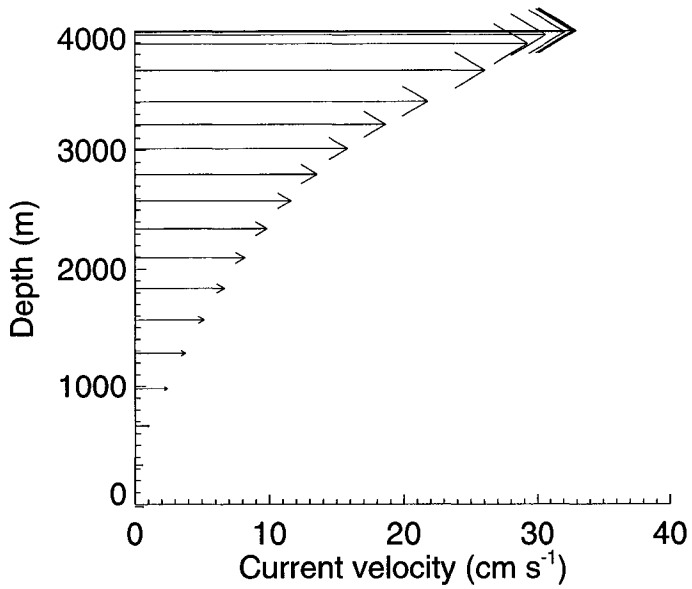

Fig. 54. Thirty-day average of the simulated current velocity (cm s^{-1}) across the SAF between 57.247°S, 65.05°W and 57.677°S, 65.833°W, which corresponds to the locations of Melville II stations 24 and 21.

fluence on the current flow in this area, especially of the fronts. The closing of deep channels by the smoothing routine is a problem with the smoothed bottom topography used in this model implementation and required changes in some areas after smoothing (section 3.1.2). When deep, narrow channels are altered as in this implementation of HOPS, this will not only change the current flow, but also has the potential to increase frictional forces that slow currents down.

The simulated subsurface drifters are 60% too slow compared to the WOCE subsurface drifters, which cannot be explained solely by the currents associated with the fronts. All of the eighteen observed WOCE subsurface drifters started in the northern Drake Passage and followed the path of the SAF into the South Atlantic. As described previously (section 4.3.2), the flow in the South Atlantic is not properly represented in the simulated circulation fields because of the model boundaries. The Brazil Current enters from the north along the coast of South America and deflects the northward-flowing Malvinas Current to the northeast, away from its usual path, and reducing its speed. This affects the speed of the simulated drifters in the South Atlantic and also their drifter paths. The simulated subsurface drifters are transported back into the north Scotia Sea and return to the South Atlantic

(cf. Fig. 35), which is not observed in the WOCE subsurface drifter trajectories. However, the flow in the South Atlantic does not influence the flow through Drake Passage and thus does not affect the transport of drifters across the Scotia Sea.

The noted discrepancies between the simulated circulation fields and observations indicate issues with the circulation dynamics included in the HOPS model and with the implementation of this model. However, the surface circulation, particularly through the Drake Passage and across the Scotia Sea, matches observations, with its northeastward flow characterized by three high speed fronts. The location of the SAF, PF, and SACCF match observations. Also, the Weddell Sea and the Brazil Current, and their associated transports match observations. In addition, mesoscale variability, an important component of the flow in this region, is found in the simulated circulation. The sizes of eddies produced by the simulated circulation field are within the range of observed spatial scales of 30 km to 100 km (Bryden, 1983) and the eddy kinetic energy produced by these mesoscale flow features is in agreement with values calculated from satellite and drifter observations.

5.1.5 Effect of Sea Ice Cover

The simulated circulation fields are produced without including the potential effects of sea ice cover. However, large areas of the Weddell Sea and areas along the west Antarctic Peninsula may be covered by sea ice for some part or all of the year. Sea ice and its associated snow cover reflect radiation and isolate the ocean from the atmosphere for a large part of the year. This affects ocean-atmosphere gas exchange and heat fluxes, and by modifying the kinetic energy input from wind, also influences the circulation of surface waters (Murphy et al., 1995). Wind stress drives sea ice motion and the frictional drag of the sea ice upon water itself sets the surface water in motion. This stress is transmitted downward through the layers of the water column in the form of an Ekman spiral and changes the direction of the flow (Wadhams, 2000). In addition, sea ice melting produces cold fresh water that tends to stabilize the surface waters and the formation of sea ice results in brine rejection, which may cause buoyancy driven circulation. These dynamics are not included in the HOPS model as it is implemented in this study. Thus, flow dynamics underneath the sea ice cover may therefore be altered and not calculated correctly in the simulated circulation fields.

5.1.6 Flow Dynamics around South Georgia

A shallow continental shelf of less than 200 m, across which deep canyons cut, extends around South Georgia to a distance of 50 to 150 km from the coast, after which the water depths rapidly increase to over 3000 m (cf. Fig. 37). General flow around South Georgia is mainly influenced by two of the circumpolar fronts, the PF and SACCF. The PF passes between Maurice Ewing Bank (cf. Fig. 1) and South Georgia (Trathan et al., 1997) ensuring there are always polar waters around the Island and resulting in the Island being heavily glaciated (>50%) (Brandon et al., 1999). The SACCF transports cold waters from the Antarctic Peninsula and north of the Weddell Sea towards South Georgia, approaching the Island's shelf break from the south and southeast (Meredith et al., submitted).

The local on-shelf waters around South Georgia are influenced by shallow water processes such as the addition of fresh-water, and heating and mixing processes due to friction and tidal stirring (Brandon et al., 1999), and, as a result, are warmer and fresher than the off-shelf waters. The off-shelf waters lack some of this forcing which results in inherent density differences between on-shelf and off-shelf waters that give rise to a baroclinic front between the two (Brandon et al., 1999). This shelf break front has been observed to the east and north of South Georgia (Brandon et al., 1999, 2000). Such fronts are common in shelf edge regions (eg. Pingree and Mardell, 1981; Marra et al., 1990) and are critical for determining the exchange of salt and heat between on- and off-shelf regions (Dever and Lentz, 1994), as well as sediments and nutrients (Falkowski et al., 1988).

Reasons for the formation of warmer, fresher on-shelf water on the eastern shelf of South Georgia are rather complex due to South Georgia having two heavily glaciated mountain ranges running along its length with mountains up to a maximum of 2934 m and 12 peaks over 2000 m (Headland, 1984). While the mean climatological winds in the southwest Atlantic are from the west (Mayes, 1985) and reach South Georgia on the west coast, Richards and Tickell (1968) show a strong lee effect on the east side of the Island, due to the mountains. The lee effect creates a microclimate and causes low humidities, a low amount of cloud formation and as a consequence more sunshine and higher air temperatures (Brandon et al., 1999). This microclimate drives greater local melting and provides a strong local fresh-water runoff from South Georgia, which coupled with shelter from prevailing westerly winds, creates the observed warm fresh water pool.

This microclimate cannot be reproduced in the simulated circulation fields around South Georgia, because there is no freshwater input and the average wind used to force the model does not include local geographic effects, which are the environmental conditions that produce the local circulation around the Island. Therefore, no local shelf front can develop in the simulated circulation fields around South Georgia. In addition, the model resolution is too coarse (10-km grid spacing) to resolve shelf fronts. The across-shelf circulation is important in determining how particles reach the shelf waters that surround South Georgia. Thus, the specific dynamics of krill transport onto shelf waters around South Georgia cannot be investigated with the HOPS model as it was implemented in this study. A high resolution model for the local South Georgia area, that includes the relevant environmental forcing and dynamics is needed.

5.2 Krill Origination Areas and Transport Pathways

The population structure of many species can be considered as an array of local populations linked by variable degrees of gene flow (Wade and McCauley, 1988). In this metapopulation concept, migrants are not only an integral part of the structure, but are indeed necessary for the survival, persistence, and expansion of the metapopulation (McQuinn, 1997). The migrants abandon their local population and cannot be selected for at the local population level, as they are lost to the local population. However, these migrants can be selected for in the population they migrated to and are therefore advantageous at the metapopulation level by ensuring survival of the distant population. This is the case for krill transported from the Antarctic Peninsula and the Weddell Sea to South Georgia. The krill population at South Georgia is assumed to be a sink population within the krill metapopulation of the Antarctic Peninsula/Scotia Sea region. The populations of krill found at the Antarctic Peninsula and in the Weddell Sea are assumed to be the source populations for the South Georgia population. For the survival of the local South Georgia krill population, therefore, input of viable krill from areas along the western Antarctic Peninsula and the Weddell Sea is needed.

The simulated transport patterns discussed in section 4.3.3 can be grouped into five areas from which particles can reach South Georgia (Fig. 55). Of these five regions there are four regions from which krill can be transported to South Georgia in a period of 10 months: the west Antarctic Peninsula, Bransfield Strait, the

Elephant Island/Scotia Sea area, and the southwest Antarctic Peninsula (Fig. 55). These locations coincide with known krill spawning areas (Marr, 1962; Siegel, 1992). Simulated drifters originating in the Bransfield Strait region need about 263 days to reach South Georgia, while those originating along the west Antarctic Peninsula need about 211 days. The difference in transport times reflects the time needed to move out of the Bransfield Strait and become entrained in the SACCF. Drifters originating near Elephant Island, however, are transported to South Georgia on average in 168 days, the shortest transit time, while drifters originating at the southwest Antarctic Peninsula have the longest transport pathways and need on average of 276 days.

In section 5.1.3 it was shown that the simulated current speeds in the SAF are about 10% slower than the average observed current speeds. However, the simulated current speeds are within the variability reported for the measurements of current speeds. Therefore, the simulated transport times of krill reported here can be seen as maximum time scenarios and indeed krill may be able to reach South Georgia 10% faster than suggested by the simulations. A shorter transport time would benefit krill and result in higher numbers of krill surviving transport than reported in this study.

Larval krill released at the west Antarctic Peninsula, in the Bransfield Strait, the Elephant Island/Scotia Sea area, and the southwest Antarctic Peninsula grow to 1+ sizes during the average time needed for drifters being transported to South Georgia, while juvenile krill grow to 2+ sizes. However, krill originating at the southwest Antarctic Peninsula grow to overall smaller sizes than krill from other areas due to long transport times with low food supply. Thus, krill spawned in the main spawning area along the Antarctic Peninsula can be transported to South Georgia, and will arrive with a size that is observed for local krill populations. However, spawning further south along the western Antarctic Peninsula is not likely to produce krill that reach South Georgia at an observed size in 10 months. The same is true for the spawning area in the far east of the Scotia Sea which does not contribute to the South Georgia population, because krill originating there are transported eastward, never reaching South Georgia. Krill located further north in Drake Passage can be transported to South Georgia, but krill are not typically found at this location (Fig. 18, Marr, 1962). In addition any krill that are positioned in the Scotia Sea along the path of the SACCF are transported to South Georgia.

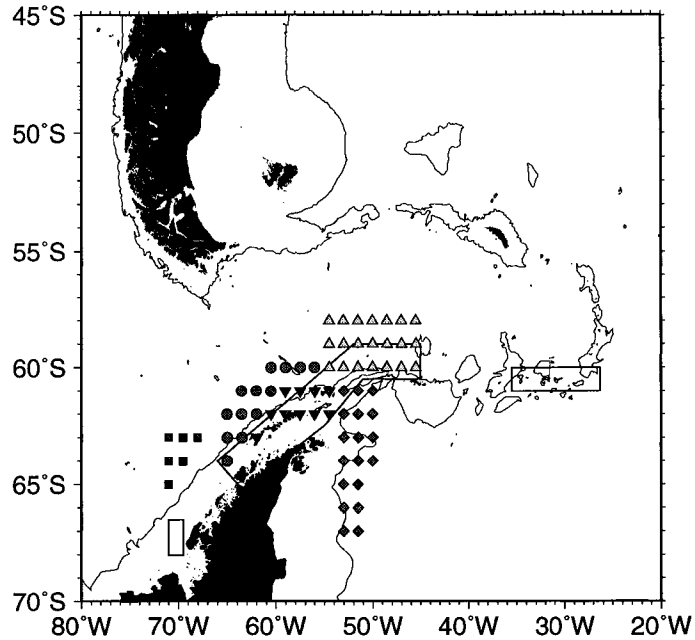

Fig. 55. Distribution of five areas around the Antarctic Peninsula that can potentially provide Antarctic krill to South Georgia. The areas are designated as: 1) western Antarctic Peninsula (•), 2) Bransfield Strait (▼), 3) Scotia Sea/Elephant Island (△), 4) southwestern Antarctic Peninsula (■), and 5) Weddell Sea (♦). Boxes indicate the areas of krill spawning identified in Marr (1962). Thin lines show the 2000-m isobath.

5.2.1 Weddell Sea

Krill originating near the continental shelf break of the Weddell Sea may reach South Georgia. An average transport time of 263 days places krill near the Weddell Scotia Confluence from where transport to South Georgia is possible. During transport from the shelf break of the Weddell Sea to the Weddell-Scotia Confluence, larval and juvenile krill do not encounter significant periods of low food supply (Appendix A, Fig. A5, Fig. A10, Fig. A15). As a result, when reaching the Weddell-Scotia Confluence, larval and juvenile krill have reached 2+ to 4+ sizes, respectively, and can continue transport from there.

Additional simulations starting in the Weddell-Scotia Confluence in November (after krill arrive there in October) show that krill require on average 10 additional months from different areas in the Weddell-Scotia Confluence to reach South Georgia (Fig. 56). Thus, krill arrive at South Georgia after a transport time of approximately

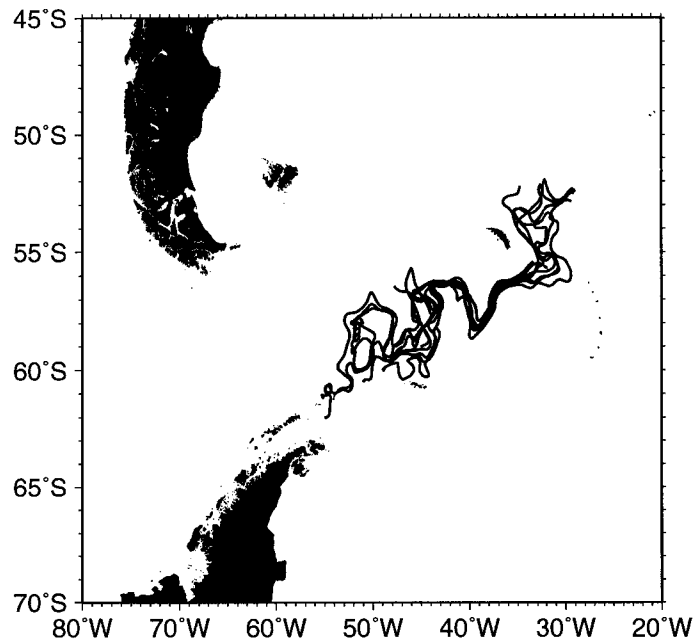

Fig. 56. Transport pathways over 10 months for drifters released at different points in the Weddell-Scotia Confluence in November.

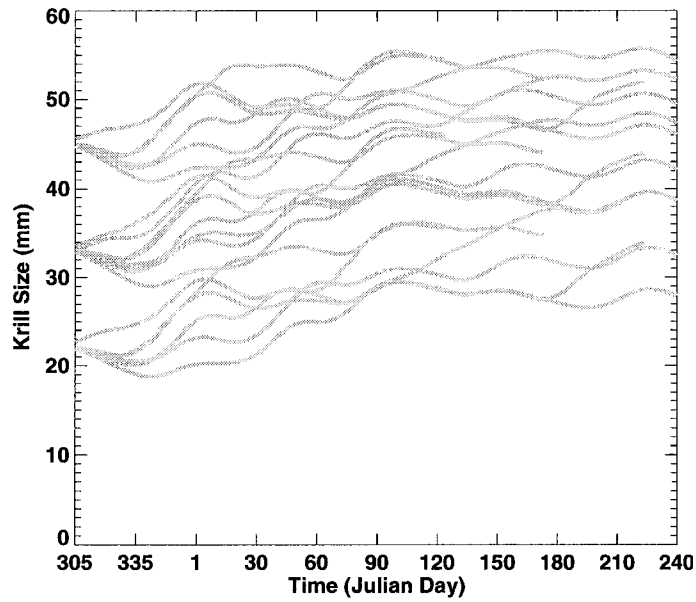

Fig. 57. Simulated growth of 22 mm krill (lower curves), 33 mm krill (middle curves), and 45 mm krill (upper curves) released in November (Year Day 305) in the Weddell-Scotia Confluence.

20 months. Concentrations of all four food sources along the simulated drifter paths that start in the Weddell-Scotia Confluence are sufficient to sustain krill during this additional transport. Simulations using the krill size-class model suggest that all krill starting from the Weddell-Scotia Confluence survive and grow during the time required for transport to South Georgia (Fig. 57). Juvenile krill (22 mm) grow to between 28 mm and 39 mm, larger subadult krill (33 mm) grow to between 39 and 46 mm, while adult krill (45 mm) reach 45 mm and 55 mm. Therefore, krill originating in the Weddell Sea can be transported to South Georgia in a time frame of approximately 20 months, thereby contributing 2+, 3+ and larger krill to the local krill population.

This potential transport of krill from the Weddell Sea to South Georgia agrees with studies that found cold water of Weddell Sea origin to the north and east of South Georgia (Deacon, 1977; Hardy and Gunther, 1935). This water has been suggested to be a main source of krill (Marr, 1962; Maslennikov and Solyankin, 1988). In addition, recorded tracks of giant icebergs showed that material of Weddell Sea origin can leave the Weddell Sea region and can be transported along the east side of South Georgia, following the general path of the SACCF (Trathan et al., 1997). The drifter and krill growth simulations done in this study support Watkins et al. (1999) who suggest that krill from the Antarctic Peninsula and the Weddell Sea may reach South Georgia and may explain the different age structures of the local krill populations.

5.2.2 Importance of the Southern ACC Front

The simulated drifter results (section 4.3) show that the currents associated with the SACCF are the main transport mechanism for krill, because the simulated distributions of larval and older krill (>20 mm) that may reach South Georgia, coincide with the path of the SACCF (Figs. 51 and 50). The simulated distributions of krill stages agree with historical krill distributions in the Scotia Sea (Fig. 18, Marr, 1962), pointing to the importance of the SACCF as a transport mechanism. Previous studies also suggest the importance of the SACCF for krill transport (Hofmann et al., 1998; Murphy et al., 1998). Observations during summer suggest that 1+ krill and, in much higher numbers 2+ krill enter the South Georgia region mainly from the east (Murphy et al., 1998; Watkins et al., 1999). The SACCF bounds the east side of South Georgia, and it was shown in this study that most krill (91%) indeed are

transported to the east side of the Island. It also agrees with the expectation that 1+ and 2+ krill reach South Georgia from the three main origination areas and are delivered there at the end of spring.

The ACC in the Drake Passage is known to shift its location during the year (Hofmann and Whitworth, 1985) or possibly over longer time scales (Klinck and Smith, 1993). A shift of the SACCF north, even of only 10 km, leaves only a fraction of the large spawning area at the Antarctic Peninsula in the path of the SACCF. This greatly reduces the possibility for transport of krill from the Antarctic Peninsula and the Weddell Sea to South Georgia as was shown in section 4.4.3. Thus, such a change in the location of the SACCF endangers the delivery of krill to South Georgia, especially from the main spawning area along the Western Antarctic Peninsula and in the Bransfield Strait. This may have a devastating effect on the krill population at South Georgia, which depends on the krill supply from further upstream. Such shifts in the SACCF may occur during the year (Hofmann and Whitworth, 1985; Hofmann and Klinck, 1998) and indicates that the transport of krill to South Georgia is not necessarily continuous throughout the year, but may be interrupted. If such a shift in the SACCF occurs about a month after spawning time, the effect may be that only very few krill are transported to South Georgia and the abundance of krill at the Island declines. This agrees with studies that report strong fluctuations in krill abundance around South Georgia (Heywood et al., 1985; Priddle et al., 1988).

An increase in winds by 70% and a northward shift of the winds, as thought to have occurred during the last glacial maximum (Crowley and Parkinson, 1988), has been shown to increase the transport of the ACC and shift its location northward by 2° latitude. Therefore, climate change processes that result in wind conditions that differ from present conditions, may shift the SACCF location northward, endangering the survival of the local South Georgia population by removing the main transport mechanism.

5.2.3 Local Effects around South Georgia

Watkins et al. (1999) noted that the krill population at the eastern end of South Georgia tends to be smaller sized and to lack the larger year classes relative to the krill population at the western end of the Island. A potential explanation for these observations is that krill are delivered to the east side of the Island by the currents

associated with the SACCF. However, the simulated length-frequency distributions at South Georgia show the opposite (Fig. 53), with only 9% of the krill arriving on the western side of the Island. Those krill that do arrive on the western side of South Georgia are not within the West Core Box, but rather are found south of 54°S on the southwest side of the Island. It has been proposed that krill are transported from the east side of South Georgia to the northwest and grow during the transport to bigger sizes (Watkins, 1999). However, none of the simulated drifters arriving on the east side of South Georgia is transported to the northwest of the Island because the circulation on the South Georgia continental shelf is not simulated correctly, as discussed in section 5.1.5. Thus, the processes that allow arrival, retention and transport of krill in local waters around South Georgia cannot be fully tested. What has been shown however, is that krill originating in areas further north in the Drake Passage (Fig. 36) may reach the western side of South Georgia, if krill were found in this area (see section 5.2).

5.2.4 Effect of Different Spawning Times on Transport

The timing of the drifter release, which simulates different spawning times, shows that early release enhances the possibility of krill reaching South Georgia, especially from the main spawning area off the western Antarctic Peninsula. In Bransfield Strait, an area with a large krill population and active reproduction (Siegel, 1992), there are regions from which the circulation does not favor transport to South Georgia and this area increases with later spawning. The change in the size of this region is due to the wind conditions, which shift from westerly winds during early spring to northwesterly winds at the beginning of summer (Fig. 6), creating less of an offshore component to the Ekman flux. Later spawning times also decrease chances for krill originating in the Weddell Sea to reach the vicinity of South Georgia. In contrast, later spawning increases the possibility for krill originating further north in Drake Passage to reach South Georgia.

Krill are believed to spawn during three or more years of their life span (Siegel, 1987; Nicol et al., 1995). It has been suggested that krill spawn multiple times during one year (Ross and Quetin, 1983), but laboratory studies were only able to demonstrate a single spawning event (Harrington and Ikeda, 1986). Nicol et al. (1995) argued that multiple spawning of krill in a season would require above average phytoplankton concentrations and krill filtration rates in order for krill to fulfill the

necessary energy input, and may not be likely. Spiridonov (1995) showed that there is considerable variation in the start, maxima, and duration of krill spawning along the Antarctic Peninsula. Spawning may start early (late November) and last long (3-3.5 months) or start early and last for a short time. Areas with variable starting times have been observed as well.

The simulations of krill growth suggest that early spawning is more beneficial for krill to survive transport to South Georgia. Thus, a single spawn at the beginning of the season, rather than multiple spawns, may result in more krill arriving at South Georgia. However, the timing of this single spawn is crucial, because of variability in food supply and circulation characteristics. The timing of spawning relative to the environmental characteristics may be part of the explanation for the year-to-year fluctuations in krill biomass at South Georgia.

5.2.5 Effect of Environmental Changes

The Antarctic Circumpolar Wave (ACW) causes anomalous sea surface temperatures (SST) and sea ice anomalies to propagate eastward around Antarctica (White and Peterson, 1996). The atmospheric response to changes in SST then produces a positive feedback to the ocean, which is the displacement of the anomalous SST to the east and thereby the eastward propagation of the ACW. Although Antarctic sea ice is predominantly annual, interannual variability has been demonstrated by satellite data (Murphy et al., 1995). Zwally et al. (1983) showed that the position of anomalies in the maximum sea ice extent fields proceeds around the Antarctic Continent with a period of approximately seven to nine years.

The timing of the advance and retreat of the sea ice edge determines the irradiance and hence the potential light available for photosynthesis in the biologically active marginal ice zone. The total irradiance may vary by as much as 50% depending on the timing of the seasonal track of the ice edge (Murphy et al., 1995) affecting primary production and higher trophic levels.

The propagation of high sea ice extent around the Antarctic imposes interannual changes in sea ice extent on the Southern Ocean ecosystem. A high concentration and long duration of sea ice is important for the overwintering of krill, especially larvae (Daly, 1990) and also provides sufficient food to krill to promote early spawning in spring. Two consecutive years of high sea ice concentration are necessary for successful recruitment of krill (Siegel and Loeb, 1995; Loeb et al., 1997). Due to the

periodic dynamics of the ACW, the extent of sea ice is shifted around Antarctic and low sea ice years follow the high sea ice years. Years of low sea ice result in less krill recruitment and a decline in krill biomass that occurs with an observed periodicity. At the same time juvenile krill originating along the west Antarctic Peninsula continental shelf are selected for by biological and environmental factors to successfully complete transport to South Georgia. The variability of sea ice extent due to the ACW therefore has a potentially large effect on the supply of krill from this source population and years of low sea ice concentrations may substantially reduce successful transport from this source population. However, due to the distance between the Antarctic Peninsula and South Georgia and the dynamics of the progressing ACW, a winter of low sea ice concentration at the Peninsula might not necessarily be a winter of low sea ice concentration at South Georgia. This may explain why in some years krill biomass is low at the Antarctic Peninsula and not at South Georgia.

The effects of the ACW on krill populations is only now being recognized. Additional, multi-year observational studies are needed in order to investigate the teleconnections between periodic changes in sea ice extent and concentration and krill abundance at the Antarctic Peninsula and South Georgia.

5.3 Food Supply

Spawning between December to February places krill in an environment in the Scotia Sea, in which chlorophyll concentrations are not always sufficient to support growth over the 168 to 276 days needed for transport to South Georgia from the four main origination areas along the Antarctic Peninsula. Sea ice algae does not provide a viable alternative food source because sea ice extent and concentration tends to be low in the Scotia Sea. Spawning in December, and therefore an early start to transport, results in a more successful krill growth than does later spawning because of higher food availability in the Scotia Sea during austral summer before the rapid decline in phytoplankton concentration during fall. The inclusion of an additional food source, such as heterotrophic food, is available only to krill larger than 18 mm (Granéli et al., 1993; Huntley et al., 1994a).

The implication of these simulations is that krill of all sizes, but mainly larval krill, rely on additional food sources during transport across the Scotia Sea, especially in winter, as has been suggested by Fach et al. (2002). This food source may be detritus (Kawaguchi et al., 1986; Holm-Hansen and Huntley, 1984; Daly, 1990)

which has been observed to be the only food fed on by krill in times of low food conditions (Daly, pers. com.). The inclusion of detritus as an additional food source has a positive influence on the growth and survival of krill, especially larvae, and is most needed during winter. Growth and survival of krill from the origination area along the Antarctic Peninsula during transport to South Georgia is most successful when krill feeds on a combination of phytoplankton, sea ice algae, detritus and copepods.

The growth rate of krill has been shown to be influenced by temperature (Poleck and Denys, 1982) in that the intermoult periods decrease with increasing temperature, indicating that increased temperature might result in a higher growth rate. Krill in the Scotia Sea experience temperatures from -1.8°C in winter up to 4°C in summer and are therefore exposed to a wide range of temperatures. The simulated krill growth rates increase in response to increased temperature only when these coincide with high food concentrations. However, the changes in krill growth rate due to temperature alone are small relative to those produced by changes in concentration of food supply (see Fach et al. 2002). Therefore, enhancements of growth rate due to increased temperature are not sufficient to compensate for a low food environment.

The krill growth simulation results (section 4.5) are based on food availability time series derived from composite CZCS and SSM/I images, which are then combined with idealized representations of heterotrophic food and detritus concentrations derived from POC:Chl$a$ relationships. Thus, these time series represent specific assumptions about how food is distributed across the Scotia Sea and once defined, the food availability and food type does not evolve along a given trajectory. However, all food is linked in the existing ecosystem and environmental changes translate into the whole food web. Therefore, such translations of environmental changes cannot be resolved in the modeling approach used here and events that increase or decrease local food concentrations are missed. However, such events may be strong enough to determine krill survival or death and should be included into the modeling approach.

Polar phytoplankton growth is mainly influenced by low temperatures, the presence or absence of sea ice, nutrient supply, and seasonal variations in available light (Smith and Sakshaug, 1990). Therefore changes in water temperature, changes in sea ice cover, and changes in wind stress that may result in increased or decreased

mixing of the water column, will have a strong effect on the growth of phytoplankton and also on the species composition. Also, POC concentrations are dependent on species composition and physiological state of the phytoplankton (Cota et al., 1992). The modeling approach used here cannot resolve such dynamics.

The life cycle of zooplankton in polar regions is also governed by the low temperatures, but in addition depends on the cycles associated with primary production (Smith and Schnack-Schiel, 1990). Thus, changes in the species composition and concentration of the phytoplankton community will change zooplankton growth and species composition, which in return affect higher predators that depend on different zooplankton species as a food source.

Environmental changes can, thus, propagate throughout the food web and are important factors determining the food supply available to krill during transport. The inclusion of the effects of environmental changes on the food supply of krill requires the development of lower trophic level models that allow autotrophic and heterotrophic food distributions to evolve over time in response to environmental conditions. Such a model will then be able to translate the repercussions of climate change discussed in section 5.2.5 into the overall food web and allow testing of these effects on food availability and on krill.

5.3.1 Deep Chlorophyll Maximum

High phytoplankton concentrations are found at depth, below 60 m, in the study area (El-Sayed and Weber, 1982; Bianchi et al., 1992; Smith et al., 1996; Tréguer and Jacques, 1992; Whitehouse et al., 1996), in the deep chlorophyll maxima. Deep chlorophyll maxima have been observed mostly in the summer/fall in the Scotia Sea (El-Sayed and Weber, 1982), at the western Antarctic Peninsula (Bianchi et al., 1992; Tréguer and Jacques, 1992; Smith et al., 1996), and near South Georgia (Whitehouse et al., 1996) and not during winter/spring (El-Sayed and Weber, 1982; Smith et al., 1996). Krill wanting to exploit this food source need to be able to reach depths of 80-100 m by vertically migrating. Krill have been observed to exhibit a diel vertical migration pattern (Marr, 1962; Nast, 1979; Kalinowski and Witek, 1980; Everson and Ward, 1980; Godlewska, 1996) and no difference was observed between female and male krill migration (Nast, 1979). However, it has been observed that there is a connection between the size of krill and the amplitude and period of migration (Nast, 1979; Godlewska, 1996; Everson and Ward, 1980), with a 24-hour period and

larger vertical migration distance (up to 100 m) associated with older krill and a 12-hour period and a smaller range of vertical migration associated with younger krill (Everson and Ward, 1980; Godlewska, 1996). This difference is believed to result from passive krill sinking in swarms following feeding (Pavlov, 1969; Everson and Ward, 1980). After digestion, krill actively ascend to the surface with high chlorophyll *a* concentrations and a segregation of krill sizes occurs because small and large krill need different periods of time for feeding and digestion, which may let larger krill be positioned above smaller krill or below (Everson and Ward, 1980). Godlewska (1996) shows that the amount of phytoplankton available for feeding is a main factor in influencing krill migration. High abundance of phytoplankton will cause krill to migrate with a maximum amplitude and longer period, while low food supply will cause krill to migrate less and in a shorter period. Krill are therefore found at average depths of 50 m to 70 m (Godlewska, 1996). There are seasonal changes in the vertical migration patterns of krill due to the availability of phytoplankton as food (Godlewska, 1996), with the depth range of migration being greatest in January.

Such krill migration and feeding behavior is not included in the modeling framework used in this study. The drifters in the simulated circulation fields remain at a fixed depth of 50 m and the HOPS model, as it was implemented in this study, does not allow for the vertical migration of drifters. Inclusion of vertical migration is needed in future studies, because concentrations of chlorophyll at depth may be an important additional food source for krill. Also, vertical migration positions krill at levels with different flow speeds (Fig. 54), which may influence overall transport times. The inclusion of behavior requires parameterization of the corresponding energy requirements in the krill growth model, linking the energy demand of krill to its current behavior. However, data on the energy expenditures associated with swimming activity is very limited (Kils, 1982) and not sufficient to parametrize this process. Thus, additional measurements of energy expenditure during swimming and vertical migration are needed.

5.3.2 Selection of Age Group?

The simulated drifter results (section 4.3) show that there are four regions from which krill can be transported to South Georgia in 10 months or less. To survive this transport, the krill need a combination of all four food sources and an early

transport start in December is more beneficial than later start times. For krill originating in region 1 this means that 85% of the larval krill starting transport in December (Table 16), and all juvenile krill survive. This is similar for krill originating in region 2 (Table 17), where 89% juveniles and 100% adults survive, as well as region 3 (Table 18) and region 4 (Table 19). The pattern of more juvenile krill than larval krill surviving transport when feeding on all four food sources is also observed for different release times.

These results show that it is possible for larval krill to be transported from specific regions to South Georgia and grow to 1+ sizes during transport. The survivors that only grow slightly during transport (e.g. 3.13 mm) are not viable when reaching South Georgia, although they survive transport in the simulation. Men'shenia and Spiridonov (1991) showed that krill development through one developmental stage takes from eight to 30 days. They calculated a relationship between temperature and developmental time that shows that if krill do not develop into the next stage within this time, development will not continue and the animal dies. Therefore, krill that remain at the same size throughout a given simulation will not survive. However, juvenile krill survive transport to South Georgia from all four regions and can grow to sizes of 2+ and 3+ krill.

Larval and juvenile krill from region 4, the southwestern Antarctic Peninsula, survive transport to South Georgia, however, krill that arrive at South Georgia are relatively small (4.13 - 13.38 mm and 26.63 - 42.13 mm) compared to those originating from the other three regions. The transport pathways of drifters originating in the southwestern Antarctic Peninsula show that drifters spend up to 4-5 months in transport toward the tip of the Antarctic Peninsula. Thus, larval and juvenile krill originating in this region may not be the primary source for krill at South Georgia. More likely, these krill supply 1+ and 2+ animals to regions 1 to 3, which are located along their transport paths.

All sizes of krill originating in the Weddell Sea are likely to survive transport to South Georgia due to their access to large amounts of sea ice algae and detrital food during the first 10 months of transport. No selection of a size class was observed for krill originating in this region. Krill arriving at South Georgia after 20 months reach sizes of 2+, 3+ and even larger size classes.

Therefore, the availability of food together with the length of time needed for transport combine to select for juvenile krill being the most able to survive the time

required for transport to South Georgia for krill originating in regions 1-4. This implies that regions 1-4 supply mainly 2+ animals. From the Weddell Sea, 2+ and 3+ animals can be delivered to South Georgia. These results agree with studies that show that usually the youngest dominant size class found at South Georgia is the 2+ class and only some years show a dominant 1+ size class (Mackintosh, 1972; Murphy et al., 1998)

5.3.3 Estimates of Krill Food Demand

Krill density estimates at South Georgia encompass a wide range of values, from 11.7 g m^{-2} for a November/December 1981 survey (Murphy et al., 1991) to 95 g m^{-2} for a January 1992 survey (Goss and Everson, 1996). Brierley et al. (1997) estimated a krill density of 40.57 g m^{-2} for the East Core Box (cf. Fig. 24) and 26.48 g m^{-2} for the West Core Box. At the Elephant Island region, Siegel et al., (2002) measured a krill abundance of 13.04 g m^{-2}, which is just slightly below the long-term running mean 13.9 g m^{-2} for this region (Siegel et al. 2002). Along the west Antarctic Peninsula values of 95 g m^{-2} were measured during the LTER study in summer, compared to 32 g m^{-2} in spring, 12 g m^{-2} in fall, and 8 g m^{-2} in winter (Lascara et al., 1999).

To estimate the amount of food that is necessary to sustain such large krill densities at South Georgia, Elephant Island, and the west Antarctic Peninsula during summer, a calculation of metabolic needs of different-sized krill was made. The maximum allowed krill growth rate in the growth model simulations is 0.25 mm d^{-1}. From the parameterizations for ingestion and respiration in the krill growth model (cf. Table 5) it can be estimated that larval krill (2 mm) need to gain 0.004558 mg C d^{-1} to achieve 0.25 mm d^{-1} growth, which in return requires a total of 312.0 mg C d^{-1} food intake. The required food intake reflects what is needed to cover the high respirational costs of larval krill and to provide energy for positive growth. These high rates may be due to the feeding parameterization for small, 2 mm, krill which is extrapolated from observations for larger krill (Hofmann and Lascara, 2000) and may overestimate metabolic needs of larval krill.

Food sources that krill may use in summer are phytoplankton, detritus and heterotrophic food. Feeding on sea ice algae in summer is unlikely because of reduced or no sea ice at the specified locations. Also, the krill density estimates are from measurements made in ice-free waters. If phytoplankton, heterotrophic food, and

detritus are fed on in equal quantities, a single larval krill would need a phytoplankton supply of 1.73 mg d^{-1}, 86.67 mg C d^{-1} carbon from heterotrophic food sources and 138.67 mg C d^{-1} from detritus.

A juvenile krill (22 mm) needs to gain 0.2637 mg C d^{-1} to achieve a growth of 0.25 mm d^{-1}, which translates into a total of 110.1 mg C d^{-1} food intake per individual because of lower respiration rates. This amount of carbon can be supplied by 0.612 mg d^{-1} of phytoplankton, 30.58 mg C d^{-1} of heterotrophic food and 48.93 mg C d^{-1} of detritus.

An adult krill (45 mm) needs to gain 1.42 mg C d^{-1} to achieve a growth of 0.25 mm d^{-1}. This requires a total of 119.21 mg C d^{-1} food intake which can be supplied by phytoplankton, heterotrophic, and detritus food of 0.663 mg d^{-1}, 33.13 mg C d^{-1}, and 52.96 mg C d^{-1}, respectively.

Using the krill density estimates for South Georgia, Elephant Island and the west Antarctic Peninsula and assuming that larval, juvenile and adult krill are present in equal numbers in each of the areas, the amount of food necessary to sustain this biomass can be calculated. The weight of the different sizes of krill can be calculated from the equations used in the growth model (Table 5), which is 0.2325 mg for a larval krill, 83.22 mg for a juvenile krill, and 162.01 mg for an adult krill. Therefore, 89.29 g C m^{-2} d^{-1} are needed to sustain krill in the East Core and 58.28 g C m^{-2} d^{-1} in the West Core Box. The Elephant Island area would need to supply 30.59 g C m^{-2} d^{-1} to feed 13.9 g m^{-2} of krill and at the west Antarctic Peninsula 95 g m^{-2} krill demand 209.08 g C m^{-2} d^{-1}.

These values seem realistic for summer conditions at South Georgia, where high average phytoplankton concentrations of 5.1 mg chl*a* m^{-3} have been measured and SeaWiFS images show intense phytoplankton blooms on the South Georgia shelf of >10 mg chl*a* m^{-3} (for review see Atkinson et al., 2001). Other studies estimate a mean phytoplankton biomass of 132 mg m^{-2} (6.6 g C m^{-2}) (Ward et al., 1995) or even 625 mg m^{-3} (31.25 g C m^{-2}) (Atkinson et al., 1996) for the surface mixed layer on the South Georgia shelf in summer. In addition, Ward et al. (1995) calculated a mean mesozooplankton biomass of 5.85 g C m^{-2} and an average of 5.54 g C m^{-2} was calculated by Atkinson et al. (1996). This would provide an average range of 12.45 to 36.47 mg C m^{-2} for both food sources and when detritus concentrations are included (POC:Chl*a* ratio of 38 in summer), a total of 17.47 to 60.54 g C m^{-2} may be available for krill to meet the demand of 58.28 g C m^{-2} d^{-1}. It should be

noted that these observed values are average values and individual patches may have a higher or lower biomass. In addition estimates of biomass vary largely between studies (Atkinson and Snÿder, 1997). At the same time the growth rate assumed here is a rather large growth rate that cannot be sustained very long.

Phytoplankton abundance data for January in the west Antarctic Peninsula region from BIOMASS cruise data is summarized by Priddle et al. (1994) and shows variations from 0.45 to 1334.5 mg chl$a$ m^{-2}, integrated over the upper 50 m. In this region areas of high phytoplankton concentrations exist, as was also observed by Holm-Hansen and Mitchell (1991), who observed phytoplankton biomass exceeding 700 mg chl$a$ m^{-2} at some stations on the west Antarctic Peninsula continental shelf. Mean phytoplankton biomass in the upper 50 m during December 1986 was 291 mg chl$a$ m^{-2} and 176 mg chl$a$ m^{-2} in January 1987 (Mitchell and Holm-Hansen, 1991a; 1991b). This phytoplankton biomass is more than that needed to sustain the high krill densities observed in this region. Including detritus concentrations derived from POC:Chl$a$ ratios, a total of 52.02 g C m^{-2} may be available to krill.

Few data on copepod distributions at the west Antarctic Peninsula are available. Schnack-Schiel and Mujica (1994) show an abundance of 2,700 copepods of the species *Calanoides acutus* per 1000 m^3 and 20,000 *Metridia gerlachi* per 1000 m^3 at the Antarctic Peninsula in January 1984, which are two dominant species of copepods. Huntley et al. (1994b) report numbers of 1,086 *Calnoides acutus* per m^2 at the end of October 1989 in the Gerlache Strait, which declined to 244 numbers m^{-2} by the end of November 1989. Again, these calculations show that it may be the patches of high food concentrations that krill depend on for their growth and survival.

5.4 Effect of Variability

5.4.1 Variability of Food Sources

The Scotia Sea is a variable environment and phytoplankton concentrations extracted from the CZCS images along drifter trajectories that are not widely separated in space and time show marked differences (Fig. 8). Similarly the sea ice time series (Fig. 10) and detritus time series extracted from the blended CZCS data (Fig. 13) suggest environmental variability occurring at a large number of scales. The circulation across the Scotia Sea is affected by the variability in the location

of the ACC fronts and is characterized by mesoscale eddies (Brandon et al., 1999). This mesoscale variability is evident in the simulated circulation fields as well, and the formation of mesoscale eddies is observed in the circulation distribution (Fig. 25). Peaks and troughs in the food time series extracted along drifter trajectories correlate with the trajectories moving through mesoscale eddies which may be located in high or low food environments. Fach et al. (2002) imposed this kind of variability with a time series of chlorophyll concentrations based on characteristics of mesoscale features seen in WOCE drifter trajectories, since the composite circulation field used did not include such features. The simulations in this study, which do include mesoscale flow variability, show that more krill survive and grow to larger sizes when feeding on phytoplankton only (Figs. 44-48A) when compared to growth of krill feeding on phytoplankton in the study including variability in an *ad hoc* manner (Fach et al., Fig. 8). This shows that the variability in food supply due to the use of a simulated circulation field that includes mesoscale variability plays a major role in the survival of krill during transport.

5.4.2 Variations in Krill Biomass at South Georgia

The results from this study show a strong connection between the krill population at South Georgia and those along the western Antarctic Peninsula, which represent the sink and the source population within the metapopulation, respectively. Transport times between these regions are relatively short, with 163 to 225 days required to cover the 1500 km distance between the two regions. Thus, changes in krill biomass at the western Antarctic Peninsula may influence the biomass at South Georgia in the same year with a relatively short lag time.

Krill abundance around South Georgia is known to fluctuate markedly (Heywood et al., 1985; Priddle et al., 1988). Studies of hydro-acoustic surveys of krill at South Georgia (Priddle et al., 1988; Brierley et al., 1997) together with data on avian and mammalian populations (Croxall et al., 1988; Croxall and Rothery, 1995; Croxall et al., 1998) show that there were four times in the last 20 years when the availability of krill at South Georgia was much reduced. These years of low krill biomass appear to reflect generally low abundance of krill throughout the South Georgia area and possibly the whole Scotia Sea (Priddle et al., 1988; Kock et al., 1994). In addition, recent studies have shown that there are major interannual changes in the krill density at South Georgia, with low concentrations of krill found during October and

much higher concentrations of krill found during December/January, and that the timing of a survey significantly effects krill estimates (Brierley et al., 2002)

Oscillations in krill biomass at Elephant Island (cf. Fig 1) have been shown to coincide with oscillations in biomass at South Georgia (Brierley et al., 1999). Changes in krill density apparent at Elephant Island in any particular year (of a total of six years) also seemed to be manifested at South Georgia in the same season, with no apparent time lag between locations (Brierley et al., 1999). The results from that study support the idea that environmental influences, recruitment success, and sea ice extent may have the same effect on both populations and that teleconnection processes between locations may transmit possible environmental-mediated changes in density across the Scotia Sea.

The variations in krill biomass seen at South Georgia can be attributed to variations in krill populations at the upstream source in the Antarctic Peninsula, in the Weddell Sea, and local populations at South Georgia, which are discussed below.

Variation Upstream

As suggested above, changes in the krill population along the western Antarctic Peninsula have an influence on the krill population at South Georgia. Thus, changes in the recruitment success of krill along the western Antarctic Peninsula may result in more or less krill being transported to South Georgia. Such recruitment success depends, for example, on the timing of spawning within the spawning season relative to environmental conditions, such as changes in the location of the SACCF and sea ice extent. It is also linked to the food supply available during krill spawning season, influencing the timing and size of the spawn.

A key feature of the physical environment that is of major importance for krill is the annual formation and retreat of sea ice (Mackintosh, 1972). The recruitment of juvenile krill in the Antarctic Peninsula region has been linked to the extent and duration of sea ice in the previous season (Siegel and Loeb, 1995; Loeb et al., 1997). The environment beneath the winter sea ice provides a favorable habitat for larval krill development (Daly, 1990) and also provides sufficient food supply for krill to promote early spawning in spring (Siegel and Loeb, 1995). A year with low sea ice concentration and short duration promotes late spawning of krill, while a year with high sea ice concentration and long duration promotes early spawning, which increases krill survival during transport (section 5.2.4). For successful recruitment of the spawned krill, a second year of high sea ice concentrations and long duration

is necessary. A minimum of two consecutive years of high sea ice concentration are needed for successful krill recruitment. The krill growth simulations suggest that juvenile krill are most likely to survive transport. Thus, seasons characterized by increased sea ice and therefore enhanced recruitment of krill can potentially provide a large source of krill for transport to South Georgia and other downstream locations.

However, a high abundance of krill at the Antarctic Peninsula may not always propagate toward South Georgia. Variability in the location of the SACCF relative to the shelf break may place it further offshore along the Peninsula (Hofmann and Klinck, 1998). Therefore, fewer krill will be entrained and transported from the region, with the result that more krill are retained along the Antarctic Peninsula (see section 5.2.2).

Although years of low krill biomass at South Georgia in general occurred during periods of low sea ice extent, there are periods of low sea ice cover (e.g. 1984/85, 1985/86) when the biomass of krill in the South Georgia area did not appear to be particularly low (Murphy et al., 1998). A possible explanation for this may be the influence of the propagating ACW, which provides more sea ice for krill survival at South Georgia after it has already passed the Antarctic Peninsula. Another explanation may be that krill originating from the Weddell Sea, which need 20 months to reach South Georgia, may have compensated in these particular years for the absence of krill from the Antarctic Peninsula.

Variation During Transport

During transport from the west Antarctic Peninsula to South Georgia krill is dependent on the food resources across the Scotia Sea. Therefore, a particularly low food year, may result in a reduction in krill survival; whereas, a high food environment will result in increased survival and potentially more krill reaching South Georgia. Timing of the transport is important with respect to food conditions, as early spawning releases krill into a potentially higher food environment.

Although hydro-acoustic estimates of krill vary considerably between years, these observations show that the krill biomass at Elephant Island is greater than that at South Georgia (Brierley et al., 1999). If this is indeed a representative observation and not due to differences in measuring krill biomass (Brierley et al., 1999), then this might be due to the dispersal of krill during transport, as suggested in Brierley et al. (1999). Or, as suggested in this study, the different survival chances of krill during transport depend on the timing of spawning in relation to the position of the SACCF

and the spawning area. Different transport pathways lead through different food concentrations (section 4.3.3) and release time and location is crucial to encountering sufficient food supply. At the same time predation of krill by predators, such as for example sea birds, whales, seals, and penguins, is an issue during transport, which is not included in the model setup used in this study.

Variation Locally

The local environment at South Georgia may also exert a large influence on the krill population. Once krill arrive at South Georgia, survival success is determined by sea ice extent, food supply, and predation. Predation on krill is an important factor at South Georgia, given the large biomass and diversity of predator species (Croxall et al., 1984; Croxall and Prince, 1987; Croxall et al., 1988; Hunt et al., 1992; Boyd et al., 1994) that depend on krill as a food source.

A shift in the SACCF may transport krill further offshore from the Island in some years or transport krill to locations even further downstream, thereby reducing the amount of krill being delivered directly to South Georgia. Also, local variability in mesoscale processes may change krill retention mechanisms (Murphy, 1995; Murphy et al., 1998; Brandon et al., 1999). For example, if the location of the shelf front found at South Georgia (section 5.1.5) moves further offshore, krill that are usually retained in the continental shelf area may be transported further offshore, and through interactions with the fast-flowing currents associated with the SACCF, may get transported further downstream and exported from the local population.

5.4.3 Estimates of Predation

Given the long transport time necessary to deliver krill to South Georgia from different source regions, it is likely that krill encounter predators along the way. Estimates of predation rates on krill are few. Boyd and Croxall (1996) calculated the demand for krill of Antarctic fur seals and macaroni penguins at South Georgia, from a combination of physiological data and diet samples, to be 32000 tons fresh mass d^{-1}. These two predators together consume >75% of the total for land-based predators (Croxall et al., 1985). Atkinson et al. (2001) calculate a total food removal for the same two species for an area off the west coast of South Georgia of 0.94 g fresh mass m^{-2} d^{-1}, compared with a mean biomass of 30 g fresh mass m^{-2}. This area includes breeding and non-breeding populations of Antarctic fur seals and macaroni

penguins. They conclude that the total removal of krill by land-based predators is on average approximately 3% d^{-1}.

These estimates, however, are calculated for the productive waters around South Georgia which have a large predator biomass and diversity of predator species (Croxall et al., 1984; Croxall and Prince, 1987; Croxall et al., 1988; Hunt et al., 1992; Boyd et al., 1994) and are not representative for other areas with predator colonies or the open ocean, which is where most of the transport time is spent. Therefore, 3% d^{-1} removal of krill (Atkinson et al., 2001) is considered a maximum estimate for predation, which cannot be applied to krill being transported across the Scotia Sea to South Georgia.

Murphy (1995) estimated the total land-based predator demand at South Georgia as a function of distance from the Island. Close to the Island the annual impact is up to 250 t km^{-2} $year^{-1}$, while at a distance of 350 km away from the Island the impact vanished. Assuming the predator demand at South Georgia is 3% d^{-1} as estimated by Atkinson et al. (2001), predator impact decreases to 2.4% d^{-1} at 75 to 130 km from the Island and diminishes to 0.45% d^{-1} at 200 km. Krill being transported to South Georgia spend most of this transport time more than 350 km away from South Georgia, which means predation is negligible. However, krill originating at the western Antarctic Peninsula spend part of their transport close to the Peninsula and in proximity to the predator colonies located there. Also, during the remainder of the transport krill are still subject to predation by whales, fish and sea birds not included in the land-based predators. Thus, a predation rate of 0.3% d^{-1} is assumed to be representative for the time of transport. This value is within the available predator estimates of 0 and 0.45% given by Murphy (1995).

The effect of predation on krill during transport to South Georgia was estimated as

$$K(t) = K_0 e^{-dt}, \tag{25}$$

where $K(t)$ is the number of krill at a certain time t during transport, K_0 is the initial number of krill at the time of release assumed to be 5000, and d is the rate of predation (0.3%). The number of krill chosen as K_0 is arbitrary and is intended to represent a small school of krill. The predation estimates are in terms of a non-dimensional ratio $(K(t)/K_0)$ that is between 0 and 1, and therefore does not change with different K_0 values.

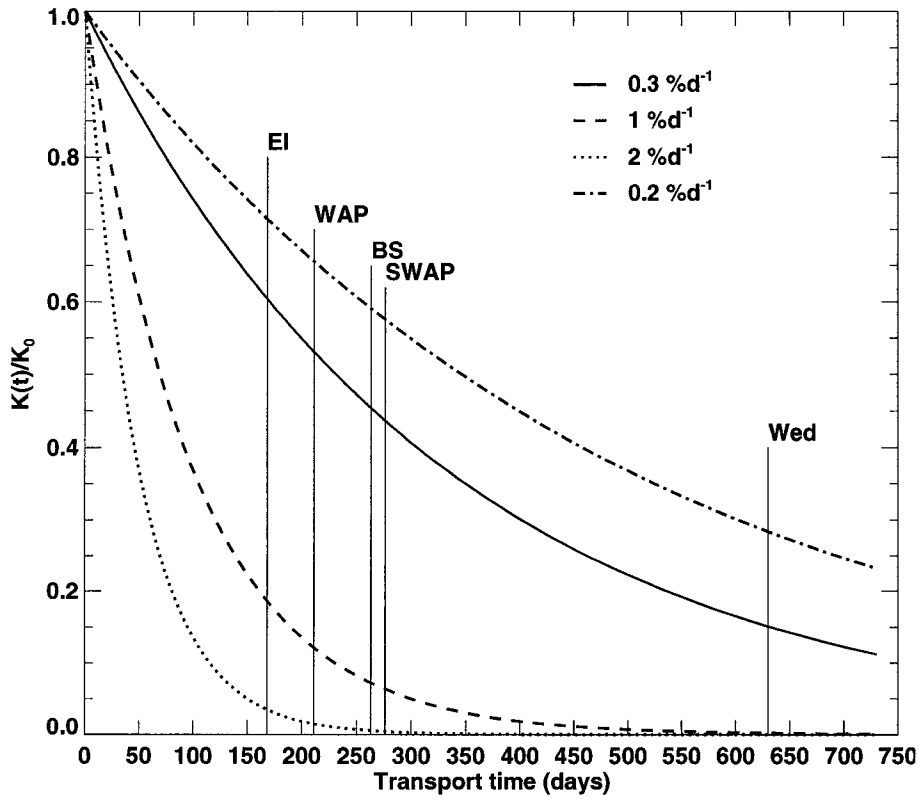

Fig. 58. Estimates of krill loss due to different rates of predation. The vertical lines indicate the average simulated transport times from the different source regions: Elephant Island (EI), west Antarctic Peninsula (WAP), Bransfield Strait (BS), southwest Antarctic Peninsula (SWAP), and Weddell Sea (Wed).

Depending on origination area, or total transport time, predation effects on krill survival differ (Fig. 58). Krill originating in the Elephant Island/Scotia Sea region have a better chance of surviving transport to South Georgia than do krill from the Weddell Sea because of the different transport times. However, krill from the Weddell Sea spend most of the transport time away from land and land-based predators and for these individuals a predation rate of 0.3% d^{-1} may be too high.

Calculations of the total time needed to remove 50% of the krill transported to South Georgia ($K(t)/K_0 = 0.5$) show a wide range for different predation rates (Fig. 58, Table 22). Krill originating at the Elephant Island/Scotia Sea region and the west Antarctic Peninsula are able to reach South Georgia before 50% are removed with a 0.3% d^{-1} predation rate. Krill originating in the Bransfield Strait region and

Table 22. Summary of the total times (days) necessary for different percent (%) of krill to be removed by different rates of predation.

	Predation Rate (%)			
Krill Removal (%)	0.2	0.3	1	2
1	5	3.4	1	0.5
10	53	35	10	5
50	347	231	69	35
90	1157	767	230	115

the southwest Antarctic Peninsula take longer to reach South Georgia, which allows >50% of the population to be removed by predation. At the same time, 82% of the Weddell Sea krill are removed before reaching South Georgia.

The above analysis indicates that predation can have a considerable effect on the successful transport of krill to South Georgia and that the potential impact on the variability of krill biomass at South Georgia cannot be neglected. Thus, the effect of predation needs to be explicitly included in future studies on krill transport. However, this will require detailed estimates of predation rates on krill as a function of the different predators and geographical regions.

6 SUMMARY

This study used a modeling frame work that couples physical and biological processes to characterize the transport and survival of larval, juvenile, and adult krill under different environmental conditions. The analysis of the results from circulation simulations, drifter simulations, and simulations of krill growth and how they answer the research questions posed for this study are summarized below.

This study defined four origination regions along the west Antarctic Peninsula that coincide with known spawning areas, and one origination area in the Weddell Sea, from which krill can potentially recruit into the local krill population at South Georgia. The main transport pathway for krill is found to be the currents associated with the SACCF and it was found that the timing of spawning is crucial for krill survival, with early spawning resulting in the highest numbers of krill reaching South Georgia, as well as providing the highest food concentrations along simulated drifter paths. However, timing of spawning is also crucial in respect to the position of the SACCF and changes in the front location may result in reduced numbers of krill reaching South Georgia. This implies that the krill population along the Antarctic Peninsula and the Weddell Sea are likely the source populations that provide krill to the sink population at South Georgia.

Krill survival during transport is dependent on the food availability along transport paths and the krill growth model simulations showed that no single food source, such as pelagic phytoplankton, detritus, sea ice algae, or zooplankton, can support continuous growth of Antarctic krill during the time needed for transport to South Georgia. However, combinations of the food sources during transport time enhanced krill survival, with heterotrophic food and detritus being particularly important during periods of low pelagic phytoplankton concentrations. It was shown that mesoscale patches of high food concentrations may be important to sustain krill in a variable food environment.

At the west Antarctic Peninsula, environmental and biological factors combine to select for juvenile krill being the age group that successfully completes transport. For krill originating in the Weddell Sea no such selection could be observed. The implication of this is that for best transport success the source population along the Antarctic Peninsula needs to provide large numbers of juvenile krill. However, it has been shown in previous studies that the recruitment success of juvenile krill depends on the occurrence of two consecutive high sea ice concentration years (Siegel and

Loeb, 1995; Loeb et al., 1997). This implies that interannual changes in the sea ice extent, such as from the ACW, potentially has a large effect on the supply of krill from this source population and years of low sea ice concentrations may substantially reduce successful transport from this source population.

The observed episodic variations in krill biomass at South Georgia result from a combination of variations at the source population, during transport, and at the local population. It has been shown in this study, that the successful transport of krill to South Georgia depends on multiple factors, such as the location of the spawning area and timing of spawning, food concentrations during transport, the variations in the location of the SACCF, and predation. It also depends on the recruitment success of the source population that may result in more or less krill being transported to South Georgia. This implies that Antarctic krill are well adapted to the variable environment in which they live. However, the many factors that need to converge to produce successful supply of krill to the sink population at South Georgia, makes the krill population at South Georgia susceptible to changes caused by climate variations or human impact.

The fact that populations at South Georgia, the west Antarctic Peninsula, and the Weddell Sea belong to the same krill metapopulation has wide reaching implications for the management strategies of this commercially exploited fisheries. Catch limits need to be revised taking into account that the separate fisheries at South Georgia and at the Antarctic Peninsula are fishing on the same population, not as previously thought on separately contained populations (Mackintosh, 1973; Makarov, 1973; Lubimova et al. 1982). This may ensure the survival of the metapopulation while sustaining the existing fishery.

This study has provided insight into which biological and environmental factors control the successful transport of krill across the Scotia Sea and their survival during that time, and with it insight into krill distribution and production in the Scotia Sea. Future modeling efforts of krill growth and survival will require inclusion of vertical migration behavior of krill with the corresponding energy dynamics. In addition, the inclusion of a lower trophic level ecosystem model is necessary to better account for dynamically changing food sources for krill and to allow for the possibility of testing the influence of environmental changes on krill growth and survival. Further, the inclusion of estimates of predation on krill is of importance because predation can account for a major source of krill mortality during transport.

Though this study has provided insight into the factors influencing krill population dynamics, many questions are still open. The effects of the ACW on krill populations is only now starting to be considered, for example. Additional, multi-year observational studies are needed in order to investigate the teleconnections between periodic changes in sea ice extent and concentration, and krill abundance at the Antarctic Peninsula and South Georgia. It is necessary to investigate the transport and retention mechanisms for krill around South Georgia more closely, to asses their importance for the local krill population and to understand krill distributions around the Island. Further studies are needed to investigate the fate of krill that are transported further downstream from South Georgia, looking at the teleconnections of krill populations all around Antarctica. It is only with such a holistic approach that the dynamics of these krill populations can be understood.

7 REFERENCES

Abbott, M.R., Richman, J.G., Nahorniak, J.S., Barksdale, B.S., 2001. Meanders in the Antarctic Polar Front Zone and their impact on phytoplankton. Deep-Sea Research II 48, 3891-3912.

Ackley, S.F., Sullivan, C.W., 1994. Physical controls on the development and characteristics of Antarctic sea ice biological communities - a review and synthesis. Deep-Sea Research 41, 1583-1604.

Angel, M.V., Fasham, M.J.R., 1983. Eddies and Biological Processes. In: Robinson, A.R. (Ed.), Eddies in marine science. Springer Verlag, Berlin, Heidelberg, New York, pp. 492-524.

Antonov, J. I., Levitus, S., Boyer, T.B., Conkright, M.E., O'Brien, T.D., Stephens, C., 1998. World Ocean Atlas 1998. Volume 1: Temperature of the Atlantic Ocean. NOAA Atlas NESDIS 27, U.S. Government Printing Office, Washington, D.C., pp. 166, CD-ROMs.

Arrigo, K., Worthen, D.L., Dixon, P., Lizotte, M.P., 1998. Primary productivity of near surface communities within Antarctic pack ice. In: Lizotte, M.P., Arrigo, K.R. (Eds.), Antarctic sea ice: biological processes, interactions, and variability, Antarctic Research Series 73, pp. 23-43.

Arrigo, K., Worthen, D.L., Lizotte, M.P., Dixon, P., Dieckmann, G., 1997. Primary production in Antarctic sea ice. Science 276, 394-397.

Astheimer, H., 1986. A length class model of the population dynamics of the Antarctic krill *Euphausia superba* Dana. Polar Biology 6, 227-232.

Astheimer, H., Krause, H., Rakusa-Suszczewski, S., 1985. Modeling individual growth of the Antarctic krill *Euphausia superba* Dana. Polar Biology 4, 65-73.

Atkinson, A., Sinclair, J.D., 2000. Zonal distribution and seasonal vertical migration of copepod assemblages in the Scotia Sea. Polar Biology 23, 46-58.

Atkinson, A., Snÿder, R., 1997. Krill-copepod interactions at South Georgia, Antarctica I. Omnivory by *Euphausia superba.* Marine Ecology Progress Series 160, 63-76.

Atkinson, A., Shreeve, R.S., Pakhomov, E.A., Priddle, J., Blight, S.P., Ward, P., 1996. Zooplankton response to a phytoplankton bloom near South Georgia, Antarctica. Marine Ecology Progress Series 144, 195-210.

Atkinson, A., Whitehouse, M.J., Priddle, J., Cripps, G.C., Ward, P., Brandon, M.A.,

2001. A productive, cold water pelagic ecosystem: a review of South Georgia, Antarctica. Marine Ecology Progress Series 216, 279-308.

Barnier, B., Marchesiello, P., de Miranda, A.P., Molines, J.-M., Coulibaly, M., 1998. A sigma-coordinate primitive equation model for studying the circulation in the South Atlantic. Part I: Model configuration with error estimates. Deep-Sea Research I 45, 543-572.

Bathmann, U.V., Scharek, R., Klaas, C., Dubischar, C.D., Smetacek, V., 1997. Spring development of phytoplankton biomass and composition in major water masses of the Atlantic sector of the Southern Ocean. Deep-Sea Research 44(1-2), 51-67.

Beckmann, A., Hellmer, H.H., Timmermann, R., 1999. A numerical model of the Weddell Sea: Large-scale circulation and water mass distribution. Journal of Geophysical Research 104, 23,375-23,391.

Bianchi, F., Boldrin, A., Cioce, F., Dieckmann, G., Kuosa, H., Larsson, A.-M., Noetig, E.-M., Sehlstedt, P.-I., Socal, G., Syvertsen, E.E., 1992. Phytoplankton distribution in relation to sea ice and nutrients in the northern Weddell Sea in early spring 1988 during EPOS. Polar Biology 12, 225-235.

Bleck, R., 2002. An Oceanic General Circulation Model Framed in Hybrid Isopycnic-Cartesian Coordinates, Ocean Modelling, 4, 55-88.

Boyd, I.L., Croxall, J.P., 1996. Preliminary estimates of krill consumption by Antarctic fur seals and macaroni penguins at South Georgia. Document WG-EMM-96/96, CCAMLR, Hobart.

Boyd, I.L., Arnould, J.P.Y., Barton, T., Croxall, J.P., 1994. Foraging behavior of Antarctic fur seals during periods of contrasting prey abundance. Journal of Animal Ecology 63(3), 703-713.

Boyer, T. P., Levitus, S., Antonov, J.I., Conkright, M.E., O'Brien, T.D., Stephens, C., 1998. World Ocean Atlas 1998. Volume 4: Salinity of the Atlantic Ocean. NOAA Atlas NESDIS 30, U.S. Government Printing Office, Washington, D.C., pp. 166, CD-ROMs.

Brandon, M.A., Murphy, E.J., Trathan, P.N., Bone, D.G., 2000. Physical conditions to the northwest of the sub-Antarctic island of South Georgia. Journal of Geophysical Research 105, 23,983-23,996.

Brandon, M.A., Murphy, E.J., Whitehouse, M.J., Trathan, P.N., Murray, A.W.A., Bone, D.G., Priddle, J., 1999. The shelf break front to the east of the sub-

Antarctic island of South Georgia. Continental Shelf Research 19, 799-819.

Bretherton, F.P., Davis, R.E., Fandry, C.B., 1976. A technique for objective analysis and design of oceanographic experiments applied to MODE-73. Deep Sea Research 23(7), 559-582.

Brierley, A.S., Watkins, J.L., Murray A.W.A., 1997. Interannual variability in krill abundance at South Georgia. Marine Ecology Progress Series 150, 87-98.

Brierley, A.S., Demer, D.A., Watkins, J.L., Hewitt, R.P., 1999. Concordance of interannual fluctuations in acoustically estimated densities of Antarctic krill around South Georgia and Elephant Island: Biological evidence of same-year teleconnections across the Scotia Sea. Marine Biology 134(4), 675-681.

Brierley, A.S., Goss, C., Grant, S.A., Watkins, J.L., Reid, K., Belchier, M., Everson, I., Jessop, M.J., Afanasyew, V., Robst, J., 2002. Significant intra-annual variability in krill distribution and abundance at South Georgia revealed by multiple acoustic surveys during 2000/01. CCAMLR Science 9, 71-82.

Brinton, E., 1985. The oceanic structure of the eastern Scotia Sea - III. Distributions of euphausiid species and their developmental stages in 1981 in relation to hydrography. Deep-Sea Research 32(10), 1153-1180.

Brinton, E., 1991. Distribution and population structures of immature and adult *Euphausia superba* in the western Bransfield Strait region during the 1986-87 summer. Deep-Sea Research 38, 1169-1193.

Brinton, E., Townsend, A.W., 1984. Regional relationships between development and growth in larvae of Antarctic krill, *Euphausia superba* from field samples. Journal of Crustacean Biology 4, 224-246.

Bryan, K., 1969. A numerical method for the study of the circulation of the world ocean. Journal of Computational Physics 4, 347-376.

Bryden, H.L., 1983. The Southern Ocean. In: Robinson, A.R. (Ed.), Eddies in Marine Science. Springer Verlag, Berlin, Heidelberg, New York, pp. 265-277.

Bryden, H.L., Heath, R.A., 1985. Energetic eddies at the northern edge of the Antarctic Circumpolar Current in the southwest Pacific. Progress in Oceanography 14, 65-87.

Bryden, H.L., Pillsbury, R.D., 1977. Variability of deep flow in the Drake Passage from year-long measurements. Journal of Physical Oceanography 7, 803-810.

v. Bodungen, B., Smetacek, V.S., Tilzer, M.M., Zeitschel, B., 1986. Primary production and sedimentation during spring in the Antarctic Peninsula region.

Deep-Sea Research 33(2), 177-194.

Buchholz, F., 1985. Moult and growth in Euphausiids, In: Siegfried, W.R., Cody, P.R., Laws, R.M. (Eds.), Antarctic nutrient cycles and food webs. Springer Verlag, Berlin, pp. 339-345.

Buchholz, F., 1991. Molt cycle and growth of Antarctic krill *Euphausia superba* in the laboratory. Marine Ecology Progress Series 69, 217-229.

Canuto, C., Hussaini, M.Y., Quarteroni, A., Zang, T.A., 1988. Spectral Methods in fluid dynamics, Springer Series in Computational Physics. Springer Verlag, New York, pp. 567.

Capella, J.E., Quetin, L.B., Hofmann, E.E., Ross, R.M., 1992. Models of the early life history of *Euphausia superba* - Part II. Lagrangian calculations. Deep-Sea Research 39(7/8), 1201-1220.

Capella, J.E., Ross, R.M., Quetin, L.B., Hofmann, E.E., 1990. A note on the structure of the upper ocean in the Bransfield Strait-South Shetland Islands region. Deep-Sea Research 39(7/8), 1221-1229.

Chelton, D.B., Schlax, M.G., Witter, D.L., Richman, J.G., 1990. GEOSAT altimeter observations of the surface circulation of the Southern Ocean. Journal of Geophysical Research 95, 17877-17903.

Cheney, R.E., Marsh, J.G., Beckley, B.D., 1983. Global mesoscale variability from colinear tracks of SEASAT altimeter data. Journal of Geophysical Research 88, 4331-4538.

Clarke, A., 1984. Lipid content and composition of Antarctic krill, *Euphausia superba* Dana. Journal of Crustacean Biology 4(Spec. No. 1), 285-294.

Clarke, A., Morris, D.J., 1983. Towards an energy budget for krill: the physiology and biochemistry of *Euphausia superba* Dana. Polar Biology 2, 69-86.

Comiso, J.C., Sullivan, C.W., 1986. Satellite microwave and *in-situ* observations of the Weddell Sea ice cover and its marginal ice zone. Journal of Geophysical Research 91, 9663-9681.

Comiso, J.C., Grenfell, T.C., Bell, D., Lange, M., Ackley, S., 1989. Passive microwave in situ observations of Weddell Sea Ice. Journal of Geophysical Research 94, 10,891-10,905.

Comiso, J.C., McClain, C.R., Sullivan, C.W., Ryan, J.P., Leonard, C.L., 1993. Coastal Zone Color Scanner pigment concentrations in the Southern Ocean and relationships to geophysical surface features. Journal of Geophysical Research

98, 2419-2451.

Cota, G.F., Smith, W.O., Nelson, D.M., Muench, R.D., Gordon, L.I., 1992. Nutrient and biogenic particulate distributions, primary productivity and nitrogen uptake in the Weddell-Scotia Sea marginal ice zone during winter. Journal of Marine Research 50, 155-181.

Cox, M.D., 1984. A primitive equation, three-dimensional model of the ocean. GFDL Ocean Group Technical Report 1, Geophysical Fluid Dynamics Laboratory, Princeton University, NJ, pp. 147.

Crowley, T.J., Parkinson, C.L., 1988. Late Pleistocene variations in Antarctic sea ice II: Effect of inter-hemispheric deep-ocean heat exchange. Climate Dynamics 3, 93-103.

Croxall, J.P., Prince, P.A., 1987. Seabirds as predators on marine resources, especially krill, at South Georgia. In: Croxall, J.P. (Ed.) Seabirds: feeding ecology and role in marine ecosystems. Cambridge University Press, Cambridge, pp. 347-368.

Croxall, J.P., Rothery, P., 1995. Population change in gentoo penguins *Pygoscelis papua* at Bird island South Georgian: potential roles of adult survival, recruitment and deferred breeding. In: Dann, P., Norman, I., Reilly, P. (Eds.) The penguins: ecology and management. Surrey Beatty and Sons, Chipping Norton, pp. 26-38.

Croxall, J.P., Prince, P.A., Ricketts, C., 1985. Relationships between prey life cycles and the extent, nature and timing of seal and seabird predation in the Scotia Sea. In: Siegfried, W.R., Condy, P.R., Laws, R.M. (Eds.), Antarctic nutrient cycles and food webs. Springer Verlag, Berlin, pp. 516-533.

Croxall, J.P., Ricketts, C., Prince, P.A., 1984. Impacts of seabirds on marine resources, especially krill, of South Georgia waters. In: Whittow, G.C., Rahn, H. (Eds.) Seabird energetics. Plenum Publishing Co., New York, pp. 285-318.

Croxall, J.P., Reid, K., Prince, P.A., 1999. Diet, provisioning and productivity responses of marine predators to differences in availability of Antarctic krill. Marine Ecology Progress Series 177, 117-131

Croxall, J.P., McCann, T.S., Prince, P.A., Rothery, R., 1988. Reproductive performance of seabirds and seals at South Georgia and Signy Island, South Orkney Islands, 1976-1987: implications for Southern Ocean. In: Sahrhage, D. (Ed.), Antarctic Ocean and resource variability. Springer Verlag, Berlin, pp. 261-285.

Croxall, J.P., Prince, P.A., Rothery, R., Wood, A.G., 1998. Population changes in albatross at South Georgia. In: Robertson, G., Gales, R. (Eds.) Albatross biology and conservation. Surrey Beatty and Sons, Chipping Norton, pp. 68-83.

Daly, K.L., 1990. Overwintering development, growth, and feeding of larval *Euphausia superba* in the Antarctic marginal ice zone. Limnology and Oceanography 35(7), 1564-1576.

Daly, K.L., Macaulay, M.C., 1991. Influence of physical and biological mesoscale dynamics on the seasonal distribution and behavior of *Euphausia superba* in the Antarctic marginal ice zone. Marine Ecology Progress Series 79, 37-66.

Deacon, G.E.R., 1977. Seasonal and annual variations in water temperature and salinity near South Georgia 1925-1937. IOS Report no. 49, Institute of Oceanographic Sciences, Wormley, pp. 30.

Deacon, G.E.R., 1982. A general account of the hydrology of the Southern Ocean. Deep-Sea Research, Part A 29, 1-28.

Dehairs, F., Kopczynska, E., Nielsen, P., Lancelot, C., Bakker, D.C.E., Koeve, W., Goeyens, L., 1997. $\partial^{13}C$ of Southern Ocean suspended organic matter during spring and early summer: regional and temporal variability. Deep-Sea Research II 44(1-2), 129-142.

Denys, C.T., Poleck, T.P., O'Leary, M.M., 1981. Biological studies of krill. Austral summer 1979/80. Antarctic Journal of the United States 15, 146-147.

Dever, E.P., Lentz, S.J., 1994. Heat and salt balances over the northern California shelf in winter and spring. Journal of Geophysical Research 99, 16,001-16,017.

Dierssen, H.M., Smith, R.C., 2000. Bio-optical properties and remote sensing ocean color algorithms for Antarctic Peninsula waters. Journal of Geophysical Research 105, 26,301-26,312.

El-Sayed, S.Z., 1977. Biological investigations of marine Antarctic systems and Stocks, Vol. 1. Scott Polar Research Institute, Cambridge, England, pp. 1-79.

El-Sayed, S.Z., 1994. History, organization and accomplishments of the BIOMASS Programme. In: El-Sayed, S.Z. (Ed.), Southern Ocean Ecology, the BIOMASS perspective. Cambridge University Press, Cambridge, pp. 1-8.

El-Sayed, S.Z., Weber, L.H., 1982. Spatial and temporal variations in phytoplankton biomass and primary production in the southwest Atlantic and Scotia Seas. Polar Biology 1, 83-90.

Ettershank, G., 1983. Age structure and cyclical annual size change in the Antarctic

krill, *Euphausia superba* Dana. Polar Biology 2, 189-193.

Ettershank, G., 1984. A new approach to the assessment of longevity in the Antarctic krill *Euphausia superba*. Journal of Crustacean Biology 4(Spec. No. 1), 295-305.

Ettershank, G., 1985. Population age structure in males and juveniles of the Antarctic krill, *Euphausia superba* Dana. Polar Biology 4(4), 199-201.

Everson, I., 1983. Variations in vertical distribution and density of krill swarms in the vicinity of South Georgia. Memoirs of National Institute of Polar Research, Special Issue 27, 84-92.

Everson, I., 1984. Marine Interactions. In: Laws, R.M. (Ed.), Antarctic Ecology, Volume 2, Academic Press, London, pp. 783-819.

Everson, I., Miller D.G.M., 1994. Krill mesoscale distribution and abundance: results and implications of research during the BIOMASS programme. In: El-Sayed, S.Z. (Ed.), Southern Ocean Ecology, the BIOMASS perspective. Cambridge University Press, Cambridge, pp. 129-143.

Everson, I., Murphy, E., 1987. Mesoscale variability in the distribution of krill *Euphausia superba*. Marine Ecology Progress Series 40, 53-60.

Everson, I., Ward, P., 1980. Aspects of Scotia Sea zooplankton. In: Bonner, W.N., Berry, R.J. (Eds.) Ecology of the Antarctic, Academic Press, London, pp. 93-101.

Fabiano, M., Povero., P., Danovaro, R., 1993. Distribution and composition of particulate organic matter in the Ross Sea (Antarctica). Polar Biology 13, 525-533.

Fabiano, M., Danovaro, R., Crisafi, E., La Ferla, R., Povero., P., Acosta-Pomar, L., 1995. Particulate matter composition and bacterial distribution in Terra Nova Bay (Antarctica) during summer 1989-1990. Polar Biology 15, 393-400.

Fach, B.A., Hofmann, E.E., Murphy, E.J., 2002. Modeling studies of Antarctic krill *Euphausia superba* survival during transport across the Scotia Sea. Marine Ecology Progress Series 231, 187-203.

Fahrbach, E., Rohardt, G., Schröder, M., Strass, V., 1994. Transport and structure of the Weddell Gyre. Annales Geophysicae 12, 840-855.

Falkowski, P.G., Flagg, C.N., Rowe, G.T., Smith, S.L., Whiteledge, T.E., Wirick, C.D., 1988. The fate of a spring phytoplankton bloom: Export or oxidation? Continental Shelf Research 88, 737-756.

Fandry, C., Pillsbury, R.D., 1979. On the estimation of absolute geostrophic volume transport applied to the Antarctic Circumpolar Current. Journal of Physical Oceanography 9(3), 449-455.

Fedoulov, P.P., Murphy, E.J., Shulgovsky, K.E., 1996. Environment-krill relations in the South Georgia marine ecosystem. CCAMLR Science 3, 13-30.

Fevolden, S.E., 1988. Biochemical genetics and population structure of *Euphausia superba*. Comparative Biochemistry and Physiology 90B(3), 507-513.

Fevolden, S.E., George, R.Y., 1984. Size frequency pattern of *Euphausia superba* in the Antarctic Peninsula waters in the austral summer of 1983. Journal of Crustacean Biology 4, 107-122.

Foster, T.D., Middleton, J.H., 1984. The oceanographic structure of the eastern Scotia Sea - I. Physical oceanography. Deep-Sea Research 31(5), 529-550.

FRAM Group, 1991. An eddy-resolving model of the Southern Ocean. EOS, Transactions of the American Geophysical Union 72(15), 169-175.

Fraser, F.C., 1936. On the development and distribution of the young stages of krill, (*Euphausia superba*). Discovery Reports 14, pp. 1-192.

Frost, B.W., 1972. Effects of size and concentration of food particles on the feeding behavior of the marine planktonic copepod *Calanus pacificus*. Limnology and Oceanography 17, 805-815.

Fu, L., Chelton, D.B., 1984. Temporal variability of the Antarctic Circumpolar Current observed from satellite altimetry. Science 226, 343-346.

Fu, L., Chelton, D.B., 1985. Observing large-scale temporal variations of ocean currents by satellite altimetry: with application to the Antarctic Circumpolar Current. Journal of Geophysical Research 90, 4721-4739.

Gangopadhyay, A., Robinson, A.R., Arango, H.G., 1997. Circulation and dynamics of the western north Atlantic. Part I: Multiscale feature models. Journal of Atmospheric and Oceanic Technology 16(4), 1314-1332.

Garrison, D.L., Sullivan, C.W., Ackley, S.F., 1986. Sea ice microbial communities in Antarctica. BioScience 36, 243-250.

Gille, S.T., 1994. Mean sea surface height of the Antarctic Circumpolar Current from GEOSAT data: Method and application. Journal of Geophysical Research 99, 18255-18273.

Gille, S.T., Kelly, K.A., 1996. Scales of spatial and temporal variability in the Southern Ocean. Journal of Geophysical Research 101, 8759-8773.

Godlewska, M., 1996. Vertical migrations of krill (*Euphausia superba* Dana). Polish Archive of Hydrobiology 43(1), 9-63.

Godlewska, M., Rakusa-Suszczewski, S., 1988. Variability of krill, (*Euphausia superba*), Dana 1852 (Crustacea, Euphauciacea), distribution and biomass in the western Antarctic (Bransfield Strait, Drake passage, Elephant Island) during 1976-1987. Investigacion Pesquera 52(4), 575-586.

Gordon, A.L., Georgi, D.T., Taylor, H.W., 1977. Antarctic Polar Front Zone in the western Scotia Sea - Summer 1975. Journal of Physical Oceanography 7, 3009-328.

Gordon, A.L., Molinelli, E., Baker, T., 1978. Large-scale relative dynamic topography of the Southern Ocean. Journal of Geophysical Research 83, 3023-3032.

Gordon, H.R. McCluney, W.R., 1975. Estimation of the depth of sunlight penetration in the sea for remote sensing. Applied Optics 14, 413-416.

Goss, C., Everson, I., 1996. An acoustic survey of Antarctic krill on the South Georgia shelf, CCAMLR subarea 48.3, in January 1992. WG-EMM-96/42 CCAMLR, Hobart, Australia.

Granéli, E., Granéli, W., Rabbani, M.M., Daugbjerg, N., Fransz, G., Cuzin-Roudy, J., Alder, V.A., 1993. The influence of copepod and krill grazing on species composition of phytoplankton communities from the Scotia-Weddell Sea. Polar Biology 13, 201-213.

Gross, T.J., Johnson, J.A., Bigg, G.R., 1995. A comparison between the FRAM (Fine Resolution Antarctic Model) results and observations in Drake Passage. Deep-Sea Research 42, 365-388.

Haidvogel, D.B., Wilkin, J.L., Young, R., 1991. A semi-spectral primitive equation ocean circulation model using vertical sigma coordinate and orthogonal curvilinear horizontal coordinates. Journal of Computational Physics 94, 151-185.

Hamner, W.M., 1984. Aspects of schooling of *Euphausia superba*. Journal of Crustacean Biology 4(Spec. No. 1), 67-74.

Hamner, W.M., 1988. Biomechanics of filter feeding in the Antarctic krill *Euphausia superba*: Review of past work and new observations. Journal of Crustacean Biology 8(2), 149-163.

Hamner, W.M., Hamner, P.P., Strand, S.W., Gilmer, R.W., 1983. Behavior of Antarctic krill *Euphausia superba*: Chemoreception, feeding, schooling and moulting. Science 220, 433-435.

Hampton, I., 1985. Abundance, distribution and behavior of *Euphausia superba* in the Southern Ocean between 15°E and 30°E during FIBEX. In: Siegfried, W.R., Condy, P.R., Laws, R.M. (Eds.), Antarctic nutrient cycles and food webs. Springer Verlag, Berlin, pp. 294-304.

Haney, R.L., 1991. On the pressure gradient force over steep topography in sigma coordinate models. Journal of Physical Oceanography 21, 610-619.

Hardy, A.C., Gunther, E.R., 1935. The plankton of the South Georgia whaling grounds and adjacent waters, 1926 – 1927. Discovery Reports 11, pp. 456.

Harmer, S.F., 1931. Southern whaling. Proceedings of the Linnean Society London 142, 85-163.

Harrington, S.A., Ikeda, T., 1986. Laboratory observations on spawning, brood size and egg hatchability of the Antarctic krill *Euphausia superba* from Prydz Bay, Antarctica. Marine Biology 92, 231-235.

Headland, R.K., 1984. The Island of South Georgia. Cambridge University Press, Cambridge, UK, pp. 293.

Hempel, I., Hempel, G., 1986. Field observations on the developmental ascent of larval *Euphausia superba* (Crustacea). Polar Biology 6, 121-126.

Heywood, K.J., King, B.A., 1996. WOCE section A23 cruise report, RRS *James Clark Ross* Cruise 10, 20th March - 6th May, 1995. UEA Cruise Report Series No. 1, University of East Anglia, Norwich, UK, pp. 75.

Heywood, R.B., Priddle, J., 1987. Retention of phytoplankton by an eddy. Continental Shelf Research 7(8), 937-955.

Heywood, R.B., Everson, I., Priddle, J., 1985. The absence of krill from the South Georgia zone, winter 1983. Deep-Sea Research 32(3), 369-378.

Hill, H.J., Trathan, P.N., Croxall, J.P., Watkins, J.L., 1996. A comparison of Antarctic krill *Euphausia superba* caught by nets and taken by macaroni penguins *Eudyptes chrysolophus*: evidence for selection? Marine Ecology Progress Series 140, 1-11.

Hofmann, E.E., 1985. The large-scale horizontal structure of the Antarctic Circumpolar Current from FGGE drifters. Journal of Geophysical Research 90, 7087-7097.

Hofmann, E.E., Klinck, J.M., 1998. Thermohaline variability of the waters overlying the west Antarctic Peninsula continental shelf. In: Jacobs, S.S., Weiss, R.F. (Eds.), Ocean, ice, and atmosphere: Interactions at the Antarctic continental

margin. Antarctic Research Series 75, pp. 67-81.

Hofmann, E.E., Whitworth III, T., 1985. A synoptic description of flow at Drake Passage from year-long measurements. Journal of Geophysical Research 90, 7177–7187.

Hofmann, E.E., Lascara, C.M., 2000. Modeling the growth dynamics of Antarctic krill (*Euphausia superba*). Marine Ecology Progress Series 194, 219-231.

Hofmann, E.E., Capella, J.E., Ross, R.M., Quetin, L.B., 1992. Models of the early life history of *Euphausia superba*. Part I. Time and temperature dependence during the descent–ascent cycle. Deep-Sea Research 39, 1177–1200.

Hofmann, E.E., Klinck, J.M., Locarnini, R.A., Fach, B.A., Murphy, E.J., 1998. Krill transport in the Scotia Sea and environs. Antarctic Science 10(4), 406-415.

Holm-Hansen, O., Huntley, M., 1984. Feeding requirements of krill in relation to food sources. Journal of Crustacean Biology, 4(Spec. No. 1), 156-173.

Holm-Hansen, O., Mitchell, B.G., 1991. Spatial and temporal distribution of phytoplankton and primary production in the western Bransfield Strait region. Deep-Sea Research 38(8/9), 961-980.

Hopkins, T.L., Lancraft, T.M., Torres, J.J., Donnelly, J., 1993. Community structure and trophic ecology of zooplankton in the Scotia Sea marginal ice zone in winter. Deep-Sea Research I 40(1), 81-105.

Hunt, G.L., Heinemann, D., Everson, I., 1992. The distribution and predator-prey interactions of macaroni penguins, Antarctic fur seals and Antarctic krill near Bird Island, South Georgia. Marine Ecology Progress Series 86, 15-30.

Huntley, M.E., Nordhausen, W., Lopez, M.D.G., 1994a. Elemental composition, metabolic activity and growth of Antarctic krill *Euphausia superba* during winter. Marine Ecology Progress Series 107, 23-40.

Huntley, M.E., Zhou, M., Lopez, M.D.G., 1994b. *Calanoides acutus* in Gerlache Strait, Antarctica II. Solving an inverse problem in population dynamics. Deep-Sea Research II 41(1), 209-227.

Ikeda, T., 1981. Metabolic activity of larval stages of Antarctic krill. Antarctic Journal of the United States 16, 161-162.

Ikeda, T., 1984a. Development of the larvae of Antarctic krill (*Euphausia superba* Dana) in the laboratory. Journal of Experimental Marine Biology and Ecology 75, 107-117.

Ikeda, T., 1984b. Sequences in metabolic rates and elemental composition (C, N,

P) during the development of *Euphausia superba* Dana and estimated food requirement during its life span. Journal of Crustacean Biology 4(Spec. No. 1), 273-284

Ikeda, T., Bruce, T., 1986. Metabolic activity and elemental composition of krill and other zooplankton from Prydz Bay, Antarctica, during early summer (November-December). Marine Biology 92, 545-555.

Ikeda, T., Dixon, P., 1982. Body shrinkage as a possible over-wintering mechanism of Antarctic krill (*Euphausia superba* Dana). Australian Journal of Marine and Freshwater Research 33, 71-76.

Ikeda, T., Kirkwood, R., 1989. Metabolism and body composition of two euphausiids (*Euphausia superba* and *E. crystallorophias*) collected from under the pack-ice off Enderby Land, Antarctica. Marine Biology 100, 301-308.

Ikeda, T., Mitchell, A.W., 1982. Oxygen uptake, ammonia excretion and phosphate excretion by krill and other Antarctic zooplankton in relation to their body size and chemical composition. Marine Biology 71, 283-298.

Ikeda, T., Dixon, P., Kirkwood, R., 1985. Laboratory observations of moulting, growth and maturation in Antarctic krill (*Euphausia superba* Dana). Polar Biology 4, 1-18.

Inoue, M., 1985. Modal decomposition of the low-frequency currents and baroclinic instability at Drake Passage. Journal of Physical Oceanography 15, 1157-1181.

Ishii, H., Omori, M., Maeda, M., Watanabe, Y., 1987. Metabolic rates and elemental composition of the Antarctic krill *Euphausia superba* Dana. Polar Biology 7, 379-382.

Jacobs, S.S., 1991. On the nature and significance of the Antarctic Slope Front. Marine Chemistry 35, 9-24.

Joyce, T.M., Patterson, S.L., 1977. Cyclonic ring formation in the Polar Front in the Drake Passage. Nature 265, 131-133.

Joyce, T.M., Patterson, S.L., Millard, Jr, R.C., 1981. Anatomy of a Cyclonic Ring in the Drake Passage. Deep-Sea Research 26(11A), 1265-1287.

Kalany, E., Kanamitsu, M., Kistler, R., Collins, W., Deaven, D., Gandin, L., Iredell, M., Saha, S., White, G., Woollen, J., Zhu, Y., Chelliah, M., Ebisuzaki, W., Higgins, W., Janowiak, J., Mo, K.C., Ropelewski, C., Wang, J., Leetmaa, A., Reynolds, R., Jenne, R., Joseph, D., 1996. The NCEP/NCAR 40-year reanalysis project. Bulletin of the American Meteorological Society 77(3), 437-471.

Kalinowski, J., Witek, Z., 1980. Diurnal vertical distribution of krill aggregations in the West Antarctic. Polish Polar Research 1, 127-146.

Kalinowski, J., Godlewska, M., Klusek, A., 1985. Distribution and stock of krill in the Bransfield Strait and the Drake Passage during December 1983–1984, BIOMASS - SIBEX. Polish Polar Research 6, 151-158.

Kato, M., Segawa, S., Tanoue, E., Murano, M., 1982. Filtering and ingestion rates of the Antarctic krill *Euphausia superba* Dana. Transactions of the Tokyo University of Fisheries 5, 167-175.

Kawaguchi, K., Matsuda, O., Ishikawa, S., Naito, Y., 1986. The overwintering strategy of Antarctic krill (*Euphausia superba*) under the coastal fast ice off the Ongul Island in Lutzow-Holm Bay, Antarctica. Memoirs of the National Institute of Polar Research, Tokyo (Special Issue) 44, 67-85.

Kemp, S., Bennet, A.G., 1932. On the distribution and movements of whales on the South Georgia and South Shetland whaling grounds. Discovery Report 6, 165-190.

Kennedy, H., Robertson, J., 1995. Variations in the isotopic composition of particulate organic carbon in the surface waters along an 88°W transect from 67°S to 54°S. Deep-Sea Research II 42(4-5), 1109-1122.

Kils, U., 1982. Swimming behavior, swimming performance and energy balance of Antarctic krill *Euphausia superba*. In: El-Sayed, S.Z. (Ed.), BIOMASS Scientific Series No.3, Cambridge, England, pp. 122.

Klinck, J.M., 1985. EOF analysis of central Drake Passage currents from DRAKE79. Journal of Physical Oceanography, 15, 288-298.

Klinck, J.M., Smith, D.A., 1993. Effect of wind changes during the last glacial maximum on the circulation in the Southern Ocean. Paleoceanography 8(4), 427-433.

Knox, G.A., 1970. Antarctic marine ecosystems. In: Laws, R.M. (Ed.), Antarctic Ecology, Volume 2, Academic Press, London, pp. 69-109.

Kock, K.-H., Wilhelms, S., Everson, I., Gröger, J., 1994. Variations in the diet composition and feeding intensity of mackerel icefish *Champsocephalus gunnari* at South Georgia (Antarctic). Marine Ecology Progress Series 108, 43-57.

Large, W.G., McWilliams, J.C., Doney, S.C., 1994. An oceanic vertical mixing scheme with a k-profile boundary layer parameterization. Technical Report NCAR 070/93 11, Boulder, Colorado.

Lascara, C.M., 1996. Seasonal and mesoscale variability in the distribution of Antarctic krill, *Euphausia superba*, west of the Antarctic Peninsula. Ph.D. thesis, Old Dominion University, pp. 167.

Lascara, C.M., Hofmann, E.E., Ross, R.M., Quetin, L.B., 1999. Seasonal variability in the distribution of Antarctic krill, *Euphausia superba*, west of the Antarctic Peninsula. Deep-Sea Research 46, 951-984.

Levitus, S., Boyer, T.P., 1994. World Ocean Atlas 1994. Volume 4: Temperature. NOAA Atlas NESDIS 4, U.S. Government Printing Office, Washington, D.C., pp. 117.

Levitus, S., Burgett, R., Boyer, T.B., 1994. World Ocean Atlas 1994. Volume 3: Salinity. NOAA Atlas NESDIS 3, U.S. Government Printing Office, Washington, D.C., pp. 99.

Loeb, V., Siegel, V., Holm-Hansen, O., Hewitt, R., Fraser, W., Trivelpiece, W., Trivelpiece, S., 1997. Effects of sea ice extent and krill or salp dominance on the Antarctic food web. Nature 387, 897-900.

Lozano, C.J., Haley, P., Arango, H., Sloan, Q., Robinson, A.R., 1994. Harvard Coastal/Deep Water Primitive Equation Model. Harvard Ocean Model Reports 52, Reports in Meteorology and Oceanography, Harvard University, Cambridge MA, pp. 1-15.

Lubimova, T.G., Makarov, R.R., Maslenikov, V.V., Shevtsow, V.V., Shust, K.V., 1982. The ecological peculiarities, stocks and role of *Euphausia superba* in the trophic structure of the Antarctic Ecosystem. (Translation of a report originally published in Russian. Trudy, VNIRO, Moscow.) In: Selected Papers Presented to the Scientific Committee of CCAMLR, Hobart, pp. 391-505.

Lutjeharms, J.R.E., Baker, Jr., D.J., 1980. A statistical analysis of the mesoscale dynamics of the Southern Ocean. Deep Sea Research Part A 27, 145-159.

Mackintosh, N.A., 1946. The Antarctic Convergence and the distribution of surface temperatures in Antarctic waters. Discovery Reports 23, 177-212.

Mackintosh, N.A., 1972. Life cycle of Antarctic krill in relation to ice and water conditions. Discovery Reports 36, pp. 94.

Mackintosh, N.A., 1973. Distribution of post-larval krill in the Antarctic. Discovery Reports 36, 95-106.

Madec, G, Delecluse, P., Imbard, M., Levy, C., 1998. OPA8.1 General circulation Model reference manual, Notes de l'IPSL 11, University Pierre et Marie Curie,

Paris, pp. 99.

Makaraov, R.R., 1973. Some peculiarities of reproduction of *Euphausia superba* Dana. In: All Union Conference on Macroplankton (abstract of papers). VNIRO, Moscow, 34-35.

Marchesiello, P., Barnier, B., de Miranda, A.P.,1998. A sigma-coordinate primitive equation model for studying the circulation in the South Atlantic. Part II: Meridional transports and seasonal variability. Deep Sea Research I 45, 573-608.

Marr, J.W.S., 1962. The natural history and geography of the Antarctic krill *Euphausia superba* Dana. Discovery Reports 32, pp. 37-465.

Marra, J., Houghton, R.W., Garside, C., 1990. Phytoplankton growth at the shelf-break front in the Middle Atlantic Bight. Journal of Marine Research 48, 851-868.

Marschall, H.-P., 1988. The overwintering strategy of the Antarctic krill under the pack-ice of the Weddell Sea. Polar Biology 9, 129-135.

Maslennikov, V.V., Solyankin, E.V., 1988. Patterns of fluctuations in hydrological conditions of the Antarctic and their effect on the distribution of Antarctic krill. In: Sarhage, D., (Ed.) Antarctic Ocean and resources variability. Springer Verlag, Berlin, pp. 209-213.

Matano, R.P., Gordon, A.L., Muench, R.D., Palma, E.D., 2002. A numerical study of the circulation in the northwestern Weddell Sea. Deep-Sea Research II 49(21), 4827-4841.

Mayes, P.R., 1985. Secular variations in cyclone frequency near the Drake Passage, southwest Atlantic. Journal of Geophysical Research 90(D3), 5829-5839.

McClain, C.R., Koblinsky, C.J., Firestone, J., Darzi, M., Yeh, E., Beckley, B.D., 1991. Examining several Southern Ocean data sets. EOS Transactions of the American Geophysical Union 72(33) 345-351.

McQuinn, I.H., 1997. Metapopulations and the Atlantic herring. Reviews in Fish Biology and Fisheries 7, 297-329.

Men'shenia, L.L, Spiridonov, V.A., 1991. Duration of the larval development of Antarctic Euphausiids as indicated by field data. Oceanology 31(4), 451-456.

Meredith, M.P., Brandon, M.A., Trathan, P.N., Murphy, E.J., Bone, D.G., Grant, S.D., Chernyshkov, P.P., Sushin, V.A., submitted. Variability in oceanographic conditions to the east and northwest of South Georgia, 1996-2001. Deep Sea

Research I.

Messinger, F., 1982. On the convergence and error problems of the calculation of the pressure gradient force in a sigma coordinate model. Geophysical and Astrophysical Fluid Dynamics 19, 105-117.

Miller, D.G.M., Hampton, I., 1989a. Biology and Ecology of the Antarctic krill (*Euphausia superba* Dana): A review. In: BIOMASS Scientific Series No. 9, Scientific Committee Antarctic Research, Cambridge, England, pp. 166.

Miller, D.G.M., Hampton, I., 1989b. Krill aggregation characteristics: spatial distribution patterns from hydro-acoustic observations. Polar Biology 10, 125-134.

Mitchell, B.G., Holm-Hansen, O., 1991a. Bio-optical properties of Antarctic Peninsula waters: Differentiation from temperate ocean models. Deep-Sea Research 38(8/9), 1009-1028.

Mitchell, B.G., Holm-Hansen, O., 1991b. Observations and modeling of the Antarctic phytoplankton crop in relation to mixing depth. Deep-Sea Research 38(8/9), 981-1007.

Morris, D.J., 1984. Filtration of *Euphausia superba* Dana: under- or over-estimates? Journal of Crustacean Biology 4(Spec. No. 1), 185-197.

Morris, D.J., Keck, A., 1984. The time course of the moult cycle and growth of *Euphausia superba* in the laboratory. Meeresforschung 30, 94-100.

Moore, J.K., Abbott, M.R., 200. Phytoplankton chlorophyll distributions and primary production in the Southern Ocean. Journal of Geophysical Research 105, 27,825-27,833.

Moore, J.K., Abbott, M.R., Richman, J.G., 1999. Location and dynamics of the Antarctic Polar Front from satellite sea surface temperature data. Journal of Geophysical Research 104, 3059-3073.

Mullin, M.M., 1963. Some factors affecting the feeding of marine copepods of the genus *Calanus*. Limnology and Oceanography 8, 239-250.

Murphy, E.J., 1995. Spatial structure of the Southern Ocean ecosystem: predator-prey linkages in Southern Ocean food webs. Journal of Animal Ecology 64, 333-347.

Murphy, E.J., Reid, K., 2001. Modeling Southern Ocean krill population dynamics: biological processes generating fluctuations in the South Georgia ecosystem. Marine Ecology Progress Series 217, 175-189.

Murphy, E.J., Everson, I., Murray A.W.A., 1991. Analysis of acoustic line-transect

data from the waters around South Georgia: estimation of krill (*Euphausia superba* Dana) biomass. In: Selected scientific papers 1991 (SC-CCMALR-SSP/8). CCMALR, Hobart, Australia, pp. 219-224.

Murphy, E.J., Clarke, A., Symon, C., Priddle, J., 1995. Temporal variation in Antarctic sea-ice: analysis of a longterm fast-ice record from the South Orkney Islands. Deep-Sea Research I 42, 1045-1062.

Murphy, E.J., Trathan, P.N., Everson, I., Parkes, G., Daunt, F., 1997. Krill fishing in the Scotia Sea in relation to bathymetry, including the detailed distribution around South Georgia. CCAMLR Science 4, 1-17.

Murphy, E.J., Watkins, J.L., Reid, K., Trathan, P.N., Everson, I., Croxall, J.P., Priddle, J., Brandon, M.A., Brierley, A.S., Hofmann, E.E., 1998. Interannual variability of the South Georgia marine ecosystem: biological and physical sources of variation in the abundance of krill. Fisheries Oceanography 7(3/4), 381-390.

Nast, F., 1979. The vertical distribution of larval and adult krill (*Euphausia superba* Dana) on a time station south of Elephant Island, South Shetlands. Meeresforschung 27, 103-118.

Nicol, S., de la Mare, W., 1993. Ecosystem management and the Antarctic krill. American Scientist 81, 36-47.

Nicol, S., Stolp, M., Hosie, G.W., 1991. Accumulation of fluorescent age pigments in a laboratory population of Antarctic krill *Euphausia superba* Dana. Journal of Experimental Marine Biology and Ecology 146(2), 153-161.

Nicol, S., Stolp, M., Cochran, T., Geijsel, P., Marshall, J., 1992. Growth and shrinkage of Antarctic krill *Euphausia superba* from the Indian Ocean sector of the Southern Ocean during summer. Marine Ecology Progress Series 89, 175-181.

Niiler, P.P., Amos, A., Hu J.-H., 1991. Water masses and 200-m relative geostrophic circulation in the western Bransfield Strait region. Deep-Sea Research 38(8/9), 943-959.

NOAA, 1988. Digital relief of the Surface of the Earth, Data Announcement 88-MGG-02. National Geophysical Data Center, Boulder, Colorado.

Nöthig, E.-M., 1988. On the ecology of the phytoplankton in the southeastern Weddell Sea (Antarctica) in January/February 1985. Berichte zur Polarforschung 53, pp. 118.

Nordhausen, W., 1989. Winter abundance and distribution of *Euphausia superba, E. crystallorophias,* and *Thysanoessa macrura* in Gerlache Strait and Crystal Sound, Antarctica. Marine Ecology Progress Series 109, 131-142.

Nordhausen, W., Huntley, M., Lopez, M.D.G., 1992. RACER: Carnivory by *Euphausia superba* during the Antarctic winter, Antarctic Journal of the United States 27(5), 181-183.

Nowlin, Jr., W.D., Clifford, M., 1982. The kinematic and thermohaline zonation of the Antarctic Circumpolar Current at Drake Passage. Journal of Marine Science 40, 481-507.

Nowlin, Jr., W.D., Klinck, J.M., 1986. The physics of the Antarctic Circumpolar Current. Reviews of Geophysics 24(3), 469-491.

Nowlin, Jr., W.D., Zenk, W., 1988. Westward bottom currents along the margin of the South Shetland Island Arc. Deep-Sea Research 35(2), 269-301.

Nowlin, Jr., Whitworth, III, T., Pillsbury, R.D., 1977. Structure and transport of the Antarctic Circumpolar Current at Drake Passage from short-term measurements. Journal of Physical Oceanography 7(6), 788-802.

Orsi, A.H., Nowlin, Jr., W.D., Whitworth, III, T., 1993. On the circulation and stratification of the Weddell Gyre. Deep-Sea Research 40, 169-203.

Orsi, A.H., Whitworth, III, T., Nowlin, Jr., W.D., 1995. On the meridional extent and fronts of the Antarctic Circumpolar Current. Deep Sea Research 42, 641-673.

Pakhomov, E.A., Perissinotto, R., Froneman, P.W., Miller, D.G.M., 1997. Energetics and feeding dynamics of *Euphausia superba* in the South Georgia region during summer of 1994. Journal of Plankton Research 18, 399-423.

Patterson, S.L., 1985. Surface circulation and kinetic energy distributions in the Southern Hemisphere oceans from FGGE drifting buoys. Journal of Physical Oceanography 15(7), 865-884.

Pavlov, V.Y., 1969. The feeding of krill and some features of its behavior. Trudy VNIRO 66, 207-222. (MAFF Translation No. NS94).

Pedlosky, J., 1987. Geophysical Fluid Dynamics, 2nd ed., Springer Verlag, New York. pp. 710.

Penduff, T., Barnier, B., Béranger, K., Verron, J., 2001. Comparison of near-surface mean and eddy flows from two numerical models of the South Atlantic Ocean. Journal of Geophysical Research 106, 16,857-16,867.

Peterson, R.G., 1988. On the transport of the Antarctic Circumpolar Current through Drake Passage and its relation to wind. Journal of Geophysical Research 93, 13,993-14,004.

Peterson, R.G., Nowlin, Jr., W.D., Whitworth, III, T., 1982. Generation and evolution of a cyclonic ring at Drake Passage in early 1979. Journal of Geophysical Research 12(7), 712-719.

Perissinotto, R., Duncombe Rae, C.M., 1990. Occurrence of anticyclonic eddies on the Prince Edward Plateau (Southern Ocean): Effects on phytoplankton biomass and production. Deep-Sea Research 37(5), 777-793.

Pillsbury, R.D., Bottero, J.S., 1984. Observations of current rings in the Antarctic Zone at Drake Passage. Journal of Marine Research 42, 853-874.

Pingree, R.D., Mardell, G.T., 1981. Slope turbulence, internal waves and phytoplankton growth at the Celtic shelf-break. Philosophical Transactions of the Royal Society of London A302, 663-682.

Poleck, T.P., Denys, C.J., 1982. Effect of temperature on the moulting, growth and maturation of the Antarctic krill *Euphausia superba* (Crustacea: Euphausiacea) under laboratory conditions. Marine Biology 70, 255-265.

Priddle, J., Brandini, F., Lipski, M., Thorley, M.R., 1994. Pattern and variability of phytoplankton biomass in the Antarctic Peninsula region: an assessment of the BIOMASS cruises. In: El-Sayed, S.Z. (Ed.) Southern Ocean Ecology: the BIOMASS perspective. Cambridge University Press, Cambridge, pp. 49-61.

Priddle, J., Croxall, J.P., Everson, I., Heywood, R.B., Murphy, E.J., Prince, P.A., Sear, C.B., 1988. Large-scale fluctuations in distribution and abundance of krill - a discussion of possible causes. In: Sahrhage, D. (Ed.) Antarctic Ocean and resources variability. Springer Verlag, Berlin, pp. 169-181.

Quetin, L.B., Ross, R.M., 1985. Feeding by Antarctic krill *Euphausia superba*: does size matter? In: Siegfried, W.R., Condy, P.R., Laws, R.M. (Eds.) Antarctic nutrient cycles and food webs. Springer Verlag, Berlin, pp. 372-377.

Quetin, L.B., Ross, R.M., 1989. Effects of oxygen, temperature and age on the metabolic rate of the embryos and early larval stages of the Antarctic krill *Euphausia superba* Dana. Journal of Experimental Marine Ecology 125, 43-62.

Quetin, L.B., Ross, R.M., 1991. Behavioral and physiological characteristics of the Antarctic krill, *Euphausia superba*. American Zoology 31, 49-63.

Quetin, L.B., Ross, R.M., Clarke, A., 1994. Krill energetics: seasonal and envi-

ronmental aspects of the physiology of *Euphausia superba*. In: El-Sayed, S.Z. (Ed.) Southern Ocean ecology: the BIOMASS perspective. Cambridge University Press, Cambridge, pp. 165-184.

Reid, K., Barlow, K.E., Croxall, J.P., Taylor, R.I., 1999a. Predicting changes in the Antarctic krill, *Euphausia superba*, population at South Georgia. Marine Biology 135, 647-652.

Reid, K., Watkins, J.L., Croxall, J.P., Murphy, J.M., 1999b. Krill population dynamics at South Georgia 1991-1997 based on data from predators and nets. Marine Ecology Progress Series 177, 103-144.

Reid, K., Trathan, P.N., Croxall, J.P., Hill, H.J., 1996. Krill caught by predators and nets: differences between species and techniques. Marine Ecology Progress Series 140, 13-20.

Reid, K., Watkins, J.L., Croxall, J.P., Murphy, E.J., 1999. Krill population dynamics at South Georgia 1991-1997, based on data from predators and nets. Marine Ecology Progress Series 177, 103-114.

Richards, P.A., Tickell W.L.N., 1968. Comparison between the weather at Bird Island and Kind Edward Point, South Georgia. British Antarctic Survey Bulletin 15, 63-69.

Röther, W., Schlitzer, R., Putzka, A., Beining, P., Bulsiewicz, K., 1993. A chlorofluoromethane and hydrographic section across Drake Passage: deep water ventilation and meridional property transport. Journal of Geophysical Research 98, 14,423-14,435.

Rosenberg, A.A., Beddington, J.R., Basson, M., 1986. Growth and longevity of krill during the first decade of pelagic whaling. Nature 324, 152-154.

Ross, R.M., Quetin, L.B., 1983. Spawning frequency and fecundity of the Antarctic krill, *Euphausia superba*. Marine Biology 77, 201-205.

Ross, R.M., Quetin, L.B., 1986. How productive are Antarctic krill? Bioscience 36(4), 264-269.

Ross, R.M., Quetin, L.B., Baker, K.S., Vernet, M., Smith, R.C., 2000. Growth limitation in young *Euphausia superba* under field conditions. Limnology and Oceanography 45(1), 31-43.

Sahrhage, D., 1988. Antarctic Ocean and resources variability. Springer-Verlag, Berlin, pp. 304.

Scharek, R., 1991. Development of phytoplankton during the late-winter/spring

transition in the eastern Weddell Sea (Antarctica). Berichte zur Polarforschung 94, pp. 195.

Schnack, S.B., 1985. Feeding by *Euphausia superba* and copepod species in response to varying concentrations of phytoplankton. In: Siegfried, W.R., Condy, P.R., Laws, R.M. (Eds.) Antarctic nutrient cycles and food webs. Springer Verlag, Berlin, pp. 311-323.

Schnack-Schiel, S.B., Mujica, A., 1994. The zooplankton of the Antarctic Peninsula region. In: El-Sayed, S.Z. (Ed.) Southern Ocean ecology: the BIOMASS perspective. Cambridge University Press, Cambridge, pp. 79-92.

Sciremammano, Jr., F., Pillsbury, R.D., Nowlin, Jr., W.D., Whitworth, III, T., 1980. Spatial scales of temperature and flow in the Drake Passage. Journal of Geophysical Research 85, 4015-4028.

Semtner, A.J., 1974. An oceanic general circulation model with bottom topography. Technical report 9, UCLA Department of Meteorology, pp. 1-99.

Shapiro, R., 1971. The use of linear filtering as a parameterization of Atmospheric Diffusion. Journal of Atmospheric Sciences 28, 523-531.

Shin, H.-C., Nicol, S., 2002. Using the relationship between eye diameter and body length to detect the effects of long-term starvation on Antarctic krill *Euphausia superba*. Marine Ecology Progress Series 239, 157-167.

Shum, C.K., Wender, R.A., Sandwell, D.T., Zhang, B.H., Nerem, R.S., Tapley, B.D., 1990. Variations of global mesoscale eddy energy observed from GEOSAT. Journal of Geophysical Research 95, 17,865-17,876.

Siegel, V., 1985. The distribution pattern of krill, *Euphausia superba* west of the Antarctic Peninsula in February 1982. Meeresforschung 30, 292-305.

Siegel, V., 1986. Structure and composition of the Antarctic krill stock in the Bransfield Strait (Antarctic Peninsula) during the Second International BIOMASS Experiment (SIBEX). Archiev für Fischereiwissenschaft 37(1), 51-72.

Siegel, V., 1987. Age and growth of Antarctic Euphausiacemetha (Crustacea) under natural conditions. Marine Biology 96, 483-495.

Siegel, V., 1988. A concept of seasonal variation of krill (*Euphausia superba*) distribution and abundance west of the Antarctic Peninsula. In: Sahrhage, D. (Ed.) Antarctic Ocean and resources variability. Springer Verlag, Berlin, pp. 219-230.

Siegel, V., 1989. Winter and spring distribution and status of the krill stock in

Antarctic Peninsula waters. Archiev für Fischereiwissenschaft 39(1), 45-72.

Siegel, V., 1992. Assessment of the krill (*Euphausia superba*) spawning stock off the Antarctic Peninsula. Archiev für Fischereiwissenschaft 41(2), 101-130.

Siegel, V., Kalinowski, J., 1994. Krill demography and small-scale processes: a review, In: El-Sayed, S.Z. (Ed.) Southern Ocean ecology, the BIOMASS perspective. Cambridge University Press, Cambridge, pp. 145-163.

Siegel, V., Loeb, V., 1994. Length and age at maturity of Antarctic krill. Antarctic Science 6 (4), 479-482.

Siegel, V., Loeb, V., 1995. Recruitment of Antarctic krill *Euphausia superba* and possible causes for its variability. Marine Ecology Progress Series 123, 45-56.

Siegel, V., Bergström, B., Mühlenhardt-Siegel, U., Thomasson, M., 2002. Demography of krill in the Elephant Island area during summer 2001 and its significance for stock recruitment. Antarctic Science 14(2), 162-170.

Sievers, H.A., Nowlin, Jr., W.D., 1984. The stratification and water masses at Drake Passage, Journal of Geophysical Research 89, 10489-10514.

Simmons, A.J., Burridge, D.M., 1981. An energy and angular momentum conserving finite difference scheme and hybrid vertical coordinates. Monthly Weather Review 109, 758-766.

Smetacek, V., Scharek, R., Gordon, L.I., Eicken, H., Fahrbach, G., Rohardt, G., Moore, S., 1992. Early spring phytoplankton blooms in ice platelet layers of the southern Weddell Sea, Antarctica. Deep-Sea Research 38, 153-168.

Smith, R.C., 1981. Remote sensing and depth distribution of ocean chlorophyll. Marine Ecology Progress Series 5(3), 359-361.

Smith, R. D., Dukowicz, J. K., Malone, R. C., 1992. Parallel Ocean General Circulation Modeling, Physica D, 60, 38-61.

Smith, R.C., Dierssen, H.M., Vernet, M., 1996. Phytoplankton biomass and productivity in the western Antarctic Peninsula region. In: Quetin, L.B., Hofmann, E.E., Ross, R.M. (Eds.) Foundations for ecological research west of the Antarctic Peninsula. American Geophysical Union, Washington D.C., pp. 333-356.

Smith, R.C., Baker, K., Fraser, W., Hofmann, E.E., Karl, D., Klinck, J.M., Quetin, L., Prézlin, B., Ross, R., Trivelpiece, W., Vernet, M., 1995. The Palmer LTER: A Long-Term Ecological Research Program at Palmer Station Antarctica. Oceanography 8, 77-86.

Smith, S.L., Schnack-Schiel, S.B., 1990. Polar Zooplankton, In: Smith, W.O. (Ed.),

Polar Oceanography Part B Chemistry, Biology, and Geology. Academic Press, San Diego, pp. 527-599.

Smith, W.O., Nelson, D.M., 1985. Phytoplankton bloom produced by a receding ice edge in the Ross Sea: spatial coherence with the density field. Science 227, 163-166.

Smith, W.O., Nelson, D.M., 1986. Importance of ice edge phytoplankton production in the Southern Ocean. Bioscience 36(4), 251-257.

Smith, W.O., Sakshaug, E., 1990. Polar Phytoplankton, In: Smith, W.O. (Ed.), Polar Oceanography Part B Chemistry, Biology, and Geology. Academic Press, San Diego, pp. 477-525.

Smith, W.O., Nelson, D.M., DiTillio, G.R., Leventer, A.R., 1996. Temporal and spatial patterns in the Ross Sea: Phytoplankton biomass, elemental composition, productivity and growth rates. Journal of Geophysical Research 101, 18,455-18,465.

Spall, M.A., 1988. Regional Ocean Modeling: Primitive Equation and Quasi-geostrophic Studies. Harvard Open Ocean Model Reports 28, Reports in Meteorology and Oceanography, Harvard University, Cambridge, MA, pp. 282.

Spall, M.A., Robinson, A.R., 1989. A new open ocean, hybrid coordinate primitive equation model. Mathematics and computers in simulation 31, 241-269.

Spiridonov, V.A., 1995. Spatial and temporal variability in reproductive timing of Antarctic krill (*Euphausia superba* Dana). Polar Biology 15(3), 161-174.

Stammer, D., Davis, R., Fu, L.-L., Fukumori, I., Giering, R., Lee., T., Marotzke, J., Marshall, J., Menemenlis, D., Niiler, P., Wunsch C., Zlotnicki, V., 1999. The consortium for estimating the circulation and climate of the ocean (ECCO) - Science goals and task plan. The ECCO Report Series, Report No.1, November 1999.

Stein, M., 1992. Variability of local upwelling off the Antarctic Peninsula. Archiev für Fischereiwissenschaft 41, 131-158.

Stramma, L., 1989. The Brazil Current transport south of 23°S. Deep-Sea Research 36(4A), 639-646.

Sun, S., de la Mare, W., Nicol, S., 1995. The compound eye as an indicator of age and shrinkage of Antarctic krill. Antarctic Science 7, 387-392.

Sun, S., 1997. Using Antarctic krill as an indicator of environmental interannual change. Korean Journal of Polar Research 8, 97-103.

Sullivan, C.W., Arrigo, K.R., McClain, C.R., Comiso, J.C., Firestone, J., 1993. Distributions of phytoplankton blooms in the Southern Ocean. Science 262, 1832-1837.

Thorley, M.R., Trathan, P.N., 1994. BIOMASS data set documentation. British Antarctic Survey, Natural Environment Research Council, High Cross, Madingley Road, Cambridge, CB3 OET, UK, pp. 28.

Thorpe, S.E., Heywood, K.J., Brandon, M.A., Stevens, D.P., 2002. Variability of the southern Antarctic Circumpolar Current front north of South Georgia. Journal of Marine Systems 37, 87-105.

Timmermann, R., Hellmer, H.H., Beckmann, A., 2002a. Simulations of ice-ocean dynamics in the Weddell Sea 1. Model configuration and validation. Journal of Geophysical Research 107, 10-1 - 10-11.

Timmermann, R., Beckmann, A., Hellmer, H.H., 2002b. Simulations of ice-ocean dynamics in the Weddell Sea 2. Interannual variability 1985-1993. Journal of Geophysical Research 107,11-1 - 11-9.

Torres, J.J., Childress, J.J., 1983. Relationship of oxygen consumption to swimming speed in *Euphausia pacifica* 1. Effects of temperature and pressure. Marine Biology 74, 79-86.

Torres, J.J., Aarset, A.V., Donnelly, J., Hopkins, T.L., Lancraft, T., Ainley, D.G., 1994. Metabolism of Antarctic micronektonic Crustacea as a function of depth, occurrence and season. Marine Ecology Progress Series 113, 207-219.

Trathan, P.N., Brandon, M.A., Murphy, E.J., 1997. Characterization of the Antarctic Polar Frontal Zone to the north of South Georgia in summer 1994. Journal of Geophysical Research 102, 10,483-10,497.

Tréguier, A.-M., and others, 1999. The CLIPPER project: High resolution modeling of the Atlantic. International WOCE Newsletter 36, 3-5.

Tréguer, P., Jacques, G., 1992. Dynamics of nutrients and phytoplankton, and fluxes of carbon, nitrogen and silicon in the Antarctic Ocean. Polar Biology 12, 149-162.

Trenberth, K.E., Olson, J.G., Large, W.G., 1989. A global ocean wind stress climatology based on ECMWF analyses. Technical Report NCAR/TN-338+STR, National Center for Atmospheric Research, Boulder, Colorado, pp. 93.

U.S. Southern Ocean GLOBEC, 2003. Report of the RVIB *Nathaniel B. Palmer* Cruise NBP02-04 to the Western Antarctic Peninsula 31 July to 18 Septem-

ber 2002. United States Southern Ocean Global Ocean Ecosystems Dynamics Program, Report Number 8, pp. 266.

Wade, M.J., McCauley, D.E., 1988. Extinction and recolonization: their effects on genetic differentiation of local populations. Evolution 42, 995-1005.

Wadhams, P., 2000. Ice in the ocean. Gordon and Breach Science Publishers, Amsterdam, The Netherlands, pp. 351.

Wallcraft, A.J., 1991. The Navy Layered Ocean Model Users Guide, NOARL Report 35, Naval Research Laboratory, Stennis Space Center, MS, pp. 21.

Ward, P., Atkinson, A., Murray, A.W.A., Wood, A.G., Williams, R., Poulet, S.A., 1995. The summer zooplankton community at South Georgia: biomass, vertical migration and grazing. Polar Biology 15, 195-208.

Watkins, J.L., 1999. A composite recruitment index to describe interannual changes in the population structure of Antarctic krill at South Georgia. CCAMLR Science 6, 71-84.

Watkins, J.L., Murray, A.W.A., Daly, H.I., 1999. Variation in the distribution of Antarctic krill *Euphausia superba* around South Georgia. Marine Ecology Progress Series 188, 149-160.

Webb, D.J., de Cuevas, B.C., Coward, A.C., 1998. The first main run of the OCCAM Global Ocean Model. Southampton Oceanography Centre, Internal Document No. 34, Southampton Oceanography Centre, Empress Dock, Southampton SO14 3ZH, U.K., pp. 43.

Webb, D.J., Killworth, P.D., Coward, A.C., Thompson, S.R., 1991. The FRAM Atlas of the Southern Ocean. Natural Environmental Research Council, pp. 67.

White, W.B., Peterson, R.G., 1996. An Antarctic circumpolar wave in surface pressure, wind, temperature, and sea ice extent. Nature 380, 699-702.

Whitehouse, M.J., Priddle, J., Trathan, P.N., Brandon, M.A., 1996. Substantial open-ocean phytoplankton blooms to the north of South Georgia, South Atlantic, during summer 1994. Marine Ecology Progress Series 140(1-3), 187-197.

Whitworth, III, T., 1983. Monitoring the transport of the Antarctic Circumpolar Current at Drake Passage. Journal of Physical Oceanography 13, 2045-2057.

Whitworth, III, T., Peterson, R.G., 1985. The volume transport of the Antarctic Circumpolar Current from three-year bottom pressure measurements. Journal of Physical Oceanography 15(6), 810-816.

Whitworth, III, T., Nowlin, Jr, W.D., Worley, S.J., 1982. The net transport of the Antarctic Circumpolar Current through Drake Passage. Journal of Physical Oceanography 12, 960-971.

Whitworth, III, T., Nowlin, Jr, W.D., Orsi, A.H., Locarnini, R.A., Smith, S.G., 1994. Weddell Sea shelf water in the Bransfield Strait and Weddell Scotia Confluence. Deep-Sea Research 41, 629-641.

Witek, Z., Kalinowski, J., Grelowski, A., 1988. Formation of Antarctic krill concentrations in relation to hydrodynamic processes and social behavior. In: Sahrhage, D., (Ed.) Antarctic Ocean and resources variability. Springer Verlag, Berlin, pp. 237-244.

WOCE, 1996. Project Status 1996, Future Aims. WOCE Report No. 138/96, WOCE Report, Southampton Oceanographic Centre, Empress Dock, Southampton, SO14 3ZH, UK, pp. 80.

Wolff, J.-P., Maier-Reimer, E., Legutke, S., 1997. The Hamburg Ocean Primitive Equation Model HOPE. Technical Report No. 13, Deutsches Klimarechenzentrum, Hamburg, Germany, pp. 110.

Zwally, H.C., Parkinson, C.L., Carsey, F., Gloersen, P., Campbell, W.J., Ramseier, R.O., 1979. Antarctic sea ice variations 1973-1976, NASA Weather Climate Rev. Pap., 56, 335-340.

Zwally, H.C., Parkinson, C.L., Comiso, J.C., 1983. Variability of Antarctic sea ice and changes in carbon dioxide. Science 220, 1005-1012.

APPENDIX A

A1. CZCS-derived phytoplankton concentration along drifter trajectories

Figures A1 to A5 show the CZCS-derived range of phytoplankton concentrations extracted along trajectories of drifters originating in five regions: the west Antarctic Peninsula, Bransfield Strait, the Scotia Sea/Elephant Island area, the southwestern Antarctic Peninsula, and the Weddell Sea.

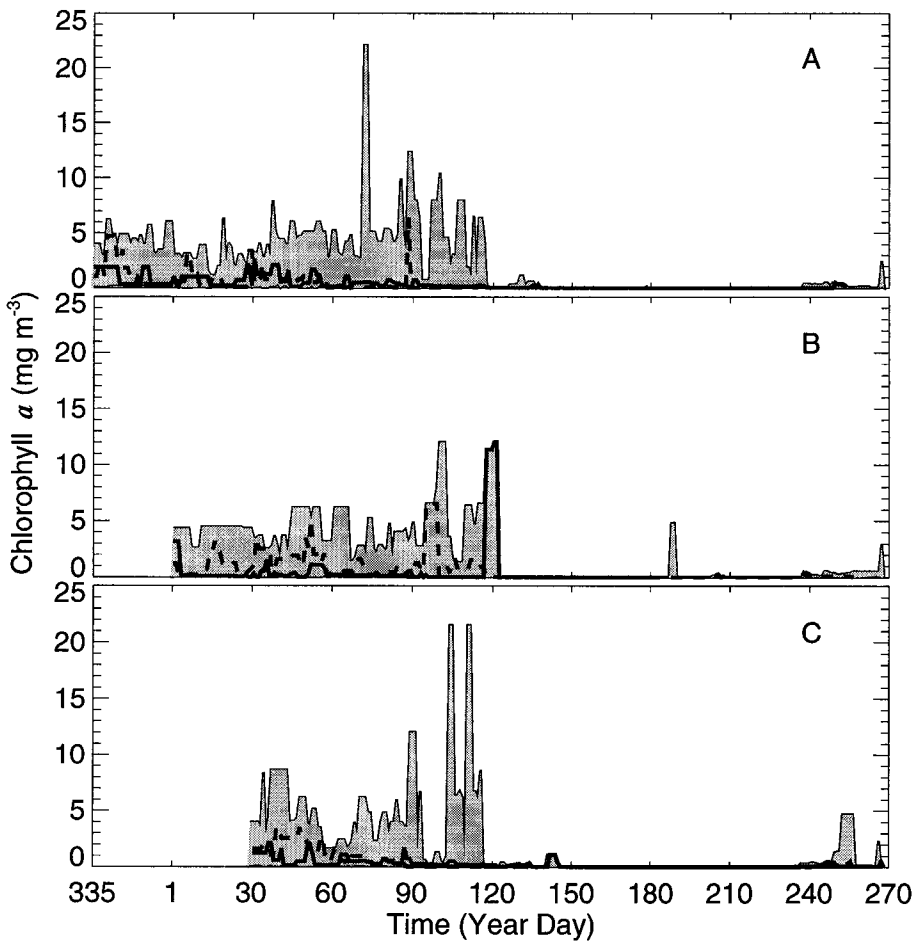

Fig. A1. Range of CZCS-derived time series of pigment concentration (mg m^{-3}) along trajectories of drifters originating at the west Antarctic Peninsula (region 1) starting in A) December (Year Day 335), B) January (Year Day 1), C) February (Year Day 32). The heavy solid line and dashed line indicate concentrations along two different particle trajectories within the range of concentrations, which is denoted by the grey shading.

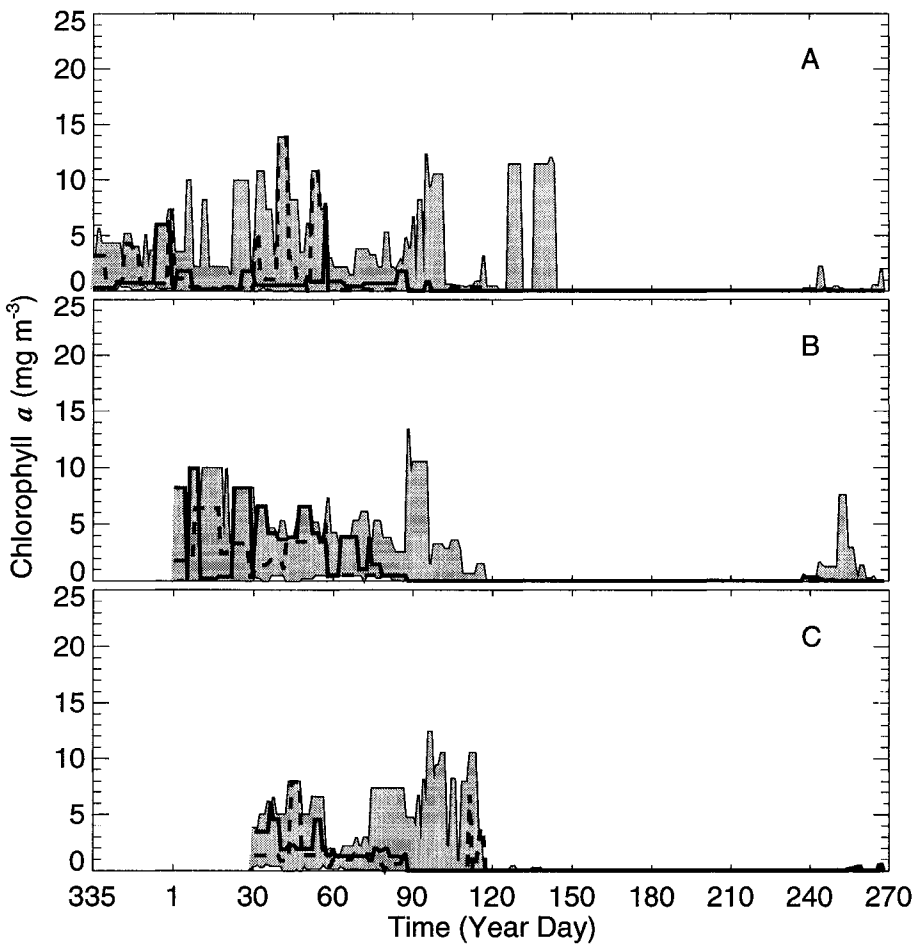

Fig. A2. Range of CZCS-derived time series of pigment concentration (mg m^{-3}) along trajectories of drifters originating in the Bransfield Strait area (region 2) starting in A) December (Year Day 335), B) January (Year Day 1), C) February (Year Day 32). The heavy solid line and dashed line indicate concentrations along two different particle trajectories within the range of concentrations, which is denoted by the grey shading.

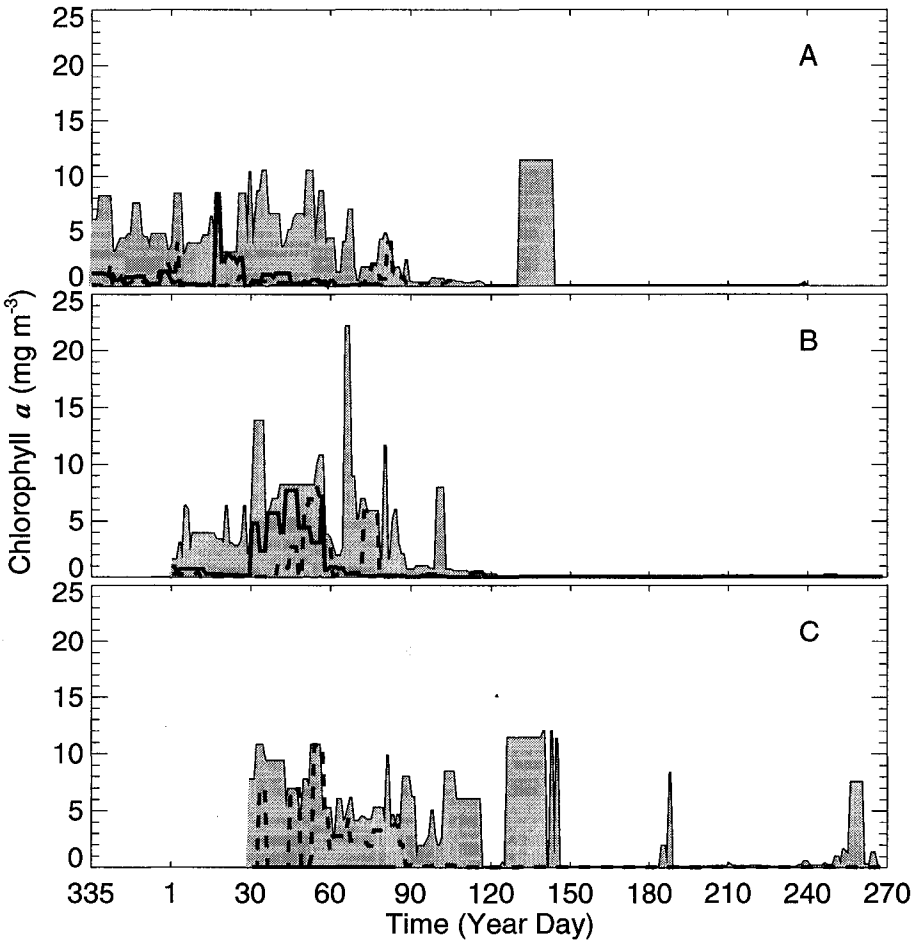

Fig. A3. Range of CZCS-derived time series of pigment concentration (mg m^{-3}) along trajectories of drifters originating in the Scotia Sea/Elephant Island area (region 3) starting in A) December (Year Day 335), B) January (Year Day 1), C) February (Year Day 32). The heavy solid line and dashed line indicate concentrations along two different particle trajectories within the range of concentrations, which is denoted by the grey shading.

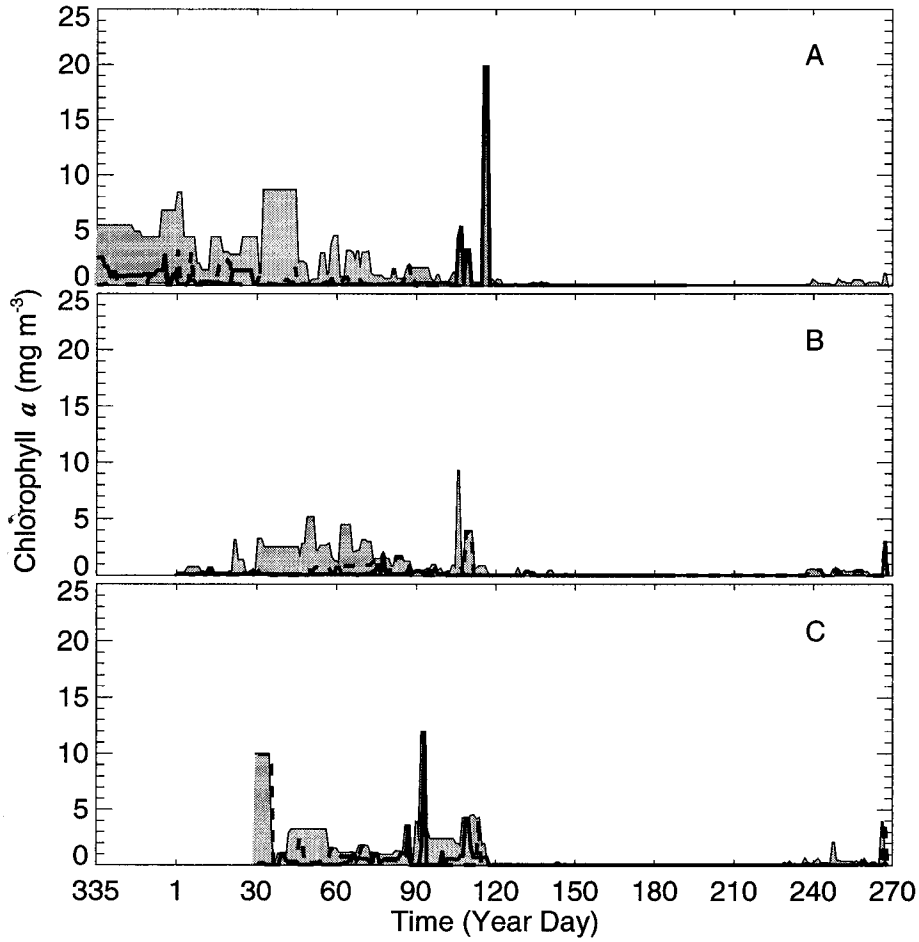

Fig. A4. Range of CZCS-derived time series of pigment concentration (mg m^{-3}) along trajectories of drifters originating in the southwestern Antarctic Peninsula area (region 4) starting in A) December (Year Day 335), B) January (Year Day 1), C) February (Year Day 32). The heavy solid line and dashed line indicate concentrations along two different particle trajectories within the range of concentrations, which is denoted by the grey shading.

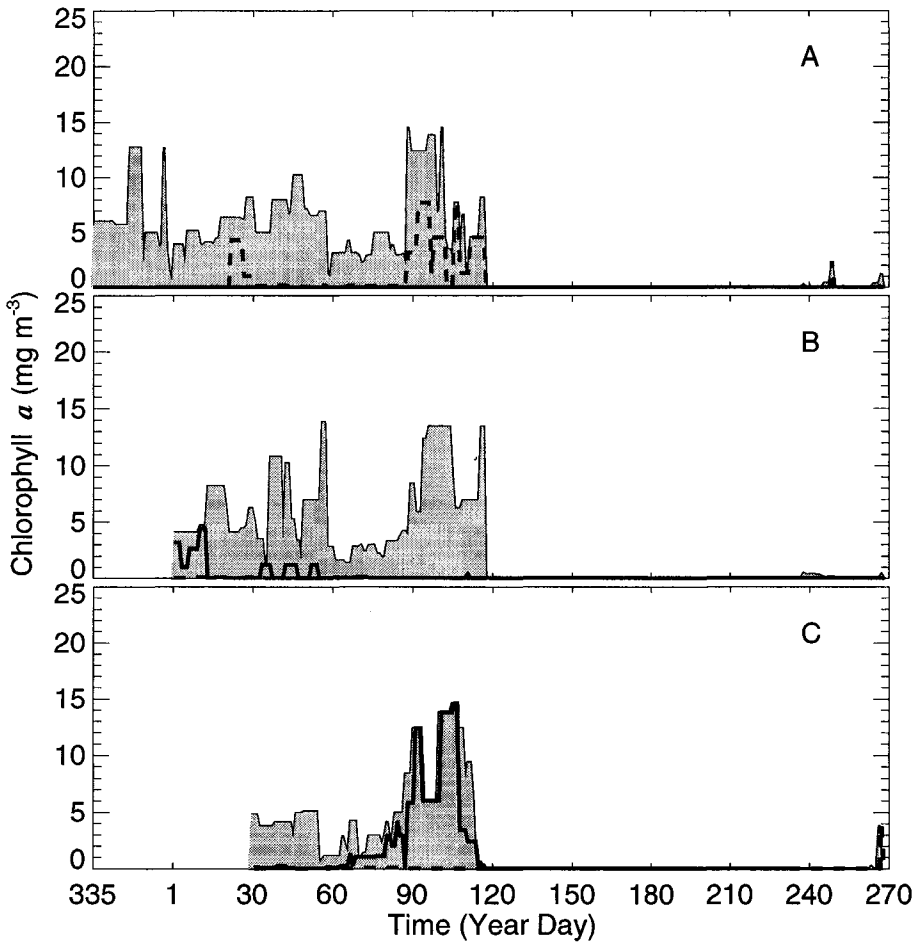

Fig. A5. Range of CZCS-derived time series of pigment concentration (mg m^{-3}) along trajectories of drifters originating in the Weddell Sea area (region 5) starting in A) December (Year Day 335), B) January (Year Day 1), C) February (Year Day 32). The heavy solid line and dashed line indicate concentrations along two different particle trajectories within the range of concentrations, which is denoted by the grey shading.

A2. SSM/I-derived sea ice algae concentration along drifter trajectories

Figures A6 to A10 show the SSM/I-derived range of sea-ice algae concentrations extracted along trajectories of drifters originating in five regions: the west Antarctic Peninsula, Bransfield Strait, the Scotia Sea/Elephant Island area, the southwestern Antarctic Peninsula, and the Weddell Sea.

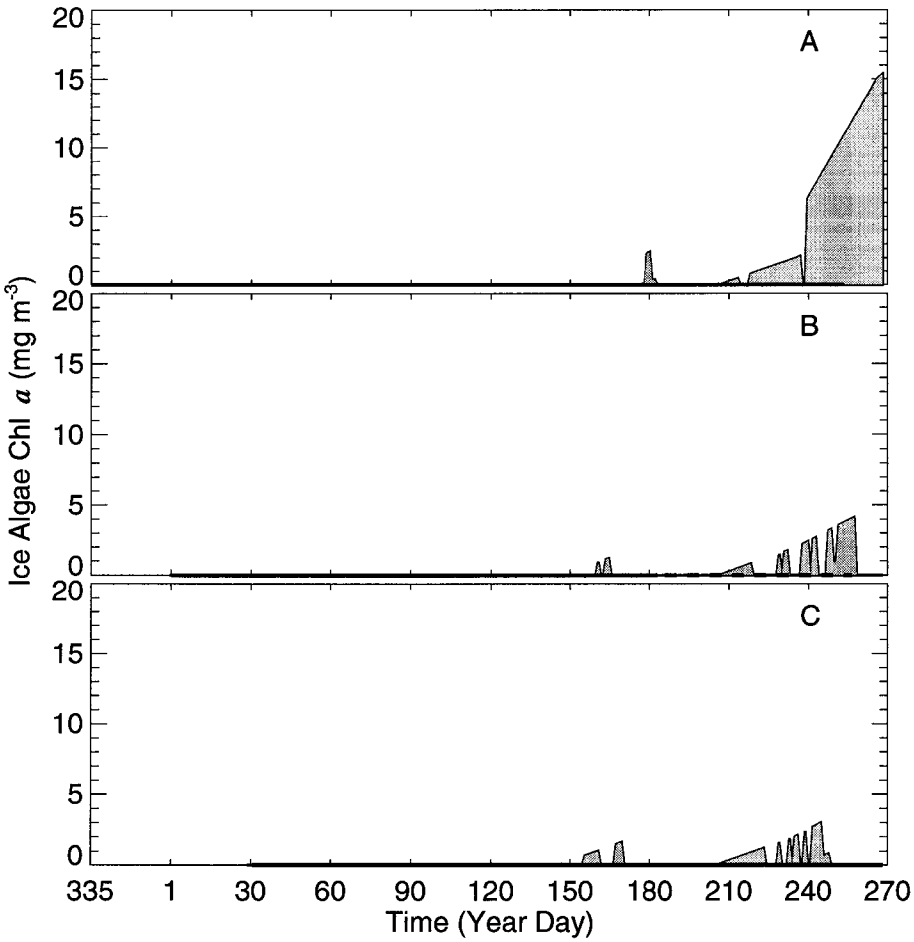

Fig. A6. Range of SSM/I-derived time series of sea ice algae concentration (mg m^{-3}) along trajectories of drifters originating at the west Antarctic Peninsula (region 1) starting in A) December (Year Day 335), B) January (Year Day 1), C) February (Year Day 32). The heavy solid line and dashed line indicate concentrations along two different particle trajectories within the range of concentrations, which is denoted by the grey shading.

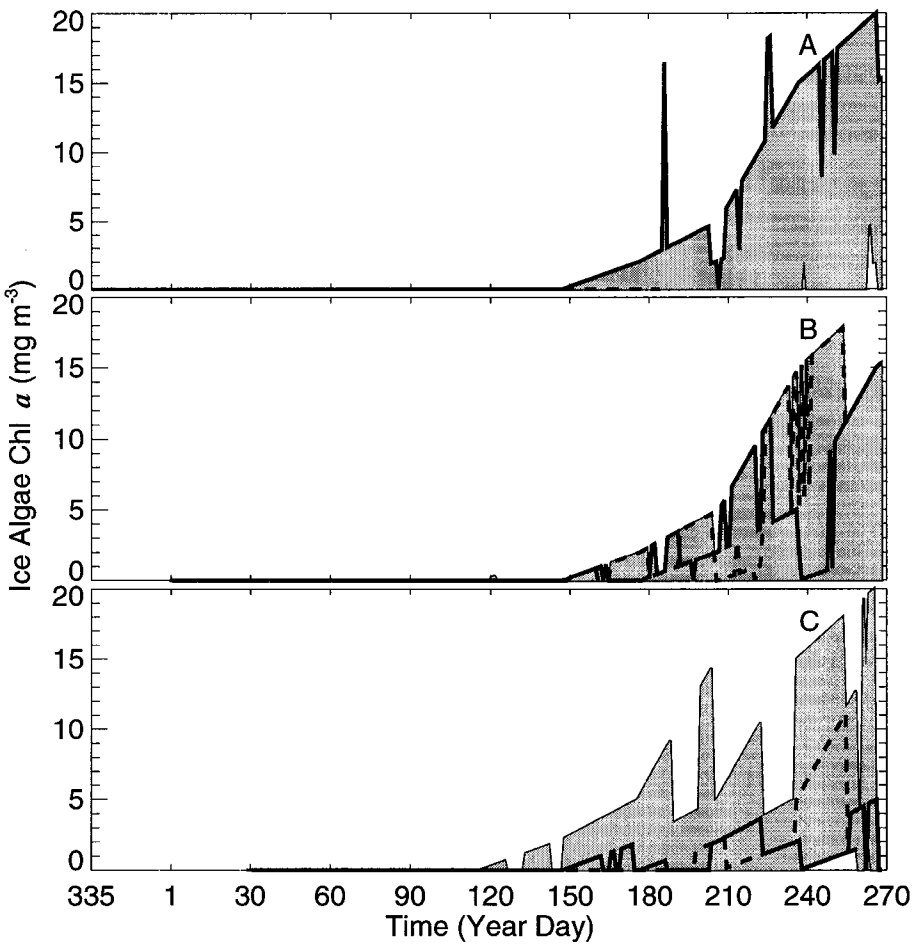

Fig. A7. Range of SSM/I-derived time series of sea ice algae concentration (mg m^{-3}) along trajectories of drifters originating in the Bransfield Strait area (region 2) starting in A) December (Year Day 335), B) January (Year Day 1), C) February (Year Day 32). The heavy solid line and dashed line indicate concentrations along two different particle trajectories within the range of concentrations, which is denoted by the grey shading.

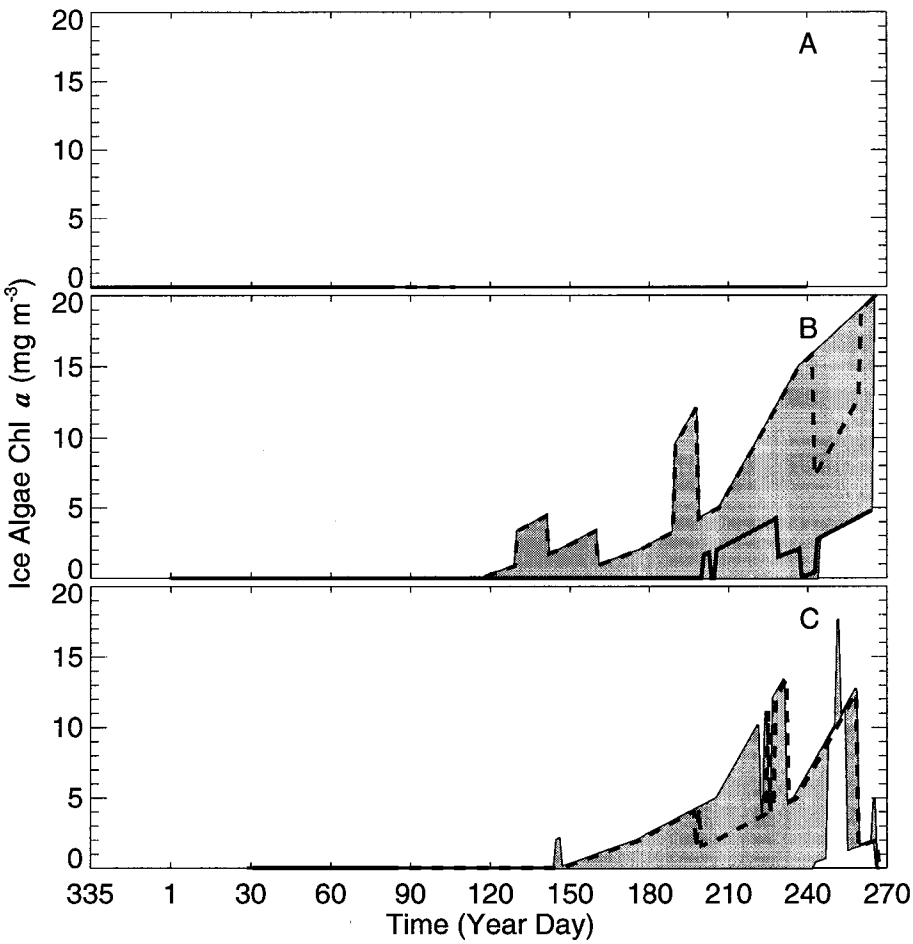

Fig. A8. Range of SSM/I-derived time series of sea ice algae concentration (mg m^{-3}) along trajectories of drifters originating in the Scotia Sea/Elephant Island area (region 3) starting in A) December (Year Day 335), B) January (Year Day 1), C) February (Year Day 32). The heavy solid line and dashed line indicate concentrations along two different particle trajectories within the range of concentrations, which is denoted by the grey shading.

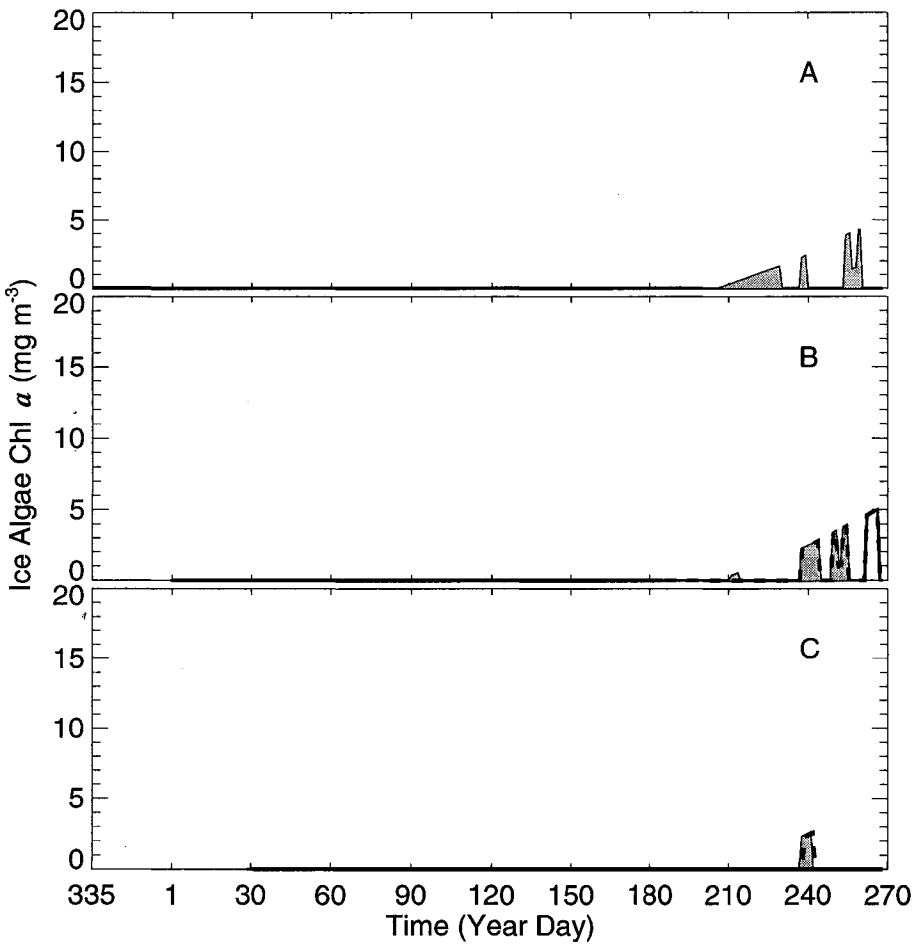

Fig. A9. Range of SSM/I-derived time series of sea ice algae concentration (mg m^{-3}) along trajectories of drifters originating in the southwestern Antarctic Peninsula area (region 4) starting in A) December (Year Day 335), B) January (Year Day 1), C) February (Year Day 32). The heavy solid line and dashed line indicate concentrations along two different particle trajectories within the range of concentrations, which is denoted by the grey shading.

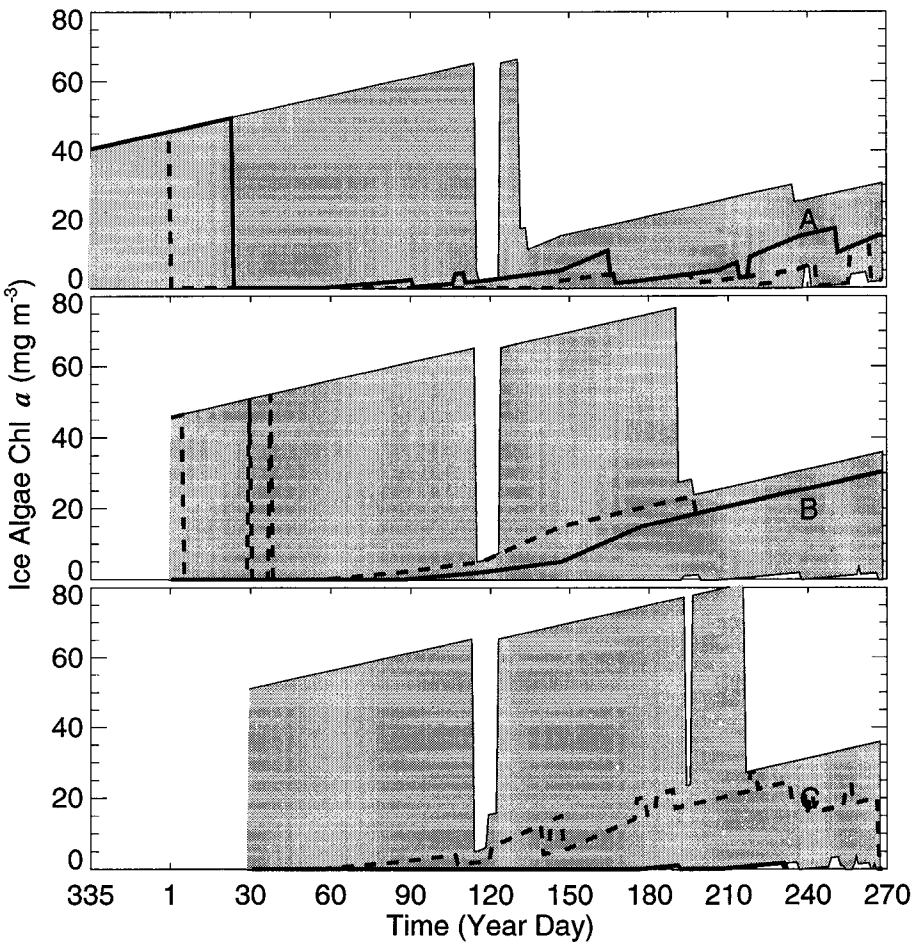

Fig. A10. Range of SSM/I-derived time series of sea ice algae concentration (mg m^{-3}) along trajectories of drifters originating in the Weddell Sea area (region 5) starting in A) December (Year Day 335), B) January (Year Day 1), C) February (Year Day 32). The heavy solid line and dashed line indicate concentrations along two different particle trajectories within the range of concentrations, which is denoted by the grey shading.

A3. Detritus concentration along drifter trajectories

Figures A11 to A15 show the CZCS chlorophyll data-derived range of sea-ice algae concentrations extracted along trajectories of drifters originating in five regions: the west Antarctic Peninsula, Bransfield Strait, the Scotia Sea/Elephant Island area, the southwestern Antarctic Peninsula, and the Weddell Sea.

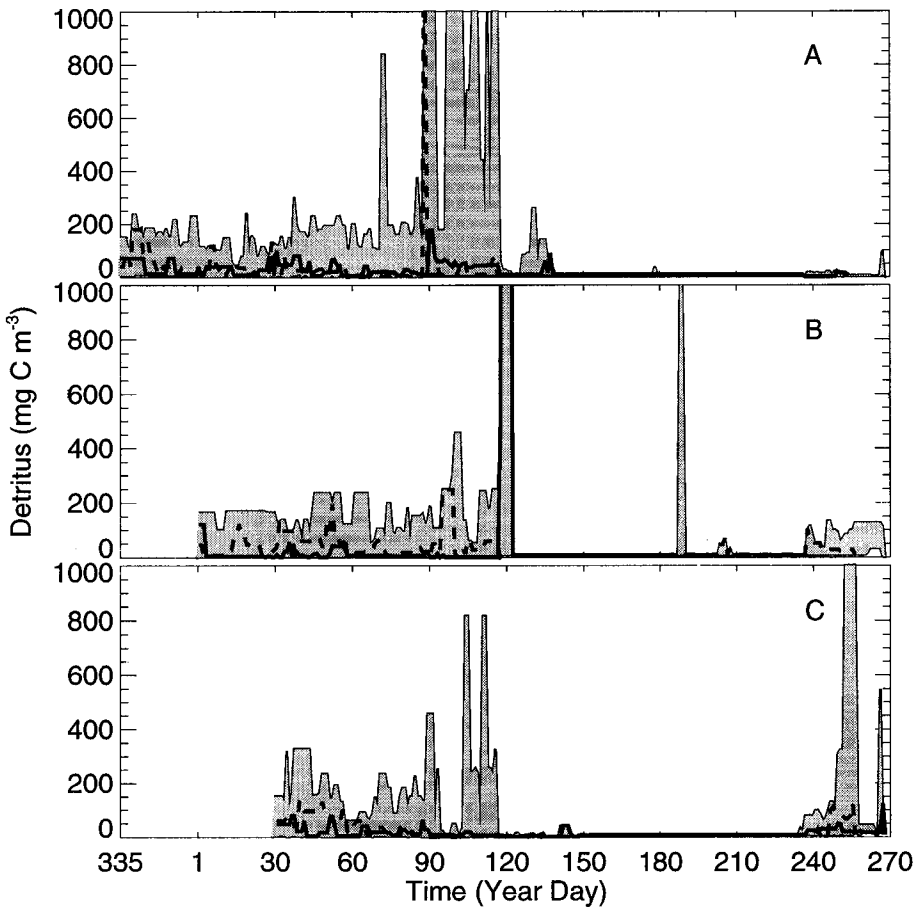

Fig. A11. Range of CZCS chlorophyll data-derived time series of detritus concentration (mg C m^{-3}) along trajectories of drifters originating at the west Antarctic Peninsula (region 1) starting in A) December (Year Day 335), B) January (Year Day 1), C) February (Year Day 32). The heavy solid line and dashed line indicate concentrations along two different particle trajectories within the range of concentrations, which is denoted by the grey shading.

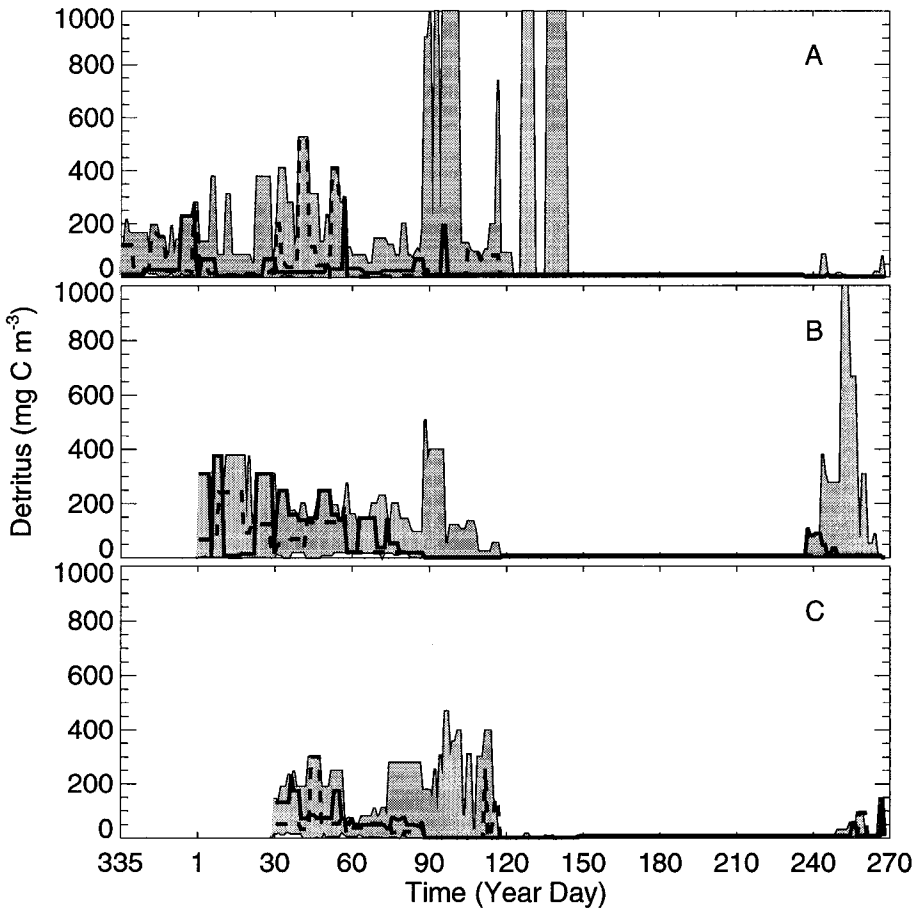

Fig. A12. Range of CZCS chlorophyll data-derived time series of detritus concentration (mg C m^{-3}) along trajectories of drifters originating in the Bransfield Strait area (region 2) starting in A) December (Year Day 335), B) January (Year Day 1), C) February (Year Day 32). The heavy solid line and dashed line indicate concentrations along two different particle trajectories within the range of concentrations, which is denoted by the grey shading.

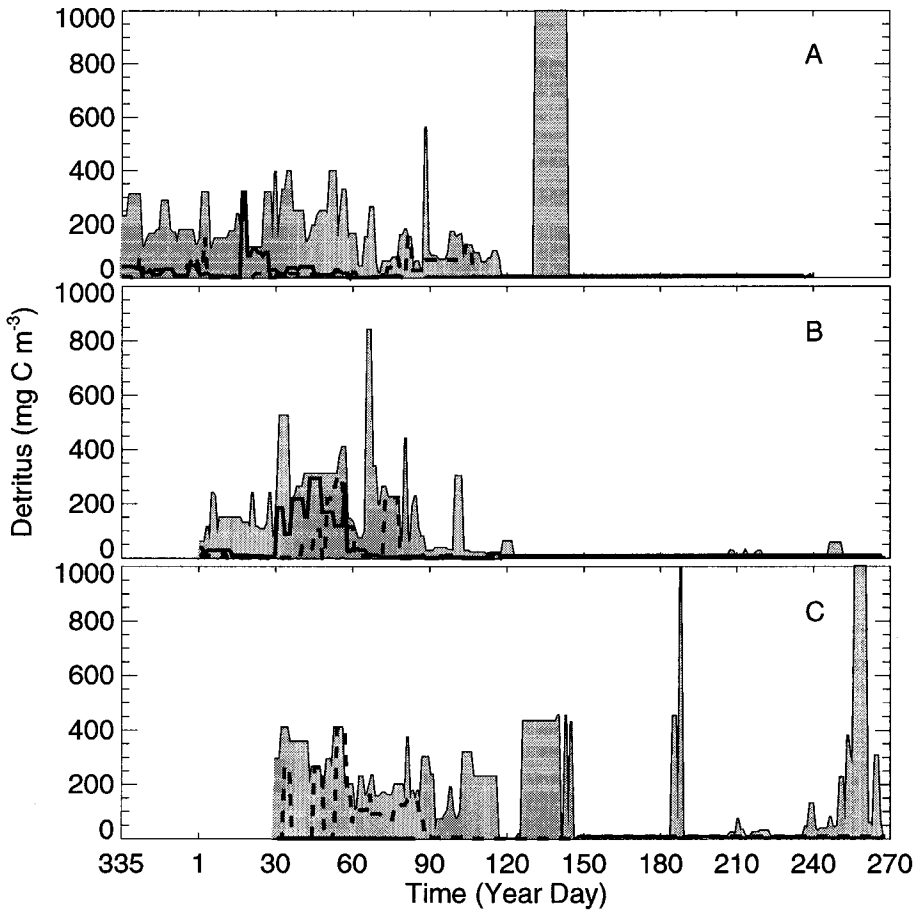

Fig. A13. Range of CZCS chlorophyll data-derived time series of detritus concentration (mg C m^{-3}) along trajectories of drifters originating in the Scotia Sea/Elephant Island area (region 3) starting in A) December (Year Day 335), B) January (Year Day 1), C) February (Year Day 32). The heavy solid line and dashed line indicate concentrations along two different particle trajectories within the range of concentrations, which is denoted by the grey shading.

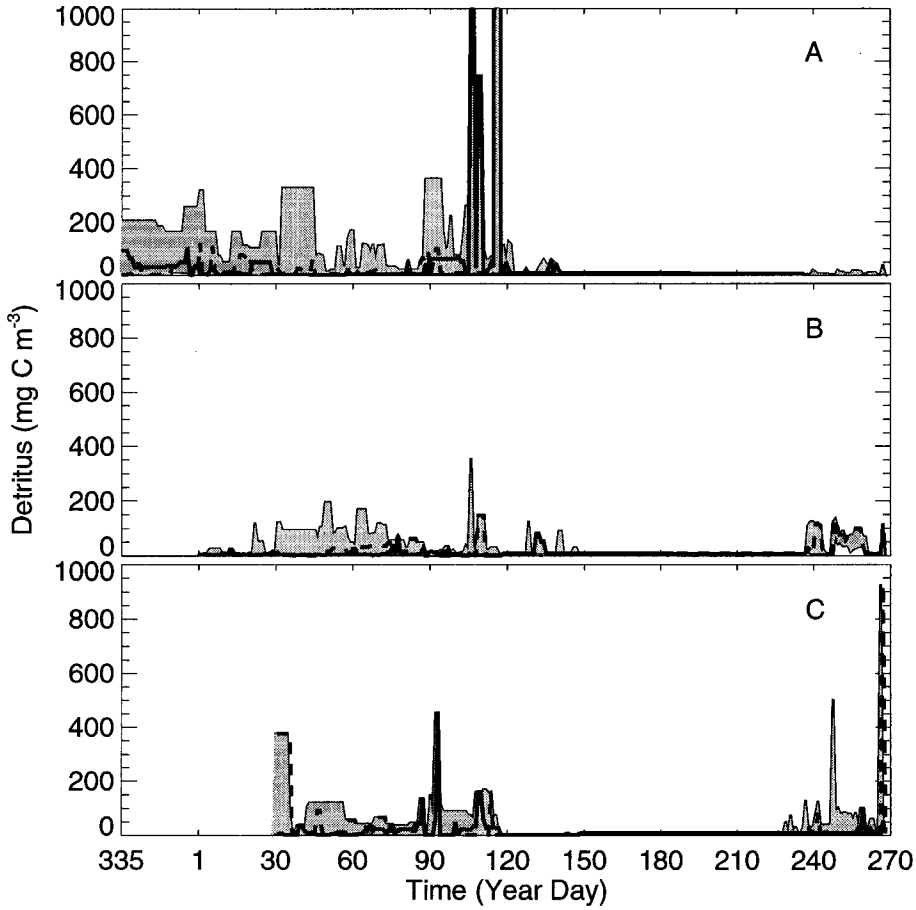

Fig. A14. Range of CZCS chlorophyll data-derived time series of detritus concentration (mg C m^{-3}) along trajectories of drifters originating in the southwestern Antarctic Peninsula area (region 4) starting in A) December (Year Day 335), B) January (Year Day 1), C) February (Year Day 32). The heavy solid line and dashed line indicate concentrations along two different particle trajectories within the range of concentrations, which is denoted by the grey shading.

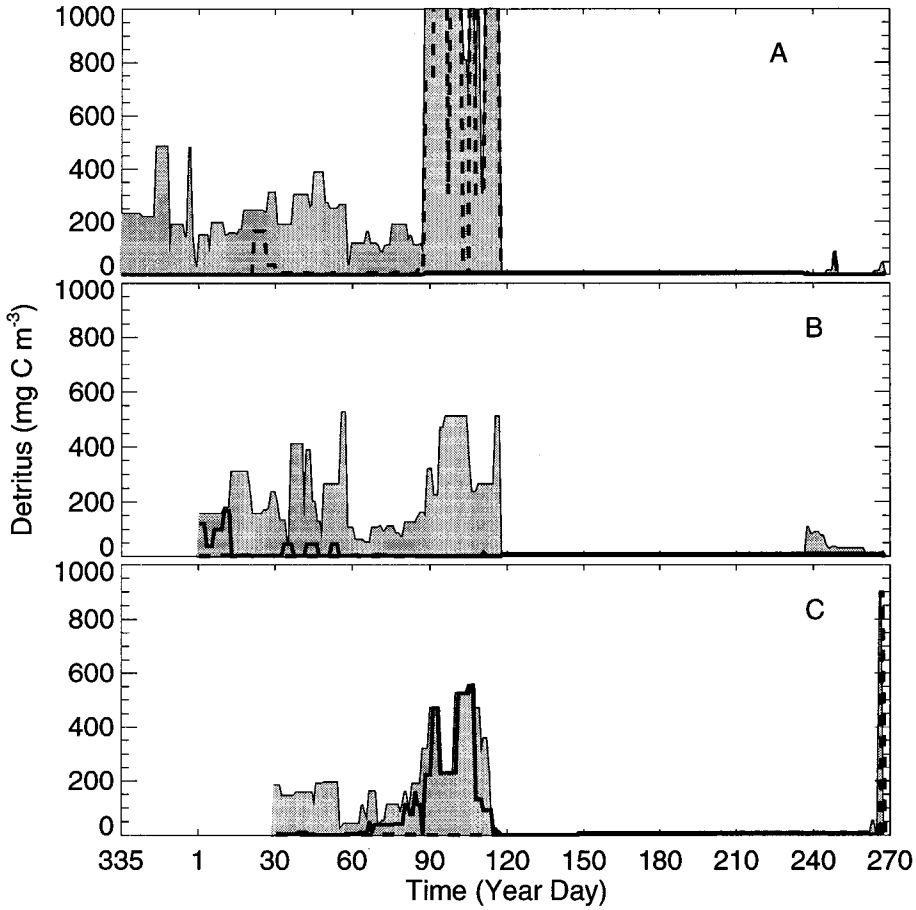

Fig. A15. Range of CZCS chlorophyll data-derived time series of detritus concentration (mg C m^{-3}) along trajectories of drifters originating in the Weddell Sea area (region 5) starting in A) December (Year Day 335), B) January (Year Day 1), C) February (Year Day 32). The heavy solid line and dashed line indicate concentrations along two different particle trajectories within the range of concentrations, which is denoted by the grey shading.

VITA

Bettina Andrea Fach
Center for Coastal Physical Oceanography
Department of Ocean, Earth, and Atmospheric Sciences
Old Dominion University
Norfolk, VA 23529

Education

Dipl-Ing., Environmental Engineering (1996)
Fachhochschule Wilhelmshaven, Germany
Ph.D., Oceanography, Old Dominion University (2003)

Publications

Fach, B.A., 1996. Development of wind conditions in the German Bight since 1965 as an important environmental influence on the coastal area. Diplomarbeit, Fachbereich Feinwerktechnik, Fachhochschule Wilhelmshaven, Germany.

Hofmann, E.E., Klinck, J.M., Locarnini R.A., Fach, B.A., Murphy, E.J., 1998. Krill transport in the Scotia Sea and environs. Antarctic Science 10(4), 406-415.

Fach, B.A., Hofmann, E.E., Murphy, E.J., 2002. Modeling studies of Antarctic krill (*Euphausia superba*) survival during transport across the Scotia Sea. Marine Ecology Progress Series 231, 187-203.

Published Abstracts

Fach, B.A., Hofmann, E.E., Klinck, J.M., Locarnini, R.A., Murphy, E.J., 1998. Relationship between biological transport and the Southern Antarctic Circumpolar Current in the Scotia Sea. EOS, Transactions AGU 79(1), 145.

Fach, B.A., Hofmann, E.E., Klinck, J.M., Locarnini, R.A., Murphy, E.J., 1998. Modeling of krill survival during transport across the Scotia Sea. EOS, Transactions AGU 79(45), 410.

Fach, B.A., Hofmann, E.E., Murphy, E.J., 1999. Krill transport and survival across the Scotia Sea: A modeling study. EOS, Transactions AGU 80(45), 305.

Fach, B.A., Hofmann, E.E., Klinck, J.M., Murphy, E.J., 2002. Modeling studies of krill survival during transport across the Scotia Sea. EOS, Transactions AGU 83(4), 367.